

# **Die Rolle des Toll-like Rezeptor 4 als Modulator metabolischer Prozesse im Tiermodell des Typ 1 Diabetes**

Inaugural-Dissertation

zur Erlangung des Doktorgrades  
der Mathematisch-Naturwissenschaftlichen Fakultät  
der Heinrich-Heine-Universität Düsseldorf

vorgelegt von

**Corinna Wessel**  
aus Neuss

Düsseldorf, Oktober 2020

aus dem Institut für Klinische Diabetologie  
des Deutschen Diabetes-Zentrums (DDZ)

Gedruckt mit der Genehmigung der  
Mathematisch-Naturwissenschaftlichen Fakultät der  
Heinrich-Heine-Universität Düsseldorf

Berichtersteller:

1. Priv.-Doz. Dr. Volker Burkart
2. Prof. Dr. Eckhard Lammert

Tag der mündlichen Prüfung: 18.03.2021

## Table of Content

<b>I</b>	<b>SUMMARY</b> .....	<b>8</b>
<b>II</b>	<b>ZUSAMMENFASSUNG</b> .....	<b>9</b>
<b>III</b>	<b>ANNOTATION TO THIS THESIS</b> .....	<b>11</b>
<b>1</b>	<b>INTRODUCTION</b> .....	<b>12</b>
1.1	Pancreatic islets and insulin.....	12
1.1.1	Glucose stimulated insulin secretion .....	12
1.1.2	Insulin effects .....	13
1.2	Diabetes mellitus .....	15
1.2.1	Type 2 diabetes.....	15
1.2.2	Type 1 diabetes.....	15
1.2.2.1	Autoimmune pathogenesis of T1D .....	16
1.2.2.2	Metabolic disorders contributing to T1D .....	17
1.2.2.3	Environmental factors modulating T1D.....	17
1.3	Potential role of insulin sensitive tissues in the pathogenesis of T1D.....	18
1.3.1	Liver in the pathogenesis of T1D.....	18
1.3.2	Adipose tissue in the pathogenesis of T1D.....	19
1.3.3	Skeletal muscle in the pathogenesis of T1D.....	20
1.4	Energy metabolism.....	20
1.5	Fatty acid metabolism.....	22
1.5.1	Free fatty acid receptors CD36 and FFAR2.....	24
1.6	Gut microbiota .....	25
1.7	Toll-like receptor family.....	26
1.7.1	Toll-like receptor 4.....	27
1.8	Animal models of type 1 diabetes .....	27
1.8.1	Non-obese diabetic mouse.....	28
1.8.2	The TLR4-deficient non-obese diabetic mouse .....	30
1.9	Interplay between energy homeostasis, gut microbiome composition and pathogenesis of T1D.....	31
1.10	Aims of this study.....	34
<b>2</b>	<b>MATERIAL AND METHODS</b> .....	<b>35</b>
2.1	Material.....	35
2.1.1	Mouse models.....	35
2.1.2	Chemicals .....	36
2.1.2.1	Chemicals for genotyping.....	36
2.1.2.2	Chemicals for physiological investigations.....	36
2.1.2.3	Chemicals for histological analysis of organs .....	36

2.1.2.4	Reagents for islet isolation .....	37
2.1.2.5	Reagents for western blot-analysis.....	37
2.1.2.6	Chemicals for magnetic resonance imaging/ spectroscopy .....	38
2.1.3	Devices .....	38
2.1.4	Consumable material .....	40
2.1.5	Buffers and reagents .....	41
2.1.6	Oligonucleotides for the determination of the TLR4 expression status .....	42
2.1.7	Antibodies .....	42
2.2	Methods.....	43
2.2.1	Genotyping of NOD TLR4 <sup>+/+</sup> and NOD TLR4 <sup>-/-</sup> mice .....	43
2.2.2	Diabetes diagnostics .....	44
2.2.3	Physiological methods.....	45
2.2.3.1	Metabolic phenotyping .....	45
2.2.3.2	Body weight, liver and fat depot measurements .....	45
2.2.3.3	Nuclear Magnetic Resonance (NMR).....	45
2.2.3.4	Blood glucose measurements .....	46
2.2.3.5	Intraperitoneal glucose and insulin tolerance test (ipGTT and ipITT) .....	46
2.2.3.6	ELISA.....	46
2.2.3.7	Determination of the HOMA-IR.....	47
2.2.3.8	FFA, TG, cholesterol, HDL, LDL and CRP levels in plasma samples .....	47
2.2.3.9	Measurement of short-chain fatty acids in plasma samples.....	47
2.2.3.10	Measurement of short-chain fatty acids in fecal samples .....	47
2.2.4	Glucose-stimulated insulin secretion from isolated islets .....	48
2.2.4.1	Islet isolation .....	48
2.2.4.2	Glucose stimulated insulin secretion from mouse pancreatic islets.....	48
2.2.5	Histological analysis of organs .....	48
2.2.5.1	Liver preparation .....	48
2.2.5.2	Preparation of frozen sections from liver tissue .....	49
2.2.5.3	Oil Red O Staining of liver sections .....	49
2.2.5.4	Preparation of frozen sections from pancreas tissue .....	49
2.2.5.5	Immunohistological insulin verification.....	50
2.2.6	Preparation of liver, muscle tissue and VAT for protein analysis .....	51
2.2.6.1	Bicinchoninic acid (BCA) assay.....	51
2.2.6.2	Western Blot-Analysis .....	53
2.2.7	Intraperitoneal glucose-tolerance-test (ipGTT) during isoflurane-anesthesia ...	56
2.2.8	Magnetic resonance imaging and spectroscopy .....	57
2.2.8.1	<sup>1</sup> H imaging and spectroscopy .....	57
2.2.8.2	<sup>31</sup> P spectroscopy .....	58

2.2.8.3	<sup>1</sup> H and <sup>31</sup> P MRS/MRI data analysis .....	59
<b>3</b>	<b>RESULTS .....</b>	<b>60</b>
3.1	Metabolic phenotyping of the NOD TLR4 <sup>-/-</sup> mouse, as a model of accelerated development of insulin-deficient diabetes.....	60
3.1.1	Age and blood glucose levels at diabetes onset in NOD mice .....	60
3.1.2	Insulin tolerance in NOD mice .....	60
3.1.3	Glucose-stimulated insulin release from isolated islets of NOD mice.....	61
3.1.4	Diabetes manifestation in NOD TLR4 <sup>+/+</sup> and NOD TLR4 <sup>-/-</sup> mice.....	62
3.1.5	Age and blood glucose levels at diabetes onset .....	62
3.1.6	Metabolic phenotyping .....	64
3.1.6.1	Water- and food intake .....	64
3.1.6.2	Physical activity.....	65
3.1.6.3	Respiratory quotient .....	66
3.1.6.4	Energy expenditure .....	67
3.1.6.5	Whole-body carbohydrate and fat oxidation rates.....	68
3.1.7	Body weight and weight of liver and visceral adipose tissue.....	69
3.1.8	Development of body weight .....	70
3.1.9	White and brown adipose tissue weight.....	70
3.1.10	Liver, VAT, NAT and BAT volume.....	71
3.1.11	Body fat mass.....	73
3.1.12	Glucose metabolism .....	73
3.1.12.1	Random blood glucose levels .....	73
3.1.12.2	Plasma glucose levels during ipGTT .....	74
3.1.12.3	Plasma insulin levels during ipGTT .....	75
3.1.12.4	HOMA-IR .....	76
3.1.12.5	Development of insulinitis and decline of beta cell mass in pancreatic islets .....	76
3.1.12.6	Effect of isoflurane-anesthesia on glucose metabolism .....	78
3.1.12.7	Effect of isoflurane-anesthesia on plasma insulin levels.....	83
3.1.13	Effect of the TLR4-expression status on lipid metabolism .....	83
3.1.13.1	Plasma free fatty acid and triglyceride levels.....	83
3.1.13.2	Plasma levels of cholesterol, HDL, LDL and CRP .....	84
3.1.13.3	Composition of fat depots.....	85
3.1.13.4	Hepatocellular lipid content .....	88
3.1.13.5	Triglyceride content in the liver.....	89
3.1.14	Fatty acid receptor expression.....	90
3.1.14.1	Expression of fatty acid receptors in liver tissue .....	90
3.1.14.2	Expression of fatty acid receptors in skeletal muscle tissue .....	91
3.1.14.3	Expression of fatty acid receptors in VAT .....	92

3.1.15	Plasma SCFA levels .....	93
3.1.16	SCFA levels in gut segments.....	95
3.1.17	Hepatic energy metabolism in NOD TLR4 <sup>-/-</sup> mice.....	98
3.1.17.1	Hepatic ATP and Pi concentrations.....	98
3.1.17.2	Hepatic PME and PDE concentrations.....	100
3.2	Effect of HFD on metabolic parameters in the prediabetic phase of NOD TLR4 <sup>-/-</sup> mice, a model of accelerated development of insulin-deficient diabetes.....	103
3.2.1	Metabolic phenotyping .....	103
3.2.1.1	Water- and food intake .....	103
3.2.1.2	Physical activity.....	104
3.2.1.3	Respiratory quotient .....	105
3.2.1.4	Energy expenditure .....	106
3.2.1.5	Whole-body carbohydrate and fat oxidation rates.....	107
3.2.2	Body weight and weight of liver and visceral adipose tissue.....	108
3.2.3	Development of body weight .....	109
3.2.4	White and brown adipose tissue weight.....	110
3.2.5	Liver, VAT, NAT and BAT volume .....	111
3.2.6	Body fat mass .....	113
3.2.7	Effect of HFD on random blood glucose levels .....	113
3.2.8	Impact of HFD on the development of insulinitis and decline of beta cell mass in pancreatic islets .....	114
3.2.9	Effect of HFD on lipid metabolism .....	116
3.2.9.1	Plasma free fatty acid and triglyceride levels.....	116
3.2.9.2	Levels of plasma cholesterol, HDL, LDL and CRP .....	117
3.2.9.3	Composition of fat depots.....	118
3.2.9.4	Hepatocellular lipid content .....	124
3.2.10	Hepatic energy metabolism in NOD TLR4 <sup>-/-</sup> mice.....	125
3.2.10.1	Hepatic ATP and Pi concentrations.....	125
3.2.10.2	Hepatic PME and PDE concentrations.....	127
<b>4</b>	<b>DISCUSSION.....</b>	<b>130</b>
4.1	Metabolic phenotyping of the NOD TLR4 <sup>-/-</sup> mouse, as a model of accelerated development of insulin-deficient diabetes.....	130
4.1.1	Effect of TLR4-deficiency in NOD mice on manifestation of insulin-deficient diabetes .....	130
4.1.2	Effect of TLR4-deficiency on body- and tissue weight of NOD mice .....	132
4.1.3	Effect of TLR4-deficiency on metabolic parameters of NOD mice .....	133
4.1.4	Effect of TLR4-deficiency in NOD mice on islet inflammation .....	134
4.1.5	Effect of TLR4-deficiency in NOD mice on glucose metabolism .....	135
4.1.6	Effect of TLR4-deficiency in NOD mice on lipid metabolism .....	136

4.1.7	Effect of TLR4-deficiency in NOD mice on SCFA levels .....	137
4.1.8	Effect of TLR4-deficiency in NOD mice on hepatic lipid, glucose and energy metabolism.....	138
4.2	Effect of HFD on metabolic parameters in the prediabetic phase of NOD TLR4 <sup>-/-</sup> mice, a model of accelerated development of insulin-deficient diabetes.....	141
4.2.1	Effect of HFD on body- and tissue weight.....	142
4.2.2	Effect of HFD on metabolic parameters.....	143
4.2.3	Effect of HFD on islet inflammation .....	144
4.2.4	Effect of HFD on lipid metabolism .....	146
4.2.5	Effect of HFD on hepatic lipid-, glucose- and energy metabolism.....	147
4.3	Limitations of this study.....	148
4.3.1	Basic problem arising from animal studies .....	148
4.3.2	Heterogeneity of NOD TLR4 <sup>+/+</sup> and NOD TLR4 <sup>-/-</sup> mice .....	148
4.3.3	Anesthesia effects.....	149
<b>5</b>	<b>CONCLUSION AND OUTLOOK.....</b>	<b>150</b>
<b>6</b>	<b>PERSONAL CONTRIBUTION TO THE MANUSCRIPTS .....</b>	<b>151</b>
<b>7</b>	<b>LIST OF ABBREVIATIONS .....</b>	<b>153</b>
<b>8</b>	<b>FIGURE INDEX.....</b>	<b>157</b>
<b>9</b>	<b>TABLE INDEX .....</b>	<b>161</b>
<b>10</b>	<b>REFERENCES.....</b>	<b>162</b>
	<b>STATUTORY DECLARATION.....</b>	<b>174</b>
	<b>EIDESSTÄTTLICHE ERKLÄRUNG.....</b>	<b>174</b>
	<b>ACKNOWLEDGEMENTS .....</b>	<b>175</b>

## I Summary

Type 1 diabetes (T1D) is the most diagnosed chronic disease in children and young adults worldwide and is characterized by an autoimmune destruction of pancreatic beta cells resulting in absolute insulin deficiency. In recent years, the incidence of T1D is continuously increasing, particularly in children at younger age. However, the mechanisms underlying the development of T1D, especially the accelerated disease development in younger children, remain unclear. Meanwhile, increasing evidence indicates that metabolic disorders in the prediabetic phase promote disease development. Recent findings identified the toll-like receptor 4 (TLR4), originally described as receptor for bacterial lipopolysaccharide, as potent regulator of metabolic processes, including obesity-associated inflammation and insulin sensitivity, thereby pointing to a role of TLR4 in the pathogenesis of T1D. Based on these considerations, the aims of the present study were to characterize disorders of the glucose-, lipid- and energy metabolism potentially contributing to accelerated diabetes development and to test whether a hypercaloric diet aggravates diabetes promoting metabolic alterations. The study was performed in a model on the background of the non-obese diabetic (NOD) mouse. Animals of a newly generated NOD mouse subline which exhibit accelerated development of insulin-deficient diabetes after deletion of the TLR4 (NOD TLR4<sup>-/-</sup>) and TLR4-expressing (NOD TLR4<sup>+/+</sup>) mice were comprehensively phenotyped in the prediabetic phase to identify potential metabolic and/or immunologic disorders associated with accelerated disease progression. To characterize the potential effects of hypercaloric nutrition on diabetes pathogenesis, animals fed a high fat diet (HFD) during the prediabetic phase were analyzed. NOD TLR4<sup>-/-</sup> mice developed diabetes earlier and with a higher incidence compared to NOD TLR4<sup>+/+</sup> mice. Compared to NOD TLR4<sup>+/+</sup> mice, NOD TLR4<sup>-/-</sup> mice showed impaired glucose tolerance and lower insulin levels during an intraperitoneal glucose tolerance test, higher body weight, elevated pancreatic islet sizes, lower hepatocellular lipid (HCL) content and decreased plasma short-chain fatty acid levels. Under HFD condition, the animals developed increased body weight, higher fat depot weights and volumes, elevated body fat mass, lipid levels and HCL independent of their TLR4 expression status. Interestingly, NOD TLR4<sup>-/-</sup> mice on HFD showed lower random blood glucose levels and higher HCL content than NOD TLR4<sup>+/+</sup> mice on HFD. In conclusion, a marked reduction of HCL content precedes the manifestation of insulin deficient diabetes in NOD TLR4<sup>-/-</sup> mice, as a model of accelerated T1D. Lower HCL in NOD TLR4<sup>-/-</sup> mice could result from lower rates of insulin-stimulated triglyceride synthesis and/or decreased insulin-suppression of lipolysis. This data improves the knowledge of metabolic disorders preceding T1D manifestation and implicates that disturbed hepatic lipid metabolism in the prediabetic phase contributes to the accelerated development of T1D, as observed in younger children.

## II Zusammenfassung

Typ 1 Diabetes (T1D) ist die weltweit am häufigsten diagnostizierte chronische Erkrankung bei Kindern und jungen Erwachsenen und ist durch eine immunvermittelte Zerstörung autologer Betazellen des Pankreas gekennzeichnet, die zu einem absoluten Insulinmangel führt. In den letzten Jahren nahm die Inzidenz des T1D kontinuierlich zu, insbesondere bei Kindern im jüngeren Alter. Die Mechanismen, die der Entwicklung von T1D zugrunde liegen, insbesondere der beschleunigten Krankheitsentwicklung bei jüngeren Kindern, bleiben jedoch unklar. Neuere Ergebnisse deuten darauf hin, dass Stoffwechselstörungen in der prädiabetischen Phase die Krankheitsentwicklung fördern. Jüngste Erkenntnisse identifizierten den Toll-like Rezeptor 4 (TLR4), der ursprünglich als Rezeptor für bakterielles Lipopolysaccharid beschrieben wurde, als potenten Regulator von Stoffwechselprozessen, einschließlich Adipositas-assoziiierter Entzündungen und Insulinsensitivität, was auf eine Rolle des TLR4 in der Pathogenese des T1D hinweist. Basierend auf diesen Betrachtungen bestand das Ziel der vorliegenden Studie darin, Störungen des Glukose-, Lipid- und Energiestoffwechsels zu charakterisieren, die möglicherweise zur beschleunigten Diabetesentwicklung beitragen, sowie zu prüfen, ob eine hyperkalorische Ernährung Diabetesbeschleunigende Stoffwechselveränderungen fördert. Die Studie wurde in einem Modell auf dem Hintergrund der non-obese diabetic (NOD) Maus durchgeführt. Tiere einer neu generierten NOD-Maus-Sublinie, die nach Deletion des TLR4 eine beschleunigte Entwicklung des Insulinmangel-Diabetes aufweisen (NOD TLR4<sup>-/-</sup>) sowie vergleichend TLR4-exprimierende (NOD TLR4<sup>+/+</sup>) NOD Mäuse, wurden in der prädiabetischen Phase umfassend phänotypisiert, um mögliche Stoffwechsel- und / oder immunologische Störungen zu identifizieren, die mit einem beschleunigten Fortschreiten der Krankheit assoziiert sind. Um die möglichen Auswirkungen einer hyperkalorischen Ernährung auf die Diabetes-Pathogenese zu charakterisieren, wurden Tiere analysiert, die während der prädiabetischen Phase eine fettreiche Ernährung (HFD) erhielten. NOD TLR4<sup>-/-</sup> Mäuse entwickelten früher und mit einer höheren Inzidenz Diabetes als NOD TLR4<sup>+/+</sup> Mäuse. Im Vergleich zu NOD TLR4<sup>+/+</sup> Mäusen zeigten NOD TLR4<sup>-/-</sup> Mäuse während eines intraperitonealen Glukosetoleranztests eine gestörte Glukosetoleranz und niedrigere Insulinspiegel, ein höheres Körpergewicht, größere pankreatische Inseln, einen niedrigeren Gehalt an hepatozellulären Lipiden (HCL) und verringerte kurzkettige Fettsäurespiegel im Plasma. Unter HFD-Bedingungen entwickelten die Tiere unabhängig von ihrem TLR4-Expressionsstatus ein erhöhtes Körpergewicht, höhere Fettdepotgewichte und -volumina, eine erhöhte Körperfettmasse, erhöhte Lipidspiegel und HCL. Interessanterweise zeigten NOD TLR4<sup>-/-</sup> Mäuse unter HFD niedrigere zufällige Blutglukosespiegel und einen höheren HCL-Gehalt als NOD TLR4<sup>+/+</sup> Mäuse. Zusammenfassend lässt sich festhalten, dass eine deutliche Verringerung des HCL-Gehalts der Manifestation des Insulinmangel-Diabetes bei NOD TLR4<sup>-/-</sup> Mäusen als einem Modell für

## Zusammenfassung

den beschleunigten T1D vorausgeht. Ein niedrigerer HCL-Gehalt in NOD TLR4<sup>-/-</sup> Mäusen könnte auf niedrigere Raten der Insulin-stimulierten Triglyceridsynthese und / oder einer verringerten Insulin-vermittelten Suppression der Lipolyse zurückzuführen sein. Die Ergebnisse der vorliegenden Studie erweitern das Wissen über Stoffwechselstörungen vor der T1D-Manifestation und implizieren, dass ein gestörter Leberlipidstoffwechsel in der prädiabetischen Phase zur beschleunigten Entwicklung von T1D beiträgt, wie sie bei jüngeren Kindern beobachtet wird.

### III Annotation to this thesis

The result and discussion parts of this thesis consist of two sections. Section one is the main part and refers partly to published original research articles and follow-up experiments, while section two describes follow-up experiments.

The first section comprises results from the NOD TLR4<sup>-/-</sup> mouse model from the publication Simon et al. [1] and Rothe et al. [2] as well as data presented at the annual conferences of the German Diabetes Association (Deutsche Diabetes Gesellschaft (DDG)) and the European Association for the Study of Diabetes (EASD).

Simon MC\*, Reinbeck AL\*, **Wessel C\***, Heindirk J, Jelenik T, Kaul K, Arreguin-Cano J, Strom A, Blaut M, Bäckhed F, Burkart V, Roden M. Distinct alterations of gut morphology and microbiota characterize accelerated diabetes onset in non-obese diabetic mice. *Journal of Biological Chemistry* 2020; 295(4):969-980.  
Original research article, \*equal contribution

Rothe M, **Wessel C**, Cames S, Szendroedi J, Burkart V, Hwang JH, Roden M. In vivo absolute quantification of hepatic  $\gamma$ -ATP concentration in mice using <sup>31</sup>P magnetic resonance spectroscopy at 11.7 T. *NMR in Biomedicine* 2020; e4422.  
Original research article

**Wessel C**, Blaut M, Roden M, Burkart V. Reduktion von kurzkettigen Fettsäuren und gestörter Glukosestoffwechsel im Tiermodell des beschleunigten Typ 1 Diabetes. *Diabetologie und Stoffwechsel* 2019; 14:S42.

**Wessel C**, Blaut M, Roden M, Burkart V. Reduced short-chain fatty acids and impaired glucose homeostasis in an animal model of accelerated type 1 diabetes. *Diabetologia* 2019; 62:S202.

**Wessel C**, Rothe M, Hwang JH, Roden M, Burkart V. Reduced hepatocellular lipid content precedes diabetes onset in a mouse model of accelerated type 1 diabetes. *Diabetologia* 2020; 365:S182.

The second section shows results from the feeding of NOD TLR4<sup>-/-</sup> mice with a high fat diet. This section describes follow-up experiments that are based on Simon et al. [1].

# 1 Introduction

## 1.1 Pancreatic islets and insulin

The pancreas is a glandular organ in the digestive system that consists of two morphologically and functionally different regions, the endocrine and exocrine pancreas [3]. The exocrine pancreas is fundamental for the synthesis of digestive enzymes like lipases and proteases, while the endocrine pancreas is important for secreting various hormones like insulin and glucagon mainly involved in the control of glucose homeostasis [3]. The endocrine functions of the pancreas are mediated by the highly specialized cell populations of the pancreatic islets also named islets of Langerhans after the anatomist Paul Langerhans who first described these structures in 1869. Islets consist of various cell types that secrete specific hormones [3]. The human pancreas contains 1-2 million islets, which are composed of different cell types similar to islets of other mammals such as mice. In contrast to human islets, which show a complex and more random distribution of the different endocrine cell types, the distribution of endocrine cells within a murine islet is characterized by a localization of beta cells in the center and a more peripheral arrangement of other cell types [3, 4]. The murine pancreas contains 2000-4000 islets. Each islet is approximately 50  $\mu\text{m}$  to 1 mm in size and contains alpha cells (approx. 15 – 20 % of total islet cells) secreting glucagon, beta cells (65-80 %) secreting insulin, delta cells (3–10 %) secreting somatostatin, gamma cells (3-5 %) secreting pancreatic polypeptides and epsilon cells (<1 %) secreting ghrelin [3, 4].

Taken together, beta cells are the most frequent cell type in pancreatic islets with the primary function of producing and secreting insulin in a tightly regulated manner [3].

### 1.1.1 Glucose stimulated insulin secretion

The hormone insulin is controlling energy homeostasis, including lipid and glucose metabolism, primarily via maintaining normoglycemia by responding to the rising and decreasing levels of blood glucose. Insulin secretion is regulated by a variety of factors including glucose, free fatty acids (FFA), lipids and glucagon [5-7]. Glucose represents the most important regulator, which enters the beta cell via the glucose transporter 2 (GLUT2), a transmembrane carrier protein that acts as a glucose sensor. Inside the beta cell, glucose is converted to pyruvate by the metabolic pathway of glycolysis. Pyruvate enters the tricarboxylic acid (TCA) cycle in the mitochondrion, which subsequently generates adenosine triphosphate (ATP). The rise of the intracellular ATP concentration is followed by the closure of the ATP sensitive potassium channels ( $K_{\text{ATP}}$ -channels) in the plasma membrane of the beta cell. The membrane depolarizes because the potential difference across the membrane becomes more positive due to the rising intracellular concentrations of potassium ions. Consequently, the voltage-dependent calcium ion channels (VDCC) open, causing calcium ions to pass the

membrane into the beta cell. The intracellular calcium levels rise and subsequently insulin containing vesicles move towards the beta cell membrane, fuse with the membrane and release insulin by exocytosis [5-7] (Figure 1).

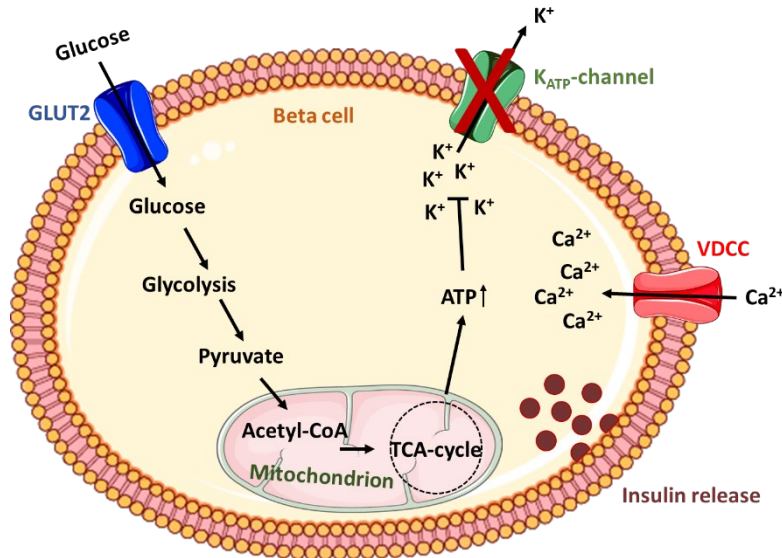


**Figure 1: Glucose stimulated insulin secretion from pancreatic beta cells.** Glucose enters the beta cell via the glucose transporter 2 (GLUT2). During the following catabolization of glucose in the tricarboxylic acid (TCA) cycle, adenosine triphosphate (ATP) is generated, which closes the ATP sensitive potassium channels (K<sub>ATP</sub>-channels), in turn hyperpolarizing the beta cell membrane. Consequently, the voltage-dependent calcium ion channels (VDCC) open, which results in an influx of calcium ions leading to the fusion of insulin vesicles with the membrane.

### 1.1.2 Insulin effects

Once insulin is secreted, it can bind to its receptor, the insulin receptor, which is located on almost every cell type of the mammalian body. After activation, the insulin receptor can phosphorylate several substrates, particularly the insulin-receptor substrates (IRS) IRS1 and IRS2 [8]. The IRS phosphorylation displays binding sites for various signaling partners and thereby initiates an intracellular signaling cascade, resulting in the activation of protein kinase B (Akt) through phosphorylation [9]. pAkt induces the translocation of the kinase receptor glucose transporter 4 (GLUT4) storage vesicle (GSV) to the plasma membrane, where GLUT4 is inserted to mediate glucose transport into the cell thereby decreasing extracellular, systemic glucose concentrations (Figure 2) [10].

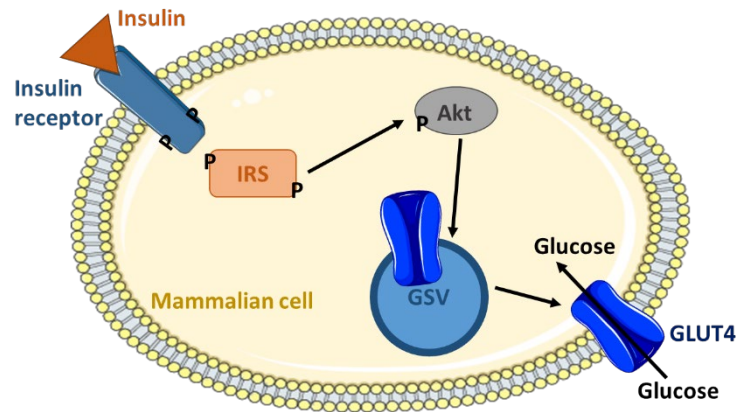


**Figure 2: Insulin signaling pathway in mammalian cells.** Insulin binds to its receptor, the insulin receptor, resulting in the phosphorylation of insulin-receptor substrates (IRS) followed by protein kinase B (Akt) phosphorylation and activation. After that, Akt induces translocation of kinase receptor glucose transporter 4 (GLUT4) storage vesicle (GSV) leading to GLUT4 insertion into the plasma membrane.

Akt activation promotes multiple cellular processes, which are regulated via insulin such as glycogenolysis but also gluconeogenesis and lipogenesis [8, 9, 11, 12]. Low blood glucose levels lead to an activation of the pathway of glycogenolysis that degrades glycogen to glucose in hepatocytes and skeletal muscle cells. Glucose molecules are released from the tissue into the blood increasing peripheral glucose levels [13]. Glycogenolysis is activated by glucagon, the antagonist of insulin, and is inhibited by insulin [14]. Gluconeogenesis is a pathway which generates glucose from noncarbohydrate precursors such as pyruvate, lactate, amino acids and glycerol. This process mainly takes place in the liver and is inhibited by insulin [15]. By these pathways, insulin inhibits glucose production, but also affects further complex signaling pathways. Another metabolic pathway, which is affected by insulin, is glycogenesis [16]. The IRS activates multiple protein kinases, which can deactivate glycogen synthase kinase leading to an active form of glycogen synthase promoting glycogenesis. During glycogenesis, glucose is added to a core of glycogen and stored as glycogen in hepatocytes and skeletal muscle cells resulting in the lowering of blood glucose levels [13]. Taken together, the above mentioned pathways represent important regulatory processes for the maintenance of blood glucose homeostasis.

In addition to the above mentioned processes, insulin inhibits the secretion of lipoproteins from the liver, stimulates lipid and glucose uptake into the adipose tissue and inhibits lipolysis as described in detail in chapter 1.5 [16, 17].

In summary, insulin is essential for the maintenance of mammalian energy homeostasis. Defects in insulin synthesis or signaling can lead to metabolic diseases such as diabetes mellitus [18, 19].

### 1.2 Diabetes mellitus

Diabetes mellitus is one of the most diagnosed diseases in the world, with the numbers continuously rising. Currently, around 463 million adults are diagnosed with diabetes worldwide and approximately 4.2 million deaths were directly caused by diabetes in 2019, making diabetes one of the leading causes of death in the world [20, 21]. Diabetes mellitus describes a group of metabolic diseases leading to impairments of glucose metabolism [22]. The main symptom is hyperglycemia (increased blood glucose levels), resulting from an absolute insulin deficiency or a progressive loss of beta cell insulin secretion associated with insulin resistance (IR) [22]. According to the disease patterns, diabetes can be categorized into four major forms: type 1 diabetes (T1D), type 2 diabetes (T2D), gestational diabetes and a group of rarely appearing diabetes forms [22].

#### 1.2.1 Type 2 diabetes

The most common form of diabetes is T2D, which accounts for up to about 90-95 % of cases worldwide and is typically associated with obesity, but also with advanced age, physical inactivity and genetic factors [22-24]. T2D is defined as a disease state mainly characterized by hyperglycemia as a consequence of relative insulin deficiency, which is due to IR, the reduced reactivity of peripheral tissues, like liver, muscle and adipose tissue, to the blood glucose lowering effect of insulin [24, 25]. Pancreatic beta cells increasingly produce insulin in the earlier stages of the disease but can compensate the rising demand for insulin during advancing IR only for a limited time. In early stages after the diagnosis of T2D, drugs like Metformin are prescribed [26]. Those drugs decrease the glucose production primarily by the liver and increase the insulin sensitivity [26]. In advanced stages of the disease, through exhaustion of beta cells, patients depend on the administration of insulin [24].

#### 1.2.2 Type 1 diabetes

T1D, previously called juvenile or insulin-dependent diabetes, is the most diagnosed chronic disease in children and young adults, which accounts for approximately 5-10 % of all diabetes cases [22, 27, 28]. T1D is defined as an autoimmune disease leading to an absolute lack of insulin due to an almost complete loss of beta cells [29, 30]. During the pathogenesis of T1D, immune cell reactivity against autologous beta cells results in the destruction of insulin-producing beta cells in the pancreatic islets [27, 29, 31]. The progressive destruction of beta cells leads to increasing blood glucose levels in patients [29]. During the clinical manifestation of the disease, severe hyperglycemia and hypoinsulinemia are often accompanied by multiple symptoms like increased urinary excretion (polyuria), an increased fluid intake (polydipsia) and increased food intake (polyphagia) [32]. Approximately one third of patients are diagnosed with

a life-threatening diabetic ketoacidosis [29]. To maintain glucose homeostasis, patients depend on regular exogenous administration of insulin throughout their life via injections or implanted pumps [27]. T1D patients show higher risks of developing severe diabetes-specific micro- and macrovascular complications including retinopathy and nephropathy as well as neurologic disorders (poly-(neuropathy)) [33]. In recent years, the incidence of T1D is increasing in younger children, especially in children under the age of seven years [27, 34]. The increasing incidence is concerning, because these patients will have T1D for a longer period of their life leading to increased risks for the development of diabetes-associated complications [35, 36]. Despite intensive clinical and experimental research efforts, the cause(s) for developing T1D and especially the accelerated development of the disease in children remain largely unknown.

### **1.2.2.1 Autoimmune pathogenesis of T1D**

The pathogenesis of T1D is described as a multi-faceted process, in which not only genetic but also environmental factors play a role in the induction of the disease [37]. The predisposition to develop T1D is determined by variations in certain gene regions. T1D-associated risk alleles are found mainly in the human leukocyte antigen (HLA) system of the major histocompatibility complex (MHC) [38, 39]. Genes of the HLA system have the largest impact on T1D risk (determining about 60 % of the risk) and can mediate either predisposing or protective effects [29, 32]. But also variations in other genes like *INS*, which encodes insulin, *CTLA4*, which encodes the cytotoxic T-lymphocyte-associated protein 4 and *IL2RA*, which encodes the interleukin-2 receptor alpha chain, can lead to an increased risk of T1D [38, 39]. However, studies in twins showed that the concordance rate for T1D is between 13 and 68 % in identical twins and only about 10 % in unidentical twins [40, 41]. This observation demonstrates that also other influences like environmental factors play an important role in the induction of T1D.

Long before the manifestation of T1D, a prediabetic phase is described. A first sign for the development of beta cell-directed immune reactivity is the appearance of autoantibodies against islet cell antigens (ICA), insulin (IAA), zinc transporter T8 (ZnT8), glutamate decarboxylase ( $GAD_{65}$ ) and tyrosin phosphatases (IA-2, IA-2 $\beta$ ) [42]. Several studies showed that increased numbers in above-mentioned autoantibodies associate with an increased risk of developing T1D [42]. Whereas autoantibodies have no beta-cell damaging effect, components of the cellular immune system, mainly macrophages and T-lymphocytes play an important role in the initiation of beta cell destruction in the prediabetic period [40]. During this phase, immune cells infiltrate the islets (insulinitis) and the beta cell mass decreases continuously as a result of the cytotoxic activities of macrophages and T-lymphocytes [40, 42]. When only approximately 40 % of functionally active beta cells are left, hyperglycemia can

occur [28, 32]. Recent studies indicate that not only beta cell-directed autoimmune processes but also the patient's lifestyle has an impact on the progression of the pathogenesis of T1D.

### ***1.2.2.2 Metabolic disorders contributing to T1D***

Investigations on the pathogenesis of T1D revealed that the progression of the disease is affected by factors that are associated with the development of obesity as a consequence of hypercaloric diet and a lack of physical activity. Consequently, an association between higher body weight and accelerated diabetes manifestation was described [43-45]. The association of high body weight with accelerated diabetes manifestation suggests that obesity and IR along with increased levels of obesity-related systemic inflammatory mediators are involved in the progression of T1D [46, 47]. Chronically elevated levels of inflammatory mediators lead to persisting subclinical inflammation in patients with adiposity [48, 49]. Recent findings further indicate that IR is associated with the progression of T1D. This association leads to the assumption, that the development of IR in predisposed patients is a risk factor for the earlier manifestation of T1D [50]. This view is supported by recent findings which demonstrate that T1D patients show an aggravation of IR with increasing adipose tissue mass and with increasing levels of the proinflammatory cytokine interleukin-6 [51].

### ***1.2.2.3 Environmental factors modulating T1D***

In humans, T1D susceptibility has been associated with several environmental factors, particularly dietary components. In genetically susceptible children, a diet enriched with omega-3 fatty acids (FA) reduced the incidence of T1D [52]. It is suggested that omega-3 FA directly bind to G-protein coupled receptor 120 on macrophages, which thereby exert anti-inflammatory effects [53]. Further studies suggest that increased intake of gluten and cow milk proteins in early life increases the risk of developing T1D [54-56]. Interestingly, a cross reactivity was shown between antibodies against cow milk proteins and p69, a beta cell surface protein [57]. Other important environmental factors that have been associated with T1D susceptibility are seasonal and geographic effects [37]. The peak of manifestations of T1D is observed in fall and winter seasons, which points to an association with the increased appearance of viral infections that are discussed as disease-precipitating events [58]. There is an inverse correlation between disease incidence and proximity to the equator [37]. Explanations for this correlation may be the reduced exposure to sunlight and ultraviolet (UV) radiation (reduced epidermal vitamin D synthesis) and lower temperature in regions in higher latitudes [37]. In non-obese diabetic (NOD) mice, a mouse model of human T1D, animals maintained at lower temperature (21 °C) exhibited a higher incidence of insulin-deficient diabetes compared to mice maintained at 23.7 °C [37]. Interestingly, vitamin D deficiency early

in life resulted in accelerated development of insulin-deficient diabetes in NOD mice [37]. NOD mice fed supplementary vitamin D were protected against the development of insulin-deficient diabetes, which correlated with a higher frequency of regulatory T-lymphocytes ( $T_{reg}$ ) in the pancreatic lymph nodes [59, 60]. It is suggested that vitamin D also regulates the immune response via inhibition of nuclear factor kappa-light-chain-enhancer of activated B cells (NF- $\kappa$ B) pathways in macrophages and dendritic cells leading to lower production of the proinflammatory cytokines interferon gamma (IFN $\gamma$ ) and interleukin-12, thereby inhibiting the development of beta cell-directed immunity [61]. In humans, vitamin D supplementation after birth also protects against the development of T1D, but could not delay the loss of beta cell function in patients with recent-onset T1D [62, 63]. Virus infections in early childhood are also discussed as diabetes-inducing environmental factors. Viruses like rotavirus or coxsackie B virus are assumed to have an impact on T1D development. Rotavirus increases intestinal permeability, which may stimulate immune responses that signal through toll-like receptors (TLR) and drive inflammation [64]. Other viruses like coxsackie B virus can directly infect islet tissue leading to inflammation in islets [37].

### **1.3 Potential role of insulin sensitive tissues in the pathogenesis of T1D**

Adipose tissue, skeletal muscle and the liver are defined as insulin sensitive tissues. In healthy individuals, glucose passes the membranes of cells of insulin-responsive adipose tissue and skeletal muscle tissue via the GLUT4 transporter. GLUT4 is activated by insulin-binding leading to various reactions like production of GLUT4 protein or translocation of existing GLUT4 from the endoplasmic reticulum (ER) to the surface of either adipose tissue or skeletal muscle cells [47]. In lean T1D patients, IR is a common feature in the liver, adipose tissue and skeletal muscle [47]. Under this condition, insulin sensitive tissues fail to properly respond to insulin and to take up glucose resulting in hyperglycemia [65]. In hepatocytes, IR results in an increased plasma glucose concentration due to the reduction of hepatic glycogen synthesis [66]. This impairment is coupled with the inability of adipocytes and skeletal muscle cells to take up glucose [66]. However, the precise pathophysiology of IR remains unclear.

#### **1.3.1 Liver in the pathogenesis of T1D**

The main functions of the liver are neutralization of toxins, regulation of lipid-, protein- and carbohydrate metabolism and production and secretion of proteins like serum albumin and fetuin A [67, 68]. The liver is supplied by both venous blood, which enters the organ from the intestinal region via the portal vein and oxygen-rich arterial blood, which enters via the hepatic artery [67]. Most of the blood enters the organ through the portal vein, which is rich in nutritional

components such as FA, glucose and amino acids but also gut microbe-derived molecules like lipopolysaccharide (LPS) [67].

Hepatic glucose- and lipid homeostases are maintained by regulation of glycogen storage, gluconeogenesis and glycogenolysis [47]. In the non-fasted state, glucose enters the hepatocytes, a cell population comprising about 80 % of the liver cells, via GLUT2 and is phosphorylated by glucokinase to generate glucose 6-phosphate (G6P). This reaction leads to a decrease in intracellular glucose levels which further elevates glucose uptake [15]. G6P can be metabolized by entering the glycolytic pathway, the TCA-cycle and oxidative phosphorylation or can be used for glycogen synthesis [15]. In the short-term fasted state, glycogen can be hydrolyzed in the liver by glycogen phosphorylase to produce glucose (glycogenolysis) [15]. In the long-term fasted state after glycogen is depleted, glucose is synthesized by hepatocytes from pyruvate, lactate, amino acids and glycerol (gluconeogenesis) [15]. Lipids can also be stored in the liver, in a process called ectopic lipid storage, which can contribute to IR [69]. Studies in rodent models showed, that short-term feeding of a HFD can lead to ectopic lipid accumulation and IR in the liver [70, 71]. Interestingly, a human study confirmed these findings. Acute administration of a diet high in saturated fat to metabolically healthy persons led to increased hepatic IR and hepatic lipid storage [72].

### 1.3.2 Adipose tissue in the pathogenesis of T1D

Adipose tissue can be divided by its localization into subcutaneous adipose tissue (SAT) and visceral adipose tissue (VAT), but also by its functionality into white adipose tissue (WAT) and brown adipose tissue (BAT). SAT comprises up to about 80 % of whole-body fat, which makes SAT the largest adipose tissue depot in the body [73]. WAT, which represents the largest proportion of the adipose tissue compartment, performs three main functions: lipid storage, lipid release and release of hormones and cytokines that modulate IR, whole-body metabolism and immunological functions [69, 74]. Triglycerides (TG) are stored in WAT and released as free fatty acids (FFA) into the circulating blood when energy is required [75]. Additionally, WAT secretes adipokines that are involved in the control of inflammation and metabolism. It also serves as a thermal insulator and has a tissue protective function against mechanical damage [75]. Compared to WAT, BAT has a higher mitochondrial content [75]. The main functions of BAT are oxidative phosphorylation and thermogenesis. BAT plays a major role in maintaining the body temperature in a physiological range via heat production [74]. Adipocytes, the dominant cell population of the adipose tissue, store FFA as TG and release FA and glycerol if required [69]. Adipocytes within the BAT are able to oxidize circulating substrates but also their own stored fat to produce heat and accelerate metabolic processes [74]. Interestingly, it could be shown that the activity and amount of BAT were much higher in lean than obese individuals [76], suggesting a role of BAT in the development of obesity. SAT has a limited

FA/lipid storage capacity to expand, which depends on the ability of the cells to recruit new or to enlarge adipocytes [69]. When the storage capacity of the SAT has reached its maximum, fat is stored in other tissues, the ectopic fat depots, particularly the liver and skeletal muscle, leading to excessive lipid accumulation in these organs, increased IR and progressive inflammation [69]. Increased lipid storage in non-SAT adipose tissue like in VAT increases the risk of metabolic and vascular disorders and the development of diseases like T2D [69].

Besides their involvement in lipid metabolism, adipocytes play an important role in the regulation of glucose-metabolism since they express GLUT4 transporters on their surface mediating the control of glucose uptake from the periphery into the tissue [69]. Interestingly, in insulin-resistant obese and in prediabetic individuals, levels of GLUT4 in adipocytes are decreased [69]. Previous findings suggest that BAT also regulates the glucose metabolism, by showing that glucose uptake was increased and whole-body insulin-sensitivity and glucose disposal was improved when BAT was activated [74]. The insulin-stimulated glucose uptake by adipose tissue contributes to only about 10 % of the prandial glucose uptake, representing a small proportion compared to the amount of glucose that can be taken up by the skeletal muscle (about 80 %) [47, 69].

### **1.3.3 Skeletal muscle in the pathogenesis of T1D**

On the cellular level, the skeletal muscle is composed of myocytes, which use fat and carbohydrates as their main energy sources [77, 78]. Based on their distribution in the skeletal muscle, lipids can be divided into intramyocellular lipids (IMCL) and extramyocellular lipids (EMCL). In myocytes, IMCL are located close to the mitochondria and serve as an important substrate pool for FA oxidation, whereas EMCL are located between the muscle fibers [78, 79]. IR in skeletal muscle develops as a consequence of impaired insulin-stimulated upregulation of GLUT4, leading to lower glucose transport into myocytes [47]. Interestingly, in obese patients with T1D or T2D, GLUT4 protein levels are decreased in skeletal muscle [47]. It is suggested that increased concentrations of IMCL and of FFA in the circulating blood activate serine kinases leading to reduced glucose transport via GLUT4 from the circulating blood into the myocytes, thereby contributing to hyperglycemia [80, 81]. Previous studies have shown, that patients with T1D have higher IMCL levels compared to healthy individuals, a finding that could be explained by increased FFA transport to the skeletal muscle resulting from the failure of low or absent insulin to repress FFA release from adipocytes [82, 83].

## **1.4 Energy metabolism**

The main source of energy in the mammalian body is glucose, which is used to generate ATP during degradation by glycolysis, TCA-cycle and finally oxidative phosphorylation in the

respiratory chain [84]. All processes, except glycolysis, are located in the mitochondria. Mitochondria are double membrane organelles consisting of the outer mitochondrial membrane, the intermembrane space and the inner mitochondrial membrane (Figure 3) [85]. During glycolysis, glucose is converted to pyruvate by multiple steps [84]. When pyruvate is converted to acetyl coenzyme A (Acetyl-CoA) it enters the TCA-cycle, a closed-loop reaction series in the mitochondria [86].

The TCA-cycle consists of multiple steps generating 3 nicotinamide adenine dinucleotide (NADH), 2 CO<sub>2</sub> and flavin adenine dinucleotide (FADH<sub>2</sub>) per 1 molecule of acetyl-CoA. NADH and FADH<sub>2</sub> provide electrons for the components of the respiratory chain located in the inner mitochondrial membrane [84, 86]. The respiratory chain includes a series of protein complexes (I – IV) and ATP synthase, which are located in the inner mitochondrial membrane and are involved in electron transfer across the membrane and oxidative phosphorylation (Figure 3, insert) [84]. The binding of NADH to the first entry point of the respiratory chain, the complex NADH dehydrogenase, and the consequential oxidation of NADH to NAD leads to a transfer of electrons from NADH to ubiquinone [84]. The second entry point of the respiratory chain and binding point of succinate is the succinate dehydrogenase, which passes electrons from the oxidation of succinate to fumarate via FAD to ubiquinone [84]. Because of the electron transfer to ubiquinone, ubiquinone is reduced to ubiquinol in the inner mitochondrial membrane leading to a transfer of electrons to the third complex, the ubiquinone/cytochrome c oxidoreductase [87]. Complex III transfers the electrons from ubiquinol to cytochrome c, which is located in the intermembrane space of the mitochondrion [87]. The cytochrome c oxidase (complex IV) finally transfers the electrons from cytochrome c to molecular oxygen (O<sub>2</sub>) [87]. O<sub>2</sub> is continuously reduced to H<sub>2</sub>O via the respiratory chain in the mitochondrial matrix [87]. The electron flux is coupled to the proton uptake from the mitochondrial matrix into the intermembrane space generating an electro-chemical gradient driving ATP synthesis [88]. The mitochondrial ATP synthase (complex V) generates ATP by controlled reflux of protons from the intermembrane space to the mitochondrial matrix (Figure 3, insert) [89, 90].

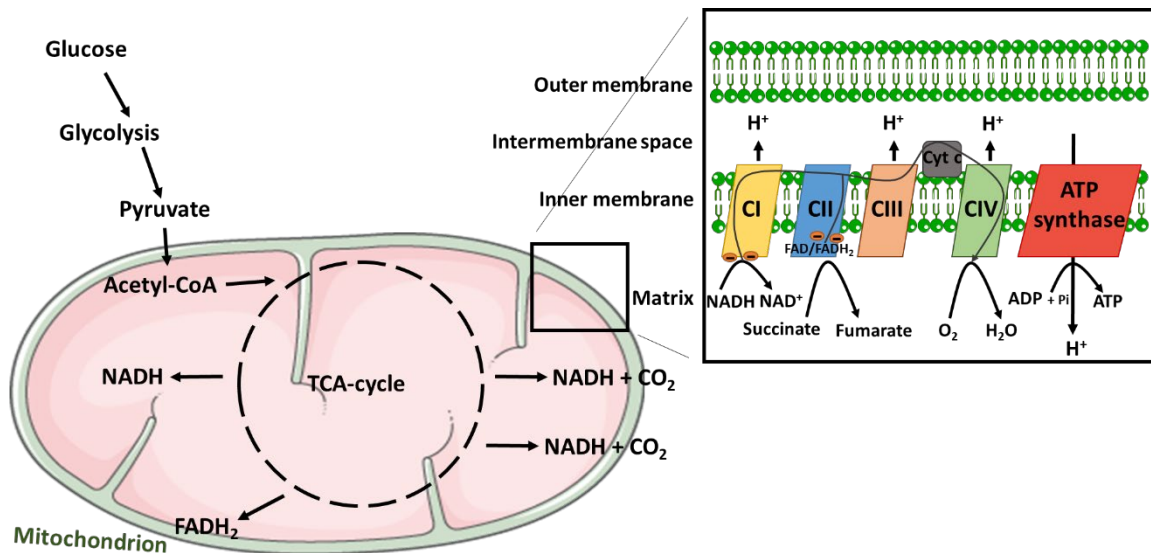


**Figure 3: Pathway of energy generation by glucose degradation from glycolysis to the tricarboxylic acid cycle and finally to the respiratory chain in mammals.** Glucose is converted to pyruvate and subsequently to acetyl coenzyme A (acetyl-CoA), which enters the TCA-cycle in the mitochondrion. In the TCA-cycle, multiple steps lead to the generation of 3 nicotinamide adenine dinucleotide (NADH), 2 CO<sub>2</sub> and flavin adenine dinucleotide (FADH<sub>2</sub>) molecules and provide electrons for the respiratory chain, where NADH binds to CI and succinate to CII in the inner mitochondrial membrane leading to an electron transport through the complexes towards the reduction of O<sub>2</sub> to H<sub>2</sub>O. During the processes, the electron flux is coupled to the proton uptake from the mitochondrial matrix into the intermembrane space leading to an electro-chemical gradient driving the ATP synthesis and producing ATP by controlling the reflux of protons from the intermembrane space to the mitochondrial matrix.

Taken together, the main cellular function of mitochondria is the maintenance of the cellular energy supply by production of ATP during oxidative phosphorylation in the respiratory chain. The TCA-cycle starts with acetyl-CoA, which can be generated from carbohydrate-derived pyruvate but also from FA degradation [86].

## 1.5 Fatty acid metabolism

The central organ for the control of FA/ lipid metabolism is the liver, which also exerts regulatory effects on energy- and glucose metabolism [91]. The hepatic FA metabolism and the storage of TG take place mainly in hepatocytes. In the gut, TG from dietary sources are emulsified by bile acids and hydrolyzed by pancreatic lipase, which leads to FA as products (lipolysis) [92]. Lipolysis takes place in the liver, but also in adipose tissue and in the circulating blood. FA in the circulating blood are mainly produced by adipose tissue lipolysis, which typically occurs during fasting [92]. In the first rate-limiting step of lipolysis in the adipose tissue, adipose triglyceride lipase (ATGL) catalyzes the hydrolysis of TG to diglycerides [92]. Hormone sensitive lipase (HSL) then catalyzes the hydrolysis of DG to monoglycerides and in the final step, monoacylglycerol lipase generates one molecule of glycerol and one molecule of FA [92]. A study in mice showed that feeding a high fat diet increases lipolysis in the adipose tissue [93]. In contrast, lipolysis in adipose tissue can be suppressed by insulin to prevent the release

of FA from TG in the fed state [94]. FA enter the circulating blood, from where they can reach different tissues to serve as substrates for the generation of energy [95]. Extracellular FA pass the hepatocyte membrane via FA receptors and enter the mitochondria [92], where they are degraded to acetyl-CoA during multiple cycles of the beta-oxidation[96]. Acetyl-CoA enters the TCA-cycle or the pathway of *de novo* lipogenesis (DNL), where acetyl-CoA is converted to FA. TG enter the lipolytic pathway within the hepatocytes or exit the hepatocytes to reach the plasma, where most of the TG are taken up by adipose tissue and skeletal muscle (Figure 4) [92]. Increased dietary glucose intake promotes DNL and the accumulation of TG in the liver [97].

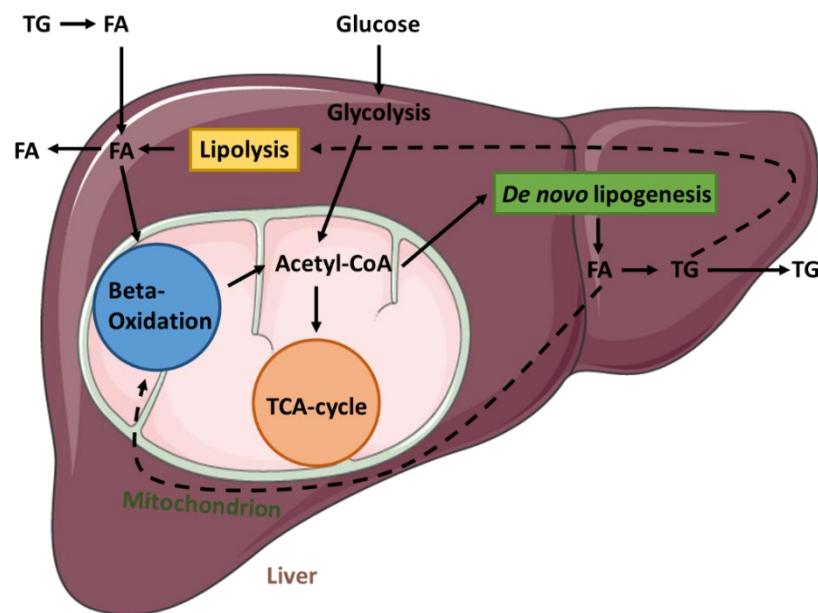


**Figure 4: Schematic representation of the fatty acid (FA) metabolism in the liver.** During lipolysis, triglycerides (TG) are converted to FA which can enter the mitochondria of hepatocytes. In the mitochondria, FA are degraded to acetyl coenzyme A (acetyl-CoA), which enters the tricarboxylic acid (TCA) cycle or the *de novo* lipogenesis (DNL). Glucose can also be converted into acetyl-CoA during glycolysis and enter the TCA-cycle or the DNL. During DNL, acetyl-CoA is used for the synthesis of FA, which are subsequently resynthesized into TG or enter beta-oxidation. TG enter the lipolytic pathway within the hepatocytes or the circulating blood and can be taken up by other tissues.

So far, research on hepatic FA metabolism focuses mainly on nonalcoholic fatty liver disease (NAFLD) and nonalcoholic steatohepatitis (NASH) and its role in the pathogenesis of IR, cardiovascular diseases and T2D [98-101]. NAFLD is the most common liver disease, with an estimated 25 % prevalence worldwide, which can lead to hepatocellular carcinoma as well as liver failure [102, 103]. It comprises fatty liver (steatosis), NASH and fibrosis/cirrhosis, diagnosed by >5 % hepatic fat accumulation in the absence of various other factors that cause fatty liver such as alcohol, drugs and viruses [103, 104]. NAFLD is tightly associated with obesity, IR, increased age and metabolic syndrome, a cluster of specific conditions that occur simultaneously including increased blood glucose, increased blood pressure, abnormal TG

concentrations and excess body fat. In less than 20 % of NAFLD patients, NAFLD can be assigned to NASH [105, 106]. NASH is defined by > 5 % hepatic steatosis with inflammation and hepatocellular injury with/ without fibrosis and is common in patients with IR or obesity [104, 105]. Interestingly, NASH was reported in children with T1D [107].

Recently it was shown that the composition of dietary fat also affects basic metabolic functions of the human liver. Excess supply of saturated FA (SFA) increases lipolysis, intrahepatic TG and induces IR, while excess supply of unsaturated FA (monounsaturated FA (MUFA) and polyunsaturated FA (PUFA)) decreases lipolysis and intrahepatic TG content [101]. These findings indicate that a diet with less fat could be beneficial to reduce intrahepatic TG and the risk of developing diabetes [101].

However, the potential impact of hepatic FA/lipid metabolism on the progression of T1D-development particularly in prediabetic persons remains largely unknown.

### 1.5.1 Free fatty acid receptors CD36 and FFAR2

In view of the above-mentioned influence of FA on glucose- and energy metabolism, it can be suggested that FFA receptors play a role in the pathogenesis of T1D. Recent studies focused on representative receptors such as cluster of differentiation 36 (CD36) and free fatty acid receptor 2 (FFAR2).

The FFA receptor CD36 is a highly glycosylated integral membrane protein with a size of 80 kD and a high affinity for long-chain fatty acids (LCFA) [108]. CD36 is widely expressed on various cell types including adipocytes, immune cells and myocytes [108]. Previous studies showed that CD36 mediates FA uptake into adipose tissue and muscle of humans and rodents [109, 110].

Besides the affinity for LCFA, CD36 can bind a variety of other ligands such as phospholipids, cholesterol as well as very low, low and high density lipoproteins (VLDL, LDL, HDL) [108]. CD36 further plays important roles in signal transduction including the activation of pathways linked to inflammation [108]. For example, in macrophages, CD36 is involved in the activation of the intracellular signaling pathway, which plays a role in foam cell formation in the pathogenesis of atherosclerosis [111]. Additionally, CD36 is involved in the activation of mitochondrial FA-oxidation by muscle cells, in the regulation of FA-induced secretion of peptides into the gut and in the regulation of calcium ion-mediated activation of phospholipases, which release arachidonic acid from phospholipids of the membrane [108]. Based on these functional properties it is suggested that CD36 plays a specific role in the control of FA metabolism, immune reactions depending on FA metabolism and consequently on the risk for the development of metabolic and immunological disorders [108]. Recent findings identifying hyperglycemia as an important stimulator of CD36-mRNA synthesis in

peripheral blood mononuclear cells from healthy individuals might link the expression of the receptor with the pathogenesis of diabetes [112]. A further study, which revealed interactions between platelet CD36 and the hyperglycemia-related prothrombotic phenotype, suggests an association of vascular complications in diabetes with CD36-mediated platelet signaling [113]. Interestingly, several population-based studies linked CD36-polymorphisms, especially polymorphisms affecting the LDL-binding domain of CD36, to increased risk of diabetes development [114-116].

Another FFA receptor, FFAR2/ G-protein-coupled receptor 43 (GPR43) is a member of the GPCR family with a size of 47 kD that binds short-chain fatty acids (SCFA) [117]. The most important agonists of FFAR2 are acetic-, propionic- and butyric acid, which are released from intestinal bacteria like Bacteroidetes and Firmicutes [118]. FFAR2 is expressed on various cell types including pancreatic alpha- and beta cells [117]. A recent study points to a role of FFAR2 in the regulation of islet mass and beta cell survival [117]. It was shown that mice lacking FFAR2 have decreased beta cell mass suggesting that FFAR2 could be a potential therapeutic target to stimulate the proliferation of beta cells in order to preserve the beta cell mass [117]. Another study in mice showed, that SCFA simulate the secretion of the gut hormone glucagon-like peptide-1 (GLP-1) via FFAR2. There is evidence that increased GLP-1 secretion has beneficial effects in patients with obesity and diabetes [119], thereby linking FFAR2 and SCFA to diabetes. Further evidence strengthens the assumption that FFAR2 is involved in the development of autoimmunity and autoimmune diseases such as T1D. A study in mice showed, that SCFA regulate the function and size of the colonic Treg pool and protect against colitis in a FFAR2-dependent manner [120]. Another study in mice lacking FFAR2 showed an increased inflammation in models of asthma, inflammatory arthritis and colitis and suggested a molecular link between SCFA-binding to FFAR2 and intestinal bacteria, diet and immune responses [121].

Taken together, FFAR2 activation seems to contribute to the association between gut microbiota and immune responses and may have an impact on the development of T1D.

### **1.6 Gut microbiota**

The majority of micro-organisms in the mammalian body is localized in the gut and called gut microbiota which includes not only bacteria but also other microbes like fungi and even viruses [122, 123]. A recent study shows that the human gut microbiome is composed of more than 35.000 bacterial species [123]. The four major microbial phyla that represent more than 90 % of the bacterial communities of the gut microbiota are Firmicutes, Bacteroides, Proteobacteria and Actinobacteria [122]. To study the gut microbiota, mainly stool samples are collected and DNA is isolated [123]. Current methods to study gut microbiome composition are 16S rRNA-

based sequencing of bacterial genes followed by bioinformatics analyses in combination with metabolomics [123]. Bacteria metabolize dietary components to produce a variety of compounds affecting the metabolism of the host. An important group of bacterial products are SCFA, which are produced in the gut by colonic microbiota through anaerobic fermentation of undigested carbohydrates, proteins, dietary fiber and starch, which cannot be degraded by digestive enzymes in the small intestine [124]. Acetic (C2)-, propionic (C3)- and butyric (C4) acid are the dominant SCFA and are present in a molar ratio of about 60:20:20 in the colon and faeces [125]. Acetic- and propionic acid are mainly produced by Bacteroidetes, whereas butyric acid is mainly produced by Firmicutes [126]. SCFA are absorbed from the gut lumen into the circulation and control various metabolic functions. Acetic acid is mainly used as a substrate for hepatic lipogenesis, propionic acid as a substrate for hepatic gluconeogenesis and butyric acid serves as the major energy substrate of colonocytes and as a stimulator of the proliferation of colonocytes [127].

Alterations of the gut microbiota composition may lead to the development of various gut-microbiota-related diseases like liver diseases, diabetes mellitus and the metabolic syndrome [106, 128-130]. A recent population-based study revealed altered gut microbiome composition in children with overt T1D at the age of 3-48 months [131]. Another study with T1D-predisposed children described an alteration in the composition of the gut microbiome with about 25 % reduction in alpha-diversity [132]. Evidence from clinical studies supports the assumption that T1D in humans is associated with increased intestinal permeability [133-135]. Investigations on the mechanisms involved in the interaction of the gut microbiome with its host organism revealed that intestinal bacteria and their products are recognized by TLR [136]. TLRs can recognize gut microbes and their products and thereby contribute to control the homeostasis of intestinal immunity [136]. During obesity or high fat intake, alterations of the gut wall integrity lead to increased concentrations of gut microbiota-derived products in the circulation. This in turn leads to the activation of TLRs on immune cells and a subsequent stimulation of inflammatory processes [136]. It is suggested that the interaction of TLRs with gut microbiota in obese individuals does not only affect immune reactivity but also metabolic processes [136].

### 1.7 Toll-like receptor family

TLRs are a family of conserved transmembrane proteins, which are expressed in many phyla [30]. The TLRs are named after the toll-protein of the *toll*-gene, discovered by Christiane Nüsslein-Volhard in *Drosophila melanogaster*. The *toll*-gene encodes a plasma membrane receptor that is involved in the control of the embryonic development of the fly [137, 138]. In mammalian animals, TLRs serve as pattern recognition receptors that can recognize pathogens based on pathogen-associated molecular patterns (PAMPs) [139, 140]. So far, 13

TLRs were described in mammalian animals and 11 in humans, which all recognize different PAMPs [141, 142]. TLRs play important roles in immune responses of the adaptive and innate immune system during the defense against pathogens [143], pointing to TLRs as important links between the adaptive and innate immune response [144]. Each TLR has selected groups of ligands comprising large arrays of bacterial, viral and also fungal structures, for example, bacteria-derived LPS which binds to TLR4 or lipoproteins which preferentially bind to TLR2 [30]. Besides the interaction of TLRs with exogenous ligands, interactions of the receptors with endogenous ligands such as mammalian stress proteins and DNA fragments were described [145-148]. Particularly, the binding of endogenous ligands qualify TLRs not only for central roles in host defense against pathogens but also in the development of autoimmune disorders like T1D [30].

### 1.7.1 Toll-like receptor 4

The toll-like receptor 4 (TLR4), an important member of the TLR family, was originally described as the receptor for bacterial LPS (a component of the cell wall of gram-negative bacteria) on innate immune cells, like dendritic cells and macrophages [139, 149]. TLR4 is important for the induction of the immune response against bacterial infections but can also mediate protective effects under conditions of inflammatory tissue damage, for example by the involvement in repair- and remodeling-processes after injuries of the lung or gut [150, 151]. The recognition of LPS by TLR4 by innate immune cells triggers a cascade of proinflammatory activation via myeloid differentiation primary response 88 (MyD88)-dependent and TRIF-dependent pathways [143, 144, 152]. Besides binding bacterial antigens like LPS, TLR4 also binds endogenous ligands such as heat shock protein 60 (HSP60), which is associated with the pathogenesis of T1D [146, 153, 154]. Further studies showed that TLR4 is also expressed on T<sub>reg</sub> [155], which are suggested to be associated with the development of T1D [156]. These studies strongly indicate that TLR4 is involved in the control of the autoimmune pathogenesis of T1D [30, 157]. Furthermore, TLR4 is also present on insulin target tissues like liver, skeletal muscle and adipose tissue, which supports its relevance for diabetes-associated metabolic disorders such as IR and obesity [158, 159]. In a mouse model of T1D it could be shown that elevated TLR4 expression correlated with increased systemic concentrations of plasma glucose and FFA, which might lead to increased IR as a consequence of obesity [1].

## 1.8 Animal models of type 1 diabetes

The ultimate goal of investigating and understanding the pathogenesis of T1D is the increase of knowledge of the disease processes in order to improve the strategies for the prevention and cure of the human disease. However, only limited studies can be performed in humans or

human tissues. Besides ethical issues and legal restrictions, other problems such as the long generation time of humans must be considered. To study the mechanisms of the pathogenesis of T1D, animal models are used. In animal models of the disease, lack of insulin production and the consequent development of insulin-deficient diabetes can be investigated after targeted chemical destruction of beta cells or by the use of models with spontaneous development of beta cell-directed immune reactivity [160, 161].

The chemically induced insulin-deficient diabetes is mainly induced by application of the beta cell toxin streptozotocin (STZ) [162]. STZ is synthesized by the bacterium *Streptomyces achromogenes* and after the injection in animals, it enters the pancreatic beta cell via the GLUT-2 transporter [162]. In the beta cell, STZ causes DNA alkylation [163] which leads to a reduction of cellular ATP followed by a decline of insulin production [162, 164]. Additionally, STZ contributes to cell death by its ability to release free radicals [162]. A disadvantage of the animal model of STZ-induced insulin-deficient diabetes is the toxic side effect of STZ, that might affect also functions of other organs of the animals [162].

An example for the spontaneous development of beta cell-directed immune reactivity leading to insulin-deficient diabetes in an animal model is the Biobreeding (BB) rat [162, 165]. About 90 % of BB rats develop diabetes typically between 8 and 16 weeks of age [162]. The development of diabetes in the BB rat model is similar to human T1D. Rats require insulin supplementation for survival and develop insulinitis with the sequential infiltration of islets by immune cell populations including macrophages, T-lymphocytes, B-lymphocytes and NK cells [162, 166]. BB rats also develop lymphopenia, which is not characteristic for T1D in humans and is regarded as a disadvantage in using the BB rat as a model for human T1D [162].

### 1.8.1 Non-obese diabetic mouse

One of the most widely used animal models for T1D is the NOD mouse. The NOD mouse was first described in a breeding colony of the Cataract Shionogi strain in the 1980s in Japan and meanwhile there are several colonies worldwide [28, 167]. The NOD mouse spontaneously develops insulin deficient diabetes that is similar to human T1D [28]. The pathogenesis of diabetes in NOD mice starts as early as 3 weeks of age, long before the clinical manifestation of diabetes, when the pancreatic islets are infiltrated by innate immune cells including macrophages, NK cells, T- and B-lymphocytes [28, 167, 168]. The advancing insulinitis leads to a progressive destruction of insulin producing beta cells [37]. Although NOD mice have an increased genetic susceptibility to develop insulin-deficient diabetes, not all mice in a colony will develop the disease [37]. The NOD mouse model shows comparable features to human T1D, but also some differences. Diabetes manifestation in NOD mice is characterized by hyperglycemia, polyuria, elevated glucose concentration in the urine (glycosuria), hypoinsulinemia and weight loss [28]. Furthermore, diabetes-predisposing variations in MHC

of the NOD mouse have high similarities with human MHC, indicative of similar disease-promoting factors in NOD mice and humans [169]. In contrast to the human disease, in which the sex has only a small impact on the risk of developing T1D, in the NOD mouse model approximately 60-80 % of female mice, but only about 10 % of male animals develop insulin-deficient diabetes [28]. First cases of diabetes manifestation are typically observed at an age of 10 weeks. While in humans, it is difficult to study the impact of environmental factors on the development of T1D, the NOD mouse model offers the possibility to control the environmental factors (for example diet), to identify their potential impact on the development of insulin-deficient diabetes [28]. Various studies in NOD mice identified distinct environmental and dietary factors that alter/decrease diabetes susceptibility, like feeding conditions [170, 171], change in gut microbiota composition [172-174] or infectious organisms [175-177]. In addition, factors like environmental temperature and epidermal vitamin D synthesis were found to play a role in the development of insulin-deficient diabetes in NOD mice [37]. Feeding of high fat diet to NOD mice was found to increase the incidence of insulin-deficient diabetes [178]. An increased incidence of insulin-deficient diabetes was also shown in NOD mice fed with wheat-enriched diets, which result in increased intestinal levels of interferon gamma (IFN $\gamma$ ) and tumor necrosis factor alpha (TNF $\alpha$ ) [179, 180]. Interestingly, mice fed with a diet low in omega-6/omega-3 FA showed a decrease in the incidence of insulin-deficient diabetes [181]. NOD mice housed under defined specific pathogen-free conditions have a higher incidence of insulin-deficient diabetes compared to NOD mice kept under non-germ-free conditions [182]. Moreover, NOD mice fed with probiotics exhibit increased interleukin-10 (IL-10) production and a lower incidence of insulin-deficient diabetes [182]. Members of the *Bacteroidetes phyla*, which are SCFA producers, are suspected to be responsible for the protection against insulin-deficient diabetes. This protection is mediated by binding of SCFA to receptors of the GPR family on immune cells leading to an anti-inflammatory response that protects from diabetes [183]. NOD mice fed with a gluten-containing diet have a higher incidence of insulin-deficient diabetes compared to mice fed a gluten-free diet. Mice fed a gluten-free diet had lower numbers of aerobic, micro-aerophilic and caecal bacteria in the gut than mice fed with a gluten-containing diet [184], suggesting a link between gluten-free diet, intestinal bacteria and insulin-deficient diabetes.

Besides experimental modifications of environmental and nutritional factors, genetic manipulations can be performed in the NOD mouse model to examine the effects of specific genes on the development of insulin-deficient diabetes [28]. NOD mice lacking nucleotide oligomerization domain -like receptors (NLRs), intracellular proteins detecting microbial products leading to activation of proinflammatory pathways, were generated to study their role in the development of autoimmune diabetes [28]. Another genetically manipulated NOD mouse

model associated with diabetes is the NOD mouse lacking TLR9. TLR9-deficient NOD mice are protected against the development of autoimmune diabetes [28]. Meanwhile, also other members of the TLR family, like TLR2 and TLR4, were genetically deleted to examine the effects of their absence on the development of insulin-deficient diabetes.

### 1.8.2 The TLR4-deficient non-obese diabetic mouse

The TLR4-deficient (TLR4<sup>-/-</sup>) NOD mouse, with a homozygous TLR4 defect, is a model for accelerated development of T1D [30]. The mice show a younger age at diabetes onset compared to NOD TLR4<sup>+/+</sup> mice [1]. In addition, these mice reveal increased immune cell infiltration (insulinitis) in the pancreatic islets during the prediabetic phase at the age of 120 days, but unchanged susceptibility of pancreatic islet cells to beta cell damaging inflammatory mediators [30]. Additionally, NOD TLR4<sup>-/-</sup> mice show decreased reactivity and proinflammatory activity of antigen-presenting cells like macrophages and dendritic cells [30]. Whereas, TLR4 deficiency shows no impact on the frequency of T<sub>reg</sub> cells, it decreases their capacity to prevent T cell proliferation [30]. T<sub>reg</sub> cells are important for the balance between stimulation of immune defense reactions and activation of mechanisms, which can prevent an overreaction of the immune system that might promote autoimmune reactivity. Thus, T<sub>reg</sub> cells are assigned a central role in the control of autoimmune reactions [30]. In the prediabetic phase, at an age of 70-90 days, NOD TLR4<sup>-/-</sup> mice show increased body weight and higher fat mass as well as higher random blood glucose concentrations. Besides diabetes-promoting immunologic alterations, NOD TLR4<sup>-/-</sup> mice also show metabolic disorders that may affect diabetes development. Compared to NOD TLR4<sup>+/+</sup> mice, NOD TLR4<sup>-/-</sup> mice show increased plasma levels of LPS, TG and FFA but similar levels of fetuin A [1], an endogenous ligand serving as mediator between TLR4 and FFA [185]. In addition to metabolic disorders, the NOD TLR4<sup>-/-</sup> mouse exhibits altered gut microbiome composition and morphology. The microbial biomass in the small intestine, cecum and colon is comparable in NOD TLR4<sup>+/+</sup> and NOD TLR4<sup>-/-</sup> mice [1]. However, NOD TLR4<sup>-/-</sup> mice display a decreased amount of Firmicutes and an increased amount of Bacteroidetes in cecum and colon [1]. NOD TLR4<sup>-/-</sup> mice show decreased longitudinal and circular muscle layers of the small intestine, which results in a decrease in total muscle thickness of these gut segments [1].

The TLR4-expression status also affects the energy and glucose homeostasis in NOD mice. NOD TLR4<sup>-/-</sup> mice show higher physical activity during the dark phase compared to NOD TLR4<sup>+/+</sup> mice [1]. Moreover, NOD TLR4<sup>-/-</sup> mice display a decreased respiratory quotient (RQ) in the light and dark phases, whereas the energy expenditure was comparable in the two phases in NOD TLR4<sup>-/-</sup> and NOD TLR4<sup>+/+</sup> mice [1]. Additionally, NOD TLR4<sup>-/-</sup> mice show an increased glucose concentration during an intraperitoneal glucose tolerance test (ipGTT) and an intraperitoneal insulin tolerance test (ipITT) pointing to disturbed glucose tolerance and

decreased whole-body insulin sensitivity [1]. Impaired glucose homeostasis of these mice is also reflected by their higher HOMA-IR values [1]. Moreover, dose-dependent glucose-stimulated insulin release from isolated pancreatic islets of NOD TLR4<sup>+/+</sup> and NOD TLR4<sup>-/-</sup> mice was comparable indicating that the TLR4-expression status does not affect the insulin secretory capacity of beta cells [1]. NOD TLR4<sup>-/-</sup> mice also show higher hepatic oxidative capacity but unchanged muscle oxidative capacity when compared to NOD TLR4<sup>+/+</sup> mice [1]. Taken together, these studies show that the TLR4-expression status has not only an effect on immunological factors and the gut microbiome composition, but also on the energy and glucose metabolism in NOD mice.

Despite extensive research efforts as outlined above, it still remains unclear which factors regulate the accelerated development of insulin-deficient diabetes in the NOD TLR4<sup>-/-</sup> mouse model.

### **1.9 Interplay between energy homeostasis, gut microbiome composition and pathogenesis of T1D**

The balance between energy storage and energy release is of central importance for health and survival of mammals [186]. Between 1975 and 2016, obesity has nearly tripled worldwide. In 2016, worldwide more than 1.9 billion adults were overweight (39 %), 650 million of these were obese (13 %) [187]. In recent years, obesity is diagnosed at a younger age group and the numbers are reaching alarming levels. In 2019, 38.2 million children under the age of five were diagnosed as overweight or obese [187]. Worldwide, more than 340 million children and adolescents were overweight or obese in 2016 [187]. The prevalence of obesity in infants, children and adolescents is rising worldwide. A major cause for rising obesity is a long-term positive energy balance as a consequence of reduced physical activity and overnutrition [187]. Patients suffering from obesity have an increased risk of developing chronic metabolic diseases such as diabetes [187, 188]. Obesity is preventable or can be reduced by pursuing a healthier lifestyle including balanced nutrition and adequate physical activity [187]. Recent studies described a link between higher body weight and accelerated T1D manifestation [43-45]. Taken together, a balanced energy homeostasis is vital to protect against overweight and obesity and consequently against the risk of developing multiple diseases such as T1D. This can be achieved by increased physical activity and most importantly healthy diet.

Specific diets including higher proportions of starch and fiber largely resistant to digestion, provide a wide range of beneficial health issues such as improving the control of blood glucose concentrations and decreasing cholesterol levels [188]. These diets also can have an impact on metabolism after degradation by bacteria in the gut. Intestinal bacteria degrade dietary components to produce various compounds, such as SCFA, that are able to modulate the metabolism of the host organism. Administration of diets with high proportions of digestion-

resistant starch or dietary fiber is associated with increased SCFA production in the gut and increased circulating SCFA in the periphery [127, 189]. Lately, various studies suggest an impact of SCFA on energy metabolism and subsequently on obesity. A study in mice suggests that obesity affects the composition of the major gut bacterial phyla. Compared to lean mice, obese (*ob/ob*) mice, unable to produce leptin, showed a 50 % reduction in the abundance of Bacteroidetes but an increase in Firmicutes [190]. Additionally, obese humans were found to have higher SCFA levels in faeces compared to lean individuals [191-193]. A recent study further suggests a link between gut microbiota and whole-body insulin sensitivity by showing that plasma SCFA are negatively associated with lipolysis and long-chain FFA levels in humans. In addition, circulating concentrations of acetate and propionate were, respectively, negatively and positively associated with insulin sensitivity [194].

Besides studies on the effect of SCFA on human energy metabolism, various studies with largely inconclusive outcomes suggest an effect of SCFA on pancreatic beta cells. In 1977, it was reported that acetate infusion in rats increased glucose-stimulated insulin secretion suggesting a positive regulatory effect of SCFA on insulin release [195]. Two other studies using isolated pancreatic rat islets exposed to acetate reported opposite results [196, 197]. A recent study showed that the loss of FFAR2 leads to impaired beta cell survival and islet mass in mice. This suggests that FFAR2 may regulate beta cell proliferation and growth, thereby connecting circulating SCFA, which activate FFAR2, with the regulation of beta cell functions and mass [117].

SCFA also play a beneficial role in liver metabolism. Acetate can serve as precursor for the synthesis of cholesterol and LCFA [126] whereas propionate serves as a substrate for gluconeogenesis [126, 198]. Increased levels of SCFA induce a switch from lipogenesis to beta-oxidation in the liver leading to an increase of energy expenditure and thereby protecting against the effect of a HFD in mice [199]. A study in rats shows, that feeding an acetate-enriched diet exhibits an increase in glycogen and citrate, but lower xylulose-5-phosphate levels in the liver, suggesting that acetate activated gluconeogenesis and inhibited glycolysis [200]. SCFA were further found to regulate the glucose metabolism by decreasing the plasma glucose concentration [126]. Studies in mice and rats showed that an oral administration of acetate and propionate leads to a decrease of blood glucose levels [201, 202]. These findings lead to the assumption that SCFA affect the plasma glucose concentration by increasing specific gut hormone levels like peptide YY and GLP-1 levels via activation of FFA receptors such as FFAR2 [126]. These gut hormones have been shown to increase the glucose uptake into the adipose tissue and skeletal muscle but also to increase insulin secretion and decrease glucagon secretion in the pancreatic islets [126]. In summary, SCFA may have a positive effect on the glucose homeostasis. SCFA not only affect the glucose metabolism but also the FA

metabolism by modulating FA synthesis, lipolysis and FA oxidation [126]. FA oxidation is activated by SCFA, whereas FA synthesis and lipolysis are inhibited by SCFA in multiple tissues leading to a decrease of FFA concentrations in the plasma and a reduction of body weight [126].

Recent findings suggest an association of the intestinal microbiome composition with the onset and progression of T1D. Studies in humans show that T1D patients have a less diverse and stable gut microbiome compared to glucose-tolerant humans [203, 204]. Furthermore, young children at the age of 0-4 years genetically predisposed to T1D, children at the age of 5-16 years with recent onset T1D or children who progress to T1D show specific alterations in gut bacterial composition associated with higher intestinal permeability (Figure 5) [132, 205]. Studies in mice show, that gut microbial metabolites particularly acetate and butyrate protect against T1D by decreasing the frequency of autoimmune T cells, enhancing gut integrity and decreasing serum levels of cytokines associated with the pathogenesis of T1D [206]. Interestingly, a recent study in mice suggested that microbiota provide signals to promote or inhibit autoimmunity via TLR [207].

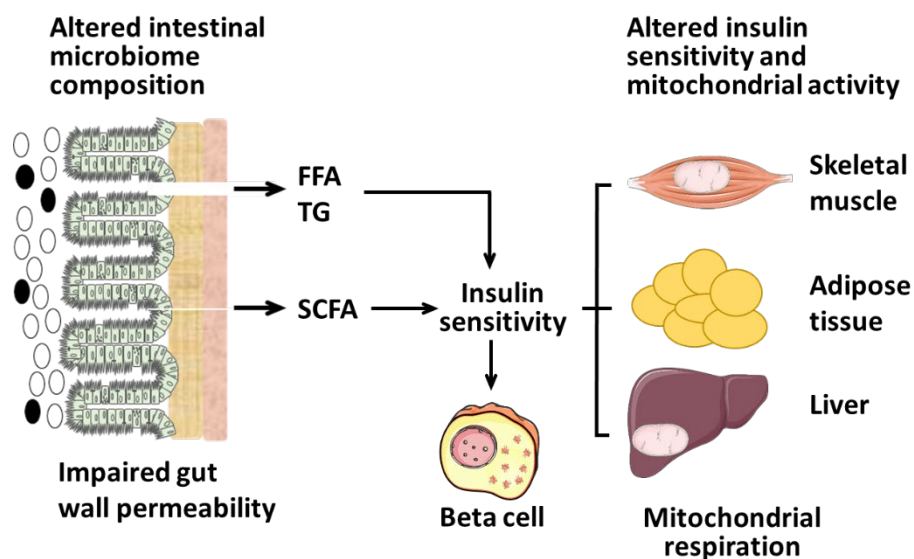


**Figure 5: Schematic representation of the interplay between the gut microbiome and energy homeostasis in T1D.** Patients with T1D show altered intestinal microbiome composition and impaired gut wall permeability. Free fatty acids (FFA), triglycerides (TG) and short-chain fatty acids (SCFA) are released from the gut into the circulating blood where they can modulate insulin sensitivity. As insulin-sensitive organs, skeletal muscle, adipose tissue and liver are involved in the control of whole-body insulin sensitivity, which in turn has an effect on beta cell function. Additionally, skeletal muscle, adipose tissue and liver can affect energy homeostasis via mitochondrial respiration. Modified after [1].

Taken together, currently available findings indicate that disorders of glucose- and lipid metabolism in the prediabetic phase accelerate the progression of the pathogenesis of T1D. However, the mechanism(s) underlying the T1D-promoting metabolic processes are largely unknown

### 1.10 Aims of this study

The manifestation of T1D is frequently preceded by metabolic disorders, which might contribute to accelerated disease development as observed in epidemiologic studies. However, the metabolic factors controlling diabetes progression in the prediabetic phase are not well understood. Therefore it is hypothesized, that multiple metabolic changes precede the development of T1D and have an impact on the progression of T1D.

To characterize the possible mechanisms underlying the diabetes development, the experiments were performed with female, prediabetic NOD TLR4<sup>-/-</sup> mice, a mouse model for accelerated development of spontaneous insulin-deficient diabetes/T1D. Therefore, it is hypothesized, that accelerated diabetes development in NOD TLR4<sup>-/-</sup> mice is associated with an impaired glucose, lipid and energy metabolism before the age of diabetes manifestation. The study focuses on the metabolism of glucose and lipids as the dominant substrates of energy metabolism before diabetes manifestation.

The development of T1D in humans is affected by metabolic changes in the prediabetic phase. Metabolic changes can be provoked by an unfavorable lifestyle in early life like obesity from hypercaloric diet and physical inactivity. Therefore, it is hypothesized, that feeding prediabetic NOD TLR4<sup>-/-</sup> mice a HFD further aggravates diabetes-promoting metabolic disorders. The study investigates metabolic changes associated with HFD-feeding before diabetes manifestation.

The expected results will contribute to improve our knowledge of metabolic processes that contribute to the accelerated development of T1D, which was recently observed in younger children. The findings will help to develop strategies to prevent or delay the progression of T1D by targeting diabetes-promoting metabolic disturbances in the prediabetic phase.

## 2 Material and methods

### 2.1 Material

#### 2.1.1 Mouse models

The NOD mouse, a mouse model for human T1D, were from the breeding colony of the German Diabetes Center [30]. NOD TLR4<sup>-/-</sup> mice were generated at the German Diabetes Center by mating NOD mice with C57BL/10ScCr (TLR4<sup>-/-</sup>) mice, kindly provided by M.A. Freudenberg (Max-Planck-Institute of Immunobiology and Epigenetics, Freiburg, Germany). The C57BL/10ScCr mouse is deficient for TLR4, due to a spontaneous deletion of the TLR4-encoding region on chromosome 4, and was used to backcross the TLR4 defect onto the NOD mouse background [30]. To transfer the TLR4 defect allele onto the NOD background, male C57BL/10ScCr mice with TLR4-deficiency were mated with female NOD mice and the TLR4 heterozygous male offspring were then backcrossed for more than 12 generations with female NOD mice to preserve NOD specific mitochondrial DNA. Heterozygous littermates from backcross generations 12-15 were intercrossed to generate NOD mice with homozygous and heterozygous TLR4-expression and with homozygous TLR4-deficiency at proportions that followed a Mendelian distribution of 1:2:1. For all experiments, only female NOD TLR4<sup>+/+</sup> and NOD TLR4<sup>-/-</sup> mice at an age between 70-90 days were used. This age range correlates with the prediabetic phase of these mice, before the manifestation of insulin deficient diabetes [30]. Follow-up of the mice until the age of 220 days revealed approximately 71 % of female NOD TLR4<sup>+/+</sup> mice develop diabetes and approximately 80 % of female NOD TLR4<sup>-/-</sup> mice develop diabetes until the age of 220 days [30].

The mice were kept under standard housing conditions (12 hours light/ 12 hours dark) in the animal facility of the German Diabetes Center and received either a standard diet (SD) (Ssniff® M-Zucht 4.5 % fat; 12 % kcal% fat; Ssniff Spezialdiäten GmbH, V1124-000, Soest) as well as water *ad libitum* or a high fat diet (HFD) from 30 to 70 days of age (Research Diets 34.9 % fat; 60 % kcal% fat, Research Diets Inc., D12492, New Brunswick, NJ USA) and water *ad libitum* (Table 1).

Table 1: Fat composition of the SD and HFD per 100 g fat and per 100 g meal. Additionally, the ratio of HFD to SD per 100 g fat and per 100 g meal was calculated.

	SD		HFD		Ratio HFD/SD	
	Per 100 g fat (%)	Per 100 g meal (%)	Per 100 g fat (%)	Per 100 g meal (%)	Per 100 g fat	Per 100 g meal
<b>SFA</b>	16.0	0.7	32.0	11.2	2.0	15.5
<b>MUFA</b>	23.3	1.1	35.9	12.5	1.5	11.4
<b>PUFA</b>	59.8	2.7	32.0	11.2	0.5	4.1

### 2.1.2 Chemicals

#### 2.1.2.1 Chemicals for genotyping

- Biozym LE Agarose Biozym, Oldendorf, Germany
- DEPC-Treated water Ambion Life Technologies Corp., Austin, Tx, USA
- Desoxyribonukleosidtriphosphate (dNTPs) Gibco BRL, Eggenstein, Germany
- Magnesium chloride (MgCl<sub>2</sub>) (50 mM) Invitrogen, Carlsbad, CA, USA
- PCR Direct Ear PeQLab Biotech GmbH, Erlangen, Germany
- PCR Reaction Buffer (10x) Invitrogen, Carlsbad, CA, USA
- Peq Gold 100 bp DNA ladder VWR Life Science, Leuven, Belgium
- Proteinase K PeQLab Biotech GmbH, Erlangen, Germany
- Red Safe Nucleic Acid Staining Solution iNtRON Biotechnology, Korea
- Taq DNA Polymerase Invitrogen, Carlsbad, CA, USA

#### 2.1.2.2 Chemicals for physiological investigations

- Glucose (40 %) SERAG Wiessner, Naila/ Bayern, Germany
- Insuman Rapid 40 I.E./ml (Insulin human) Sanofi-Aventis, Frankfurt am Main, Germany
- Mouse insulin ELISA kit Mercodia, Uppsala, Sweden
- Sodium chloride (NaCl) (0.9 %) Fresenius Kabi Germany GmbH, Bad Homburg, Germany

#### 2.1.2.3 Chemicals for histological analysis of organs

- 2-Methylbutane, ≥ 99 % Roth, Karlsruhe, Germany
- 2-Propanol, ≥ 99.95 % Roth, Karlsruhe, Germany
- Acetone VWR, Radnor, PA, USA
- Bovine Serum Albumin (BSA) SERVA, Heidelberg, Germany
- DAKI Polyclonal Guinea Pig Anti-Insulin (primary antibody) DAKO, Carpinteria, CA, USA
- Entellan Merck, Darmstadt, Germany
- Ethanol Merck, Darmstadt, Germany
- Hematoxylin Roth, Karlsruhe, Germany
- Hydrogen peroxide (H<sub>2</sub>O<sub>2</sub>) (30 %) Roth, Karlsruhe, Germany
- Kaiser's glycerol gelatin Merck, Darmstadt, Germany
- Liquid DAB+Substrate Chromogen System Agilent, Santa Clara, CA, USA
- Methanol (≥ 99.9%) Roth, Karlsruhe, Germany
- Oil Red O Solution Sigma-Aldrich, Steinheim, Germany
- Paraformaldehyde (PFA) Merck, Darmstadt, Germany
- PBS Rotifair 10x pH 7.4 Roth, Karlsruhe, Germany

## Material and methods

- Saponin Sigma-Aldrich, Steinheim, Germany
- Sucrose Sigma Life Science, St. Louis, MO, USA
- VECTASTAIN ABC Kit Vector Laboratories, Burlingame, CA, USA
- VECTASTAIN Anti-Guinea Pig IgG Biotinylated Antibody (secondary antibody) (ABC Kit) Vector Laboratories, Burlingame, CA, USA
- VECTASTAIN Normal Goat serum (ABC Kit) Vector Laboratories, Burlingame, CA, USA
- Xylol (Isomere) (> 98 %) Roth, Karlsruhe, Germany

### 2.1.2.4 Reagents for islet isolation

- Albumine bovine Fraction V pH 7.0 (BSA) SERVA Feinbiochemica GmbH & Co., Heidelberg, Germany
- Calcium chloride (CaCl<sub>2</sub>) AppliChem, Darmstadt, Germany
- D(+)-Glucose monohydrate Merck Darmstadt, Germany
- DMEM (1x) Gibco life technologies, Paisley, UK
- Fetal calf serum (FCS) PAA Laboratories GmbH, Pasching, Germany
- Harks' Balanced Salts (HBSS) Gibco life technologies, Paisley, UK
- HEPES AppliChem, Darmstadt, Germany
- Liberase TL Research Grade Roche Diagnostics GmbH, Mannheim, Germany
- Magnesium sulfate (MgSO<sub>4</sub>) AppliChem, Darmstadt, Germany
- Monopotassium phosphate (KH<sub>2</sub>PO<sub>4</sub>) AppliChem, Darmstadt, Germany
- Potassium chloride (KCl) AppliChem, Darmstadt, Germany
- Sodium chloride (NaCl) AppliChem, Darmstadt, Germany

### 2.1.2.5 Reagents for western blot-analysis

- 2-Mercaptoethanol Sigma-Aldrich, St. Louis, MO, USA
- 4x Laemmli Buffer Bio-Rad, Hercules, CA, USA
- Acrylamide 4K-Solution AppliChem, Darmstadt, Germany
- Ammonium persulfate (APS) Sigma-Aldrich, St. Louis, MO, USA
- Bovine Serum Albumin (BSA) SERVA, Heidelberg/New York, Germany/USA
- Clarity Western ECL Substrate Bio-Rad, Hercules, CA, USA
- Methanol (≥ 99.9 %) Roth, Karlsruhe, Germany
- Milk powder AppliChem, Darmstadt, Germany
- PageRuler Prestained Protein Ladder Thermo Fisher Scientific, Waltham, MA, USA
- Ponceau S-solution AppliChem, Darmstadt, Germany

## Material and methods

- Rotifair TBS 7.6 Roth, Karlsruhe, Germany
- Rotifair TG-Western Roth, Karlsruhe, Germany
- Rotiphorese 10x SDS-PAGE Roth, Karlsruhe, Germany
- SDS solution (10 %) AppliChem, Darmstadt, Germany
- Trans-Blot Transfer Medium Pure Nitrocellulose Membrane (0.45 µm) Bio-Rad, Hercules, CA, USA
- Tetramethylethylenediamine (TEMED) SERVA, Heidelberg/New York, Germany/USA
- TRIS Hydrochloride (Tris-HCl) Roth, Karlsruhe, Germany
- Tween 20 ICN Biomedicals, Irvine, CA, USA

### 2.1.2.6 Chemicals for magnetic resonance imaging/ spectroscopy

- Glucose G20 (20 %) Fresenius Kabi, Bad Homburg, Germany
- Glucose (40 %) SERAG Wiessner GmbH, Naila/Bayern, Germany
- Isoflurane-Piramal Piramal Critical Care, Hallbergmoos, Germany
- Methylendiphosphonic acid (MDPA) (1 M) Sigma-Aldrich, St. Louis, MO, USA
- Sodium chloride (NaCl) (0.9 g) Fresenius Kabi, Bad Homburg, Germany

### 2.1.3 Devices

- Anesthetic gas evaporator / isoflurane NorVap, Skipton UK
- Autoclave Webeco, Selmsdorf, Germany
- Binocular (Wilovert) Wilhelm Will KG, Wetzlar-Nauborn, Germany
- BioDocAnalyze biometra CORE Life Sciences, Laguna Niguel, CA, USA
- Centrifuge (Biofuge Fresco) Heraeus, Hanau, Germany
- Centrifuge S810R Eppendorf, Hamburg, Germany
- ChemiDoc Imaging System Bio-Rad, Hercules, CA, USA
- Cobas C311 analyzer Roche, Diagnostics GmbH, Mannheim, Germany
- Double-tuned <sup>31</sup>P/<sup>1</sup>H birdcage volume resonator (40 mm inner diameter) Bruker, Karlsruhe, Germany
- DP73 (Camera of the microscope DMRBE) Olympus, Tokio, Japan
- EchoMRI™-100 System EchoMRI, Houston, TX, USA
- ELISA-washer Nunc-ImmunoWash12 Thermo Fisher Scientific, Waltham, MA, USA
- Flake-Ice Machine (AF 100) Scotsman, Mailand, Italy
- Filtration hood LaminAir TL2472 Heraeus, Hanau, Germany
- Filtration hood LaminAir HB2472 Heraeus, Hanau, Germany
- Gel chamber AGS GmbH, Heidelberg, Germany

## Material and methods

- Heat block with magnetic mixer RCT basic, IKA, Staufen, Germany
- Heat block (Thermomixer 5436) Eppendorf, Hamburg, Germany
- Horizontal Bruker Biospin 117/16 USR Paravision 6.0.1, Bruker Corporation, Billerica, USA
- Immersion circulator SC100 Thermo Scientific, Braunschweig, Germany
- Incubator Cytoperm 2 Heraeus instruments Thermo Scientific, Braunschweig, Germany
- Intuos Pro Paper Edition L (Pen tablet) Wacom, Kazo, Japan
- Jung Frigocut 2800E (Cryostat) Leica, Nussloch, Germany
- Magnetic heating plate (IKAMAG RET) IKA, Staufen, Germany
- Magnetic heating plate (RCT basic) IKA, Staufen, Germany
- Microscope (Axiovert 25) Carl Zeiss, Oberkochen, Germany
- Microscope (Leica DMRBE) Leica, Nussloch, Germany
- Milli-Q System (IQ 7000) Merck, Darmstadt, Germany
- Mini-PROTEAN Tetra Cell Bio-Rad, Hercules, CA, USA
- Minishaker MS1 (Vortex-Schüttler) IKA, Staufen, Germany
- Multipette Eppendorf, Hamburg, Germany
- Olympus DP73 Olympus, Münster, Germany
- Oxygraph-2k Oroboros Instruments, Innsbruck, Austria
- PCR Express Thermal Cycler Thermo Hybaid, Garching, Germany
- Perfusion Line Braun, Melsungen, Germany
- pH 211 Microprocessor pH Meter Hanna Instruments, Kehl, Germany
- PhenoMaster 4050 TSE Systems, Bad Homburg, Germany
- Pipet (Reference, Research) Eppendorf, Hamburg, Germany
- Pipet controller Easypet Eppendorf, Hamburg, Germany
- PowerPac 200 Electrophoresis Power Supply Bio-Rad, Hercules, CA, USA
- Precision Xceed Abbott Diabetes Care, Wiesbaden, Germany
- Pressure pad/respiratory transducer Graseby Medical LTD., Watford, UK
- Quadrature <sup>1</sup>H birdcage volume resonator Bruker, Karlsruhe, Germany
- REAX 2000 (Vortex-Shaker) Heidolph, Schwabach, Germany
- Rocking shaker Karl Hecht, Sondheim v. d. Rhön, Germany
- Scale BP610 Sartorius, Göttingen, Germany
- Scale BTG-2002 Phoenix Instrument, Garbsen, Germany
- Scale A200S Sartorius, Göttingen, Germany
- Shaker (Titramax 100) Heidolph, Schwabach, Germany
- Short and spacer glass plates Bio-Rad, Hercules, CA, USA

## Material and methods

- Stainless Steel Beads, 5 mm	QIAGEN, Hilden, Germany
- Synergy 2 Multi-Mode Microplate Reader	Bio-Rad, Hercules, CA, USA
- Tissue Lyser Adapter Set 2x 24	QIAGEN, Hilden, Germany
- TissueLyser II	QIAGEN, Hilden, Germany
- Ultrasonic bath Sonorex RK102	Bandelin, Berlin, Germany
- Vasofix Safety 24G	Braun, Melsungen, Germany
- Veterinary Fluosorber	Harvard Apparatus, Cambridge, UK
- Water bath C12	Lauda, Königshofen, Germany

### 2.1.4 Consumable material

- Blood glucose test strips FreeStyle precision	Abbott Diabetes Care, Wiesbaden, Germany
- CellStar Tubes („Falcons“) 15+50 ml	Greiner Bio-One, Kremsmünster, Germany
- Cover sheeting	Becton Dickinson, San Jose, CA, USA
- Cover slip	Thermo Fisher Scientific, Waltham, MA, USA / Gerhard Menzel, Braunschweig, Germany
- Cryovial 1.2 ml	Biozym Scientific GmbH, Oldendorf, Germany
- Dako Pen	Agilent, Santa Clara, CA, USA
- Filtration unit 0.2 µm, 500 ml	Nalge Nunc International, NY, USA
- Glas pipet (CELLSTAR)	Greiner Bio-One, Kremsmünster, Germany
- ImmEdge Hydrophobic Barrier PAP Pen	Vector Laboratories, USA
- Low Profile Microtome Blades (Leica 819)	Leica, Nussloch, Germany
- Menzel-Gläser Superfrost Plus (Microscope slides)	Thermo Fisher Scientific, Waltham, MA, USA / Braunschweig, Germany
- Microvette CB300	Sarstedt, Nümbrecht, Germany
- Needles	Braun, Melsungen, Germany
- Needles Microlance 3	Becton Dickinson, San Jose, CA, USA
- Parafilm M	Bemis, Neenah, WI, USA
- Peel-A-Way Disposable Embedding Molds	Polysciences, Warrington, PA, USA
- Razor blade	Apollo, Solingen, Germany
- Spherical NMR bulb (microsphere)	Wilmad lab glass, Vineland, NJ, USA
- Surgical scalpels	Braun, Melsungen, Germany
- Syringe 1, 2, 5, 10, 20 ml	Braun, Melsungen, Germany
- Syringe filters 25 mm	PALL corporation, Ann Arbor, MI, USA
- Tissue-Tek O.C.T. Compound	Sakura Finetek, Alphen aan den

## Material and methods

- Transfer pipet	Rijn, Netherlands
- Tissue Culture Dish	Corning, Corning, NY, USA
	Falcon, Becton Dickinson, Heidelberg, Germany
- Well plates 6, 48, 96	Falcon, Becton Dickinson, Heidelberg, Germany
- Well plates 96	Gibco, Life Technologies, Karlsruhe, Germany

Consumable materials that are not listed above are components of standard lab equipment.

### 2.1.5 Buffers and reagents

DNA loading buffer (6x)	0.25 ml Bromophenol blue 69.5 ml DEPC-Water 0.25 ml Xylene cyanol 30 ml Glycerol
PCR buffer (10x), pH 8.3	100 mM Tris 500 mM KCl 1 % Triton X-100 100 ml DNase and RNase free Aqua dest.
TBE Puffer, pH 8.1	121.1 g Tris 61.8 g Boric acid 7.44 g EDTA 10.165 g MgCl <sub>2</sub> x 6H <sub>2</sub> O 1000 ml Aqua dest.
Krebs-Ringer buffer, pH 7.35	3.45 g NaCl 0.179 g KCl 0.082 g KH <sub>2</sub> PO <sub>4</sub> 0.148 g MgSO <sub>4</sub> x 7H <sub>2</sub> O 0.184 g CaCl <sub>2</sub> x 2H <sub>2</sub> O 1.191 g HEPES 0.25 % BSA Fraction 5
Islet cell culture medium	500 ml DMEM 1 g/l Glucose 5 ml Antibiotic-Antimycotic 5 ml Sodium pyruvate 5 ml L-Glutamine 50 ml Donor Calf Serum 2.5 ml Glucose solution 20 %
Collagenase Solution	0.5 U/ml in PBS

**2.1.6 Oligonucleotides for the determination of the TLR4 expression status**

Table 2: Nucleotide sequences of the primers for detection of the TLR4 expression status.

Gen	Sense primer	Antisense primer	Company	Size (bp)
<b>TLR4-wildtype</b>	5'- CAG TCG GTC AGC AAA CGC CTT CTT C -3'	5'- CAA GGC AGG CTA GCA GGA AAG GGT -3'	Eurofins MWG Operon, Elsberg, Germany	401
<b>TLR4-defect</b>	5'- GCA AGT TTC TAT ATG CAT TCT C -3'	5'- CCT CCA TTT CCA ATA GGT AG -3'	Eurofins MWG Operon, Elsberg, Germany	140

**2.1.7 Antibodies**

Table 3: List of primary antibodies with information of species, dilution, molecular weight and company.

Primary antibody	Species	Dilution	Molecular weight (kDa)	Company
<b>Anti-FFAR2/GPR43</b>	Rabbit	1:1000	~47	Merck Millipore, Billerica, MA, USA
<b>CD36/SR-B3</b>	Goat	1:2000	88	R&Dsystems, Minneapolis, MN, USA
<b>β-Actin (C4)</b>	Mouse	1:1000	43	Santa Cruz Biotechn., Dallas, TX, USA

Table 4: List of secondary antibodies with information of species, dilution, molecular weight and company.

Secondary antibody	Species	Dilution	Company
<b>Goat anti-rabbit IgG-HRP</b>	Goat	1:1000	Cell Signaling, Danvers, MA, USA
<b>Mouse anti-goat IgG-HRP</b>	Mouse	1:1000	Santa Cruz Biotechn., Dallas, TX, USA
<b>Goat anti-mouse IgG-HRP</b>	Goat	1:5000	Merck Millipore, Billerica, MA, USA

**2.2 Methods**

**2.2.1 Genotyping of NOD TLR4<sup>+/+</sup> and NOD TLR4<sup>-/-</sup> mice**

To determine the TLR4 expression status, the wildtype TLR4-gene and the TLR4-deletion were examined. To isolate DNA from mouse ears, the required amount of PCR Direct Ear buffer was mixed with Proteinase K (i.e. add 10 µl Proteinase K (0.2 mg/dl) to 100µl PCR Direct Ear buffer). 110 µl of the solution was added to each ear in a tube. The ear pieces were incubated at 56 °C for 1-2 hours or until they were dissolved. To stop the Proteinase K activity, the tubes were incubated at 85 °C for 45 minutes and afterwards centrifuged for 10 seconds to obtain the DNA pellets. The tubes were stored at 4° C overnight or the procedure was continued. A volume of 1 µl of DNA solution was used for the further analyses. The components for each sample were prepared according to Table 5.

Table 5: The components for each sample for the genotyping of mouse ears.

<b>Components</b>	<b>Volume (µl)</b>
<b>DEPC-water</b>	19.35
<b>10x PCR Reaction Buffer</b>	2.5
<b>MgCl<sub>2</sub> (50 mM)</b>	1.25
<b>dNTP (each 25 mM)</b>	0.25
<b>Primer sense (20 pmol)</b>	0.20
<b>Primer antisense (20 pmol)</b>	0.20
<b>Taq polymerase (5 U/µl)</b>	0.25
	/24

The polymerase chain reaction (PCR) is a method that is used to amplify any known DNA sequence by generating multiple copies of this specific DNA segment. The method is divided into three steps: denaturation, annealing and elongation. In the first step, the DNA is heated up which leads to single stranded DNA because hydrogen bonds between complementary bases melt. In the second step, the temperature is reduced to let the primers bind to the single stranded DNA. In the last step, a high-temperature resistant taq-polymerase synthesizes a new DNA strand complementary to the single stranded DNA. Multiple loops of the three steps are necessary to amplify the DNA segment. The PCR was run in a thermocycler with the following settings (Table 6 and 7):

Table 6: The PCR program for the detection of the TLR4-gene.

Steps	Temperature (°C)	Time (min.)	Loops
1	94	02:00	1
2	94	00:20	30 x
3	60.4	00:50	
4	72	00:30	
5	72	07:00	1
6	4	∞	

Table 7: The PCR program for the detection of the TLR4-defect.

Steps	Temperature (°C)	Time (min.)	Loops
1	94	02:00	1
2	94	00:20	30 x
3	48.4	00:30	
4	72	00:30	
5	72	07:00	1
6	4	∞	

The agarose gel for separation of the PCR products was prepared by mixing agarose, 5x TBE buffer and H<sub>2</sub>O in appropriate amounts and the mixture was heated up until the agarose was dissolved. Afterwards, the mixture was cooled down, 1 µl RedSafe dye per 50 ml gel was added and the gel was poured into the running chamber. When the gel was solidified, the DNA size standards and the samples were loaded and the gel was run for 45 minutes at 90 V. Afterwards, images were taken by a BioDocAnalyze UV star imager to identify the bands corresponding to the TLR4-wildtype or the TLR4-expressing genotype.

### 2.2.2 Diabetes diagnostics

The age of the animals at diabetes onset and the blood glucose levels at diabetes onset were documented and analyzed over 10 years. Diabetes was diagnosed, when the blood glucose levels of unfasted mice were above 250 mg/dl on three consecutive days.

### 2.2.3 Physiological methods

#### 2.2.3.1 Metabolic phenotyping

For metabolic phenotyping, the mice were characterized by a system (PhenoMaster) for automatic detection of metabolic parameters. This system allows long-time monitoring of mice in regular cages, which represent a stress-free environment for the mice. During the measurement, the mice were kept under standard conditions (12 hours light/ 12 hours dark; food and water *ad libitum*). One measurement always included 2 light- and 2 dark-phases. Before the start of the measurement the body weight and body composition were determined and documented. Parameters of physical activity, indirect calorimetry and the intake of food and water were measured simultaneously for each individual mouse in the interval mentioned before.

The physical activity of the mice was determined by interruptions of infrared light beams, which surround the cage in X- and Y-axis. The interruption of one of the light beams was registered by the system as one count. The results of the indirect calorimetry were used to assess the RQ ( $V\text{CO}_2/V\text{O}_2$ ) and energy consumption. The food and water intake of the mice was measured by sensors and documented in regularly intervals. Ambient air was pumped into the measurement-cages but also into a reference-cage (without mouse) with a flow rate of 0.4 l/min. In the outflowing air  $\text{O}_2$  and  $\text{CO}_2$  concentrations were determined.

#### 2.2.3.2 Body weight, liver and fat depot measurements

The whole body weight, the liver weight and the VAT, NAT, WAT and BAT weight of the mice were measured. During HFD, the body weight of the mice was monitored and measured weekly from the age of 30 to 70 days.

#### 2.2.3.3 Nuclear Magnetic Resonance (NMR)

The body composition of the mice was analyzed by the use of a nuclear magnetic resonance (NMR) system. The device measures the proportions of the body-fat-mass and the fat free body mass non-invasively in unanesthetized mice. The measurement takes approximately 1 minute and duplicates and generates values. After calibrating the machine with a canola oil filled cylinder, the mice were put in a cylinder of acrylic glass and carefully fixed with a stamp. The cylinder was inserted into the device and exposed to a magnetic field. The protons of hydrogen atoms in the tissue, which have an intrinsic angular momentum (spin), adjust to the field direction of the magnetic field. Another high-frequency impulse is sent vertically to the magnetic field and shortly distracts the aligned nuclear spins of the protons. When their nuclear spins return to the field direction of the magnetic field, energy is released and can be registered

as a signal. The analysis of the amplitude, the duration and the spatial distribution of the signals allow to determine the tissue composition [208, 209].

### **2.2.3.4 Blood glucose measurements**

Blood glucose was measured from the tail vein by using a glucose meter. Approximately 1-2 mm of tissue was cut from the tip of the mouse tail with sharp scissors. A drop of blood was applied to the test strip. Mice with blood glucose levels above 250 mg/dl were classified as diabetic [30].

### **2.2.3.5 Intraperitoneal glucose and insulin tolerance test (ipGTT and ipITT)**

The intraperitoneal glucose tolerance test (ipGTT) was performed in mice after 6 hours of fasting. After measuring the basal blood glucose levels, the mice were injected with glucose (2 g/kg body weight) and the blood glucose levels were measured at the time points: 5, 15, 30, 60, 90 and 120 minutes after the injection. Additionally, plasma samples were taken at two time points (basal and 15 minutes after injection) to determine the insulin levels by ELISA (2.2.3.6).

The intraperitoneal insulin tolerance test (ipITT) was performed in mice after 6 hours of fasting. Human fast acting insulin (0.75 U/kg body weight) was injected and blood glucose was measured from the tail tip at time points 0 (basal glucose levels) and 15, 30, 45, 60, 75, 90, 105 and 120 minutes after the injection.

### **2.2.3.6 ELISA**

The mouse insulin ELISA kit from Mercodia was used to determine insulin levels in mouse plasma or supernatant of pancreatic islets. On a precoated microplate, a volume of 5 µl of calibrators, controls and samples was used for the procedure. A volume of 100 µl of enzyme conjugate was added into each well and the microplate was incubated for 2 hours at 18-25 °C on a plate shaker. The microplate was washed 6 times with wash buffer followed by the addition of 200 µl of Substrate TMB to all wells. Afterwards, the microplate was incubated for 30 minutes and 50 µl of Stop Solution was added to each well. The microplate was placed back on the plate shaker for approximately 5 seconds and was then analyzed by 450 nm via a microplate reader.

### **2.2.3.7 Determination of the HOMA-IR**

The HOMA-IR (homeostatic model assessment-insulin resistance) is used to assess the whole body insulin resistance. To calculate the HOMA-IR, the fasting blood glucose and the fasting insulin concentration is required. The blood glucose concentration was measured from blood from the tail vein after 6 hours of fasting by using a blood glucose meter (2.2.3.4). The insulin concentration was measured by an ELISA test (2.2.3.6). The HOMA-IR was calculated according to the formula [210]:

$$\text{HOMA-IR} = ((\text{fasting blood glucose (mg/dl)}) \times (\text{fasting insulin concentration (U/ml)})) / 405$$

### **2.2.3.8 FFA, TG, cholesterol, HDL, LDL and CRP levels in plasma samples**

For the analysis of the peripheral blood lipids, plasma samples were collected and stored at -80 °C. From each sample, 100 µl were used for the analysis. The concentrations of TG, FFA, cholesterol, HDL, LDL and CRP were determined in the Biomedical Laboratory of the German Diabetes Center in Düsseldorf using a Cobas c311 Analyzer.

### **2.2.3.9 Measurement of short-chain fatty acids in plasma samples**

Blood was collected from the heart in a Microvette CB 300 which contains EDTA to prevent clotting. The Microvettes were cooled on ice. The blood samples were centrifuged at 10.000 xg for 5 minutes at 18-25 °C. The supernatant was transferred into new tubes and the centrifugation step was repeated. The plasma samples were aliquoted and stored at -80 °C. Approximately 100 µl of blood plasma were required for the method. The blood samples were analyzed at the Mayo Clinic (Rochester, MN, USA) and analyzed as previously described with minor modifications [211, 212]. Acetic acid, propionic acid, butyric acid, isobutyric acid, valeric acid, isovaleric acid, isocaproic acid and hexanoic acid were determined using gas chromatography-mass spectrometry (GC-MS).

### **2.2.3.10 Measurement of short-chain fatty acids in fecal samples**

Stool samples of the small intestine, cecum and colon were collected in separate 2 ml tubes, immediately frozen on dry ice and stored at -80 °C for further use. The stool samples were analyzed at the Department of Gastrointestinal Microbiology (German Institute of Human Nutrition) in Potsdam-Rehbruecke (Germany) as described previously [213]. An amount of at least 20 mg fecal material per sample was required for the analyses. Acetic acid, propionic acid, butyric acid, isobutyric acid, valeric acid and isovaleric acid were determined using GC-MS.

### 2.2.4 Glucose-stimulated insulin secretion from isolated islets

#### 2.2.4.1 Islet isolation

Pancreata of mice were perfused with 2 ml of Liberase TL (385 µl Liberase TL dissolved in 10.5 ml HBSS without FCS) solution, which consists of proteolytic enzymes which degrade the extracellular matrix of tissue to allow the release of individual pancreatic islets. The perfused pancreata were incubated for 19 minutes at 37 °C in a shaking water bath. Under the bench, the pancreata were homogenized manually by using a transfer pipette. The tissue homogenate was transferred to a 15 ml tube and filled with HBSS up to 14 ml. The samples were rigorously shaken, centrifuged for one minute at 320 xg and 4 °C and the supernatant was discarded. The pellet was resuspended in 4 ml medium (DMEM, 11 mM glucose + 10 % FCS) and two more 15 ml tubes with 3 ml medium were prepared. Islets were hand-picked with a pipette from a black petridish under a binocular on a cold metal plate into a new tube and the step was repeated for further enrichment of the islets. Finally, the islets were transferred to a bacterial 6-well plate, which prevents adherence. The islets were incubated overnight (37 °C, 5 % CO<sub>2</sub>) in 3 ml medium.

#### 2.2.4.2 Glucose stimulated insulin secretion from mouse pancreatic islets

To measure the insulin secretion from mouse pancreatic islets, KRH-Buffer was prepared. After adding 0.25 % BSA to the KRH-buffer, the pH was adjusted to 7.35 and the buffer was sterilized by filtration.

After incubation over night, the islets were transferred into a new 6-well plate with KRH-buffer (2.8 mM glucose) and counted. In each well of a 96-well plate, 10 islets were transferred with KRH-buffer (2.8 mM glucose) and incubated at 37 °C for 2 hours. Afterwards, the supernatant was discarded and the islets were treated with KRH-buffer with different glucose concentrations like 2.8 mM, 5.5 mM, 11 mM and 28 mM glucose for 24 hours (37 °C, 5 % CO<sub>2</sub>). After the incubation, 200 µl of the supernatant of each well was transferred into new tubes and stored by -80 °C for ELISA (2.2.3.6).

### 2.2.5 Histological analysis of organs

#### 2.2.5.1 Liver preparation

Liver (left lateral lobe) was removed from mice and transferred to 1.5 ml tubes containing 1 ml of 4 % PFA in PBS (pH 7.4) at room temperature. The organ samples were shaken on a plate shaker overnight.

After the fixation of the organ samples, they were washed with 1x PBS two times for 30 minutes each and immersed in 20 % sucrose in 1x PBS overnight. Then, the organs were transferred

to peel-a-way moulds with Tissue-Tek, frozen with methylbutane on dry ice and stored at -80 °C for further use.

### **2.2.5.2 Preparation of frozen sections from liver tissue**

Frozen sections of the liver were prepared on a microtome cryostat, which allowed to cut 5 µm thick sections. The cryochamber was cooled down to -30 °C an hour before starting to cut the samples and the specimens were separately cooled down to -16 °C. The microscope slides were labeled and of each tissue sample 3-4 sections per microscope slide were collected. The microscope slides were dried overnight at room temperature and stored at -80 °C until further use.

### **2.2.5.3 Oil Red O Staining of liver sections**

The Oil Red O stock solution was prepared by mixing 0.5 g Oil Red O and 100 ml isopropanol (99 %). The solution was prepared in a 50 ml tube by adding the following parameters:

- 6 parts by volume Oil Red O stock solution
- 4 parts by volume Aqua bidest.

The working solution had to incubate at room temperature overnight before used (18-24 hours). After overnight incubation, the working solution was centrifuged for 3-4 minutes and the supernatant (working solution) was carefully transferred into a new tube. The Oil Red O staining was performed as follows:

- |                                     |                      |
|-------------------------------------|----------------------|
| 1. 40% Isopropanol                  | 5 minutes            |
| 2. Oil Red O working solution       | 10 minutes           |
| 3. Milli-Q water                    | 5 seconds            |
| 4. Nuclei staining with hematoxylin | 2 minutes            |
| 5. Tap water                        | more than 10 minutes |

The slides were mounted by applying Kaisers Glyceringelatine (melting temperature: 30-40 °C) and a cover slip.

Imaging and analysis of the sections were performed using a Leica DMRBE microscope with cellSens Dimension Software (Olympus).

### **2.2.5.4 Preparation of frozen sections from pancreas tissue**

Pancreata were removed from animals and transferred to peel-a-way moulds with Tissue-Tek, frozen with methylbutane on dry ice and stored at -80 °C for further use.

The frozen pancreas samples were cut on a microtome cryostat, which allowed to cut 6 µm thick slices. The cryochamber was cooled down to -30 °C and the specimen was separately

cooled down to -30 °C. Sequential thin sections with a thickness of 6 µm were prepared and 3-4 sections were collected per microscopic slide. The microscope slides were air dried for 1 hour at room temperature and then fixed with acetone for 10 minutes. After drying, the slides were stored at -20 °C or were further used for insulin verification.

### ***2.2.5.5 Immunohistological insulin verification***

The frozen slides were thawed and dried for approximately 20-30 minutes at room temperature. The slides were washed with 1x PBS for 5 minutes. Afterwards the activity of endogenous peroxidases was blocked with 0.3 % H<sub>2</sub>O<sub>2</sub> in methanol for 30 minutes, followed by 3x 2 minutes of washing with 1x PBS. The insulin detection was performed by using the VECTASTAIN ABC Kits, containing blocking buffer, secondary antibody and reagents for the avidin-biotin complex. The slides were blocked by blocking buffer for 20 minutes and the primary antibody (guinea pig anti insulin) was applied and incubated for at least 18 hours. After the incubation, the slides were washed with 1x PBS for 3x 2 minutes. The secondary antibody (anti-guinea pig IgG biotinylated) was applied and incubated on the slides for 30 minutes. The slides were washed again with 1x PBS for 3x 2 minutes. The secondary antibody (ABC Kit) is biotinylated and specifically binds the primary antibody. The slides were washed with 1x PBS for 3x 2 minutes and afterwards a mixture of avidin and biotinylated horseradish peroxidase was applied to the tissues. The horseradish peroxidase serves as a reporter enzyme. Avidin binds to the biotinylated horseradish peroxidase and binds to the biotinylated secondary antibody after application to the tissue. The slides were washed with 1x PBS for 3x 2 minutes and then DAB was applied on the thin sections under the microscope. DAB is a substrate for the horseradish peroxidase, which finally leads to staining of tissue areas that contain insulin. The staining reaction with DAB was stopped when applying Milli-Q water to the slides. Thereafter, hematoxylin was applied for staining of nuclei for 10 minutes. The excess hematoxylin was washed off under flowing tap water for 10 minutes. To preserve the tissue sections, the tissue was dehydrated by an alcohol series of 70, 80 and 99 % ethanol, each for 5 minutes. After incubation with xylol to remove residual ethanol for 5 minutes, the slides were embedded in Entellan, dried for approximately 24 hours and stored at room temperature.

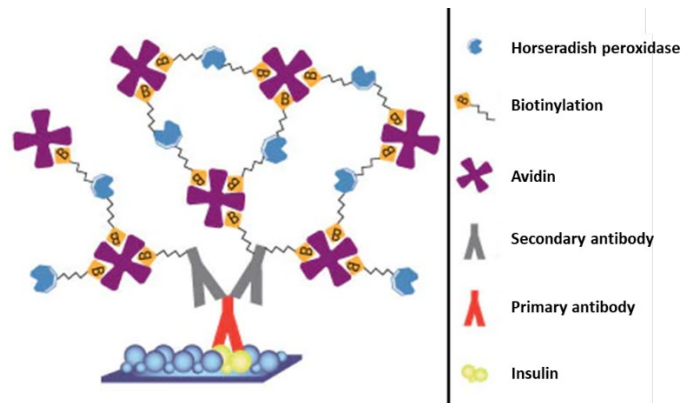


**Figure 6: Schematic representation of insulin detection using specific antibodies and the Avidin-Biotin complex formation.** The primary antibody specifically binds to insulin. The biotinylated secondary antibody then binds the primary antibody. When the Avidin-Biotin Complex is added, the Avidin binds the Biotin of the secondary antibody and of the horseradish peroxidase. Modified from: <https://www.thermofisher.com/de/de/home/life-science/protein-biology/protein-biology-learning-center/protein-biology-resource-library/pierce-protein-methods/avidin-biotininteraction.html>.

Imaging and morphometric analysis of the pancreatic sections were performed by using a Leica DMRBE microscope with cellSens Dimension Software. One tissue slice per mouse was analyzed. Islets with an area  $<500 \mu\text{m}^2$  were excluded from the analysis. The insulinitis score shows the stage of the islet infiltration by immune cells and was defined as follows: 0= no insulinitis, 1= very low to peri-insulinitis ( $<10\%$ ), 2= infiltration  $<50\%$  of the islet area, 3= infiltration  $>50\%$  of the islet area.

## 2.2.6 Preparation of liver, muscle tissue and VAT for protein analysis

Approximately 40 mg of liver, muscle or VAT was frozen on dry ice and homogenized in the presence of 1 mL of 1x PBS (+ 1 mM EDTA, Triton X-100 and 1 % Polyoxyethylene-10-tridecylether) by using a tissue lyser. The mixture was shaken 2x 2 minutes at a frequency of 25/s for the liver and VAT samples and 2x 2 minutes at a frequency of 30/s for the muscle samples. Thereafter, the homogenate was centrifuged at 10,000 g at 4 °C for 20 minutes. The supernatant was collected and incubated at 70 °C for 5 minutes. The centrifugation step was repeated with the same parameters. The samples were stored at -80 °C for further use.

### 2.2.6.1 Bicinchoninic acid (BCA) assay

The Pierce BCA Protein Assay Kit is used to determine and quantify the concentration of proteins. In the BCA Protein Assay,  $\text{Cu}^{2+}$  ions are reduced by proteins to  $\text{Cu}^+$  and those react with the bicinchoninic acid, forming a complex that is purple colored. This complex absorbs light at the specific wavelength of 562 nm, which was measured by the spectrophotometer. The standards for the quantification of the protein concentrations were prepared as follows:

Table 8: The preparation of standards for the BCA assay.

Vial	Volume of diluent (µl)	Volume + source of BSA (µl)	Final BSA concentration (µg/ml)	Vial volume (µl)
<b>A</b>	0	300 of Stock	2000	300
<b>B</b>	125	375 of Stock	1500	325
<b>C</b>	325	325 of Stock	1000	325
<b>D</b>	175	175 of vial B dilution	750	350
<b>E</b>	325	325 of vial C dilution	500	325
<b>F</b>	325	325 of vial E dilution	250	325
<b>G</b>	325	325 of vial F dilution	125	350
<b>H</b>	450	300 of vial G dilution	50	350
<b>I</b>	400	400 of vial H dilution	25	700
<b>J</b>	400	100 of vial I dilution	5	500
<b>K</b>	400	0	0 = Blank	400

1x PBS (+ 1 mM EDTA, Titriplex III and 1 % Polyoxyethylene-10-tridecylether) was used as the diluent. The volume of the BCA Working Reagent (WR) was calculated according to the following formula:

$$(\# \text{ standards} + \# \text{ unknowns}) \times (\# \text{ replicates}) \times (\text{volume of WR per sample}) = \text{total volume WR required}$$

In the present thesis duplicates of standards and duplicates or triplicates of unknowns were used. The WR was prepared by mixing 50 parts of BCA reagent A with 1 part of BCA reagent B. The samples were diluted 1:5 in the diluent.

After that, 25 µl of each standard or sample were transferred into a 96-well plate and 200 µL of WR were added to each well. The plate was shaken for 30 seconds on a plate shaker, then covered and incubated at 37 °C for 30 minutes. Afterwards, the plate was cooled down to room temperature and measured at 562 nm with a spectrophotometer. The measurement of the blank was subtracted from all other standards and samples and a standard curve was prepared.

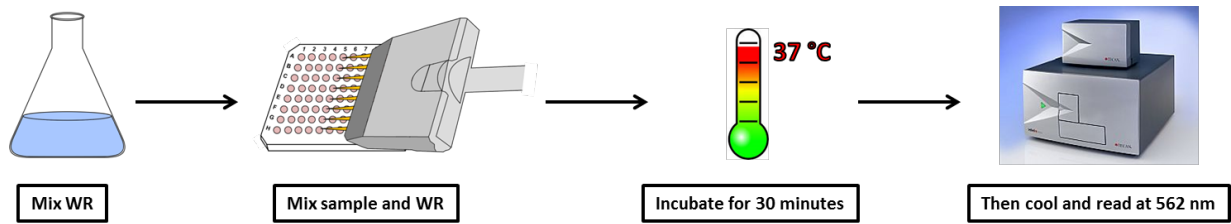


**Figure 7: Procedure of BCA for protein quantification in a 96-well plate format.** The working reagent (WR) is mixed together and standards, samples and the WR are transferred to a 96-well plate. The plate is incubated by 37 °C for 30 minutes. After the incubation, the plate is cooled down and read at 562 nm in a spectrophotometer.

### 2.2.6.2 Western Blot-Analysis

By the use of the Western Blot method, specific proteins and/or post-translational modifications (PTMs) on proteins can be detected and quantified, if antibodies recognizing the proteins/PTMs are available. A polyacrylamide SDS-PAGE (polyacrylamide gel electrophoresis) gel is used to separate proteins according to their molecular weight under the influence of an electrical field. The SDS (sodium dodecyl sulfate) detergent in the gel linearizes the proteins and makes them more negatively charged. The proteins will move toward the positive anode at different rates depending only on their molecular weight/ size. Two different gels with different buffers and the running buffer in the tank are affecting the transfer of proteins from the cathode (negative) to the anode (positive). The upper stacking gel has a pH of 6.8, the lower separating gel a pH of 8.8 and the running buffer a pH of 8.3. When the electric field is turned on, negatively charged glycine ions in the pH 8.3 running buffer enter the stacking gel and lose their charge/ become neutrally charged. Thus, the glycine ions move very slowly in the electric field. The negatively charged chloride ions from Tris-HCl in the buffer form an ion band in front of the glycine because they move faster through the gel. The separation from Tris and the chloride ions forms a voltage gradient and pulls the glycine along behind it. When the two fronts, the chloride front and glycine front, sweep through the protein samples, the proteins are captured in between and pulled towards the separating gel, until they are near the stacking/separating gel border. Glycine becomes negatively charged again when it passes the interface to the separating gel because of the pH switch to 8.8, and moves much faster, passing the proteins. As a result, the proteins arrive at the interface of the stacking and separating gel at the same time. Once the proteins have entered the separating gel, they are separated by their molecular weight because higher weight moves more slowly through the

## Material and methods

acrylamide pores of the gel. The proteins are transferred from the gel to the nitrocellulose membrane by an electric field in a blotting stack that was assembled as follows:

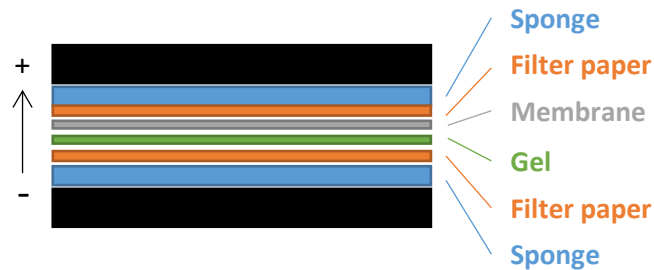


**Figure 8: The order of the blotting stack for Western Blot analysis from the anode to the cathode.** First a sponge and a filter paper are placed on the bottom (negative pole) before the gel is positioned on it. After that, the membrane is placed right on the gel and on the top (positive pole) a filter paper and another sponge is added.

After the transfer, the proteins on the membrane are reversibly stained by Ponceau solution which non-selectively stains proteins, allowing for checking and documenting the transfer of proteins onto the membrane. Afterwards, the membrane was blocked (either with BSA or milkproteins), so that the antibodies used later on can bind specifically to the proteins. The primary antibody is applied to identify the proteins of interest. The secondary antibody is directed against the species of the primary antibody and binds to it. To detect the protein bands, the membrane was incubated with a luminol-based chemiluminescent-substrate which is converted by horseradish peroxidase (HRP) (bound to the secondary antibody), releasing photons. The photons were detected by an BioDocAnalyze biometra device and the band intensities were quantified by using the software Image Lab 6.0 from BIO-RAD.

To start the analyses of distinct proteins of mouse organs, the samples and components were prepared (Table 9) in separate tubes and incubated at 95 °C for 5 minutes. Thereafter, the tubes were put on ice and stored overnight at -20 °C.

Table 9: The amount of the components used for Western Blotting.

Components	Volume [ $\mu$ l]
45 $\mu$ g in 45 $\mu$ l	X
4x Laemmli Buffer + 20 % $\beta$ -Mercaptoethanol	15
Fill up with buffer to 60 $\mu$ l	Y
<b>Total</b>	60

The Western Blot SDS-PAGE gel consists of the lower separating gel (15 %) and the upper stacking gel (4 %). The components of the separating gel for Western Blotting were mixed as follows:

Table 10: The components of the 15 % separating gel of the Western Blot.

Components	Volume
30 % Acrylamide	5.0 ml
H <sub>2</sub> O	2.3 ml
Tris-HCl 1.5 M pH 8.8	2.5 ml
10 % SDS	100 µl
10 % APS	100 µl
TEMED	5 µl

The components of the stacking gel (4 %) for Western Blotting were mixed as follows:

Table 11: The components of the 4 % stacking gel of the Western Blot.

Components	Volume
30 % Acrylamide	670 µl
H <sub>2</sub> O	3.6 ml
Tris-HCl 1.0 M pH 6.8	625 µl
10 % SDS	50 µl
10 % APS	50 µl
TEMED	5 µl

The gels were transferred into the Mini-PROTEAN Tetra System, the device was filled with running buffer and 5 µl of the protein ladder and equal amounts of protein samples (20 µl) were loaded in the pockets of the gel. Any empty lanes were loaded with 5 µl 4x Laemmli Buffer to prevent tilted running of the SDS-Page gel. The gel was run at 90 V and 400 mA for approximately 2 hours. In the meantime, the transfer buffer with 20 % Methanol was prepared and cooled on ice. The stack for blotting was assembled (see Figure 8).

The proteins were transferred from the gel to the membrane at 100 V and 400 mA for 90 minutes in a Mini-Protean Chamber which was constantly chilled by surrounding ice. Afterwards, the membrane was shaken in Ponceau-solution for 15 minutes at room temperature. After pictures were taken of the Ponceau-stained membrane, the membrane was cut (if necessary for concurrent multiple antibody incubations) and the Ponceau-solution was washed out with H<sub>2</sub>O. The membrane was blocked with blocking solution for 1 hour. The appropriate dilutions of primary antibodies in blocking buffer were mixed (Table 3). Blocking solution consisted of 5 % milk powder or BSA dissolved in 1x TBST ( 0.1 % Tween 20)

## Material and methods

according to the instruction of the individual antibody. The membrane was shaken and incubated for at least 16 hours at 4 °C in the primary antibody solution.

After an overnight incubation in primary antibody solution, the membrane was washed for three times with 1x TBST for 10 minutes each. Appropriate dilutions of secondary antibodies were prepared in blocking buffer (Table 4). The membrane was shaken and incubated in the secondary antibody dilution for 1 hour at room temperature. Then the membrane was washed three times with TBST for 10 minutes each. For the detection of protein bands, the Clarity Western ECL Substrate was used. The membrane was incubated for 5 minutes in the substrate. The ChemiDoc Imager from BIO-RAD and the ImageLab 6.0 software from BIO-RAD were used for developing images.

### 2.2.7 Intraperitoneal glucose-tolerance-test (ipGTT) during isoflurane-anesthesia

Mice were fasted for 6 hours and the basal blood glucose levels were measured in blood samples from the tail tip. The mice were placed in a chamber, which was then flooded by a gas mixture of isoflurane (1-3 % v/v) and air (start at time point -15 min). The first 1.5 minutes, 3 % v/v isoflurane with an air flow-rate of 1 ml/min was used and afterwards 1-1.8 % isoflurane with an air flow-rate of 0.5 ml/min was used. When the mice were entirely anesthetized, they were removed from the isoflurane-flooded chamber and placed on a sledge. The mice had to wear a mask through the entire experiment to receive isoflurane. The respiration of the mice was between 35-70 breaths/min while in anesthesia throughout the entire experiment. After 15 minutes in anesthesia, the blood glucose level was measured again (time point 0 min). Immediately after the measurement, the mouse was injected intraperitoneally with 2 g glucose /kg body weight dissolved in 0.9 % NaCl or the same volume of 0.9 % NaCl and the blood glucose levels were measured at time points: 5, 15, 30, 60, 90 and 120 minutes.

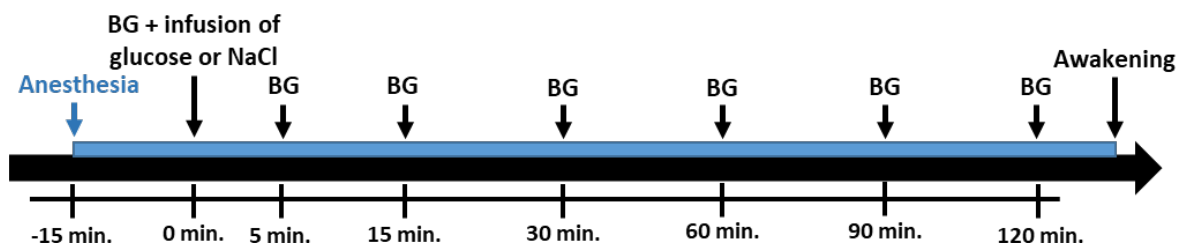


**Figure 9: Schematic presentation of the time course of the intraperitoneal glucose-tolerance-test (ipGTT) under isoflurane-anesthesia.** Anesthesia started at time point -15 minutes and the basal blood glucose levels were measured right before the mouse was injected intraperitoneally with either glucose or NaCl. The blood glucose (BG) levels of the mice were measured at various time points until 120 minutes.

### 2.2.8 Magnetic resonance imaging and spectroscopy

All magnetic resonance imaging and spectroscopy measurements (MRI/MRS) were performed in a horizontal Bruker Biospin 117/16 USR by using the ParaVision 6.0.1 software (Bruker Corporation, Billerica, MA, USA).  $^1\text{H}$  MRI and MRS protocols were performed by using a quadrature  $^1\text{H}$  birdcage volume resonator with 40 mm inner diameter and the  $^{31}\text{P}$  MRS protocol was measured by using a double-tuned  $^{31}\text{P}/^1\text{H}$  birdcage volume resonator with 40 mm diameter. The body temperature of the mice was kept at 35-37 °C with warm water circulating through a MR-compatible sled below the animal. The respiration frequency of the mice was monitored by a pressure pad/respiratory transducer attached to the back of the mouse. Body weight and blood glucose levels were determined before the start of the measurements. Inhalation anesthesia was initiated by placing the mice in a chamber, which was then flooded by a gas mixture of isoflurane (1-3 % v/v) and air. The first 1.5 minutes, 3 % v/v isoflurane with an air flow-rate of 1 ml/min was used. During the experiment, anesthesia was maintained by 1-1.8 % isoflurane with an air flow-rate of 0.5 ml/min. The respiration frequency of the mice was kept between 35-70 breaths/min while in anesthesia throughout the entire experiment.

#### 2.2.8.1 $^1\text{H}$ imaging and spectroscopy

After the mice were placed on the sled in the scanner, the coils were tuned and matched. As the mice vary in size, each animal distorts the electromagnetic field differently. In order to optimize the measurements, the coil had to be adjusted/tuned for each mouse. Localizer was used to for orientation in the mouse body and to find the optimal position of the investigated tissue. Two different sequences of Turbo Rapid Acquisition with Relaxation Enhancement (RARE) followed the localizer with two different directions (sagittal, transversal), to improve the resolution of the images for the MRI analysis and the voxel positioning. Volumes of selected voxels ranged from 2x1x3 (BAT) - 2x2x2 mm<sup>3</sup> (HCL, VAT and WAT) and each voxel was carefully placed within the to be investigated tissue. Before starting  $^1\text{H}$  MRS,  $B_0$  map shimming/manual shimming was performed to improve the homogeneity of the magnetic field. An average full width at half maximum (FWHM) was 60 Hz. Hepatocellular lipid content was determined by point resolved spectroscopy (PRESS) with and without variable power radiofrequency pulses with optimized relaxation delays (VAPOR) water suppression. The

water peak served as a reference in all hepatocellular lipid spectroscopy measurements. Lipid composition was determined by stimulated echo acquisition mode (STEAM) [2].

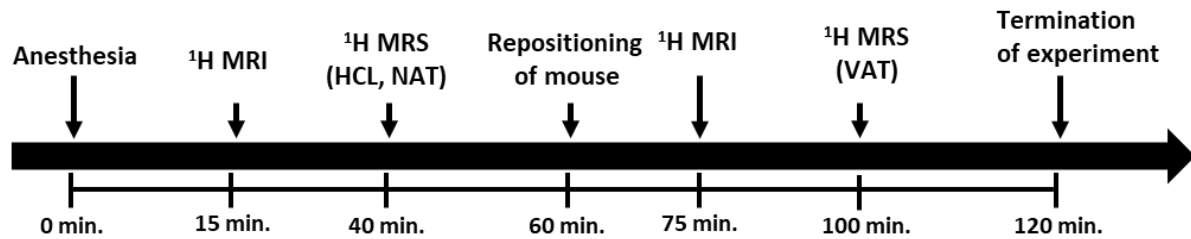


**Figure 10: Schematic representation of the  $^1\text{H}$  MRS protocol.** Anesthetized mice were placed in the scanner which takes around 15 minutes and the mouse was correctly positioned and imaged by using MRI. After that, the amount of HCL, WAT, BAT and NAT was determined by MRS. The mouse was repositioned in the scanner to measure the VAT amount. After about 120 minutes, the experiment was terminated.

### 2.2.8.2 $^{31}\text{P}$ spectroscopy

After fasting for 6 hours, the mice were prepared and anesthetized as mentioned above (2.2.8.1). After placing the mice on the sled, a peripheral venous catheter (braunule) was placed intraperitoneally and a flexible tube with a syringe was attached. The syringe was filled with either 20 % glucose in 0.9 % NaCl or 0.9 % NaCl-solution and was attached to the sled. Coil tuning/matching, localizer, turboRARE and shimming setups were performed as mentioned above (2.2.8.1). Volumes of selected voxels for this protocol were the same size for  $^1\text{H}$  MRS and  $^{31}\text{P}$  MRS, but  $>125\text{ mm}^3$  (as much as possible without muscle contamination; typical voxel size:  $12\times 4\times 4\text{ mm}^3$ ) and each voxel was carefully placed within the to be investigated tissue. An average FWHM was 90 Hz. The external phosphorus reference (18  $\mu\text{l}$  microsphere with 1 M methylene diphosphonic acid (MDPA) dissolved in water) was placed on the sled beneath the mouse and served as reference for all  $^{31}\text{P}$  measurements [2]. The reference concentration was prepared to match *in vivo* signal intensities of a mouse liver. To measure the external reference, a  $^{31}\text{P}$  non-localized singlepulse of the reference was acquired.  $\gamma$ -ATP, inorganic phosphate (Pi), phosphomonoester (PME) and phosphodiester (PDE) levels in the mouse liver were determined by using 3D image-selected *in vivo* spectroscopy (ISIS). After the measurements were completed, 2 g glucose /kg body weight or the same volume of NaCl were injected intraperitoneally without repositioning the mouse. After 15 minutes, the ISIS sequence with exactly the same voxel as before was started in order to compare  $\gamma$ -ATP and Pi levels of the same area before and after injection. Between those two measurements, two PRESS sequences were run (with/without water suppression) with the same voxel as placed for the ISIS [2]. Measuring HCL in the  $^{31}\text{P}$  protocol is important for the correction (especially under high fat diet condition). Because adipocytes contain no to very little  $^{31}\text{P}$  metabolites, high liver fat can lower the  $^{31}\text{P}$  levels in the liver.

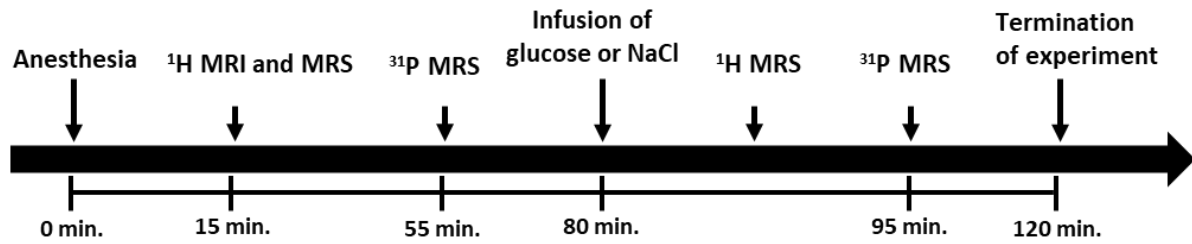


**Figure 11: Schematic representation of the <sup>31</sup>P MRS protocol.** Anesthetized mice were placed in the scanner which takes around 15 minutes and the mouse was correctly positioned, imaged and the liver fat was measured by using MRI and MRS. The  $\gamma$ -ATP, Pi, PME and PDE levels in mouse liver were determined by MRS. After that, the mouse was injected with glucose or NaCl and after 15 minutes the  $\gamma$ -ATP, Pi, PME and PDE levels in mouse liver were measured again. In between those two measurements, the liver fat was measured again. After about 120 minutes the experiment was terminated.

### 2.2.8.3 <sup>1</sup>H and <sup>31</sup>P MRS/MRI data analysis

All spectra were processed and analyzed using jMRUI 5.0 software (EC Human Capital Mobility Networks, France) with the option ‘Advanced Method for Accurate, Robust, and Efficient Spectral fitting’ (AMARES) algorithm for quantification of each peak in cooperation with Maik Rothe [2].

The volumes of the liver, VAT, BAT and WAT were determined using the software ImageJ. The images of the tissue resulting from MRI were analyzed by the “freehand selection” tool, which was used to highlight the area to measure.

### 3 Results

#### 3.1 Metabolic phenotyping of the NOD TLR4<sup>-/-</sup> mouse, as a model of accelerated development of insulin-deficient diabetes

This section contains results from the original research articles “Distinct alterations of gut morphology and microbiota characterize accelerated diabetes onset in non-obese diabetic mice” (Simon et al. [1]) and “In vivo absolute quantification of hepatic  $\gamma$ -ATP concentration in mice using <sup>31</sup>P magnetic resonance spectroscopy at 11.7 T” (Rothe et al. [2]), as well as data presented at the annual conferences of the DDG and EASD. For the analyses of the potential effect of the TLR4-deficiency in NOD mice on metabolic processes, female prediabetic NOD TLR4<sup>+/+</sup> and NOD TLR4<sup>-/-</sup> mice were metabolically phenotyped.

##### 3.1.1 Age and blood glucose levels at diabetes onset in NOD mice

To investigate the age and blood glucose levels at diabetes onset in animals of the parental NOD mouse strain, a group of female NOD mice was observed over two years. Diabetes was diagnosed, when the blood glucose levels of unfasted mice were above 250 mg/dl on three consecutive days. The results show, that NOD mice developed diabetes at the age of 169±5 days with a blood glucose concentration of 437±4 mg/dl (Figure 12).

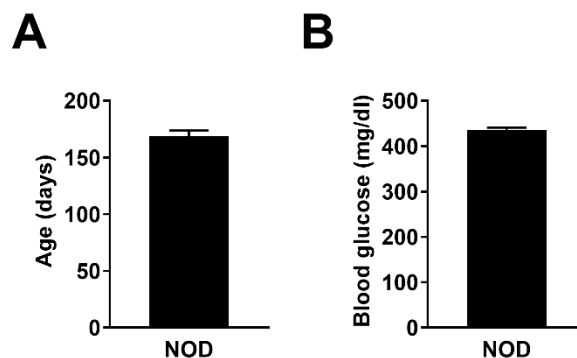


**Figure 12: Age and blood glucose concentrations at diabetes onset in female NOD mice.** The age at diabetes onset (A) was defined as the first of three consecutive days with blood glucose levels above 250 mg/dl in NOD mice. Blood glucose levels (B) were documented at the time of diabetes manifestation. Data are given as means ± SEM. n=177.

##### 3.1.2 Insulin tolerance in NOD mice

To analyze the insulin tolerance of 70-90 days old, normoglycemic NOD mice, an ipITT was performed. After 6 hours of fasting, the animals were injected intraperitoneally with insulin (0.75 U/kg body weight) and the blood glucose concentrations were measured at time point 0 (baseline, before insulin injection) and 15, 30, 45, 60, 75, 90, 105 and 120 minutes after injection. NOD mice had a blood glucose concentration of 96±8 mg/dl at baseline (Figure 13). During the ipITT, the blood glucose levels decreased to 64±3 mg/dl at 120 minutes.

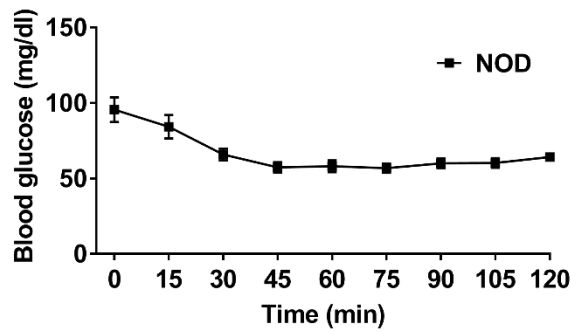


**Figure 13: Blood glucose levels during an intraperitoneal insulin tolerance test in NOD mice.** After a 6-hour period of fasting, an intraperitoneal insulin tolerance test was performed by injecting 0.75 U/kg body weight insulin intraperitoneally into female 70-90 days old NOD mice. The blood glucose concentration was measured over 120 minutes. Data are given as means  $\pm$  SEM. n=10.

### 3.1.3 Glucose-stimulated insulin release from isolated islets of NOD mice

To assess the insulin secretory capacity of islets of NOD mice in the prediabetic phase, pancreatic islets of fasted female normoglycemic 70-90 days old NOD mice were isolated and exposed to different glucose concentrations of 2.8, 5.5, 11 and 28 mM glucose to examine the insulin release at different glucose levels. The insulin released from the islets was quantified by ELISA. Islets treated with 28 mM glucose showed higher insulin release ( $187.5 \pm 19.7$  ng/ml) compared to islets treated with 2.8 ( $125.3 \pm 14.5$  ng/ml) or 5.5 mM glucose ( $115.2 \pm 11.0$  ng/ml) ( $p < 0.05$ ) (Figure 14).

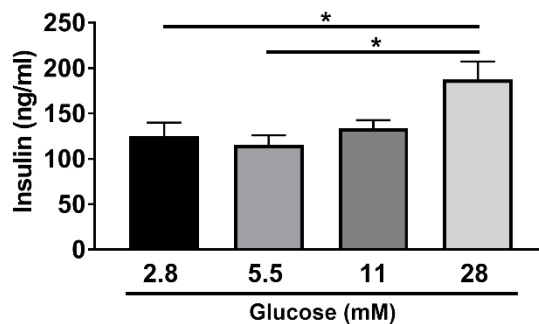


**Figure 14: Higher insulin release from cultivated pancreatic islets of NOD mice exposed to 28 mM glucose compared to islets treated with lower glucose concentrations.** After a 6-hour period of fasting, pancreatic islets of female prediabetic NOD mice were isolated and treated with either 2.8, 5.5, 11 or 28 mM glucose. The insulin released into the islet culture supernatant was quantified by ELISA. Data are given as means  $\pm$  SEM. n=6-10. \* $p < 0.05$  by one-way ANOVA.

### 3.1.4 Diabetes manifestation in NOD TLR4<sup>+/+</sup> and NOD TLR4<sup>-/-</sup> mice

To analyze the impact of the TLR4-expression status on the development of diabetes in NOD mice, diabetes manifestations of female and male NOD TLR4<sup>+/+</sup> and NOD TLR4<sup>-/-</sup> mice in the mouse colony were monitored over more than 10 generations. Diabetes was diagnosed, when the blood glucose levels of non-fasted mice were above 250 mg/dl on three consecutive days. The results showed, that 70 % of female NOD TLR4<sup>+/+</sup> mice and 76 % of female NOD TLR4<sup>-/-</sup> mice developed diabetes in their life span. In contrast, only 21 % of male NOD TLR4<sup>+/+</sup> mice and 31 % of male NOD TLR4<sup>-/-</sup> mice developed diabetes (Figure 15). A higher proportion of female NOD TLR4<sup>+/+</sup> mice developed diabetes compared to male NOD TLR4<sup>+/+</sup> mice (female: 92 of 132 mice developed diabetes; male: 38 of 184 mice developed diabetes) ( $p < 0.001$ ). Furthermore, a higher proportion of female NOD TLR4<sup>-/-</sup> mice developed diabetes compared to male NOD TLR4<sup>-/-</sup> mice (female: 119 of 157 mice developed diabetes; male: 63 of 202 mice developed diabetes) ( $p < 0.001$ ) (Figure 15).

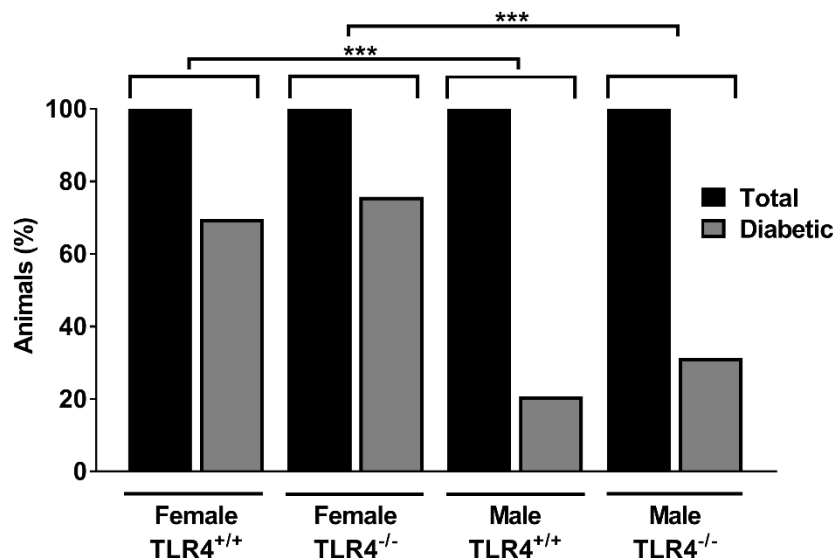


**Figure 15: Diabetes incidence in female and male NOD TLR4<sup>+/+</sup> and NOD TLR4<sup>-/-</sup> mice.** Diabetes manifestation was documented and analyzed over several generations in female and male NOD TLR4<sup>+/+</sup> and NOD TLR4<sup>-/-</sup> mice. The proportions of observed mice and mice that developed diabetes during the observation period are shown in percent. Diabetes was diagnosed when the blood glucose levels of non-fasted mice were above 250 mg/dl on three consecutive days. Female mice n=132-157, male mice n=184-202. \* $p < 0.001$  by Fisher's exact test.

### 3.1.5 Age and blood glucose levels at diabetes onset

To further investigate the influence of the TLR4-expressing status on the development of diabetes in female and male NOD TLR4<sup>+/+</sup> and NOD TLR4<sup>-/-</sup> mice, the age at diabetes onset was documented for each genotype. The results show, that the mean age of diabetes manifestation was  $151 \pm 4$  days in female NOD TLR4<sup>-/-</sup> mice, whereas female NOD TLR4<sup>+/+</sup> mice reached their mean age of diabetes manifestation in  $165 \pm 7$  days, around two weeks later ( $p < 0.05$ ) (Figure 16A,B). Compared to female mice, male NOD TLR4<sup>+/+</sup> and NOD TLR4<sup>-/-</sup> mice

developed diabetes later at the age of  $190 \pm 8$  days and  $186 \pm 9$  days, respectively ( $p < 0.05$  and  $p < 0.001$ ) (Figure 16A).

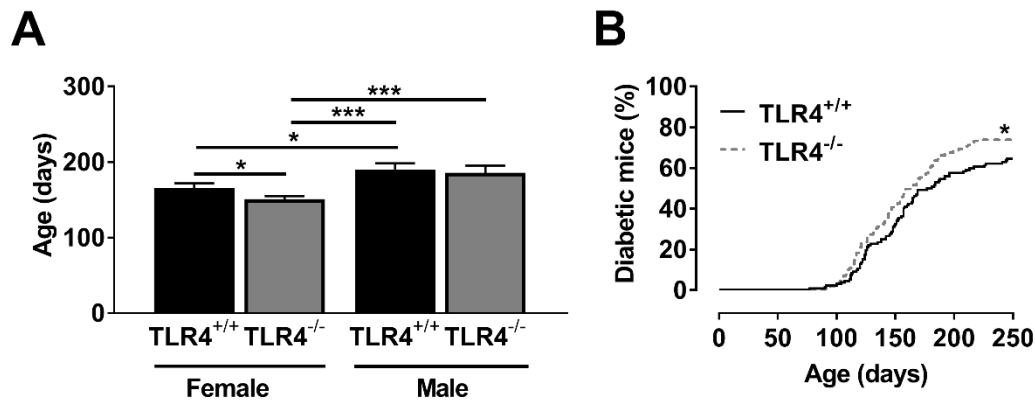


**Figure 16: Accelerated diabetes development in female NOD TLR4<sup>-/-</sup> mice compared to NOD TLR4<sup>+/+</sup>.** Diabetes manifestation was documented and analyzed over several generations in female and male NOD TLR4<sup>+/+</sup> and NOD TLR4<sup>-/-</sup> mice (A). The development of diabetes was monitored in female NOD TLR4<sup>+/+</sup> and NOD TLR4<sup>-/-</sup> mice (B) until the age of 250 days. The age at diabetes onset was defined as the first of three consecutive days with blood glucose levels above 250 mg/dl. Data are given as means  $\pm$  SEM and as a survival curve. Female mice  $n=92-119$ , male mice  $n=38-63$ . \* $p < 0.05$ , \*\*\* $p < 0.001$  by survival curve (curve comparison) and one-way ANOVA.

At the time of diabetes manifestation, the blood glucose levels of non-fasted female NOD TLR4<sup>+/+</sup> and NOD TLR4<sup>-/-</sup> mice were measured and documented. NOD TLR4<sup>+/+</sup> and NOD TLR4<sup>-/-</sup> mice showed comparable blood glucose levels at diabetes onset (TLR4<sup>+/+</sup>:  $430 \pm 8$  mg/dl; TLR4<sup>-/-</sup>:  $429 \pm 7$  mg/dl) (Figure 17).

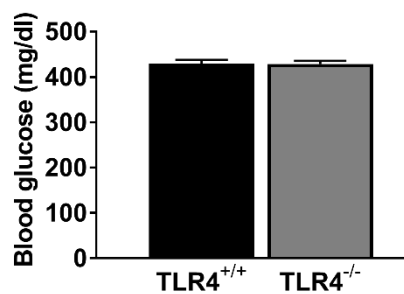


**Figure 17: Comparable blood glucose concentrations in female NOD TLR4<sup>+/+</sup> mice and NOD TLR4<sup>-/-</sup> mice at the time of diabetes manifestation.** Diabetes was diagnosed when the blood glucose levels of non-fasted mice were above 250 mg/dl on three consecutive days. Data are given as means  $\pm$  SEM.  $n=92-119$ .

Based on the findings that female NOD TLR4<sup>+/+</sup> and NOD TLR4<sup>-/-</sup> mice showed higher diabetes incidence and developed diabetes earlier compared to male mice, all further experiments of this thesis were performed only with female mice, also in accordance with previous studies with the NOD mouse model [28].

Moreover, as the thesis focused on the elucidation of the effects of TLR4 on the pathogenesis of autoimmune diabetes i.e. before disease manifestation, all further investigations were performed in animals at an age of 70-90 days, corresponding to the prediabetic phase.

### 3.1.6 Metabolic phenotyping

To characterize possible effects of the TLR4-expression status on the metabolism of female, prediabetic 70-90 days old NOD TLR4<sup>+/+</sup> and NOD TLR4<sup>-/-</sup> mice, basic metabolic parameters of the animals were analyzed including food and water intake, physical activity, energy expenditure and the RQ. Each parameter was measured during two light- and two dark-phases (each phase 12 hours light/ 12 hours dark) after an adaption period of the animals to the housing conditions of the metabolic test system for one light-/dark-phase. For food and water intake, the data from both light-phases and both dark-phases were combined to a total of 24 hours. For the other metabolic parameters, the mean of both light-phases and both dark-phases was calculated. The parameters “food intake” and “water intake” were monitored over the entire measurement period, which includes the adaption period, both light-phases and both dark-phases.

#### 3.1.6.1 Water- and food intake

During the light- and dark-phases, the animals had free access to food and water. The food and water intake was higher in the dark-phases compared to the light-phases in NOD TLR4<sup>+/+</sup> and NOD TLR4<sup>-/-</sup> mice ( $p < 0.001$ ) (Figure 18A,B). NOD TLR4<sup>+/+</sup> and NOD TLR4<sup>-/-</sup> mice showed comparable intake of water and food during the light-phases and dark-phases (Figure 18A,B). In the light-phases, the water intake of NOD TLR4<sup>+/+</sup> and NOD TLR4<sup>-/-</sup> mice ranged from  $0.10 \pm 0.01$  to  $0.11 \pm 0.03$  ml/g body weight and in the dark-phases from  $0.21 \pm 0.02$  to  $0.24 \pm 0.02$  ml/g body weight (Figure 18A). The food intake ranged from  $0.10 \pm 0.02$  to  $0.12 \pm 0.01$  g/g body weight in the light-phases and was about  $0.25 \pm 0.02$  g/g body weight in the dark-phases in NOD TLR4<sup>+/+</sup> and NOD TLR4<sup>-/-</sup> mice (Figure 18B). After the entire measurement period of 72 hours (including the adaption period, two light-phases and two dark-phases), NOD TLR4<sup>+/+</sup> and NOD TLR4<sup>-/-</sup> mice had comparable total water intake (TLR4<sup>+/+</sup>:  $0.43 \pm 0.03$ ; TLR4<sup>-/-</sup>:  $0.44 \pm 0.02$  ml\* $g$  body weight<sup>-1</sup>\*72 h<sup>-1</sup>), respectively food intake (TLR4<sup>+/+</sup>:  $0.47 \pm 0.02$ ; TLR4<sup>-/-</sup>:  $0.47 \pm 0.01$  g\* $g$  body weight<sup>-1</sup>\*72 h<sup>-1</sup>) (Figure 18C,D).

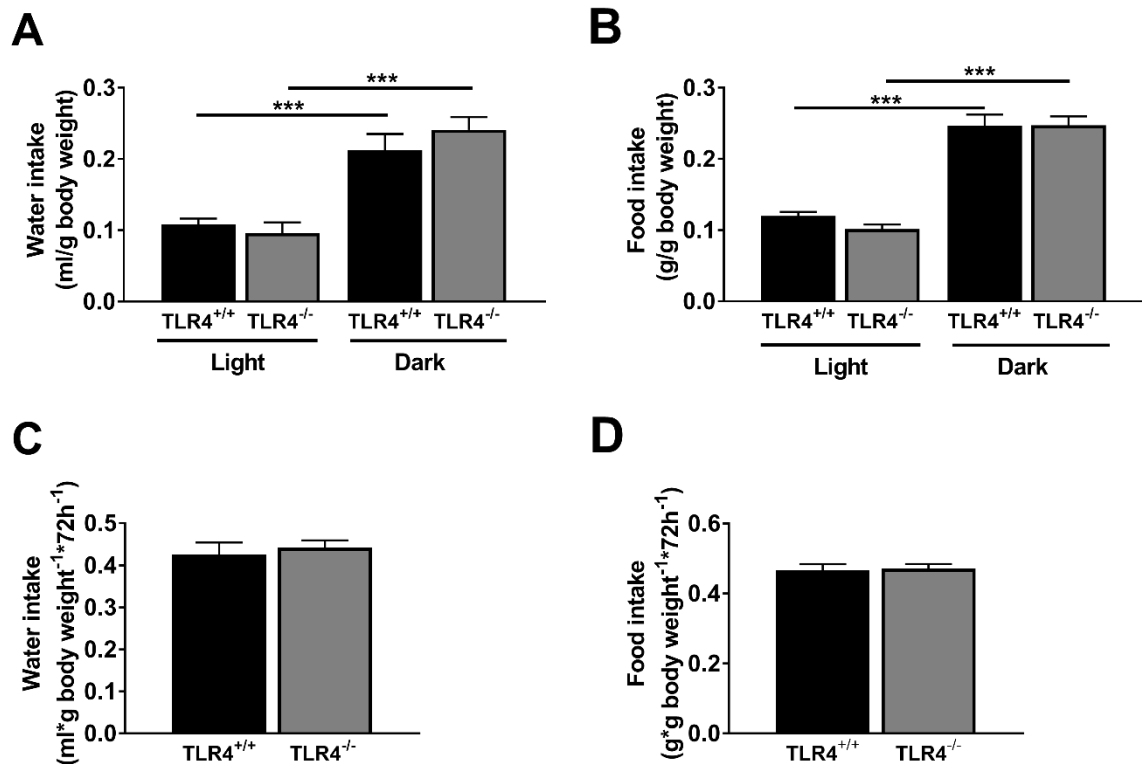


**Figure 18: Comparable water and food intake of female prediabetic NOD TLR4<sup>+/+</sup> and NOD TLR4<sup>-/-</sup> mice.** Female prediabetic NOD TLR4<sup>+/+</sup> and NOD TLR4<sup>-/-</sup> mice were analyzed in a system that measures metabolic parameters like water (A) and food (B) intake over 2 light- and 2 dark-phases. Water intake (C) and food intake (D) after the entire measurement period of 72 hours was determined. The data show the water and food intake in ml/g body weight and g/g body weight, respectively. Data are given as means ± SEM. n= 7-10. \*\*\*p<0.001 by one-way ANOVA.

### 3.1.6.2 Physical activity

The physical activity was measured during the measurement period of 2 light- and 2 dark-phases. The cages are surrounded by a metal frame, which emits infrared rays along the x- and y-axes and every time a mouse interrupts a beam one count is registered. The physical activity of the mice was increased in both dark-phases compared to the light-phases in NOD TLR4<sup>+/+</sup> and NOD TLR4<sup>-/-</sup> mice (Figure 19A). The mean physical activity was higher in the dark-phases compared to the light-phases in NOD TLR4<sup>+/+</sup> and NOD TLR4<sup>-/-</sup> mice (TLR4<sup>+/+</sup>: Dark-phases: 2406±328; light-phases: 974±133 counts) (p<0.001) (TLR4<sup>-/-</sup>: dark-phases: 2346±164; light-phases: 900±113 counts) (p<0.01) (Figure 19B). There was no difference in the physical activity of NOD TLR4<sup>+/+</sup> and NOD TLR4<sup>-/-</sup> mice in the light-phases and the dark-phases.

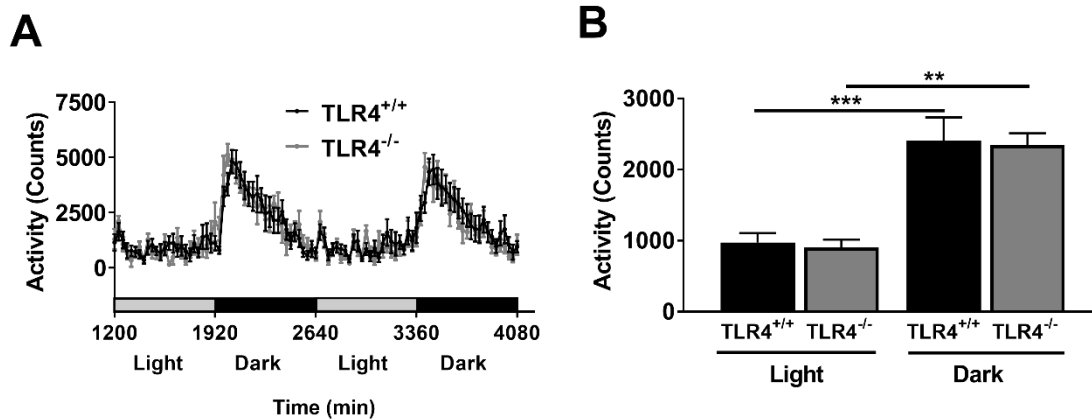


**Figure 19: Comparable physical activity in female prediabetic NOD TLR4<sup>+/+</sup> and NOD TLR4<sup>-/-</sup> mice.** The physical activity of female prediabetic NOD TLR4<sup>+/+</sup> and NOD TLR4<sup>-/-</sup> mice was analyzed in a system that detects metabolic parameters over 2 light- and 2 dark-phases. The data show the physical activity in counts (A) and the mean of both light-phases and both dark-phases (B). Data are given as means  $\pm$  SEM.  $n = 7-11$ . \*\* $p < 0.01$ , \*\*\* $p < 0.001$  by one-way ANOVA.

### 3.1.6.3 Respiratory quotient

The RQ was determined by measuring the CO<sub>2</sub> production and the O<sub>2</sub> consumption and calculating the ratio VCO<sub>2</sub>/VO<sub>2</sub>. The CO<sub>2</sub> production was higher in the dark-phases compared to the light-phases in both NOD TLR4<sup>+/+</sup> and NOD TLR4<sup>-/-</sup> mice (Dark-phases: TLR4<sup>+/+</sup>: 94.6 $\pm$ 3.2; TLR4<sup>-/-</sup>: 96.4 $\pm$ 5.0 ml/h; light-phases: TLR4<sup>+/+</sup>: 69.5 $\pm$ 2.2; TLR4<sup>-/-</sup>: 71.0 $\pm$ 1.6 ml/h) (both  $p < 0.001$ ) (Figure 20A). Moreover, both, NOD TLR4<sup>+/+</sup> and NOD TLR4<sup>-/-</sup> mice revealed higher O<sub>2</sub> consumption in the dark-phases than the light-phases (Dark-phases: TLR4<sup>+/+</sup>: 100.1 $\pm$ 3.3; TLR4<sup>-/-</sup>: 101.3 $\pm$ 2.2 ml/h; light-phases: TLR4<sup>+/+</sup>: 78.8 $\pm$ 1.8; TLR4<sup>-/-</sup>: 80.5 $\pm$ 1.7 ml/h) (both  $p < 0.001$ ) (Figure 20B). NOD TLR4<sup>+/+</sup> and NOD TLR4<sup>-/-</sup> mice showed comparable CO<sub>2</sub> production and O<sub>2</sub> consumption in the light-phases and in the dark-phases. The RQ serves as an indicator for the metabolized substrate. During an energy production exclusively from carbohydrates the RQ is 1, during an energy production exclusively from proteins the RQ is 0.81 and during an energy production exclusively from fat the RQ is 0.7. The feeding of mice with a standard diet results in a RQ in a range from about 0.88 to 0.95 depending on the phase. The RQ showed peak values in both dark-phases in NOD TLR4<sup>+/+</sup> and NOD TLR4<sup>-/-</sup> mice (Figure 20C). The mean RQ in both light- and both dark-phases was higher in the dark-phases compared to the light-phases in NOD TLR4<sup>+/+</sup> and NOD TLR4<sup>-/-</sup> mice (Dark-phases: TLR4<sup>+/+</sup>: 0.94 $\pm$ 0.01; TLR4<sup>-/-</sup>: 0.95 $\pm$ 0.01; light-phases: TLR4<sup>+/+</sup>: 0.88 $\pm$ 0.01; TLR4<sup>-/-</sup>: 0.88 $\pm$ 0.01) (both  $p < 0.001$ ) (Figure 20D). There was no difference in RQ between the two genotypes in the light phases and in the dark phases.

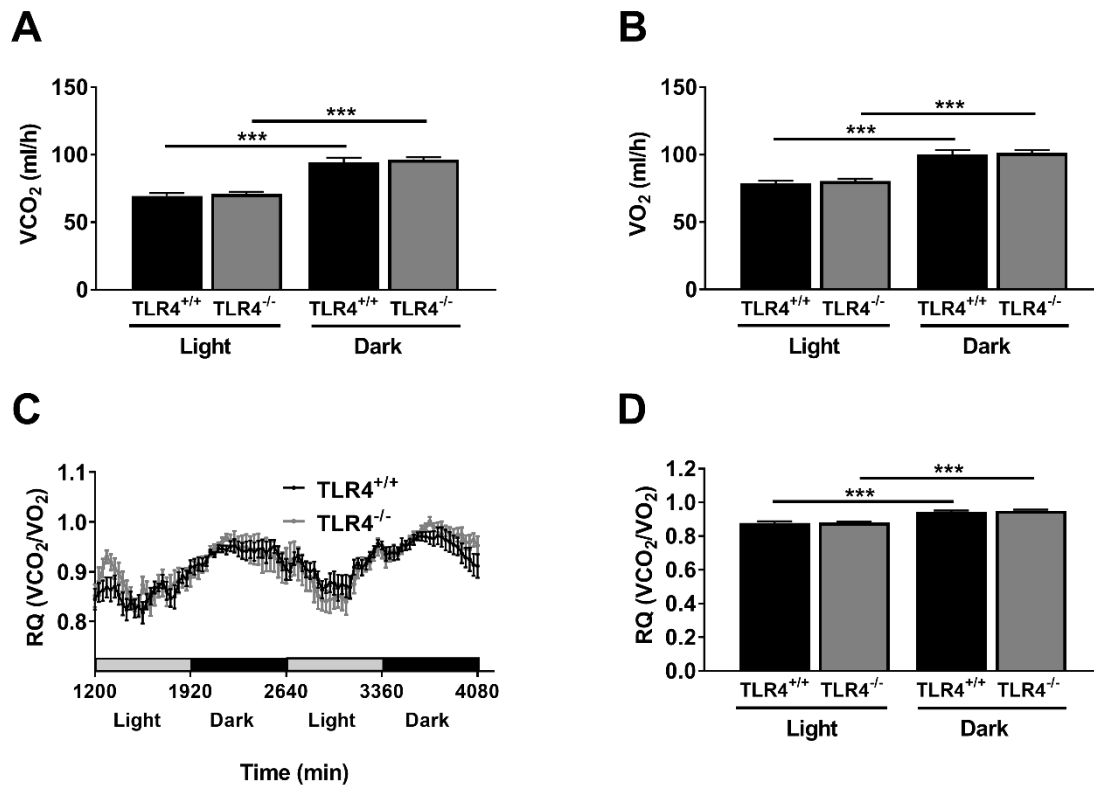


**Figure 20: Comparable respiratory quotient in female prediabetic NOD TLR4<sup>+/+</sup> and NOD TLR4<sup>-/-</sup> mice.** The VCO<sub>2</sub>, VO<sub>2</sub> and RQ of female prediabetic NOD TLR4<sup>+/+</sup> and NOD TLR4<sup>-/-</sup> mice were analyzed in a system that detects metabolic parameters over 2 light- and 2 dark-phases. The data show the volumes of produced CO<sub>2</sub> (VCO<sub>2</sub>) (A) and consumed O<sub>2</sub> (VO<sub>2</sub>) (B) in ml/h and the RQ as VCO<sub>2</sub>/VO<sub>2</sub> (C+D) and as mean of both light-phases and both dark-phases. Data are given as means ± SEM. n= 7-11. \*\*\*p<0.001 by one-way ANOVA.

#### 3.1.6.4 Energy expenditure

The energy expenditure of the animals was calculated from the VO<sub>2</sub> and VCO<sub>2</sub> parameters during 2 light- and 2 dark-phases. In NOD TLR4<sup>+/+</sup> and NOD TLR4<sup>-/-</sup> mice, the highest energy expenditure was observed during the dark-phases and the lowest during the light-phases (Figure 21A). Mean energy expenditure was higher in the dark-phases compared to the light-phases in NOD TLR4<sup>+/+</sup> and NOD TLR4<sup>-/-</sup> mice (Dark-phases: TLR4<sup>+/+</sup>: 21.5±0.5; TLR4<sup>-/-</sup>: 22.0±0.4 kcal·h<sup>-1</sup>·kg<sup>-1</sup>; light-phases: TLR4<sup>+/+</sup>: 16.7±0.3; TLR4<sup>-/-</sup>: 17.2±0.3 kcal·h<sup>-1</sup>·kg<sup>-1</sup>) (both p<0.001) (Figure 21B). There was no difference in energy expenditure between the two genotypes in the light phases and in the dark phases.

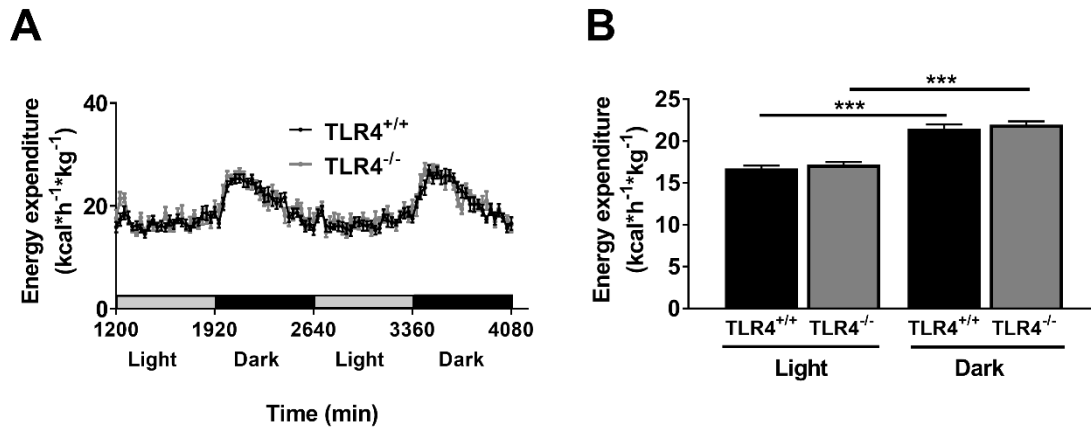


**Figure 21: Comparable energy expenditure in female prediabetic NOD TLR4<sup>+/+</sup> and NOD TLR4<sup>-/-</sup> mice.** The energy expenditure of female prediabetic NOD TLR4<sup>+/+</sup> and NOD TLR4<sup>-/-</sup> mice was analyzed in a system that detects metabolic parameters over 2 light- and 2 dark-phases. The data show the kinetics of energy expenditure (A) and the means of both light-phases and both dark-phases in kcal\*h<sup>-1</sup>\*kg<sup>-1</sup> (B). Data are given as means ± SEM. n= 7-11. \*\*\*p<0.001 by one-way ANOVA.

### 3.1.6.5 Whole-body carbohydrate and fat oxidation rates

The whole-body CHO and FAO rates were calculated from the VO<sub>2</sub> and VCO<sub>2</sub> parameters determined during 2 light- and 2 dark-phases in NOD TLR4<sup>+/+</sup> and NOD TLR4<sup>-/-</sup> mice. The whole-body CHO rates were highest in the dark-phases compared to light-phases in NOD TLR4<sup>+/+</sup> and NOD TLR4<sup>-/-</sup> mice (Dark-phases: TLR4<sup>+/+</sup>: 1.84±0.09; TLR4<sup>-/-</sup>: 1.92±0.04 mg/min; light-phases: TLR4<sup>+/+</sup>: 1.07±0.08; TLR4<sup>-/-</sup>: 1.10±0.05 mg/min) (both p<0.001) (Figure 22A). NOD TLR4<sup>+/+</sup> and NOD TLR4<sup>-/-</sup> mice showed comparable whole-body CHO rates in the light-phases and in the dark-phases. In contrast, whole-body FAO rates were highest in the light-phases compared to dark-phases in NOD TLR4<sup>+/+</sup> and NOD TLR4<sup>-/-</sup> mice (Dark-phases: TLR4<sup>+/+</sup>: 0.15±0.02; TLR4<sup>-/-</sup>: 0.13±0.02 mg/min; light-phases: TLR4<sup>+/+</sup>: 0.26±0.02; TLR4<sup>-/-</sup>: 0.26±0.02 mg/min) (both p<0.01) (Figure 22B). There was no difference in whole-body FAO between the two genotypes in the light phases and in the dark phases.

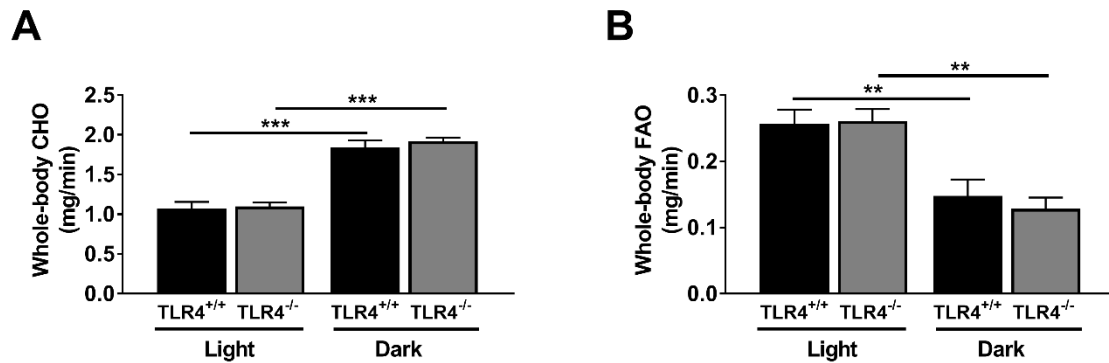


**Figure 22: Comparable whole-body carbohydrate and fat oxidation rates in female prediabetic NOD TLR4<sup>+/+</sup> and NOD TLR4<sup>-/-</sup> mice.** The CHO and FAO rates of female prediabetic NOD TLR4<sup>+/+</sup> and NOD TLR4<sup>-/-</sup> mice were analyzed in a system that detects metabolic parameters over 2 light- and 2 dark-phases. The data show the CHO rates (A) and the FAO rates (B) in mg/min. The means of both light-phases and both dark-phases are shown. Data are given as means  $\pm$  SEM.  $n = 7-11$ . \*\* $p < 0.01$ , \*\*\* $p < 0.001$  by one-way ANOVA.

### 3.1.7 Body weight and weight of liver and visceral adipose tissue

The body weight and the weights of the liver and VAT were determined from female prediabetic mice aged 70-90 days to examine the possible impact of the TLR4-expression status on these parameters. Compared to NOD TLR4<sup>+/+</sup> mice, NOD TLR4<sup>-/-</sup> mice showed increased body weight (TLR4<sup>+/+</sup>: 24.44 $\pm$ 0.18; TLR4<sup>-/-</sup>: 25.25 $\pm$ 0.28 g) ( $p < 0.05$ ) (Figure 23A). Furthermore, liver and visceral adipose tissue (VAT) were removed from the mice and the weights of the organs were determined. The weight of the liver was comparable between NOD TLR4<sup>+/+</sup> and NOD TLR4<sup>-/-</sup> mice (TLR4<sup>+/+</sup>: 1.15 $\pm$ 0.03; TLR4<sup>-/-</sup>: 1.14 $\pm$ 0.03 g) (Figure 23B). Moreover, VAT weight showed no differences between NOD TLR4<sup>+/+</sup> and NOD TLR4<sup>-/-</sup> mice (TLR4<sup>+/+</sup>: 0.23 $\pm$ 0.03; TLR4<sup>-/-</sup>: 0.35 $\pm$ 0.05 g) (Figure 23C).

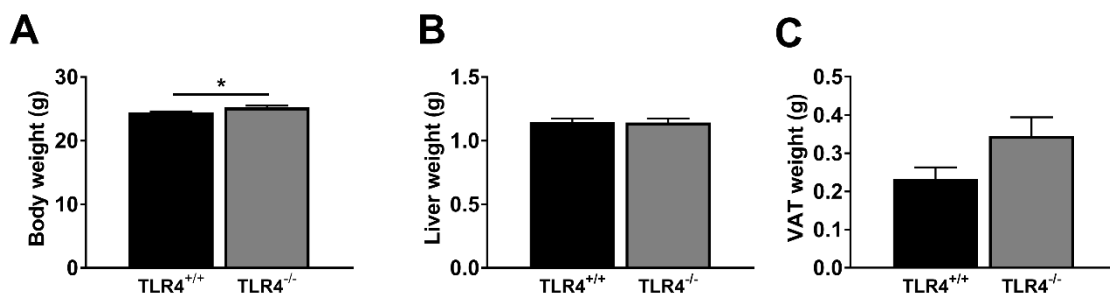


**Figure 23: Increased body weight, but comparable liver and visceral adipose tissue weight in NOD TLR4<sup>-/-</sup> mice compared to NOD TLR4<sup>+/+</sup> mice.** The body weight (A) in g, and the weights of liver (B) and VAT (C) in g were measured from female prediabetic NOD TLR4<sup>+/+</sup> and NOD TLR4<sup>-/-</sup> mice at the age of 70-90 days. Data are given as means  $\pm$  SEM.  $n = 6-10$ . \* $p < 0.05$  by Student's t-test.

### 3.1.8 Development of body weight

The body weight development was monitored in female prediabetic NOD TLR4<sup>+/+</sup> and NOD TLR4<sup>-/-</sup> mice, to examine the possible impact of the TLR4-expression status on the gain of body weight before diabetes manifestation. To this end, the weight of NOD TLR4<sup>+/+</sup> and NOD TLR4<sup>-/-</sup> mice was determined weekly between 30 and 70 days of age. NOD TLR4<sup>+/+</sup> and NOD TLR4<sup>-/-</sup> mice showed comparable body weight development during the observational period (Figure 24).

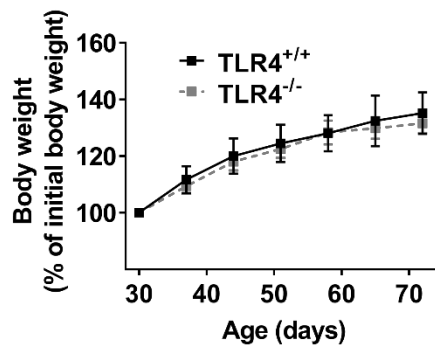


**Figure 24: Comparable body weight development in female prediabetic NOD TLR4<sup>+/+</sup> mice and NOD TLR4<sup>-/-</sup> mice.** The body weight of female prediabetic NOD TLR4<sup>+/+</sup> and NOD TLR4<sup>-/-</sup> mice was determined from the age of 30 to 70 days and shown as percent body weight gain. Data are given as means  $\pm$  SEM. n=7-11.

### 3.1.9 White and brown adipose tissue weight

The WAT and BAT weight was determined in female prediabetic NOD TLR4<sup>+/+</sup> and NOD TLR4<sup>-/-</sup> mice aged 70-90 days to examine a potential impact of the TLR4-expression status on the development of the neck adipose tissue (NAT) depots. The WAT and BAT weights were determined separately and added to obtain the total weight of the NAT. NOD TLR4<sup>+/+</sup> and NOD TLR4<sup>-/-</sup> mice had comparable weight of NAT (TLR4<sup>+/+</sup>: 51.9 $\pm$ 4.2; TLR4<sup>-/-</sup>: 53.0 $\pm$ 3.8 mg/10 g body weight) (Figure 25A). Furthermore, similar weight of BAT was measured in NOD TLR4<sup>+/+</sup> and NOD TLR4<sup>-/-</sup> mice (TLR4<sup>+/+</sup>: 20.8 $\pm$ 2.0; TLR4<sup>-/-</sup>: 22.8 $\pm$ 2.6 mg/10 g body weight) (Figure 25B). Moreover, no differences were found in WAT weight of NOD TLR4<sup>+/+</sup> and NOD TLR4<sup>-/-</sup> mice (TLR4<sup>+/+</sup>: 31.1 $\pm$ 2.9; TLR4<sup>-/-</sup>: 30.2 $\pm$ 1.6 mg/10 g body weight) (Figure 25C).

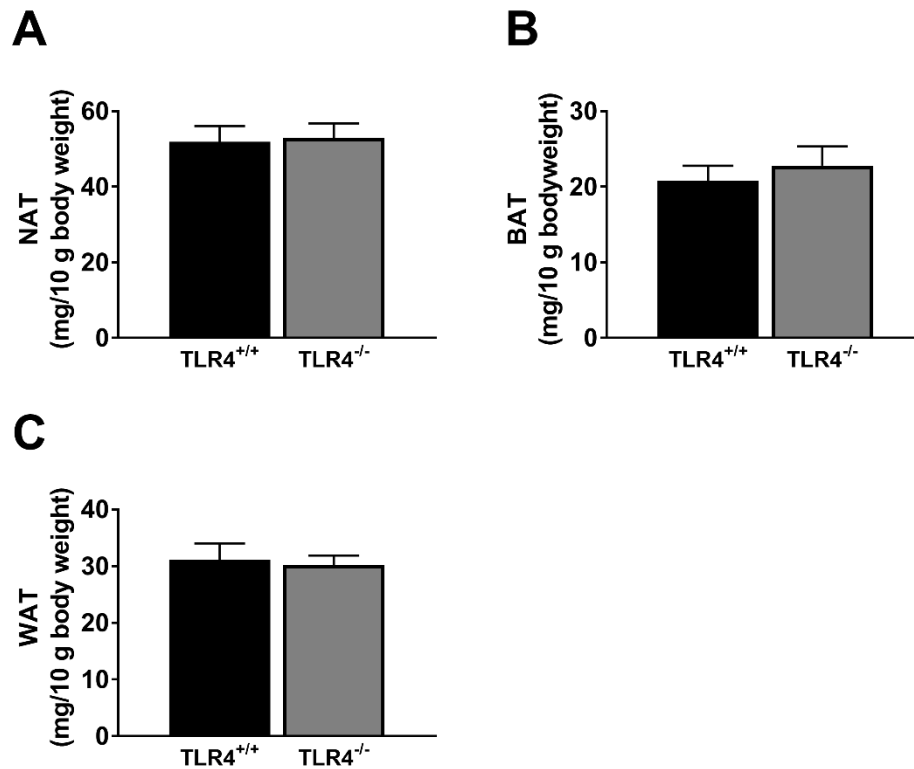


**Figure 25: Comparable weights of NAT, BAT and WAT in female prediabetic NOD TLR4<sup>+/+</sup> mice and NOD TLR4<sup>-/-</sup> mice.** The total NAT weight (A), BAT weight (B) and WAT weight (C) in mg/10 g body weight were measured from female prediabetic NOD TLR4<sup>+/+</sup> and NOD TLR4<sup>-/-</sup> mice at the age of 70-90 days. Data are given as means  $\pm$  SEM. n=6-9.

### 3.1.10 Liver, VAT, NAT and BAT volume

The potential effect of the TLR4-expression status on the volume of liver, VAT, NAT and BAT was determined in female prediabetic 70-90 days old NOD TLR4<sup>+/+</sup> and NOD TLR4<sup>-/-</sup> mice. The volume of each tissue was measured by encircling the shape of the tissue in each slice sequentially obtained by MRI in the axial direction and analyzing each slide to determine the entire tissue volume (Figure 26A-D). NOD TLR4<sup>+/+</sup> and NOD TLR4<sup>-/-</sup> mice showed comparable volumes of liver (TLR4<sup>+/+</sup>:  $0.47 \pm 0.01$ ; TLR4<sup>-/-</sup>:  $0.44 \pm 0.02$  ml/10g body weight) (Figure 26A) and VAT (TLR4<sup>+/+</sup>:  $0.11 \pm 0.01$ ; TLR4<sup>-/-</sup>:  $0.12 \pm 0.02$  ml/10g body weight) (Figure 26B). The NAT consists of the BAT and WAT, however the BAT volume was separately visualized and quantified. The entire NAT volume was similar in NOD TLR4<sup>+/+</sup> and NOD TLR4<sup>-/-</sup> mice (TLR4<sup>+/+</sup>:  $37.7 \pm 3.1$ , TLR4<sup>-/-</sup>:  $41.4 \pm 3.7$   $\mu$ l/10g body weight) (Figure 26C), as well as the BAT volume (TLR4<sup>+/+</sup>:  $18.3 \pm 0.7$ ; TLR4<sup>-/-</sup>:  $19.2 \pm 1.1$   $\mu$ l/10g body weight) (Figure 26D).

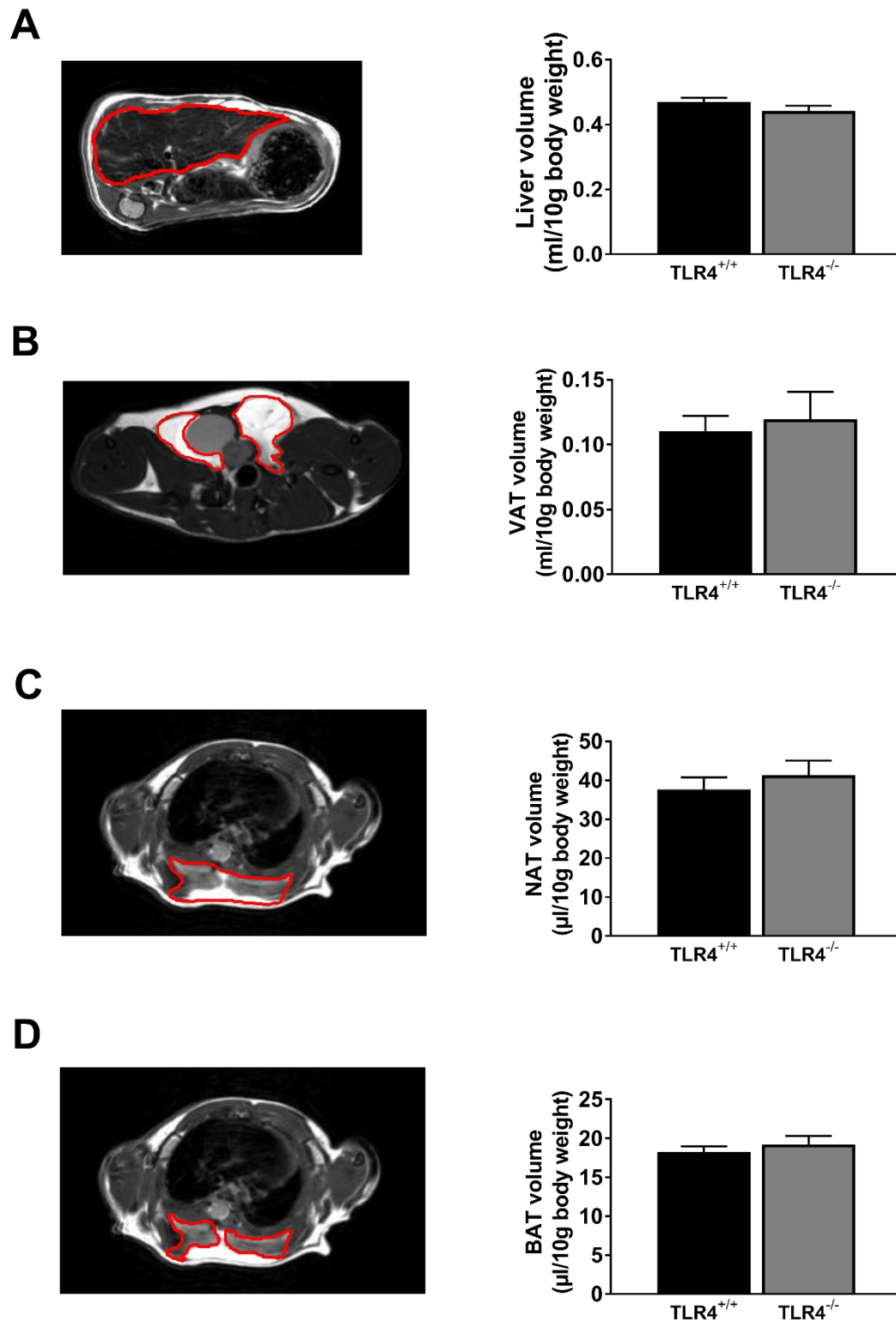


**Figure 26: Volumes of liver, VAT, NAT and BAT of female prediabetic NOD TLR4<sup>+/+</sup> and NOD TLR4<sup>-/-</sup> mice.** The volumes of the liver and fat depots were measured by encircling the tissue shapes in each MRI-derived slice in axial direction and analyzing each slice to determine the entire tissue volume in female prediabetic NOD TLR4<sup>+/+</sup> and NOD TLR4<sup>-/-</sup> mice. The volumes of liver (A), VAT (B), NAT (C) and BAT (D) were determined in NOD TLR4<sup>+/+</sup> and TLR4<sup>-/-</sup> mice. Data are given as means  $\pm$  SEM. n=6.

### 3.1.11 Body fat mass

To analyze the potential effect of TLR4-expression on body fat mass development, the body composition of female prediabetic NOD TLR4<sup>+/+</sup> and NOD TLR4<sup>-/-</sup> mice was determined at the age of 30 and 70 days by NMR. At the two time points, the proportion of fat free mass was comparable in both genotypes in a range between 81.5±0.8 and 84.4±0.7 %. The amount of the total fat mass was also comparable in a range between 12.3±0.5 and 13.6±0.5 % for both genotypes and the two time points (Figure 27).

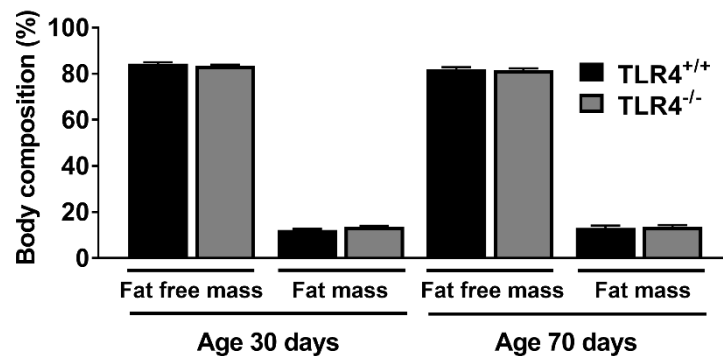


**Figure 27: Comparable body composition of female NOD TLR4<sup>+/+</sup> and NOD TLR4<sup>-/-</sup> mice at 30 and 70 days of age.** The body composition of 30 and 70 days old female NOD TLR4<sup>+/+</sup> and NOD TLR4<sup>-/-</sup> mice was analyzed by differentiating in fat free mass and fat mass by NMR. Data show the proportion of fat free mass and fat mass as percent of the whole body weight. Data are given as means ± SEM. n=7-11.

### 3.1.12 Glucose metabolism

To investigate the effect of the TLR4-expression status on parameters of the glucose metabolism in female NOD TLR4<sup>+/+</sup> and NOD TLR4<sup>-/-</sup> mice before the age of diabetes manifestation at the age of 70-90 days, random blood glucose levels were determined and the degrees of glucose tolerance and insulin resistance were assessed. Blood glucose levels of 90-250 mg/dl were considered as normal range, whereas blood glucose levels above 250 mg/dl indicated hyperglycemia (and diabetes).

#### 3.1.12.1 Random blood glucose levels

Random blood glucose concentrations of non-fasted female prediabetic NOD TLR4<sup>+/+</sup> and NOD TLR4<sup>-/-</sup> mice were determined in the morning between 9 and 11 am, to examine the possible impact of the TLR4 expression status on the blood glucose metabolism. NOD TLR4<sup>-/-</sup> mice showed increased blood glucose concentrations compared to NOD TLR4<sup>+/+</sup> mice (TLR4<sup>+/+</sup>: 113±3; TLR4<sup>-/-</sup>: 123±3 mg/dl) (p<0.05) (Figure 28).

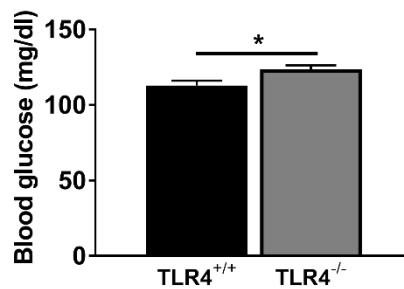


**Figure 28: Increased random blood glucose levels in NOD TLR4<sup>-/-</sup> compared to NOD TLR4<sup>+/+</sup> mice.** The random blood glucose levels were measured in non-fasted female prediabetic mice at the age of 70-90 days. Data are given as means  $\pm$  SEM. n=13-21. \*p<0.05 by Student's t-test.

### 3.1.12.2 Plasma glucose levels during ipGTT

To assess the glucose tolerance of NOD TLR4<sup>+/+</sup> and NOD TLR4<sup>-/-</sup> mice, an ipGTT was performed. After 6 hours of fasting, 70-90 days old normoglycemic mice were injected intraperitoneally with 2 g/kg body weight glucose and the blood glucose levels were measured at time point 0 (baseline, before glucose injection) and 5, 15, 30, 60, 90 and 120 minutes after injection. The basal blood glucose levels of fasted NOD TLR4<sup>+/+</sup> and NOD TLR4<sup>-/-</sup> mice were in a similar range (TLR4<sup>+/+</sup>: 89 $\pm$ 6; TLR4<sup>-/-</sup>: 87 $\pm$ 4 mg/dl) (Figure 29A). Interestingly, compared to NOD TLR4<sup>+/+</sup> mice, NOD TLR4<sup>-/-</sup> mice had higher blood glucose levels at time points 5 minutes (TLR4<sup>+/+</sup>: 115 $\pm$ 7; TLR4<sup>-/-</sup>: 144 $\pm$ 7 mg/dl) and 15 minutes (TLR4<sup>+/+</sup>: 157 $\pm$ 13; TLR4<sup>-/-</sup>: 202 $\pm$ 11 mg/dl) after glucose injection (both p<0.05). After 90 minutes, the blood glucose levels of both, NOD TLR4<sup>+/+</sup> and NOD TLR4<sup>-/-</sup> mice, have returned to baseline concentrations (at 0 minutes) (TLR4<sup>+/+</sup>: 93 $\pm$ 7; TLR4<sup>-/-</sup>: 83 $\pm$ 4 mg/dl) (Figure 29A).

The area under the curve (TLR4<sup>+/+</sup>: 7335 $\pm$ 734; TLR4<sup>-/-</sup>: 8867 $\pm$ 246 mg\*dl<sup>-1</sup>\*120 min<sup>-1</sup>) and the incremental area under the curve, which can be divided into the total area (TLR4<sup>+/+</sup>: 2174 $\pm$ 685; TLR4<sup>-/-</sup>: 3677 $\pm$ 381 mg\*dl<sup>-1</sup>\*120 min<sup>-1</sup>) and net area (TLR4<sup>+/+</sup>: 2019 $\pm$ 766; TLR4<sup>-/-</sup>: 3677 $\pm$ 381 mg\*dl<sup>-1</sup>\*120 min<sup>-1</sup>), showed no differences of the blood glucose levels during ipGTT between the different genotypes (Figure 29B-D).

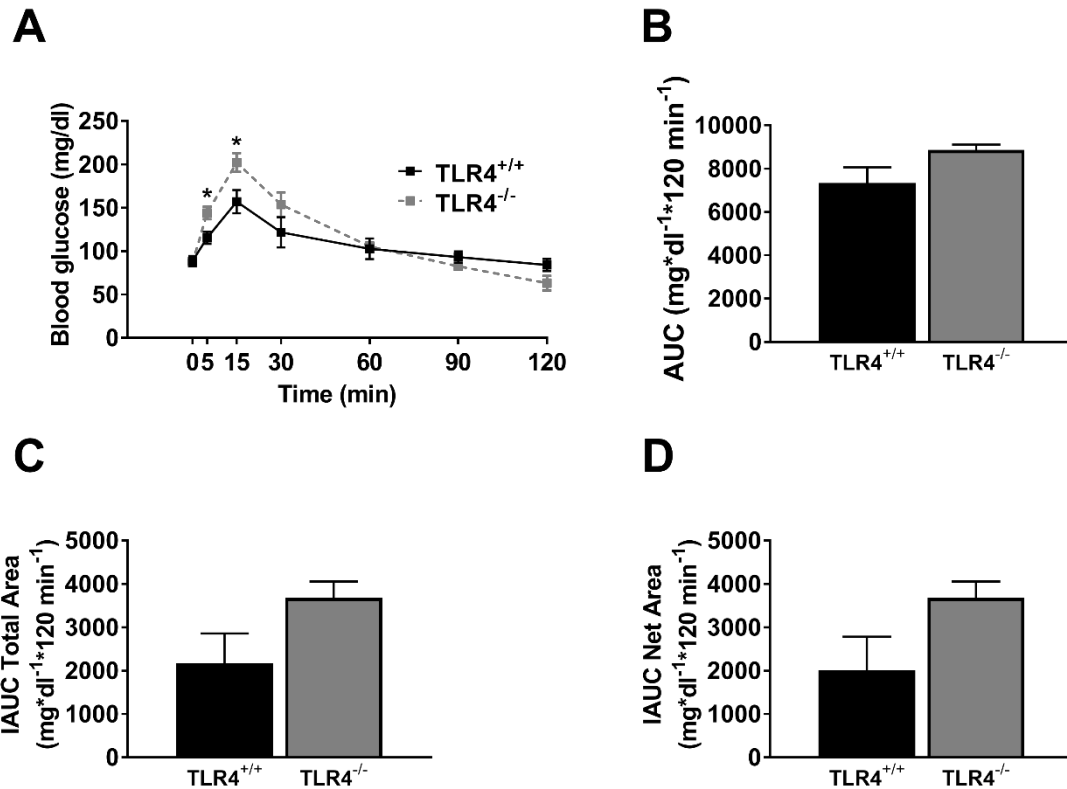


**Figure 29: Increased blood glucose levels during an intraperitoneal glucose tolerance test in NOD TLR4<sup>-/-</sup> mice compared to NOD TLR4<sup>+/+</sup> mice.** After a 6-hour period of fasting, an intraperitoneal glucose tolerance test was performed by injecting 2 g/kg body weight glucose intraperitoneally into female prediabetic NOD TLR4<sup>+/+</sup> and NOD TLR4<sup>-/-</sup> mice. The blood glucose concentration was measured over 120 minutes (A). The area under the curve (AUC) was calculated in mg\*dl<sup>-1</sup>\*120min<sup>-1</sup> (B). The incremental area under the curve was determined in the above mentioned mice and divided into the total area (positive peaks plus negative peaks) (C) and the net area (positive peaks minus negative peaks) in mg\*dl<sup>-1</sup>\*120min<sup>-1</sup> (D). Data are given as means  $\pm$  SEM. n=4-5. \*p<0.05 by Student's t-test.

### 3.1.12.3 Plasma insulin levels during ipGTT

Plasma samples were collected from NOD TLR4<sup>+/+</sup> and NOD TLR4<sup>-/-</sup> mice during an ipGTT (chapter 3.1.12.2) before glucose injection and 15 minutes after glucose injection. The insulin concentrations in these samples were determined by ELISA. Before glucose injection, NOD TLR4<sup>+/+</sup> and NOD TLR4<sup>-/-</sup> mice showed comparable plasma insulin concentrations (TLR4<sup>+/+</sup>: 0.65 $\pm$ 0.12; TLR4<sup>-/-</sup>: 0.47 $\pm$ 0.12  $\mu$ g/l). However, 15 minutes after the glucose injection, NOD TLR4<sup>-/-</sup> mice showed a lower plasma insulin concentration compared to NOD TLR4<sup>+/+</sup> mice (TLR4<sup>-/-</sup>: 0.59 $\pm$ 0.08; TLR4<sup>+/+</sup>: 1.03 $\pm$ 0.15  $\mu$ g/l) (p<0.05) (Figure 30).

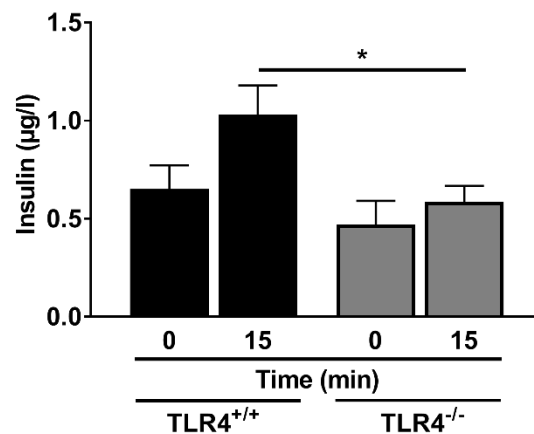


**Figure 30: Lower insulin levels 15 minutes after glucose injection in NOD TLR4<sup>-/-</sup> mice compared to NOD TLR4<sup>+/+</sup> mice.** After a 6-hour period of fasting, an intraperitoneal glucose tolerance test was performed by injecting 2 g/kg body weight glucose intraperitoneally into female prediabetic NOD TLR4<sup>+/+</sup> and NOD TLR4<sup>-/-</sup> mice. Plasma samples were collected at baseline (0, before glucose injection) and 15 minutes after injection and their insulin concentration was determined by ELISA. Data are given as means  $\pm$  SEM. n=5-7. \*p<0.05 by Student's t-test.

#### 3.1.12.4 HOMA-IR

The determination of the HOMA-IR index allows to assess insulin resistance. After 6 hours of fasting, the glucose concentration and the insulin concentration of NOD TLR4<sup>+/+</sup> and NOD TLR4<sup>-/-</sup> mice were determined to calculate the HOMA-IR. The HOMA-IR index was comparable in NOD TLR4<sup>+/+</sup> mice and NOD TLR4<sup>-/-</sup> mice (TLR4<sup>+/+</sup>: 4.28 $\pm$ 1.19; TLR4<sup>-/-</sup>: 3.39 $\pm$ 0.89) (Figure 31).

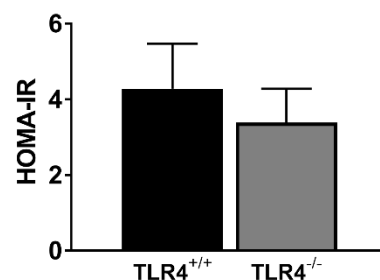


**Figure 31: Comparable HOMA-IR of female prediabetic NOD TLR4<sup>+/+</sup> and NOD TLR4<sup>-/-</sup> mice.** After a 6-hour period of fasting, the glucose concentration and the insulin concentration of female prediabetic NOD TLR4<sup>+/+</sup> and NOD TLR4<sup>-/-</sup> mice were determined to calculate the HOMA-IR. Data are given as means  $\pm$  SEM. n=5-7.

#### 3.1.12.5 Development of insulinitis and decline of beta cell mass in pancreatic islets

To analyze the effect of the TLR4-expression status on insulinitis and beta cell loss, sections of pancreatic tissue from female 70-90 days old NOD TLR4<sup>+/+</sup> and NOD TLR4<sup>-/-</sup> mice were examined by (immuno-) histochemical methods.

Evaluation of the total islet area revealed that NOD TLR4<sup>-/-</sup> mice had larger areas (53792±4834 μm<sup>2</sup>) compared to NOD TLR4<sup>+/+</sup> mice (38291±3778 μm<sup>2</sup>) (p<0.05) (Figure 32A). In addition, the insulin-positive areas of the pancreatic islets were determined to investigate the effect of the TLR4-expression status on the decline of the pancreatic beta-cell mass in NOD mice. However, there was no difference in the proportions of insulin-positive areas of the total islet area between the two genotypes (TLR4<sup>+/+</sup>: 56.6±1.2 %; TLR4<sup>-/-</sup>: 54.0±1.0 %) (Figure 32B).

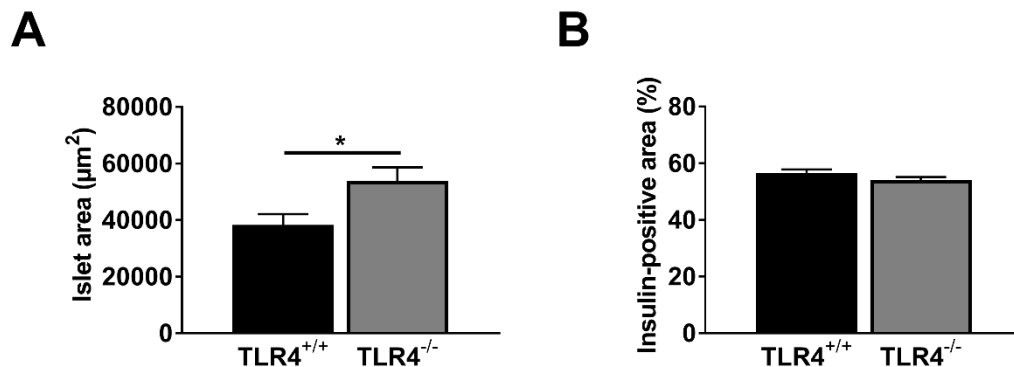


**Figure 32: Total area and insulin-positive area of pancreatic islets of NOD TLR4<sup>+/+</sup> and NOD TLR4<sup>-/-</sup> mice.** The total area of pancreatic islets was measured (A). The relative insulin positive area was measured in female prediabetic NOD TLR4<sup>+/+</sup> and NOD TLR4<sup>-/-</sup> mice (B). 339-425 pancreatic islets were analyzed per genotype. Islet areas less than 500 μm<sup>2</sup> were excluded. Data are given as means ± SEM. n=9-10. \*p<0.05 by Student's t-test.

The severity of islet inflammation was categorized into scores 0-3 based on the progression of inflammation. Score 0 defines non infiltrated islets, score 1 includes islets with an infiltration less than 10 % and peri-insulinitis, whereas score 2 reflects infiltration less than 50 % and score 3 infiltration more than 50 % (Figure 33A).

Furthermore, the degree of immune cell infiltration of pancreatic islets was determined in NOD TLR4<sup>+/+</sup> and NOD TLR4<sup>-/-</sup> mice. Affected islets of both genotypes were separated into their infiltration rate and showed comparable proportions for each range of infiltrated area (Figure 33B).

Pancreatic islets of NOD TLR4<sup>+/+</sup> and NOD TLR4<sup>-/-</sup> mice were categorized into four scores and their proportion of the total islet number was calculated. NOD TLR4<sup>+/+</sup> mice showed the highest area proportion of score 0 with 55.5 %, followed by NOD TLR4<sup>-/-</sup> mice with around 47.9 %. The lowest amount of islets with a proportion of around 3-6 % were assigned to score 1. About 40-50 % of the islets account for score 2 and score 3. There was no difference between the genotypes in the four categories (Figure 33C).

In addition, the correlation between islet area and insulinitis-score was determined. Independent of the TLR4-expression status, pancreatic islets with areas exceeding 200000 μm<sup>2</sup> showed predominantly higher infiltration rates reflected by scores 2 and 3 (p<0.001) (Figure 33D).

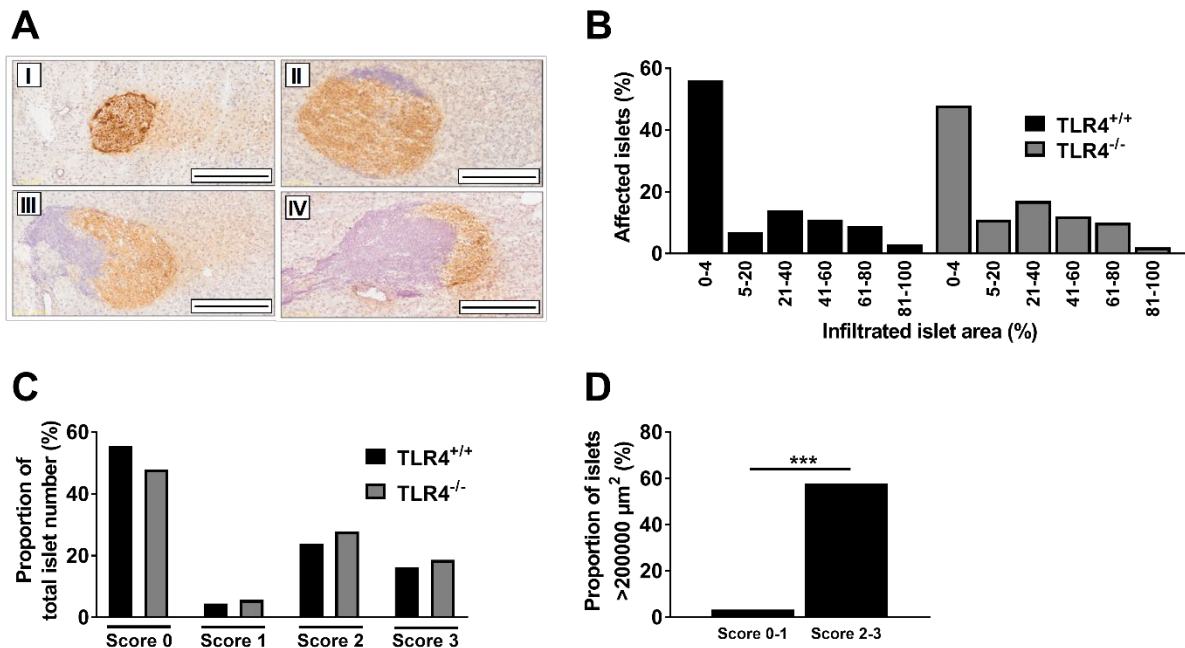


**Figure 33: Representative histological images of pancreatic islets and their classification into insulitis-scores, the infiltrated islet area and the association of islet area and insulitis-scores in NOD TLR4<sup>+/+</sup> and NOD TLR4<sup>-/-</sup> mice.** The insulitis score is shown (A) from a non-infiltrated islet (Score 0) (I), an islet with an infiltration area less than 10 % (Score 1) (II), an islet with an infiltration area less than 50 % (Score 2) (III) and with more than 50 % infiltration (Score 3) (IV). The scale bars represent 200  $\mu\text{m}^2$ . The amount of islets with a certain infiltration rate were analyzed from all examined animals and expressed as cumulative proportions of afflicted islets (B). The severity of insulitis was assessed by categorizing into four insulitis-scores: Score 0= no insulitis, 1= <10 % and peri-insulitis, 2= <50 % infiltration, 3= >50 % infiltration (C). The proportion of islets with an area >200000  $\mu\text{m}^2$  and scores 0-1 and 2-3 were determined (D). Islet areas less than 500  $\mu\text{m}^2$  were excluded. n= 9-10. \*\*\*p<0.001 by Fisher's exact test.

### 3.1.12.6 Effect of isoflurane-anesthesia on glucose metabolism

In pilot-studies for the MRS/MRI measurements, the effect of the anesthetic isoflurane on the blood glucose concentration was examined in female prediabetic 70-90 days old NOD TLR4<sup>+/+</sup> and NOD TLR4<sup>-/-</sup> mice during an ipGTT. After 6 hours of fasting, mice were anesthetized with isoflurane (anesthetized animals) and injected with either glucose (2 g/kg body weight) or equal volumes of NaCl. The blood glucose concentrations were documented at -15 minutes (baseline, before initiation of anesthesia), 0 (15 minutes in anesthesia, before glucose injection) and 5, 15, 30, 60, 90, and 120 minutes after glucose injection. Before isoflurane administration at -15 minutes, fasted NOD TLR4<sup>+/+</sup> and NOD TLR4<sup>-/-</sup> mice showed comparable blood glucose levels in a normal range between 80-127 mg/dl (Figure 34A,B). Anesthesia by isoflurane inhalation was initiated immediately after blood glucose measurements at -15 minutes. At 0 minutes, the mice were injected intraperitoneally with either a glucose- or 0.9 % NaCl solution. As shown in Figure 34A, at 0 minutes, anesthetized NOD TLR4<sup>+/+</sup> mice injected with NaCl (234 $\pm$ 21 mg/dl) showed higher blood glucose concentrations compared to unanesthetized NOD TLR4<sup>+/+</sup> mice injected with glucose (89 $\pm$ 6 mg/dl) (p<0.001). At 5 minutes after injections, anesthetized NOD TLR4<sup>+/+</sup> mice injected with glucose showed higher blood

## Results

glucose levels ( $259\pm 37$  mg/dl) compared to unanesthetized NOD TLR4<sup>+/+</sup> mice injected with glucose ( $115\pm 7$  mg/dl) ( $p < 0.001$ ). From 15 minutes until 120 minutes after injections, anesthetized NOD TLR4<sup>+/+</sup> mice injected with glucose showed higher blood glucose concentrations compared to anesthetized NOD TLR4<sup>+/+</sup> mice injected with NaCl and unanesthetized NOD TLR4<sup>+/+</sup> mice injected with glucose ( $p < 0.001$ ). After 30 minutes, anesthetized NOD TLR4<sup>+/+</sup> mice injected with glucose showed a blood glucose maximum of  $451\pm 19$  mg/dl compared to anesthetized NOD TLR4<sup>+/+</sup> mice injected with NaCl ( $187\pm 18$  mg/dl) and unanesthetized NOD TLR4<sup>+/+</sup> mice injected with glucose ( $122\pm 18$  mg/dl) ( $p < 0.001$ ). Nonlinear regression analysis revealed that the three curves were different ( $p < 0.001$ ) (Figure 34A). At 0 minutes, anesthetized NOD TLR4<sup>-/-</sup> mice (Glucose injection group:  $168\pm 5$ ; NaCl injection group:  $185\pm 17$  mg/dl) showed “similar” glucose concentrations compared to unanesthetized NOD TLR4<sup>-/-</sup> mice injected with glucose ( $87\pm 4$  mg/dl) (Figure 34B). At 5 minutes after injection, anesthetized NOD TLR4<sup>-/-</sup> mice injected with glucose ( $274\pm 24$  mg/dl) showed higher blood glucose levels compared to unanesthetized NOD TLR4<sup>-/-</sup> mice injected with glucose ( $144\pm 7$  mg/dl) ( $p < 0.05$ ). After 15 minutes until 120 minutes, anesthetized NOD TLR4<sup>-/-</sup> mice injected with glucose showed higher blood glucose concentrations compared to anesthetized NOD TLR4<sup>-/-</sup> mice injected with NaCl and unanesthetized NOD TLR4<sup>-/-</sup> mice injected with glucose ( $p < 0.001$ ). After 30 minutes, anesthetized NOD TLR4<sup>-/-</sup> mice injected with glucose showed a blood glucose maximum of  $414\pm 18$  mg/dl compared to anesthetized NOD TLR4<sup>-/-</sup> mice injected with NaCl ( $166\pm 15$  mg/dl) and unanesthetized NOD TLR4<sup>-/-</sup> mice injected with glucose ( $154\pm 14$  mg/dl) ( $p < 0.001$ ). Nonlinear regression analysis revealed that the three curves were different ( $p < 0.05-0.001$ ) (Figure 34B). Comparison of the blood glucose curves of anesthetized NOD TLR4<sup>+/+</sup> and NOD TLR4<sup>-/-</sup> mice injected with glucose revealed similar blood glucose concentrations over the period of 120 minutes (Figure 34C). The kinetics of blood glucose levels of anesthetized NOD TLR4<sup>+/+</sup> and TLR4<sup>-/-</sup> mice injected with NaCl also showed comparable blood glucose levels over the period of 120 minutes (Figure 34D).

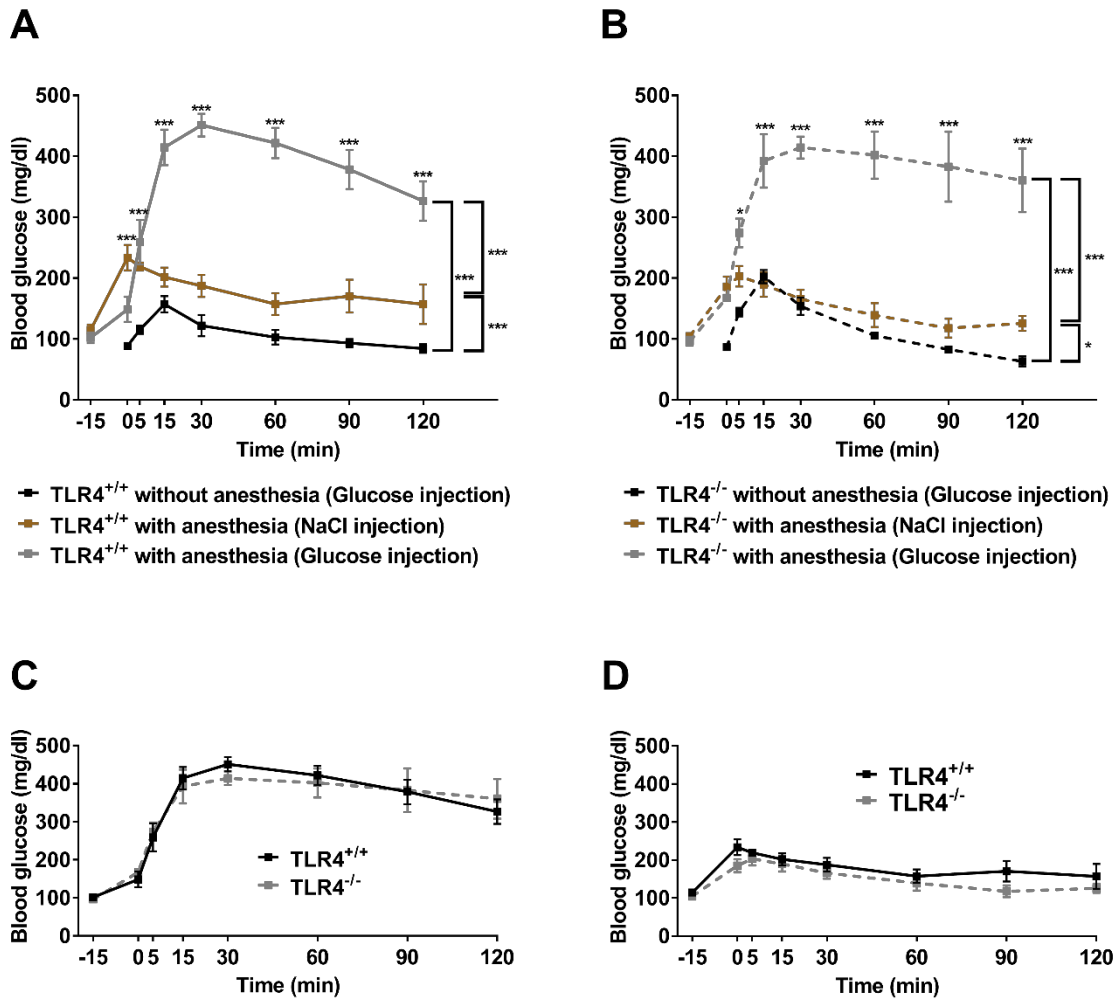


**Figure 34: The effect of the anesthetic isoflurane on the blood glucose levels during an ipGTT in female prediabetic NOD TLR4<sup>+/+</sup> and NOD TLR4<sup>-/-</sup> mice.** The blood glucose levels of female prediabetic NOD TLR4<sup>+/+</sup> mice (A) and NOD TLR4<sup>-/-</sup> mice (B) unanesthetized (black curve), with anesthesia and NaCl injection (brown curve) and with anesthesia and glucose injection (grey curve) were determined. The blood glucose levels of NOD TLR4<sup>+/+</sup> and NOD TLR4<sup>-/-</sup> mice under isoflurane inhalation with glucose injection (C) and with NaCl injection (D) were compared. Data are given as means  $\pm$  SEM.  $n=3-5$ . \* $p<0.05$ , \*\*\* $p<0.001$  by one-way ANOVA and nonlinear regression.

At the end of the observation period, at 120 minutes, glucose-treated unanesthetized NOD TLR4<sup>+/+</sup> mice (0 min:  $89\pm 6$ ; 120 min:  $84\pm 7$  mg/dl) and anesthetized NOD TLR4<sup>+/+</sup> mice with NaCl injection (0 min:  $115\pm 9$ ; 120 min:  $157\pm 33$  mg/dl) showed blood glucose concentrations comparable to the levels at the beginning of the experiment (Figure 35A). Interestingly, anesthetized NOD TLR4<sup>+/+</sup> mice with glucose injection did not return to their initial blood glucose levels, but showed higher blood glucose concentrations at the end ( $327\pm 32$  mg/dl) compared to the beginning of the experiment ( $102\pm 9$  mg/dl) ( $p<0.001$ ). Glucose treated anesthetized NOD TLR4<sup>+/+</sup> mice ( $327\pm 32$  mg/dl) showed higher blood glucose levels at 120 minutes than either NaCl-treated anesthetized NOD TLR4<sup>+/+</sup> mice ( $157\pm 33$  mg/dl) or glucose-treated unanesthetized NOD TLR4<sup>+/+</sup> mice ( $84\pm 7$  mg/dl) (both  $p<0.001$ ) (Figure 35A).

## Results

Glucose-treated unanesthetized NOD TLR4<sup>-/-</sup> mice (0 min: 87±4; 120 min: 63±9 mg/dl) and anesthetized NOD TLR4<sup>-/-</sup> mice injected with NaCl (0 min: 105±6; 120 min: 126±12 mg/dl) showed comparable blood glucose concentrations at the beginning and at the end of the experiment (Figure 35B). In anesthetized NOD TLR4<sup>-/-</sup> mice injected with glucose, the blood glucose levels at the end of the experiment (360±52 mg/dl) were higher than at the beginning (97±7 mg/dl) ( $p < 0.001$ ). Glucose-treated anesthetized NOD TLR4<sup>-/-</sup> mice, showed higher blood glucose levels at 120 minutes (360±52 mg/dl) than either NaCl-treated anesthetized NOD TLR4<sup>-/-</sup> mice (126±12 mg/dl) or glucose-treated unanesthetized NOD TLR4<sup>-/-</sup> mice (63±9 mg/dl) (both  $p < 0.001$ ) (Figure 35B).

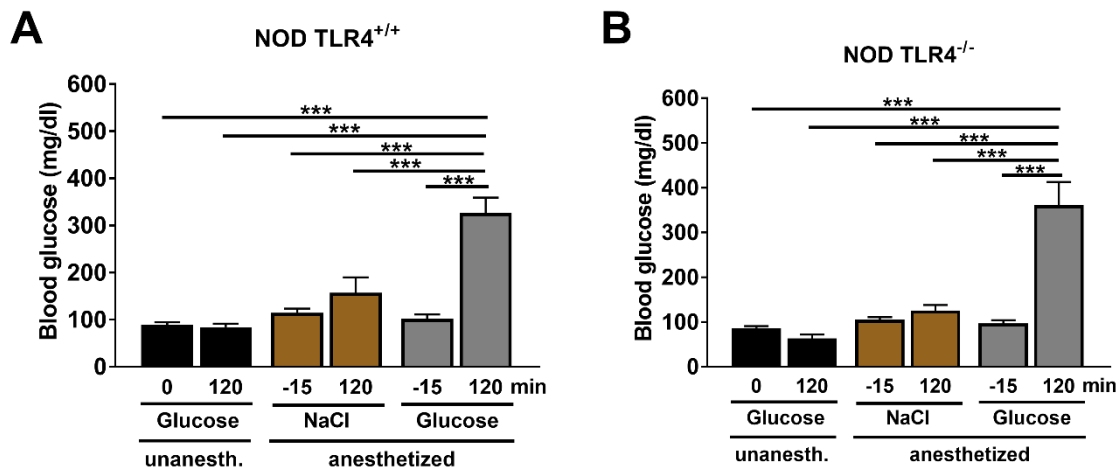


**Figure 35: Effect of isoflurane anesthesia on blood glucose levels of NOD TLR4<sup>+/+</sup> and NOD TLR4<sup>-/-</sup> mice at the beginning and the end of an ipGTT.** The blood glucose levels of NOD TLR4<sup>+/+</sup> mice (A) and NOD TLR4<sup>-/-</sup> mice (B) without anesthesia (black bars), with anesthesia and NaCl injection (brown bars) and with anesthesia and glucose injection (grey bars) were determined at the beginning (0 minutes) and the end (120 minutes) of an ipGTT. Data are given as means ± SEM. n=3-5. \*\*\* $p < 0.001$  by one-way ANOVA.

For further comparison of the blood glucose concentrations, the area (AUC) and the incremental area (iAUC) under the respective concentration-time curves were determined (Figure 36A). The iAUC was calculated as total area (positive peaks plus negative peaks). The calculation of the AUC showed, that anesthetized NOD TLR4<sup>+/+</sup> mice with an injection of either NaCl (23760±2483 mg/(dl x 2h)) ( $p < 0.05$ ) or glucose (48436±3245 mg/(dl x 2h)) ( $p < 0.001$ ) showed higher blood glucose concentrations during the ipGTT compared to glucose-treated unanesthetized mice (12936±1058 mg/(dl x 2h)). Additionally, the blood glucose levels of anesthetized NOD TLR4<sup>+/+</sup> mice injected with glucose were higher during the ipGTT compared to anesthetized mice injected with NaCl ( $p < 0.001$ ). The determination of the iAUC (total area) showed, that glucose-treated anesthetized NOD TLR4<sup>+/+</sup> mice (34666±2696 mg/(dl x 2h)) showed higher blood glucose concentrations during the ipGTT compared to NaCl-treated anesthetized mice (10794±3879 mg/(dl x 2h)) and glucose-treated unanesthetized mice (3270±835 mg/(dl x 2h)) ( $p < 0.001$ ) (Figure 36A). The calculation of the AUC in NOD TLR4<sup>-/-</sup>

## Results

mice showed, that glucose-treated anesthetized mice ( $47635 \pm 3486$  mg/(dl x 2h)) showed higher blood glucose concentrations during the ipGTT compared to NaCl-treated anesthetized mice ( $19843 \pm 1990$  mg/(dl x 2h)) and glucose-treated unanesthetized mice ( $13880 \pm 450$  mg/(dl x 2h)) ( $p < 0.001$ ) (Figure 36B). There was no difference in the AUC between NaCl-treated anesthetized NOD TLR4<sup>-/-</sup> mice and glucose-treated unanesthetized mice. The determination of the iAUC (total area) showed, that glucose-treated anesthetized NOD TLR4<sup>-/-</sup> mice ( $34607 \pm 4285$  mg/(dl x 2h)) showed higher blood glucose concentrations during the ipGTT compared to NaCl-treated anesthetized mice ( $6143 \pm 1537$  mg/(dl x 2h)) and glucose-treated unanesthetized mice ( $4440 \pm 405$  mg/(dl x 2h)) ( $p < 0.001$ ) (Figure 36B).

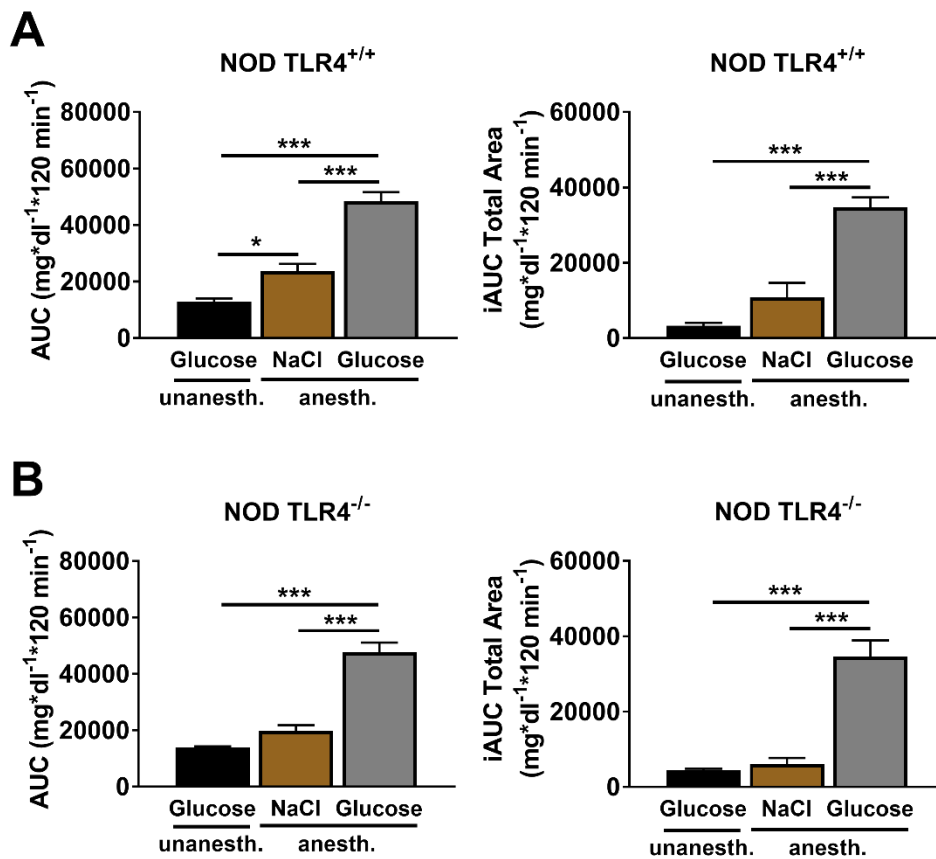


**Figure 36: Area under the glucose concentration time curve and incremental area under the curve of an ipGTT in female prediabetic NOD TLR4<sup>+/+</sup> and NOD TLR4<sup>-/-</sup> mice.** The area and the incremental area under the respective concentration-time curves were determined in female prediabetic NOD TLR4<sup>+/+</sup> (A) and NOD TLR4<sup>-/-</sup> mice (B) without anesthesia but glucose injection and with anesthesia treatment with either NaCl injection or glucose injection. The incremental area under the curve was determined in the above-mentioned groups of mice and shown as total area. Data are given as means  $\pm$  SEM.  $n=4-5$ . \* $p < 0.05$ , \*\*\* $p < 0.001$  by one-way ANOVA.

### 3.1.12.7 Effect of isoflurane-anesthesia on plasma insulin levels

The effect of anesthesia by isoflurane on plasma insulin levels during an ipGTT was determined in female prediabetic 70-90 days old NOD-TLR4<sup>+/+</sup> and NOD TLR4<sup>-/-</sup> mice. The plasma insulin levels were measured 15 minutes after initiation of anesthesia (15 min) and again 15 minutes after glucose injection (30 min). After 15 minutes of anesthesia, NOD TLR4<sup>-/-</sup> mice showed higher plasma insulin levels compared to NOD TLR4<sup>+/+</sup> mice (TLR4<sup>+/+</sup>: 1.13±0.20; TLR4<sup>-/-</sup>: 2.13±0.03 µg/l) (p<0.05). After glucose injection, NOD TLR4<sup>-/-</sup> mice showed higher plasma insulin levels compared to NOD TLR4<sup>+/+</sup> mice (TLR4<sup>+/+</sup>: 1.08±0.20; TLR4<sup>-/-</sup>: 2.03±0.18 µg/l) (p<0.05). No difference was detectable in insulin levels before (15 min) and after glucose injection (30 min) in NOD TLR4<sup>+/+</sup> and NOD TLR4<sup>-/-</sup> mice (Figure 37).

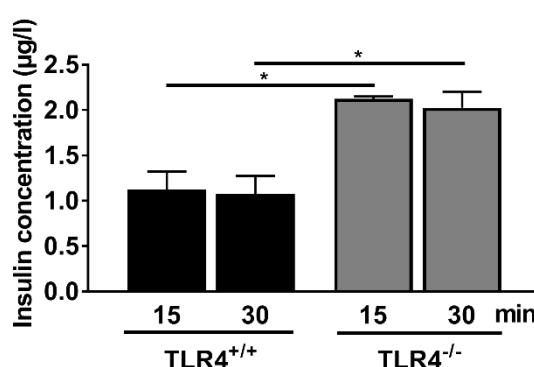


**Figure 37: Effect of isoflurane anesthesia on plasma insulin levels in female prediabetic NOD TLR4<sup>+/+</sup> and NOD TLR4<sup>-/-</sup> mice.** Plasma insulin concentrations were measured in female prediabetic NOD TLR4<sup>+/+</sup> and NOD TLR4<sup>-/-</sup> mice at 15 and 30 minutes after glucose injection. Data are given as means ± SEM. n=2-4. \*p<0.05 by Student's t-test.

### 3.1.13 Effect of the TLR4-expression status on lipid metabolism

To investigate the possible effect of the TLR4-expression status on lipid homeostasis, plasma samples of non-fasted female prediabetic 70-90 days old NOD TLR4<sup>+/+</sup> and NOD TLR4<sup>-/-</sup> mice were analyzed for parameters of lipid metabolism such as FFA, TG, HDL and LDL.

#### 3.1.13.1 Plasma free fatty acid and triglyceride levels

Plasma FFA and TG levels were analyzed from samples of non-fasted female prediabetic NOD TLR4<sup>+/+</sup> and NOD TLR4<sup>-/-</sup> mice. NOD TLR4<sup>+/+</sup> and NOD TLR4<sup>-/-</sup> mice showed comparable FFA concentrations in the plasma (TLR4<sup>+/+</sup>: 741.9±82.0; TLR4<sup>-/-</sup>: 920.7±102.4 µmol/l) (Figure 38A). Additionally, similar TG concentrations in the plasma of NOD TLR4<sup>+/+</sup> and NOD TLR4<sup>-/-</sup> mice were found (TLR4<sup>+/+</sup>: 143.1±12.2; TLR4<sup>-/-</sup>: 160.6±15.1 mg/dl) (Figure 38B).

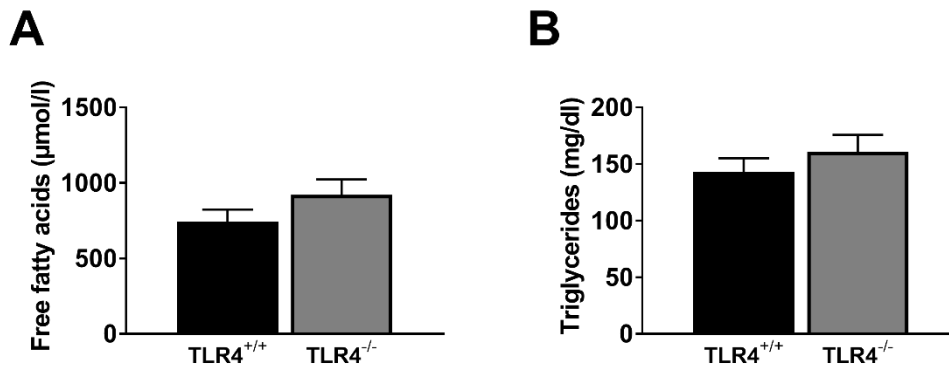


**Figure 38: Comparable plasma free fatty acid and triglyceride levels in female prediabetic NOD TLR4<sup>+/+</sup> and NOD TLR4<sup>-/-</sup> mice.** Free fatty acid levels in µmol/l (A) and triglyceride concentrations in mg/dl (B) were measured in the plasma of non-fasted female prediabetic NOD TLR4<sup>+/+</sup> and NOD TLR4<sup>-/-</sup> mice at the age of 70-90 days. Data are given as means ± SEM. n=10.

### 3.1.13.2 Plasma levels of cholesterol, HDL, LDL and CRP

Plasma samples of female prediabetic NOD TLR4<sup>+/+</sup> and NOD TLR4<sup>-/-</sup> mice, aged 70-90 days, were analyzed for their cholesterol, HDL, LDL and CRP levels. NOD TLR4<sup>+/+</sup> and NOD TLR4<sup>-/-</sup> mice showed comparable cholesterol concentrations (TLR4<sup>+/+</sup>: 78.3±2.4; TLR4<sup>-/-</sup>: 75.4±2.0 mg/dl) (Figure 39A). Plasma HDL and LDL analyses revealed no difference between NOD TLR4<sup>+/+</sup> and NOD TLR4<sup>-/-</sup> mice (HDL: TLR4<sup>+/+</sup>: 48.9±1.6; TLR4<sup>-/-</sup>: 50.4±1.4 mg/dl; LDL: TLR4<sup>+/+</sup>: 10.9±0.28; TLR4<sup>-/-</sup>: 10.4±0.36 mg/dl) (Figure 39B,C). Furthermore, NOD TLR4<sup>+/+</sup> and NOD TLR4<sup>-/-</sup> mice showed similar plasma levels of CRP (TLR4<sup>+/+</sup>: 0.126±0.030; TLR4<sup>-/-</sup>: 0.128±0.029 mg/dl) (Figure 39D).

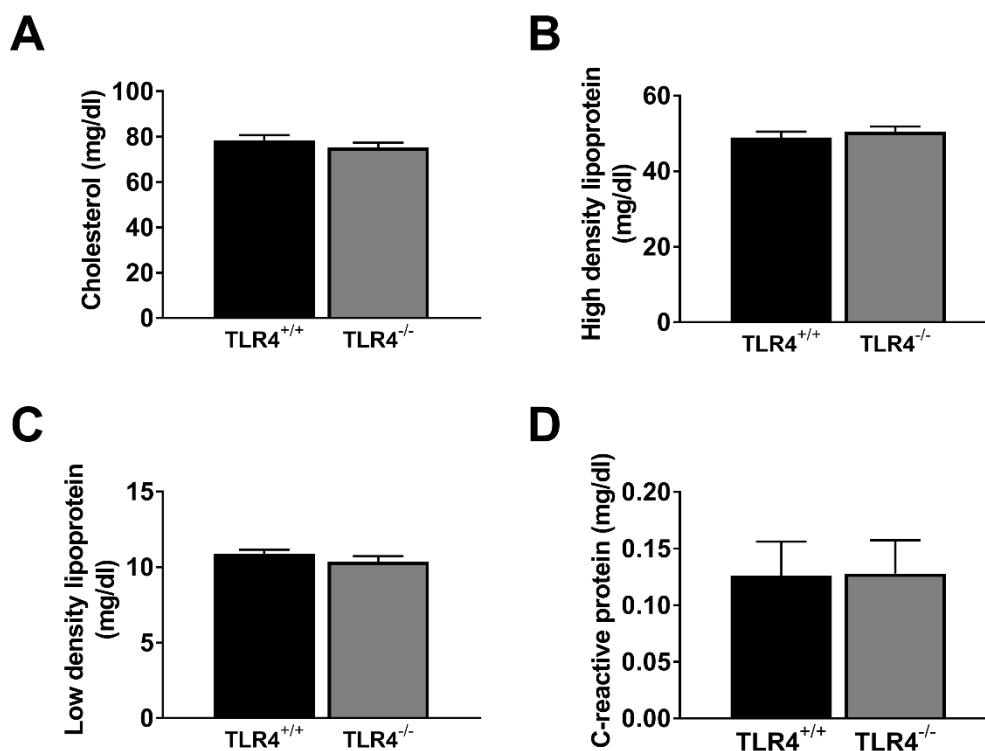
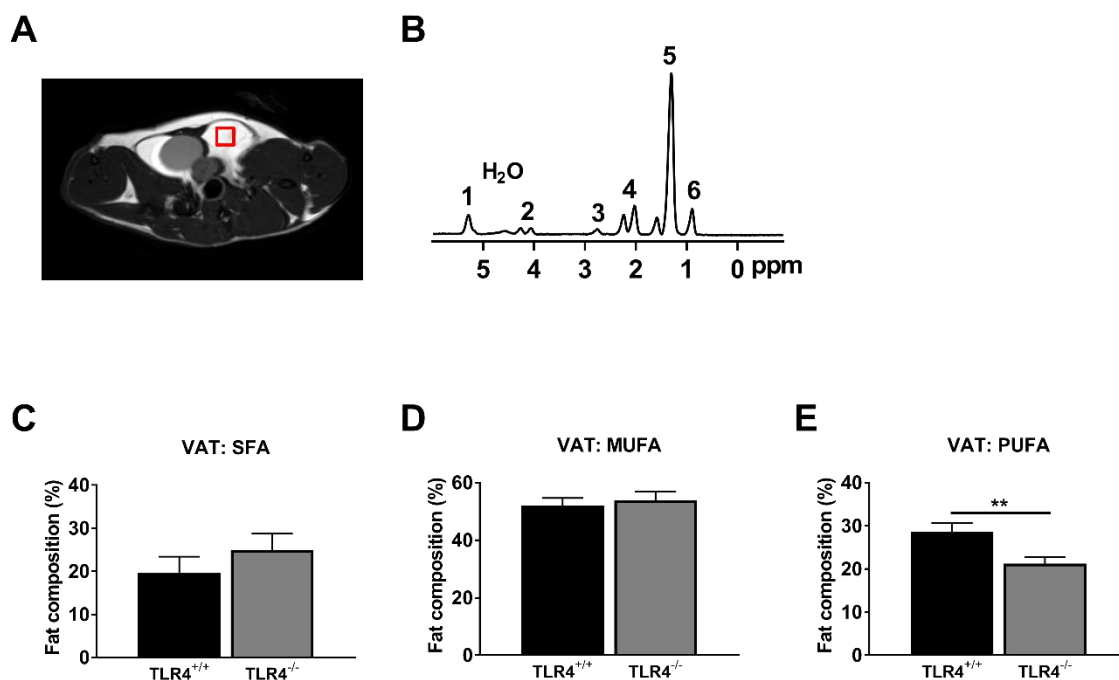


**Figure 39: Comparable plasma cholesterol, high and low density lipoprotein and C-reactive protein levels in female prediabetic NOD TLR4<sup>+/+</sup> and NOD TLR4<sup>-/-</sup> mice.** Concentrations of cholesterol in mg/dl (A), high density lipoprotein in mg/dl (B), low density lipoprotein in mg/dl (C) and C-reactive protein in mg/dl (D) were measured in the plasma of female prediabetic NOD TLR4<sup>+/+</sup> and NOD TLR4<sup>-/-</sup> mice. Data are given as means  $\pm$  SEM. n=10.

### 3.1.13.3 Composition of fat depots

To analyze a possible effect of the TLR4-expression status on lipid composition of different fat depots, <sup>1</sup>H MRS was applied in female prediabetic 70-90 days old NOD TLR4<sup>+/+</sup> and NOD TLR4<sup>-/-</sup> mice. Fat depots including VAT, NAT (BAT and WAT) and BAT were visualized and their SFA, MUFA and PUFA contents were quantified.

The voxel positioning in axial direction in the VAT depot of the mice to measure the FA composition is shown in Figure 40A and Figure 40B shows a representative <sup>1</sup>H MRS spectrum of VAT with the H<sub>2</sub>O reference peak. The peak assignments of SFA, MUFA and PUFA with location and type were determined (Table 12). NOD TLR4<sup>+/+</sup> and NOD TLR4<sup>-/-</sup> mice showed comparable proportions of SFA (TLR4<sup>+/+</sup>: 19.6 $\pm$ 3.8; TLR4<sup>-/-</sup>: 24.9 $\pm$ 3.9 %) and MUFA (TLR4<sup>+/+</sup>: 52.1 $\pm$ 2.6; TLR4<sup>-/-</sup>: 53.9 $\pm$ 3.0 %) in VAT (Figure 40C,D). Interestingly, NOD TLR4<sup>-/-</sup> mice showed a lower percentage of PUFA in VAT compared to NOD TLR4<sup>+/+</sup> mice (TLR4<sup>+/+</sup>: 21.2 $\pm$ 1.5; TLR4<sup>-/-</sup>: 28.7 $\pm$ 2.0 %) (p<0.01) (Figure 40E).



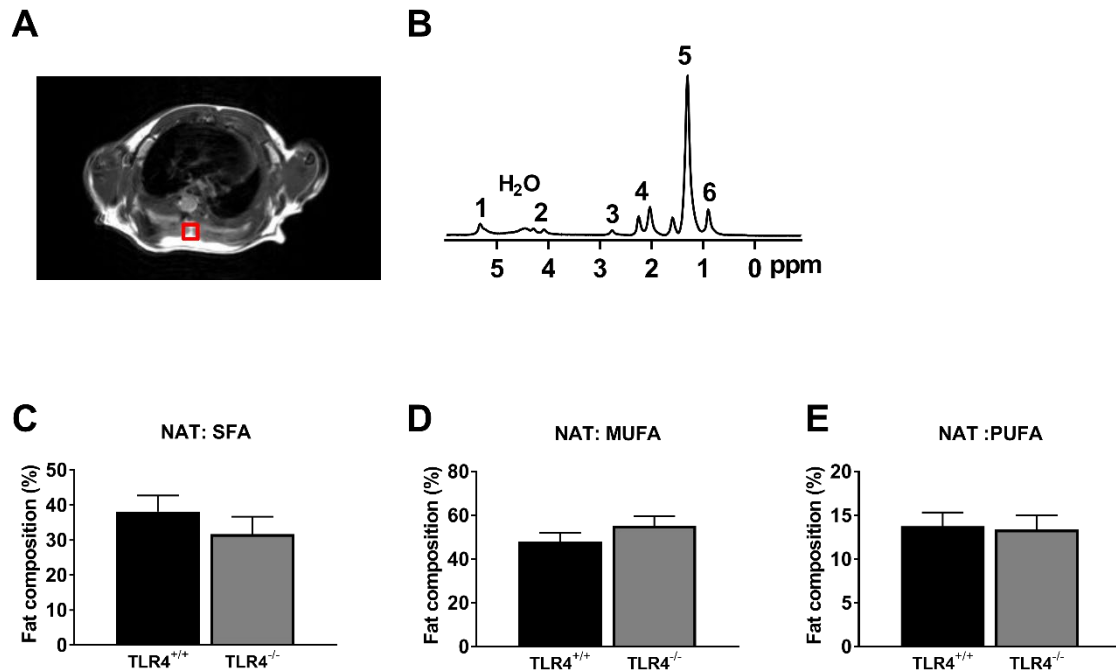
**Figure 40: Effect of the TLR4-expression status on fat composition of VAT in female prediabetic NOD TLR4<sup>+/+</sup> and NOD TLR4<sup>-/-</sup> mice.** Voxel positioning in axial direction in VAT to determine the FA composition (A) and a representative <sup>1</sup>H MRS VAT spectrum with fat peak assignments (B). Fat peak assignment: 1: -CH=CH- and -CH-O-CO-, 2: -CH<sub>2</sub>-O-CO-, 3: -CH=CH-CH<sub>2</sub>-CH=CH-, 4: -CO-CH<sub>2</sub>-CH<sub>2</sub>- and -CH<sub>2</sub>-CH=CH-CH<sub>2</sub>-, 5: -CO-CH<sub>2</sub>-CH<sub>2</sub>- and -(CH<sub>2</sub>)<sub>n</sub>-, 6: -(CH<sub>2</sub>)<sub>n</sub>-CH<sub>3</sub> [214]. The percentage of SFA (C), MUFA (D) and PUFA (E) of total FA (total FA= 100 %) in VAT in NOD TLR4<sup>+/+</sup> and NOD TLR4<sup>-/-</sup> mice was determined by MRS (Table 12). Data are given as means ± SEM. n=11-19. \*\*p<0.01 by Student's t-test.

Table 12: Peak assignments with location (ppm) and type [214].

Peak	Location (ppm)	Assignment	Type
1	5.29	-CH=CH-	Olefinic
	5.19	-CH-O-CO-	Glycerol
Water	4.70	H <sub>2</sub> O	-
2	4.20	-CH <sub>2</sub> -O-CO-	Glycerol
3	2.75	-CH=CH-CH <sub>2</sub> -	Diacyl
		CH=CH-	
4	2.24	-CO-CH <sub>2</sub> -CH <sub>2</sub> -	α-Carboxyl
	2.02	-CH <sub>2</sub> -CH=CH-CH <sub>2</sub> -	α-Olefinic
5	1.60	-CO-CH <sub>2</sub> -CH <sub>2</sub> -	β-Carboxyl
	1.30	-(CH <sub>2</sub> ) <sub>n</sub> -	Methylene
6	0.90	-(CH <sub>2</sub> ) <sub>n</sub> -CH <sub>3</sub>	Methyl

To measure the FA composition in the NAT, which consists of the WAT and BAT depots, the voxel was positioned in axial direction in the NAT depot of the NOD TLR4<sup>+/+</sup> and NOD TLR4<sup>-/-</sup> mice (Figure 41A). A representative <sup>1</sup>H MRS spectrum of NAT with the H<sub>2</sub>O reference peak is shown in Figure 41B. The peak assignments for SFA, MUFA and PUFA were determined with their location and type (Table 12). NOD TLR4<sup>+/+</sup> mice and NOD TLR4<sup>-/-</sup> mice showed

comparable proportions of SFA (TLR4<sup>+/+</sup>: 38.2±4.6; TLR4<sup>-/-</sup>: 31.7±5.0 %), MUFA (TLR4<sup>+/+</sup>: 48.1±4.0; TLR4<sup>-/-</sup>: 55.1±4.6 %) and PUFA (TLR4<sup>+/+</sup>: 13.8±1.6; TLR4<sup>-/-</sup>: 13.4±1.7 %) in the NAT (Figure 41C-E).



**Figure 41: Effect of the TLR4-expression status on fat composition of the NAT in female prediabetic NOD TLR4<sup>+/+</sup> and NOD TLR4<sup>-/-</sup> mice.** Voxel positioning in axial direction in the NAT to determine the FA composition (A) and a representative <sup>1</sup>H MRS NAT spectrum with fat peak assignments (B). Fat peak assignment: 1: -CH=CH- and -CH-O-CO-, 2: -CH<sub>2</sub>-O-CO-, 3: -CH=CH-CH<sub>2</sub>-CH=CH-, 4: -CO-CH<sub>2</sub>-CH<sub>2</sub>- and -CH<sub>2</sub>-CH=CH-CH<sub>2</sub>-, 5: -CO-CH<sub>2</sub>-CH<sub>2</sub>- and -(CH<sub>2</sub>)<sub>n</sub>-, 6: -(CH<sub>2</sub>)<sub>n</sub>-CH<sub>3</sub> (Table 12). The percentage of SFA (C), MUFA (D) and PUFA (E) of total FA (total FA= 100 %) in NAT in NOD TLR4<sup>+/+</sup> and NOD TLR4<sup>-/-</sup> mice was determined by MRS. Data are given as means ± SEM. n=20-22.

The composition of fatty acids in VAT was compared to the fatty acid composition in NAT in female prediabetic 70-90 days old NOD TLR4<sup>+/+</sup> and NOD TLR4<sup>-/-</sup> mice. NOD TLR4<sup>+/+</sup> mice showed lower amounts of SFA in VAT (19.6±3.8 %) than NAT (38.2±4.6 %) (p<0.05), but NOD TLR4<sup>-/-</sup> mice showed similar amounts of SFA in VAT (24.9±3.9 %) and NAT (31.7±5.0 %). Additionally, NOD TLR4<sup>+/+</sup> and NOD TLR4<sup>-/-</sup> mice showed comparable amounts of MUFA in VAT (TLR4<sup>+/+</sup>: 52.1±2.6; TLR4<sup>-/-</sup>: 53.9±3.0 %) and NAT (TLR4<sup>+/+</sup>: 48.1±4.0; TLR4<sup>-/-</sup>: 55.1±4.6 %). Interestingly, a higher amount of PUFA was found in VAT (TLR4<sup>+/+</sup>: 28.7±2.0; TLR4<sup>-/-</sup>: 21.2±1.5 %) compared to similar PUFA levels in NAT (TLR4<sup>+/+</sup>: 13.8±1.6; TLR4<sup>-/-</sup>: 13.4±1.7 %) in both NOD TLR4<sup>+/+</sup> and NOD TLR4<sup>-/-</sup> mice (p<0.01-0.001).

To analyze FA composition in BAT, the voxel was positioned in axial direction in the BAT of NOD TLR4<sup>+/+</sup> and NOD TLR4<sup>-/-</sup> mice (Figure 42A). A representative <sup>1</sup>H MRS spectrum of BAT with the H<sub>2</sub>O reference peak and SFA, MUFA and PUFA peaks assignments is shown in Figure 42B. NOD TLR4<sup>+/+</sup> mice and NOD TLR4<sup>-/-</sup> mice showed comparable percentages of SFA

(TLR4<sup>+/+</sup>: 19.0±8.0; TLR4<sup>-/-</sup>: 33.4±9.0 %), MUFA (TLR4<sup>+/+</sup>: 51.7±4.0; TLR4<sup>-/-</sup>: 40.2±9.9 %) and PUFA (TLR4<sup>+/+</sup>: 29.3±6.5; TLR4<sup>-/-</sup>: 26.4±5.3 %) in their BAT depots (Figure 42C-E).

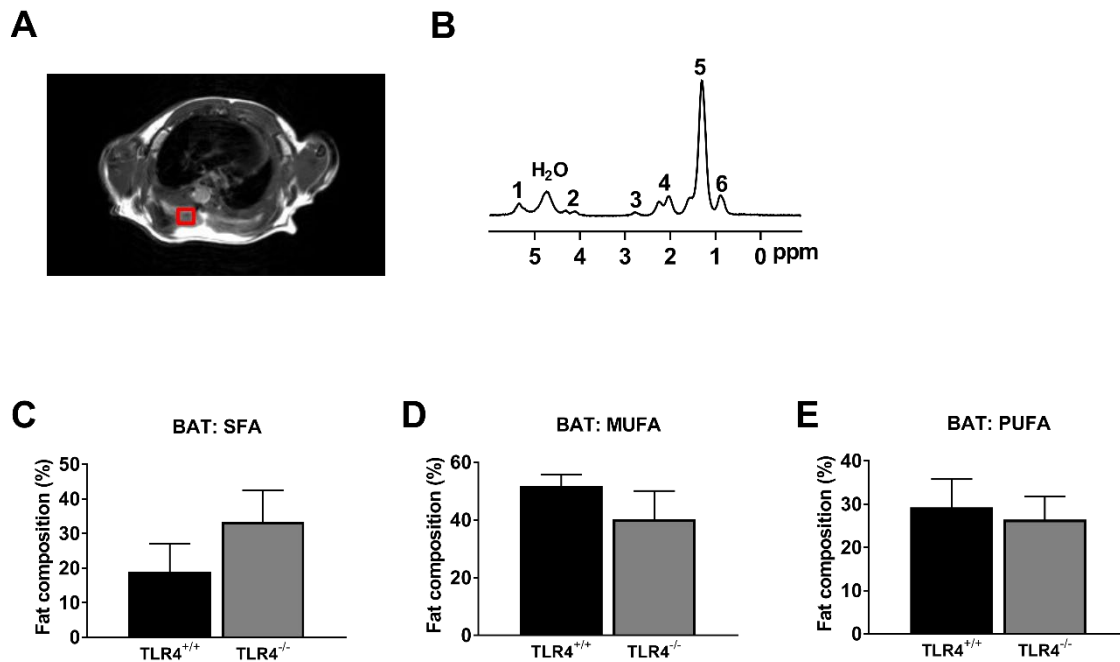


**Figure 42: Effect of TLR4-expression status on fat composition of the BAT in female prediabetic NOD TLR4<sup>+/+</sup> and NOD TLR4<sup>-/-</sup> mice.** Voxel positioning in axial direction in the BAT to measure the FA (A) and a representative <sup>1</sup>H MRS BAT spectrum with fat peak assignments (B). Fat peak assignment: 1: -CH=CH- and -CH-O-CO-, 2: -CH<sub>2</sub>-O-CO-, 3: -CH=CH-CH<sub>2</sub>-CH=CH-, 4: -CO-CH<sub>2</sub>-CH<sub>2</sub>- and -CH<sub>2</sub>-CH=CH-CH<sub>2</sub>-, 5: -CO-CH<sub>2</sub>-CH<sub>2</sub>- and -(CH<sub>2</sub>)<sub>n</sub>-, 6: -(CH<sub>2</sub>)<sub>n</sub>-CH<sub>3</sub> (Table 12). The percentages of SFA (C), MUFA (D) and PUFA (E) of total FA (total FA= 100 %) in BAT in NOD TLR4<sup>+/+</sup> and NOD TLR4<sup>-/-</sup> mice were determined by MRS. Data are given as means ± SEM. n=5-6.

### 3.1.13.4 Hepatocellular lipid content

To investigate the effect of TLR4-deficiency on the accumulation of liver fat, the amount of HCL in female prediabetic NOD TLR4<sup>+/+</sup> and NOD TLR4<sup>-/-</sup> mice was measured by MRS. The voxel positioning in coronal (left) and axial (right) direction in the liver to quantify the lipid content is shown in Figure 43A. A representative <sup>1</sup>H MRS spectrum of the liver with the H<sub>2</sub>O reference peak and CH<sub>2</sub> and CH<sub>3</sub> peaks is shown in Figure 43B. Interestingly, NOD TLR4<sup>-/-</sup> mice showed a lower percentage of HCL signal intensity compared to NOD TLR4<sup>+/+</sup> mice (TLR4<sup>+/+</sup>: 4.2±0.8; TLR4<sup>-/-</sup>: 2.4±0.3 %) (p<0.05) (Figure 43C).

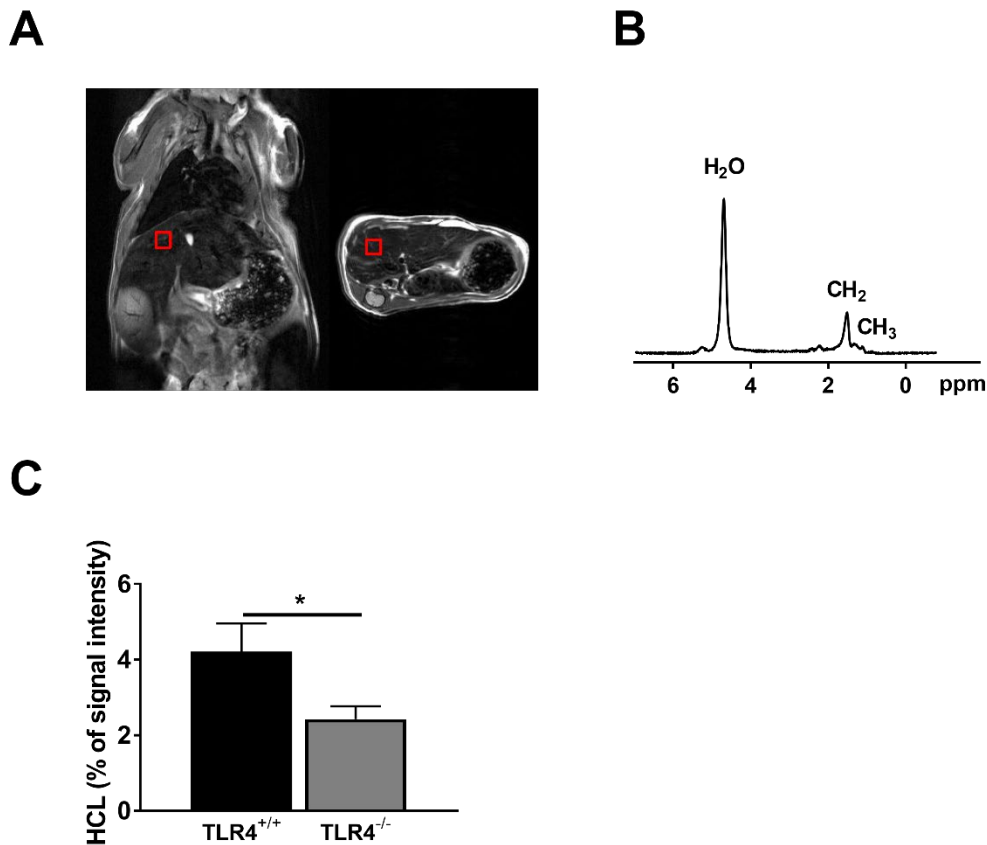


**Figure 43: Lower HCL levels in NOD TLR4<sup>-/-</sup> mice compared to NOD TLR4<sup>+/+</sup> mice.** Voxel positioning in coronal (left) and axial (right) direction in the liver to analyze lipid composition (A) and a representative <sup>1</sup>H MRS liver spectrum (B). HCL content was analyzed in female prediabetic NOD TLR4<sup>+/+</sup> and NOD TLR4<sup>-/-</sup> mice (C). Data are given as means ± SEM. n=17-18. \*p<0.05 by Student's t-test.

### 3.1.13.5 Triglyceride content in the liver

The potential effect of the TLR4-expression status on TG content in liver tissue was analyzed via histological liver sections in female prediabetic 70-90 days old NOD TLR4<sup>+/+</sup> and NOD TLR4<sup>-/-</sup> mice. On each section, lipids were stained, visualized and the means of the lipid containing areas were plotted against the total areas of the liver sections. NOD TLR4<sup>+/+</sup> and NOD TLR4<sup>-/-</sup> mice showed similar TG content in the liver (TLR4<sup>+/+</sup>: 36.5±8.0; TLR4<sup>-/-</sup>: 40.1±3.3 μm<sup>2</sup>/10.000 μm<sup>2</sup> hepatic tissue) (Figure 44A). The lipid containing areas were categorized according to their size of 0-10, 20-30, 40-70, 80-140 and 150-310 lipid containing areas in μm<sup>2</sup>/10.000 μm<sup>2</sup> hepatic tissue. There was no difference in the frequency distribution of the TG containing area size in NOD TLR4<sup>+/+</sup> and NOD TLR4<sup>-/-</sup> mice (Figure 44B).

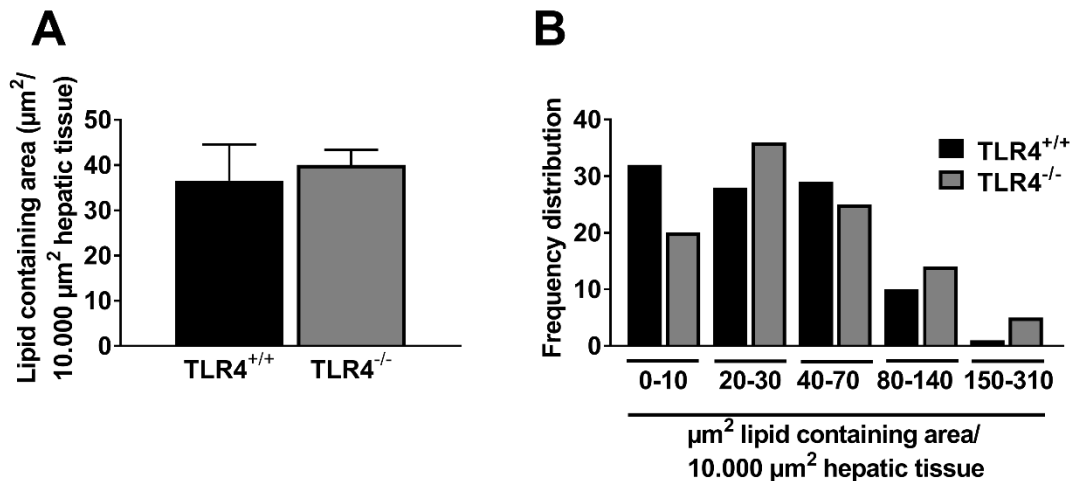


**Figure 44: Effect of the TLR4-expression status on the triglyceride content in liver tissue in female prediabetic NOD TLR4<sup>+/+</sup> and NOD TLR4<sup>-/-</sup> mice.** The proportion of the lipid containing area of the total analyzed area was determined in liver tissue of female prediabetic NOD TLR4<sup>+/+</sup> and NOD TLR4<sup>-/-</sup> mice (A). The frequency distribution was measured from each liver section that was analyzed and categorized by area size in 0-10, 20-30, 40-70, 80-140 and 150-310  $\mu\text{m}^2$  lipid containing area/10.000  $\mu\text{m}^2$  hepatic tissue (B). Data are given as means  $\pm$  SEM. n=7.

### 3.1.14 Fatty acid receptor expression

The possible effect of the TLR4-expression status on the expression of fatty acid receptors CD36 and FFAR2 in liver, skeletal muscle and VAT of female prediabetic 70-90 days old NOD TLR4<sup>+/+</sup> and NOD TLR4<sup>-/-</sup> mice was analyzed by western blotting using beta-actin as reference protein. For each analysis, a representative blot and graph are shown.

#### 3.1.14.1 Expression of fatty acid receptors in liver tissue

NOD TLR4<sup>+/+</sup> and NOD TLR4<sup>-/-</sup> mice showed similar relative CD36 expression levels in liver tissue (TLR4<sup>+/+</sup>: 2.17 $\pm$ 0.52; TLR4<sup>-/-</sup>: 2.27 $\pm$ 0.30 relative expression) (Figure 45A). The relative expression of FFAR2 in liver tissue was also comparable in NOD TLR4<sup>+/+</sup> and NOD TLR4<sup>-/-</sup> mice (TLR4<sup>+/+</sup>: 0.42 $\pm$ 0.09; TLR4<sup>-/-</sup>: 0.45 $\pm$ 0.10 relative expression) (Figure 45B).

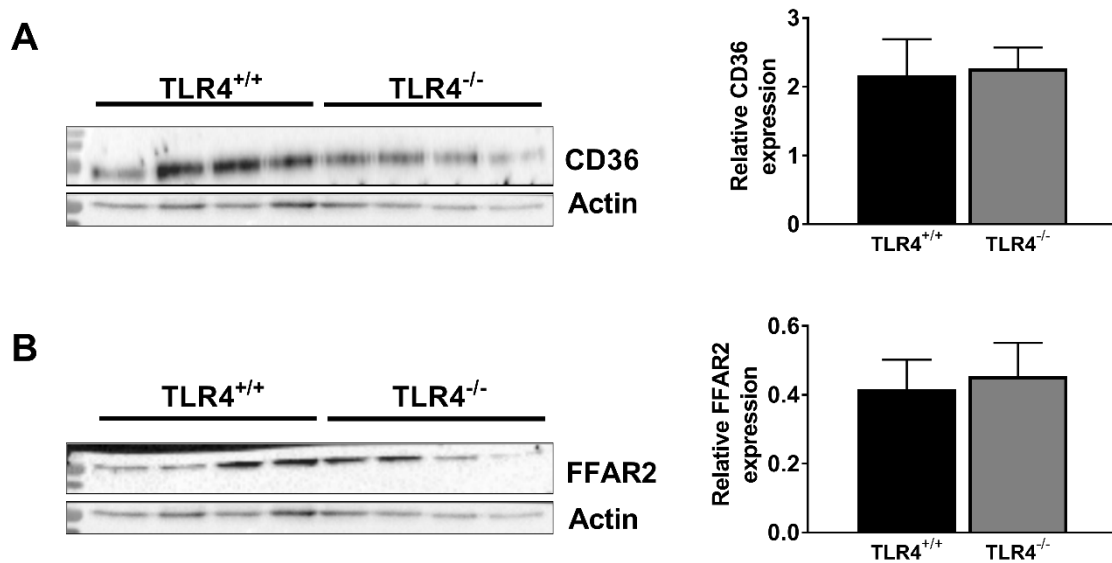


**Figure 45: Effect of the TLR4-expression status on protein expression of the FA receptors CD36 and FFAR2 in liver tissue of female prediabetic NOD TLR4<sup>+/+</sup> and NOD TLR4<sup>-/-</sup> mice.** Signals after blotting and relative expression of CD36 (A) and FFAR2 (B) in liver tissue of female prediabetic NOD TLR4<sup>+/+</sup> and NOD TLR4<sup>-/-</sup> mice are shown. CD36 and FFAR2 antibodies were used for detection and beta-actin served as protein reference. Data are given as means  $\pm$  SEM. n=7-8.

### 3.1.14.2 Expression of fatty acid receptors in skeletal muscle tissue

NOD TLR4<sup>+/+</sup> and NOD TLR4<sup>-/-</sup> mice showed similar relative CD36 expression levels in skeletal muscle tissue (TLR4<sup>+/+</sup>:  $3.19 \pm 0.84$ ; TLR4<sup>-/-</sup>:  $5.44 \pm 1.44$  relative expression) (Figure 46A). The relative expression of FFAR2 in skeletal muscle tissue was also comparable in NOD TLR4<sup>+/+</sup> and NOD TLR4<sup>-/-</sup> mice (TLR4<sup>+/+</sup>:  $2.35 \pm 0.56$ ; TLR4<sup>-/-</sup>:  $3.16 \pm 1.02$  relative expression) (Figure 46B).

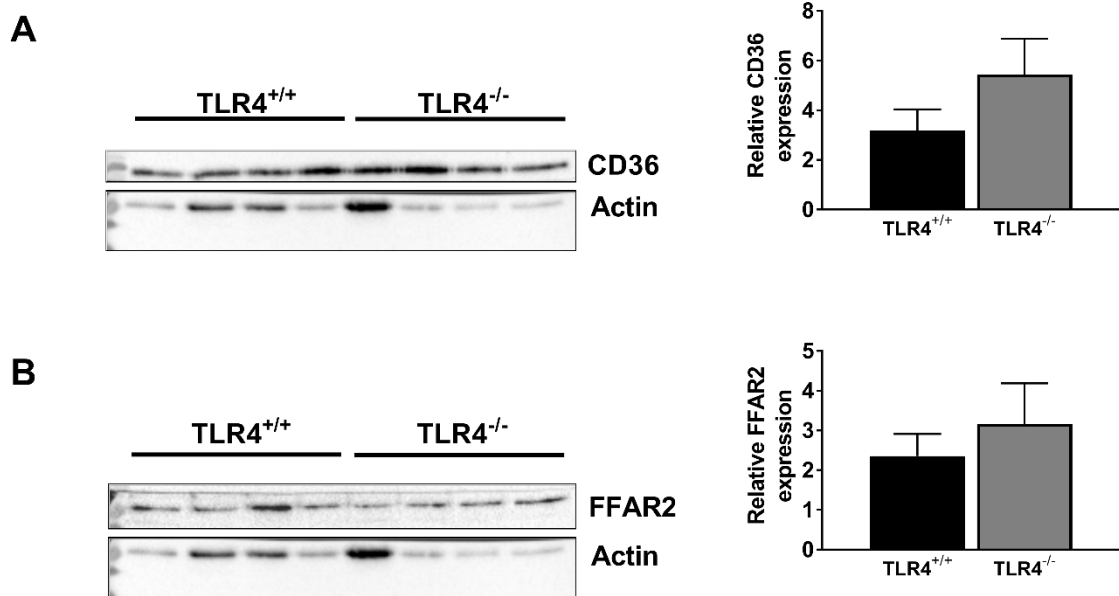


**Figure 46: Effect of the TLR4-expression status on protein expression of the FA receptors CD36 and FFAR2 in skeletal muscle tissue of female prediabetic NOD TLR4<sup>+/+</sup> and NOD TLR4<sup>-/-</sup> mice.** Signals after blotting and relative expression of CD36 (A) and FFAR2 (B) in skeletal muscle tissue of female prediabetic NOD TLR4<sup>+/+</sup> and NOD TLR4<sup>-/-</sup> mice are shown. CD36 and FFAR2 antibodies were used for detection and beta-actin served as protein reference. Data are given as means  $\pm$  SEM. n=4.

### 3.1.14.3 Expression of fatty acid receptors in VAT

FFAR2 was not detectable in VAT by western blotting. NOD TLR4<sup>+/+</sup> and NOD TLR4<sup>-/-</sup> mice showed similar relative CD36 expression levels in VAT (TLR4<sup>+/+</sup>: 2.42 $\pm$ 0.27; TLR4<sup>-/-</sup>: 4.09 $\pm$ 1.42 relative expression) (Figure 47).

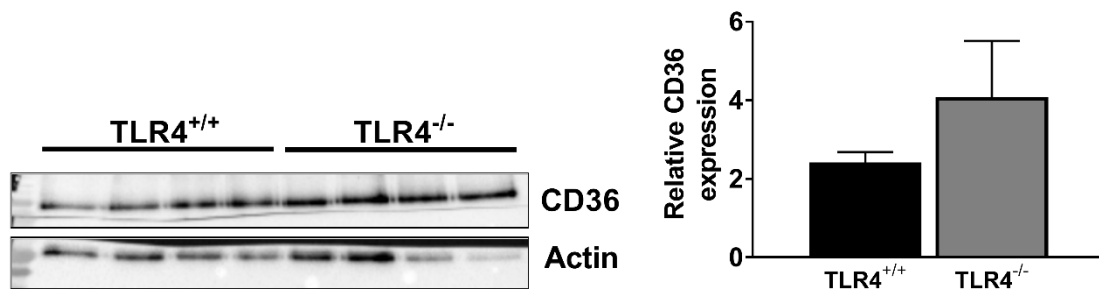


**Figure 47: Effect of the TLR4-expression status on protein expression of the FA receptors CD36 and FFAR2 in VAT of female prediabetic NOD TLR4<sup>+/+</sup> and NOD TLR4<sup>-/-</sup> mice.** Signals after blotting and relative expression of CD36 in VAT of NOD TLR4<sup>+/+</sup> and NOD TLR4<sup>-/-</sup> mice are shown. CD36 antibody was used for detection and beta-actin served as protein reference. Data are given as means  $\pm$  SEM. n=6-10.

### 3.1.15 Plasma SCFA levels

The SCFA content of plasma samples from non-fasted female prediabetic 70-90 days old NOD TLR4<sup>+/+</sup> and NOD TLR4<sup>-/-</sup> mice was measured by GC/MS, to determine the possible effect of the TLR4-expression status on plasma SCFA levels before diabetes manifestation.

Blood samples of NOD TLR4<sup>-/-</sup> mice showed lower total SCFA content compared to samples of NOD TLR4<sup>+/+</sup> mice (TLR4<sup>-/-</sup>: 137.8±2.9; TLR4<sup>+/+</sup>: 160.7±5.0 µM) (p<0.001) (Figure 48A).

To further determine the SCFA levels in plasma samples, individual SCFA were measured and quantified. The concentrations of the most abundant SCFA acetic acid, propionic acid and butyric acid were determined as well as the levels of isobutyric acid, valeric acid, isovaleric acid, isocaproic acid and hexanoic acid.

Compared to NOD TLR4<sup>+/+</sup> mice, NOD TLR4<sup>-/-</sup> mice showed lower levels of the most abundant SCFA acetic acid, propionic acid and butyric acid (Acetic acid: TLR4<sup>+/+</sup>: 147.8±3.9; TLR4<sup>-/-</sup>: 130.4±2.7 µM) (p<0.01) (Propionic acid: TLR4<sup>+/+</sup>: 8.8±0.8; TLR4<sup>-/-</sup>: 5.1±0.4 µM) (p<0.001) (Butyric acid: TLR4<sup>+/+</sup>: 2.7±0.4; TLR4<sup>-/-</sup>: 1.3±0.3 µM) (p<0.05) (Figure 48B).

Concentrations of less abundant SCFA like isobutyric acid, isovaleric acid and hexanoic acid were also lower in NOD TLR4<sup>-/-</sup> mice compared to NOD TLR4<sup>+/+</sup> mice (Isobutyric acid: TLR4<sup>+/+</sup>: 0.35±0.09; TLR4<sup>-/-</sup>: 0.13±0.04 µM) (p<0.05) (Isovaleric acid: TLR4<sup>+/+</sup>: 0.29±0.01; TLR4<sup>-/-</sup>: 0.25±0.02 µM) (p<0.05) (Hexanoic acid: TLR4<sup>+/+</sup>: 0.36±0.08; TLR4<sup>-/-</sup>: 0.08±0.05 µM) (p<0.01) (Figure 48B).

However, comparable valeric acid and isocaproic acid concentrations were found in plasma samples of NOD TLR4<sup>+/+</sup> and NOD TLR4<sup>-/-</sup> mice (Valeric acid: TLR4<sup>+/+</sup>: 0.37±0.02; TLR4<sup>-/-</sup>: 0.28±0.04 µM; Isocaproic acid: TLR4<sup>+/+</sup>: 0.16±0.01; TLR4<sup>-/-</sup>: 0.17±0.02 µM) (Figure 48B).

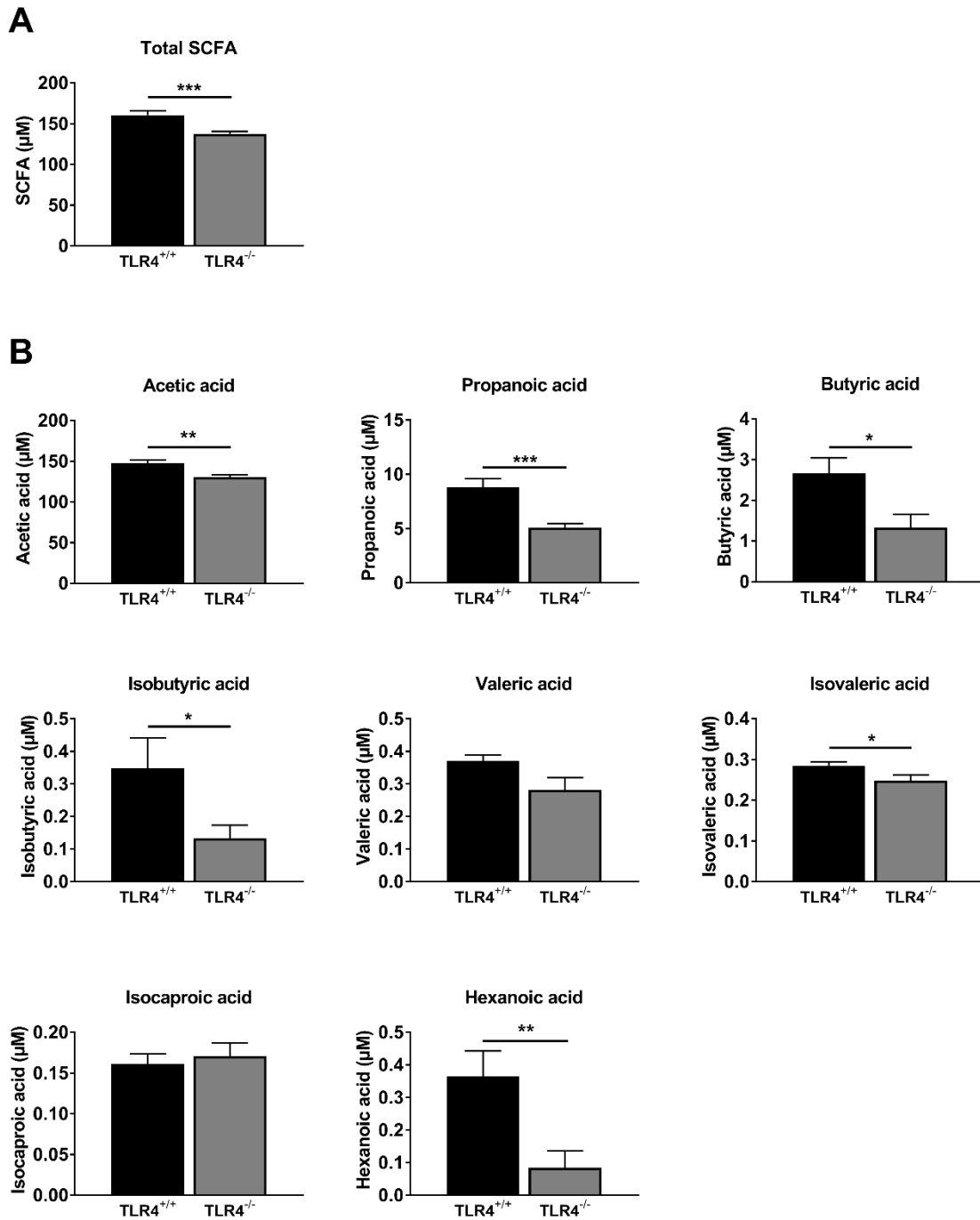


**Figure 48: Lower SCFA plasma concentrations in NOD TLR4<sup>-/-</sup> mice compared to NOD TLR4<sup>+/+</sup> mice.** Concentrations of SCFA were determined in plasma of non-fasted female prediabetic 70-90 days old NOD TLR4<sup>+/+</sup> and NOD TLR4<sup>-/-</sup> mice by GC/MS. Data of total SCFA in μM (A) and individual SCFA in μM (B) were analyzed. Data are given as means ± SEM. n=10. \*p<0.05, \*\*p<0.01, \*\*\*p<0.001 by Student's t-test.

### 3.1.16 SCFA levels in gut segments

Since plasma samples showed altered SCFA levels in NOD TLR4<sup>-/-</sup> mice, the intraluminal concentrations of SCFA in gut segments of non-fasted female prediabetic 70-90 days old NOD TLR4<sup>+/+</sup> and NOD TLR4<sup>-/-</sup> mice were analyzed. The concentration of SCFA content of acetic acid, propionic acid, butyric acid, isobutyric acid, valeric acid and isovaleric acid was measured in the small intestine, cecum and colon.

The concentration of SCFA content of each gut segment showed comparable SCFA concentrations in NOD TLR4<sup>+/+</sup> mice and NOD TLR4<sup>-/-</sup> mice (Small intestine: TLR4<sup>+/+</sup>: 670±63; TLR4<sup>-/-</sup>: 606±34 µmol/l; Cecum: TLR4<sup>+/+</sup>: 6213±448; TLR4<sup>-/-</sup>: 5485±253 µmol/l; Colon: TLR4<sup>+/+</sup>: 3278±432; TLR4<sup>-/-</sup>: 3142±333 µmol/l) (Figure 49).

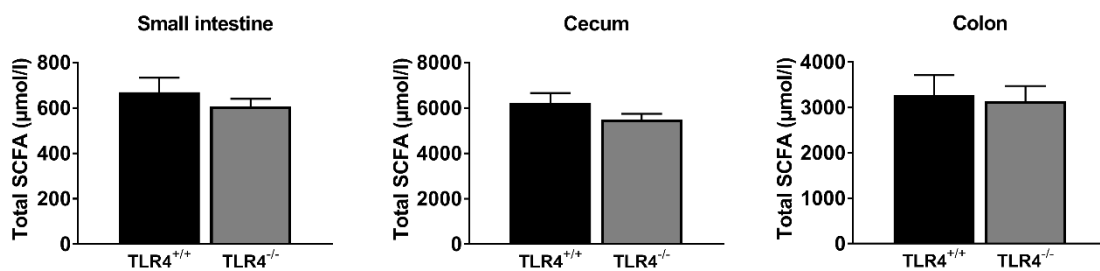


**Figure 49: Comparable SCFA concentrations in small intestine, cecum and colon of female prediabetic NOD TLR4<sup>+/+</sup> and NOD TLR4<sup>-/-</sup> mice.** Intraluminal concentrations in µmol/l of SCFA in small intestine, cecum and colon were measured in non-fasted female prediabetic NOD TLR4<sup>+/+</sup> and NOD TLR4<sup>-/-</sup> mice. Data are given as means ± SEM. n=8-10.

To further investigate the SCFA levels in the gut segments, single SCFA were analyzed and quantified in the lumen of small intestine, cecum and colon of non-fasted female prediabetic 70-90 days old NOD TLR4<sup>+/+</sup> and NOD TLR4<sup>-/-</sup> mice. NOD TLR4<sup>+/+</sup> and NOD TLR4<sup>-/-</sup> mice showed comparable SCFA content in each gut compartment. The two distal gut segments, cecum and colon, showed the highest SCFA concentrations compared to the small intestine (Figure 50).

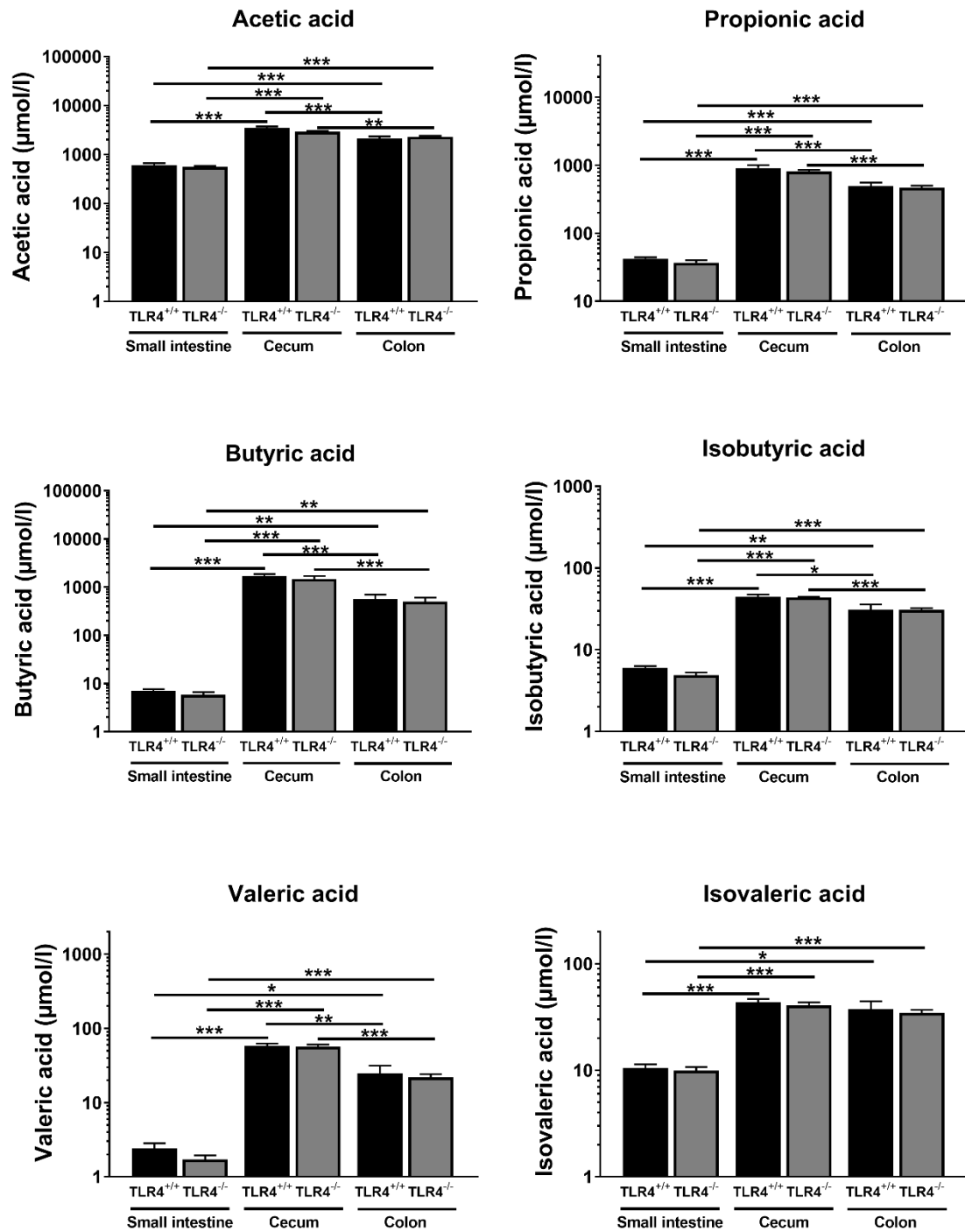


**Figure 50: Effect of the TLR4-expression status on intraluminal concentrations of SCFA in gut segments of female prediabetic NOD TLR4<sup>+/+</sup> and NOD TLR4<sup>-/-</sup> mice.** Concentrations of SCFA were determined by GC/MS in the lumen of the small intestine, cecum and colon of non-fasted female prediabetic NOD TLR4<sup>+/+</sup> and NOD TLR4<sup>-/-</sup> mice. Data are given as means  $\pm$  SEM. n=8-10. \*p<0.05, \*\*p<0.01, \*\*\*p<0.001 by one-way ANOVA.

## Results

For further analyses, the ratios of the SCFA concentrations in plasma and in the gut segments were calculated. Detailed analyses of the individual gut segments revealed, that the ratios between plasma and small intestine for acetic acid and butyric acid concentrations were comparable between NOD TLR4<sup>+/+</sup> and NOD TLR4<sup>-/-</sup> mice (Acetic acid: TLR4<sup>+/+</sup>: 0.28±0.04; TLR4<sup>-/-</sup>: 0.25±0.01; Butyric acid: TLR4<sup>+/+</sup>: 0.36±0.07; TLR4<sup>-/-</sup>: 0.25±0.06). However, compared to NOD TLR4<sup>+/+</sup> mice, NOD TLR4<sup>-/-</sup> mice showed a lower ratio between plasma and small intestine for propionic acid concentrations (TLR4<sup>+/+</sup>: 0.22±0.03; TLR4<sup>-/-</sup>: 0.14±0.01) (p<0.01) (Figure 51A).

Furthermore, the ratios between plasma and cecum for acetic acid concentrations revealed comparable levels for NOD TLR4<sup>+/+</sup> and NOD TLR4<sup>-/-</sup> mice (TLR4<sup>+/+</sup>: 0.045±0.004; TLR4<sup>-/-</sup>: 0.046±0.003). But the ratios between the concentrations of plasma and cecum for propionic acid and butyric acid respectively were about two-fold lower in NOD TLR4<sup>-/-</sup> than in NOD TLR4<sup>+/+</sup> mice (Propionic acid: TLR4<sup>+/+</sup>: 0.011±0.002; TLR4<sup>-/-</sup>: 0.006±0.001) (p<0.05) (Butyric acid: TLR4<sup>+/+</sup>: 0.0018±0.0003; TLR4<sup>-/-</sup>: 0.0007±0.0002) (p<0.01) (Figure 51B).

The ratios between plasma and colon for acetic acid and butyric acid showed comparable concentrations for NOD TLR4<sup>+/+</sup> and NOD TLR4<sup>-/-</sup> mice (Acetic acid: TLR4<sup>+/+</sup>: 0.070±0.007; TLR4<sup>-/-</sup>: 0.058±0.004; Butyric acid: TLR4<sup>+/+</sup>: 0.006±0.002; TLR4<sup>-/-</sup>: 0.002±0.001). However, the ratios between plasma and colon for propionic acid were lower in NOD TLR4<sup>-/-</sup> than in NOD TLR4<sup>+/+</sup> mice (TLR4<sup>+/+</sup>: 0.018±0.002; TLR4<sup>-/-</sup>: 0.011±0.001) (p<0.05) (Figure 51C).

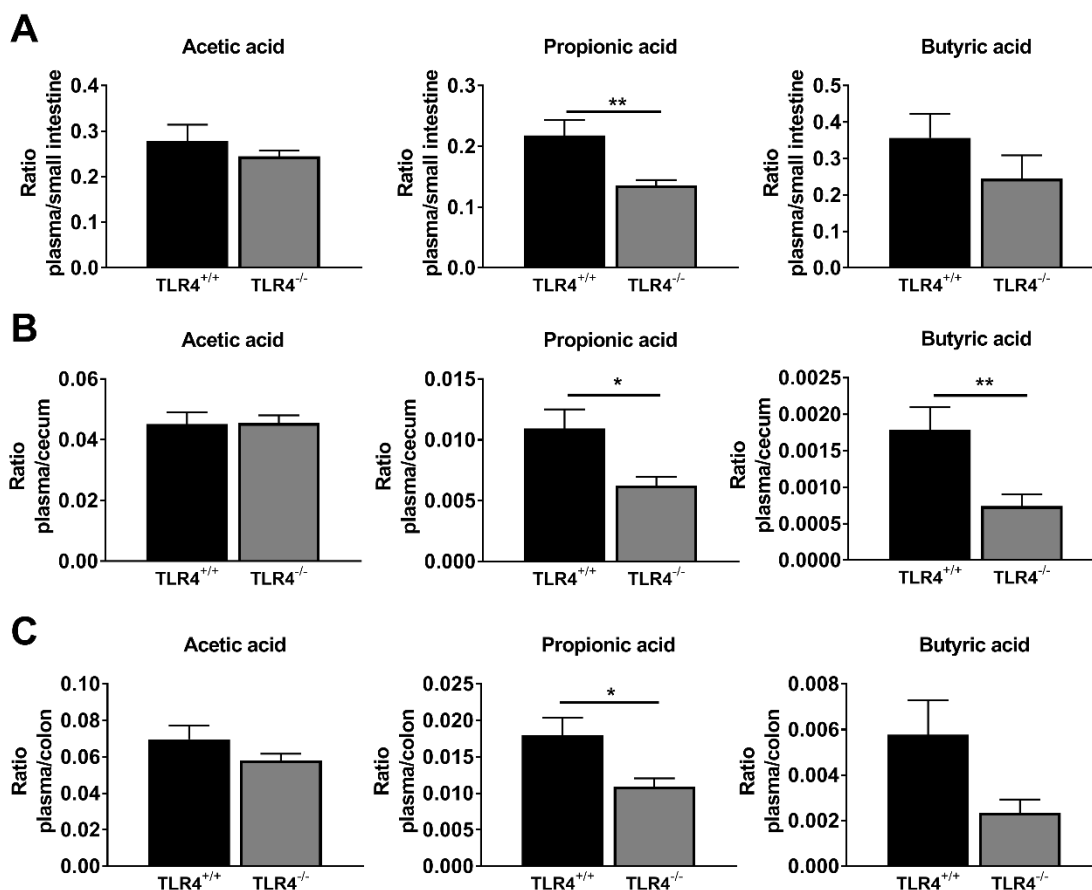


**Figure 51: Ratios of SCFA concentrations between plasma and gut segments in female prediabetic NOD TLR4<sup>+/+</sup> and NOD TLR4<sup>-/-</sup> mice.** Ratios of the concentrations of the three most abundant plasma SCFA and SCFA of the small intestine (A), cecum (B) and colon (C) of non-fasted female prediabetic NOD TLR4<sup>+/+</sup> and NOD TLR4<sup>-/-</sup> mice were calculated. Data are given as means  $\pm$  SEM. n=9-10. \*p<0.05, \*\*p<0.01 by Student's t-test.

### 3.1.17 Hepatic energy metabolism in NOD TLR4<sup>-/-</sup> mice

To analyze the potential effect of the TLR4-expression status on the hepatic energy metabolism,  $\gamma$ -ATP, Pi, PME and PDE contents were determined in NOD TLR4<sup>+/+</sup> and NOD TLR4<sup>-/-</sup> mice via MRS.

#### 3.1.17.1 Hepatic ATP and Pi concentrations

To examine the possible effect of the TLR4-expression status on the ATP concentration in the liver of female prediabetic 70-90 days old NOD TLR4<sup>+/+</sup> and NOD TLR4<sup>-/-</sup> mice, livers of mice were analyzed by <sup>31</sup>P MRS. The voxel was positioned in coronal (left) and axial (right) direction in the liver (Figure 52A) and hepatic  $\gamma$ -ATP and Pi content were measured by <sup>31</sup>P MRS in NOD TLR4<sup>+/+</sup> and NOD TLR4<sup>-/-</sup> mice (Figure 52B). NOD TLR4<sup>+/+</sup> and NOD TLR4<sup>-/-</sup> mice showed comparable  $\gamma$ -ATP (TLR4<sup>+/+</sup>: 1.62 $\pm$ 0.09; TLR4<sup>-/-</sup>: 1.42 $\pm$ 0.07 mmol/l) and Pi (TLR4<sup>+/+</sup>: 1.12 $\pm$ 0.08; TLR4<sup>-/-</sup>: 1.11 $\pm$ 0.05 mmol/l) content in their livers (Figure 52C,D).

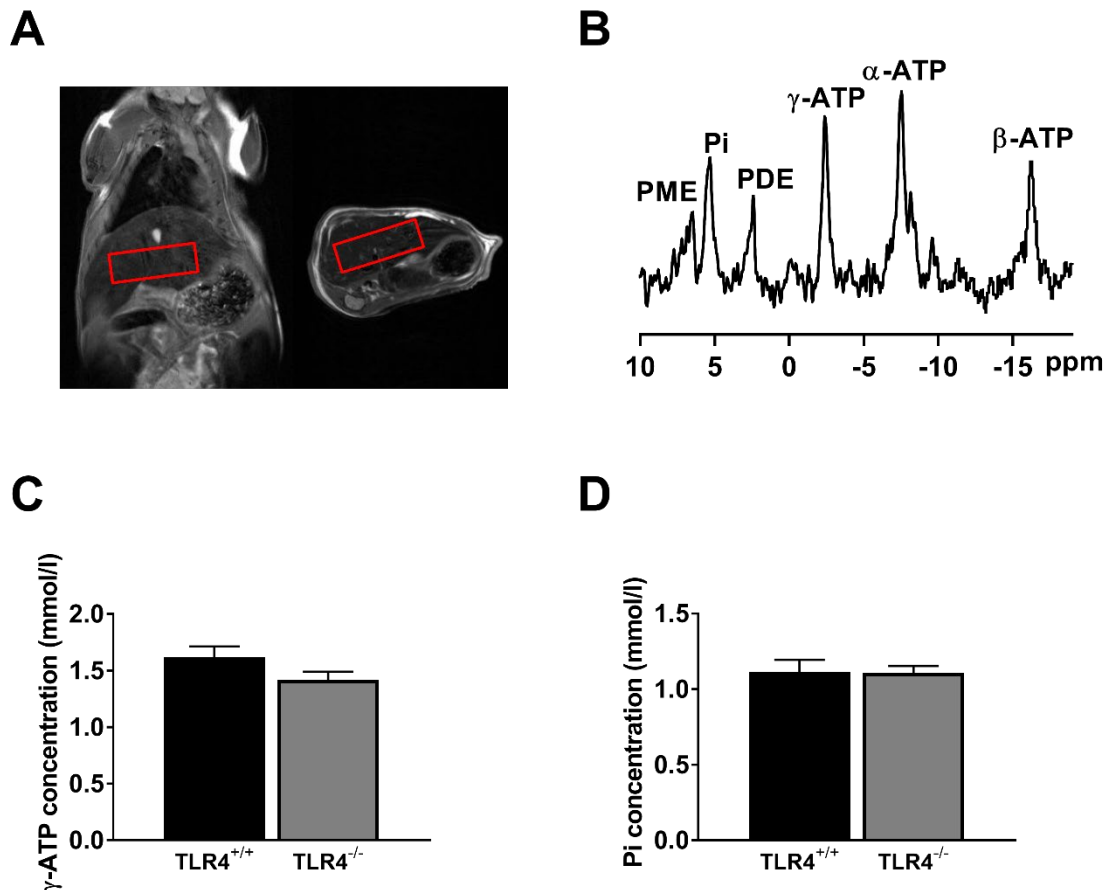


**Figure 52: Similar  $\gamma$ -ATP and Pi levels in the liver of female prediabetic NOD TLR4<sup>+/+</sup> and NOD TLR4<sup>-/-</sup> mice.** Voxel positioning in coronal (left) and axial (right) direction in the liver to measure  $\gamma$ -ATP and Pi concentrations (A) and a representative <sup>31</sup>P MRS liver spectrum (B). Hepatic  $\gamma$ -ATP (C) and Pi (D) content was analyzed in female prediabetic NOD TLR4<sup>+/+</sup> and NOD TLR4<sup>-/-</sup> mice. Data are given as means  $\pm$  SEM. n=13-16.

<sup>31</sup>P measurements were performed before and after intraperitoneal injection of 2g/kg glucose and the  $\gamma$ -ATP and Pi content was determined in the identical liver area before and 15 minutes after the glucose injection in female prediabetic 70-90 days old NOD TLR4<sup>+/+</sup> and NOD TLR4<sup>-/-</sup> mice. Comparable amounts of hepatic  $\gamma$ -ATP were measured in NOD TLR4<sup>+/+</sup> and NOD TLR4<sup>-/-</sup> mice before (TLR4<sup>+/+</sup>: 1.62 $\pm$ 0.09; TLR4<sup>-/-</sup>: 1.42 $\pm$ 0.07 mmol/l) and after (TLR4<sup>+/+</sup>: 1.50 $\pm$ 0.09; TLR4<sup>-/-</sup>: 1.65 $\pm$ 0.05 mmol/l) glucose injection (Figure 53A). Interestingly, the difference in  $\gamma$ -ATP concentrations measured before and after glucose showed that NOD TLR4<sup>-/-</sup> mice have a lower  $\gamma$ -ATP concentration before and a higher  $\gamma$ -ATP concentration after glucose injection compared to NOD TLR4<sup>+/+</sup> mice (TLR4<sup>+/+</sup>: -0.12 $\pm$ 0.06; TLR4<sup>-/-</sup>: 0.23 $\pm$ 0.06 mmol/l) ( $p < 0.001$ ) (Figure 53B). Additionally, NOD TLR4<sup>+/+</sup> and NOD TLR4<sup>-/-</sup> mice showed similar concentrations of Pi in the liver before (TLR4<sup>+/+</sup>: 1.12 $\pm$ 0.08; TLR4<sup>-/-</sup>: 1.11 $\pm$ 0.05 mmol/l) and after (TLR4<sup>+/+</sup>: 1.07 $\pm$ 0.08; TLR4<sup>-/-</sup>: 1.06 $\pm$ 0.06 mmol/l) glucose injection (Figure 53C). Furthermore, the difference in Pi concentrations measured before and after glucose injection

showed no differences between the genotypes (TLR4<sup>+/+</sup>:  $-0.046 \pm 0.07$ ; TLR4<sup>-/-</sup>:  $-0.049 \pm 0.07$  mmol/l) (Figure 53D).

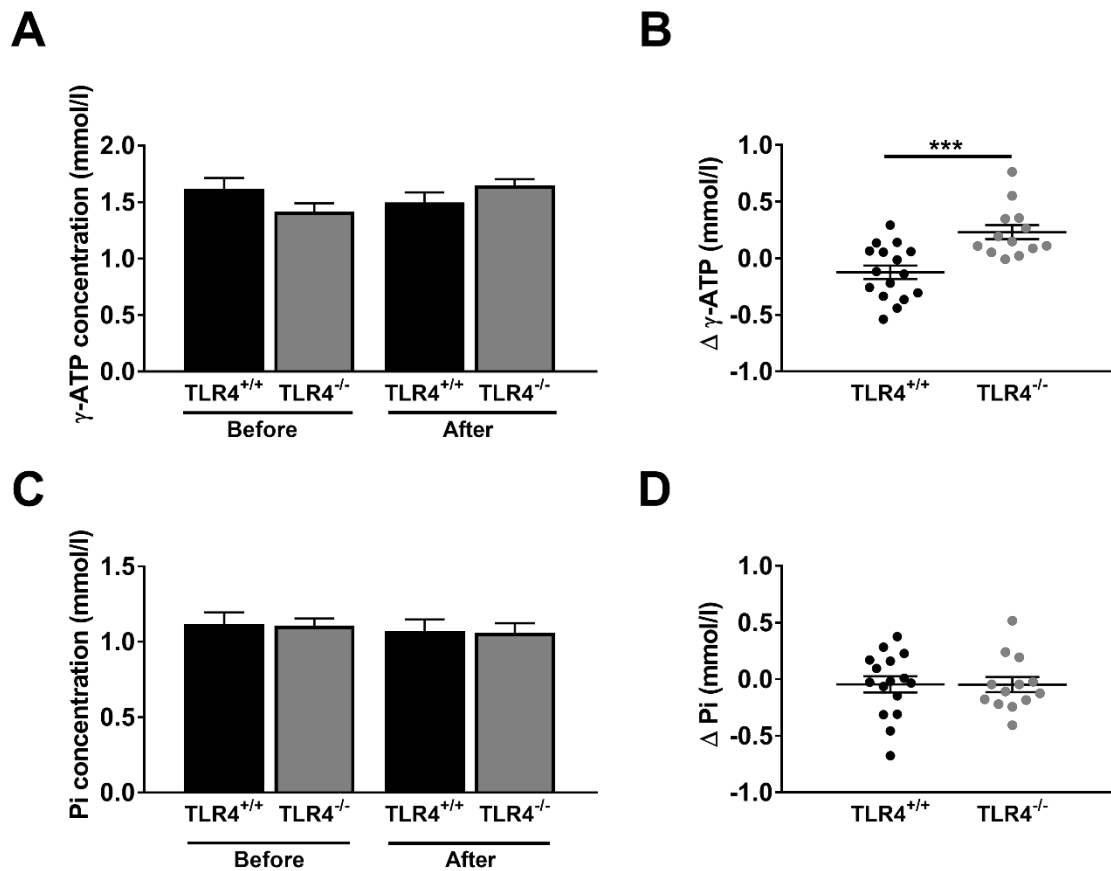


**Figure 53: Hepatic  $\gamma$ -ATP and Pi concentrations before and after glucose injection in female prediabetic NOD TLR4<sup>+/+</sup> and NOD TLR4<sup>-/-</sup> mice.** The hepatic  $\gamma$ -ATP (A) concentrations of female prediabetic NOD TLR4<sup>+/+</sup> and TLR4<sup>-/-</sup> mice before and after intraperitoneal glucose injection were analyzed and their differences were calculated (B). The hepatic Pi concentrations (C) were determined and Pi differences (D) in NOD TLR4<sup>+/+</sup> and TLR4<sup>-/-</sup> mice were calculated.  $\Delta$ =  $\gamma$ -ATP and Pi levels after – before glucose injection in mmol/l. Data are given as means  $\pm$  SEM. n=13-16. \*\*\*p<0.001 by Student's t-test.

### 3.1.17.2 Hepatic PME and PDE concentrations

The effect of the TLR4-expression status on PME and PDE concentrations in the liver was measured in female prediabetic 70-90 days old NOD TLR4<sup>+/+</sup> and NOD TLR4<sup>-/-</sup> mice. For these measurements, the voxel was positioned in coronal (left) and axial (right) direction in the liver (Figure 54A) and hepatic PME and PDE contents were measured by <sup>31</sup>P MRS (Figure 54B). NOD TLR4<sup>+/+</sup> and NOD TLR4<sup>-/-</sup> mice showed comparable PME (TLR4<sup>+/+</sup>:  $1.13 \pm 0.08$ ; TLR4<sup>-/-</sup>:  $1.08 \pm 0.07$  mmol/l) and PDE (TLR4<sup>+/+</sup>:  $0.198 \pm 0.04$ ; TLR4<sup>-/-</sup>:  $0.202 \pm 0.03$  mmol/l) content in the liver (Figure 54C,D).

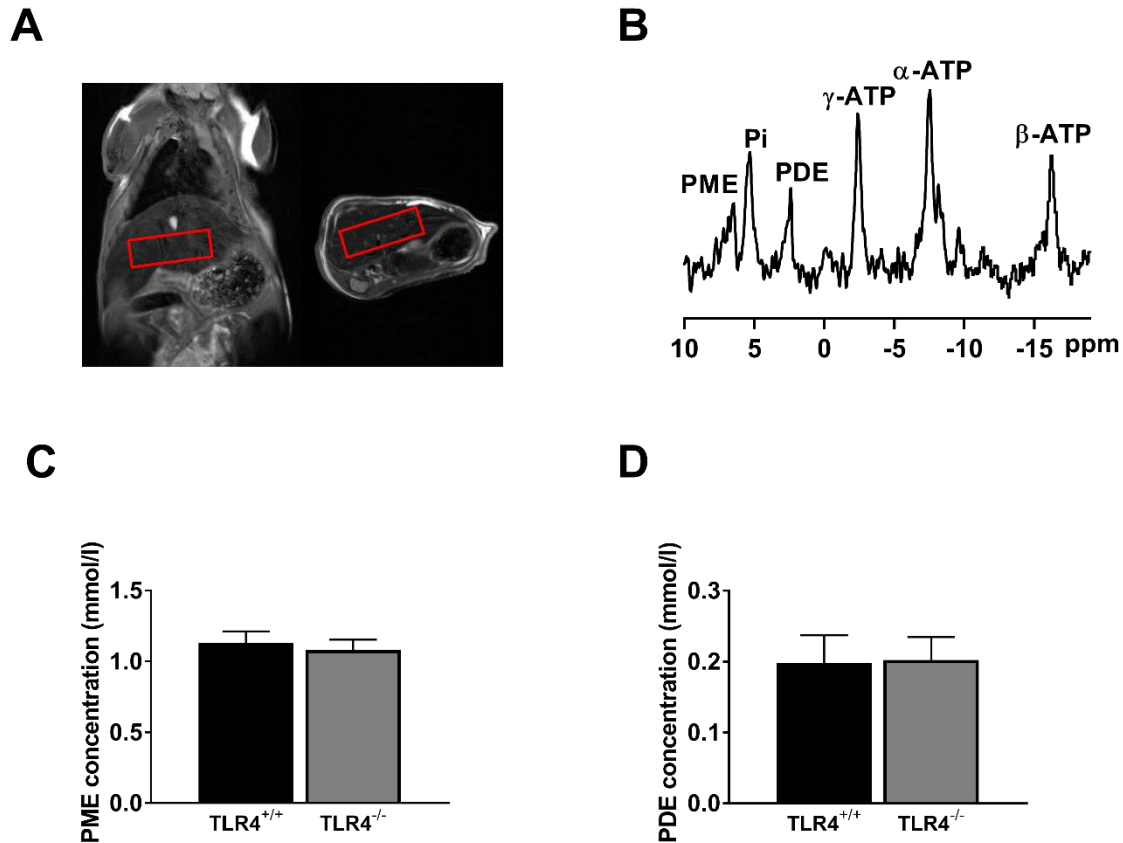


**Figure 54: Similar PME and PDE levels in the liver of female prediabetic NOD TLR4<sup>+/+</sup> and NOD TLR4<sup>-/-</sup> mice.** Voxel positioning in coronal (left) and axial (right) direction in the liver to measure PME and PDE concentrations (A) and a representative <sup>31</sup>P MRS liver spectrum (B). Hepatic PME (C) and PDE (D) contents were analyzed in female prediabetic NOD TLR4<sup>+/+</sup> and NOD TLR4<sup>-/-</sup> mice. Data are given as means ± SEM. n=11-13.

<sup>31</sup>P measurements were performed before and after intraperitoneal injection of 2g/kg glucose and the PME and PDE content in the liver was determined in the identical liver area before and 15 minutes after the glucose injection in female prediabetic 70-90 days old NOD TLR4<sup>+/+</sup> and NOD TLR4<sup>-/-</sup> mice. Comparable amounts of hepatic PME were measured in NOD TLR4<sup>+/+</sup> and NOD TLR4<sup>-/-</sup> mice before (TLR4<sup>+/+</sup>: 1.10±0.08; TLR4<sup>-/-</sup>: 1.08±0.07 mmol/l) and after (TLR4<sup>+/+</sup>: 1.40±0.13; TLR4<sup>-/-</sup>: 1.26±0.09 mmol/l) glucose injection (Figure 55A). Moreover, the change in PME concentration measured before and after glucose injection showed no differences in NOD TLR4<sup>+/+</sup> and NOD TLR4<sup>-/-</sup> mice (TLR4<sup>+/+</sup>: 0.31±0.18; TLR4<sup>-/-</sup>: 0.19±0.09 mmol/l) (Figure 55B).

No changes in hepatic PDE concentrations after glucose injection were observed in both genotypes (before: TLR4<sup>+/+</sup>: 0.20±0.05; TLR4<sup>-/-</sup>: 0.21±0.03 mmol/l; after: TLR4<sup>+/+</sup>: 0.20±0.05; TLR4<sup>-/-</sup>: 0.17±0.04 mmol/l) (Figure 55C). Additionally, the change in PDE concentration measured before and after glucose injection showed no differences between the two genotypes (TLR4<sup>+/+</sup>: 0.006±0.045; TLR4<sup>-/-</sup>: -0.042±0.034 mmol/l) (Figure 55D).

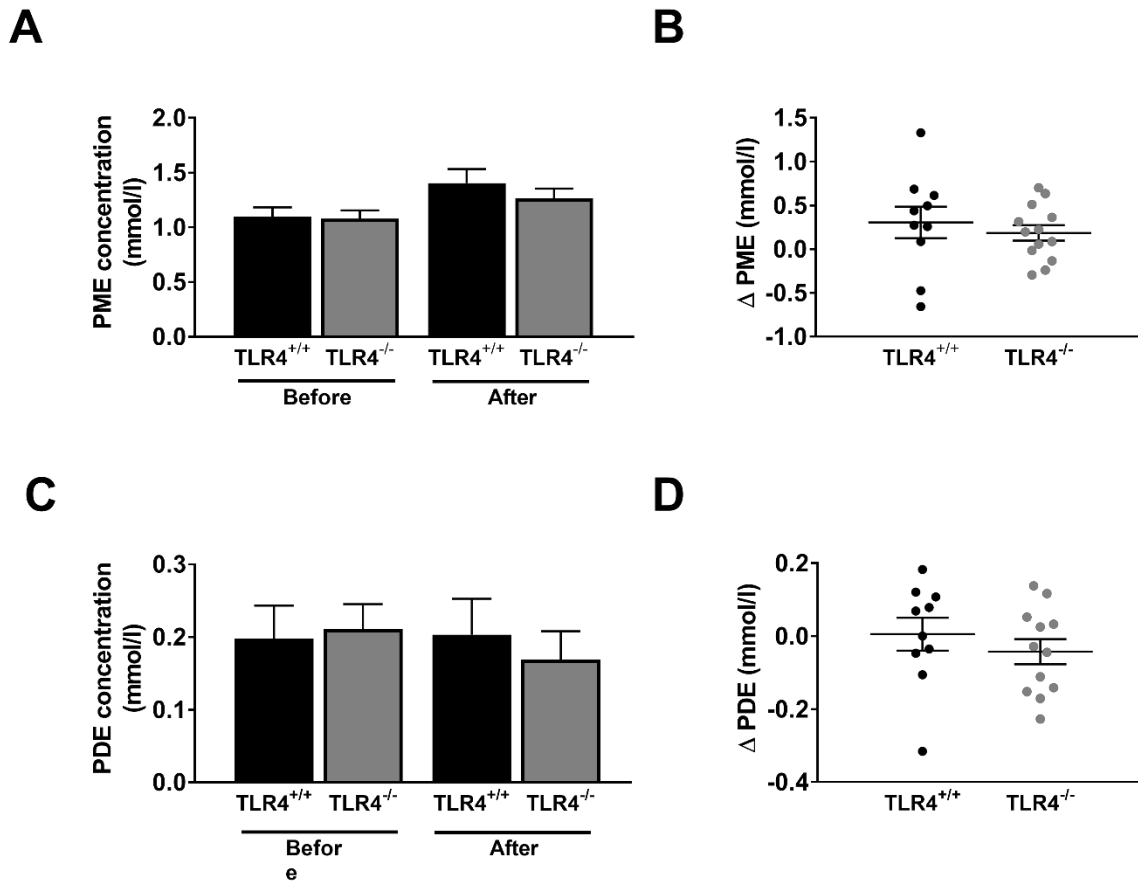


**Figure 55: Hepatic PME and PDE concentrations before and after glucose injection in female prediabetic NOD TLR4<sup>+/+</sup> and NOD TLR4<sup>-/-</sup> mice.** The hepatic PME (A) concentration in female prediabetic NOD TLR4<sup>+/+</sup> and NOD TLR4<sup>-/-</sup> mice before and after glucose injection were analyzed and the differences calculated (B). The hepatic PDE concentrations (C) were measured and the differences in PDE concentrations (D) were determined in NOD TLR4<sup>+/+</sup> and TLR4<sup>-/-</sup> mice.  $\Delta$  = PME and PDE levels after – before glucose injection in mmol/l. Data are given as means  $\pm$  SEM. n=10-13.

### 3.2 Effect of HFD on metabolic parameters in the prediabetic phase of NOD TLR4<sup>-/-</sup> mice, a model of accelerated development of insulin-deficient diabetes

The second section of this thesis focused on the analysis of the potential effects of a higher fat intake on the metabolism in NOD TLR4<sup>-/-</sup> mice. To this end, NOD TLR4<sup>+/+</sup> and NOD TLR4<sup>-/-</sup> mice were fed a HFD from an age of 30 days to an age of 70-90 days followed by metabolic phenotyping of the animals.

#### 3.2.1 Metabolic phenotyping

To characterize a possible effect of HFD-feeding in NOD TLR4<sup>+/+</sup> and NOD TLR4<sup>-/-</sup> mice on metabolic parameters, basic metabolic parameters such as food and water intake, physical activity, respiratory quotient and energy expenditure were analyzed. Each parameter was measured during two light- and two dark-phases (each phase 12 hours light/ 12 hours dark) after an adaptation period of the animals to the housing conditions of the metabolic test system for one light and one dark phase. The data for food and water intake were combined from both light-phases and both dark-phases. For the other metabolic parameters, the mean of both light-phases and both dark-phases was determined.

##### 3.2.1.1 Water- and food intake

Animals had free access to water and food during the light- and dark-phase measurements. The water intake of NOD TLR4<sup>+/+</sup> and NOD TLR4<sup>-/-</sup> mice fed with HFD was comparable in the light-phases and in the dark-phases and between the genotypes (Figure 56A). NOD TLR4<sup>+/+</sup> and NOD TLR4<sup>-/-</sup> mice fed with HFD had lower water intake in the dark-phases compared to NOD TLR4<sup>+/+</sup> and NOD TLR4<sup>-/-</sup> mice fed with SD (TLR4<sup>+/+</sup>: SD: 0.21±0.02; HFD: 0.12±0.01 ml/g body weight; TLR4<sup>-/-</sup>: SD: 0.24±0.02; HFD: 0.11±0.01 ml/g body weight) (all p<0.001) (Figure 56A). After 72 hours, NOD TLR4<sup>+/+</sup> and NOD TLR4<sup>-/-</sup> mice fed with HFD revealed lower total water intake than mice fed with SD (TLR4<sup>+/+</sup>: SD: 0.43±0.03; HFD: 0.24±0.02 ml\*g body weight<sup>-1</sup>\*72 h<sup>-1</sup>; TLR4<sup>-/-</sup>: SD: 0.44±0.02; HFD: 0.24±0.02 ml\*g body weight<sup>-1</sup>\*72 h<sup>-1</sup>) (both p<0.001) (Figure 56B).

The food intake of mice fed with HFD could not be measured during the phases as the device for the registration of food uptake is not designed for holding sticky substances such as pellets with a high fat content. To overcome this issue, the HFD was weighed and placed in each cage on a culture dish and only at the end of the experiment (72 hours) the remaining HFD was weighed again. After 72 hours in the system, NOD TLR4<sup>+/+</sup> and NOD TLR4<sup>-/-</sup> mice fed with HFD showed lower food intake compared to mice on SD (TLR4<sup>+/+</sup>: SD: 0.47±0.02; HFD:

$0.33 \pm 0.02 \text{ g} \cdot \text{g body weight}^{-1} \cdot 72 \text{ h}^{-1}$ ; TLR4<sup>-/-</sup>: SD:  $0.47 \pm 0.01$ ; HFD:  $0.32 \pm 0.02 \text{ g} \cdot \text{g body weight}^{-1} \cdot 72 \text{ h}^{-1}$ ) (Figure 56C).

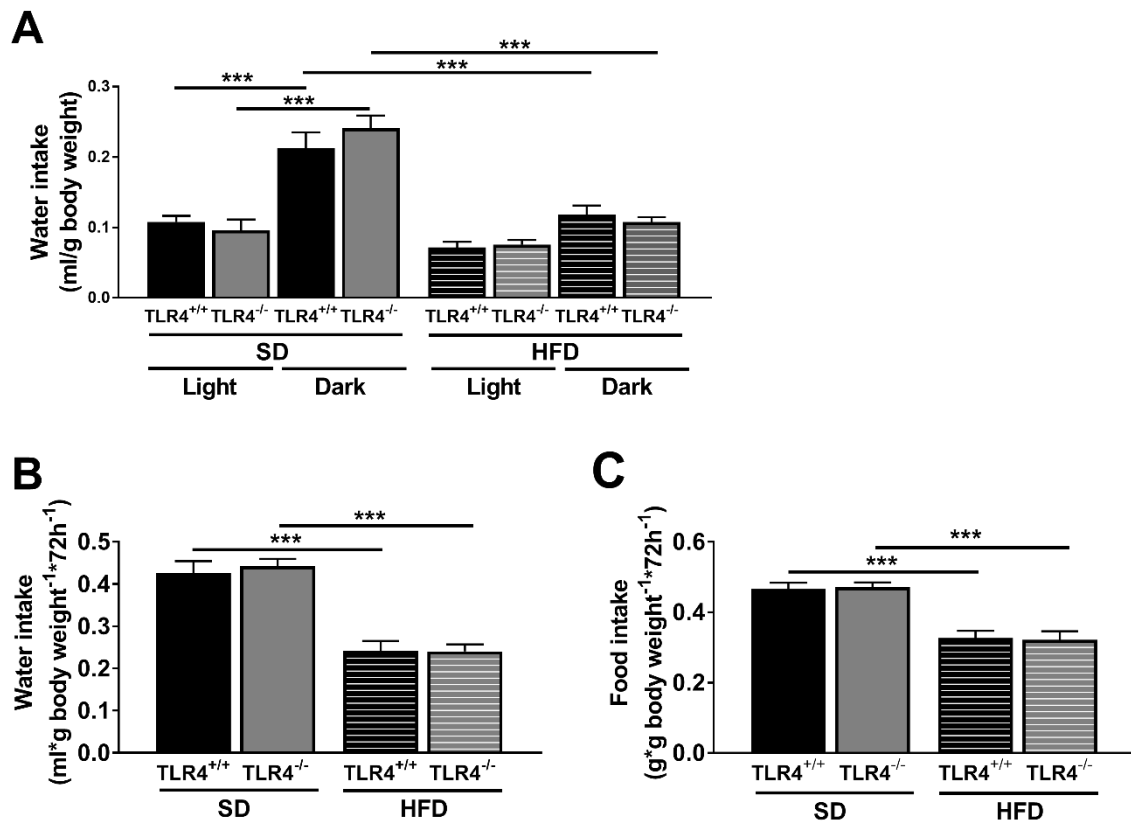


**Figure 56: Comparable water and food intake in female prediabetic NOD TLR4<sup>+/+</sup> and NOD TLR4<sup>-/-</sup> mice fed with either SD or HFD.** Female prediabetic NOD TLR4<sup>+/+</sup> and NOD TLR4<sup>-/-</sup> mice fed with SD or HFD were analyzed in a system that measures metabolic parameters such as water (A+C) and food (B) intake over 2 light- and 2 dark-phases. The data show the water and food intake in ml/g body weight and g/g body weight in two light-phases and two dark-phases. Data are given as means  $\pm$  SEM. n= 7-10. \*\*\*p<0.001 by one-way ANOVA.

### 3.2.1.2 Physical activity

During the light- and dark-phase measurements, the physical activity was measured for a period of 2 light- and 2 dark-phases. The physical activity of the mice is assessed by the number of interruptions of infrared beams registered as “counts”. The physical activity was increased in both dark-phases compared to the light-phases in NOD TLR4<sup>+/+</sup> and NOD TLR4<sup>-/-</sup> mice fed with HFD, similar to mice fed with SD (Figure 57A). NOD TLR4<sup>+/+</sup> and NOD TLR4<sup>-/-</sup> mice fed with HFD showed a higher mean physical activity in the dark-phases compared to the light-phases (Dark-phases: TLR4<sup>+/+</sup>:  $2269 \pm 152$ ; TLR4<sup>-/-</sup>:  $1906 \pm 170$  counts; light-phases: TLR4<sup>+/+</sup>:  $804 \pm 85$ ; TLR4<sup>-/-</sup>:  $691 \pm 102$  counts) (p<0.01-0.001) (Figure 57B). There was no difference between the genotypes and the diets in the light-phases and in the dark-phases.

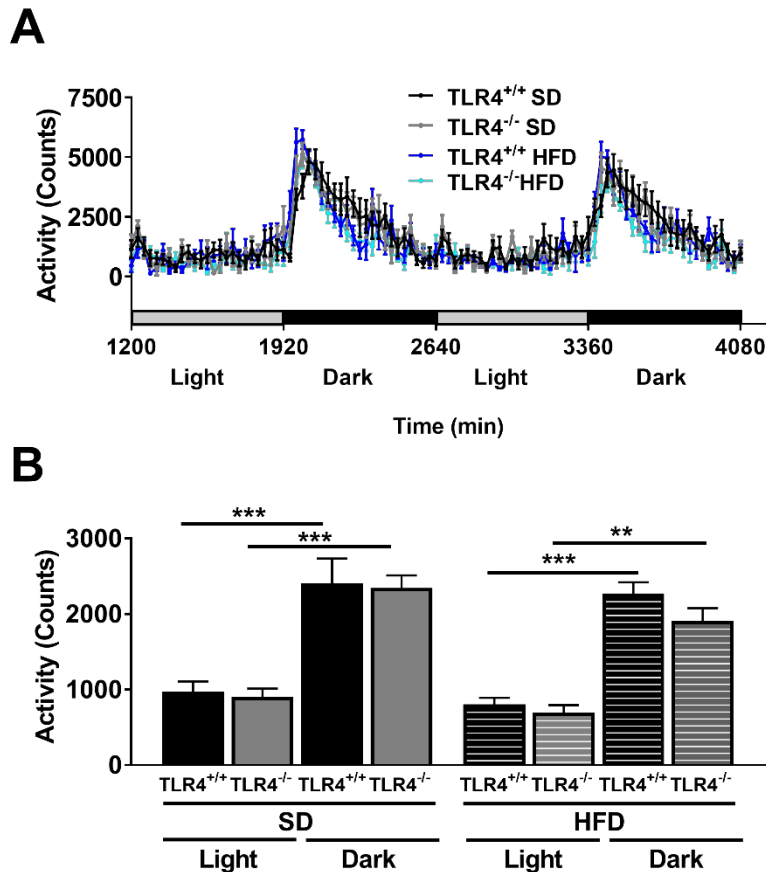


**Figure 57: Comparable physical activity in female prediabetic NOD TLR4<sup>+/+</sup> and NOD TLR4<sup>-/-</sup> mice fed with SD or HFD.** The physical activity of female prediabetic NOD TLR4<sup>+/+</sup> and NOD TLR4<sup>-/-</sup> mice fed with SD or HFD was analyzed in a system that detects metabolic parameters over 2 light- and 2 dark-phases. The data show the physical activity in counts and the mean of both light-phases and both dark-phases. Data are given as means  $\pm$  SEM. n= 7-10. \*\*p<0.01, \*\*\*p<0.001 by one-way ANOVA.

### 3.2.1.3 Respiratory quotient

The RQ was determined from the CO<sub>2</sub> production and the O<sub>2</sub> consumption (VCO<sub>2</sub>/VO<sub>2</sub>). The CO<sub>2</sub> production was lower in animals fed with HFD compared to animals fed with SD in the dark-phases (SD: TLR4<sup>+/+</sup>: 94.6 $\pm$ 3.2; TLR4<sup>-/-</sup>: 96.4 $\pm$ 1.9 ml/h; HFD: TLR4<sup>+/+</sup>: 83.2 $\pm$ 2.2; TLR4<sup>-/-</sup>: 83.1 $\pm$ 3.0 ml/h) (p<0.05) (Figure 58A). Interestingly, NOD TLR4<sup>+/+</sup> mice fed with HFD showed higher CO<sub>2</sub> production in the dark-phases (83.2 $\pm$ 2.2 ml/h) than in the light-phases (71.6 $\pm$ 1.5 ml/h) (p<0.05). Comparing the O<sub>2</sub> consumption of these animals, NOD TLR4<sup>+/+</sup> and NOD TLR4<sup>-/-</sup> mice on HFD revealed higher O<sub>2</sub> consumptions in the dark-phases (TLR4<sup>+/+</sup>: 106.0 $\pm$ 2.2; TLR4<sup>-/-</sup>: 105.0 $\pm$ 3.4 ml/h) than the light-phases (TLR4<sup>+/+</sup>: 90.9 $\pm$ 1.5; TLR4<sup>-/-</sup>: 91.5 $\pm$ 3.5 ml/h) (p<0.05-0.01) (Figure 58B). Additionally, NOD TLR4<sup>+/+</sup> mice fed with HFD showed higher O<sub>2</sub> consumptions in the light-phases compared to NOD TLR4<sup>+/+</sup> mice fed with SD (SD: 78.8 $\pm$ 1.8; HFD: 90.9 $\pm$ 1.5 ml/h) (p<0.05).

Feeding of the mice with a HFD leads to a RQ from 0.78 to 0.79 depending on the phase. The RQ showed similar kinetics in both light-phases and both dark-phases in NOD TLR4<sup>+/+</sup> and NOD TLR4<sup>-/-</sup> mice fed with HFD (Figure 58C). The mean RQ in both light- and both dark-phases was comparable in the light-phases and the dark-phases in NOD TLR4<sup>+/+</sup> and NOD TLR4<sup>-/-</sup> mice fed with HFD (Figure 58D). Animals on HFD (Light-phases: TLR4<sup>+/+</sup>: 0.79±0.01; TLR4<sup>-/-</sup>: 0.79±0.01; dark-phases: TLR4<sup>+/+</sup>: 0.78±0.01; TLR4<sup>-/-</sup>: 0.79±0.01) showed lower RQ rates compared to mice on SD (Light-phases: TLR4<sup>+/+</sup>: 0.88±0.01; TLR4<sup>-/-</sup>: 0.88±0.01; dark-phases: TLR4<sup>+/+</sup>: 0.94±0.01; TLR4<sup>-/-</sup>: 0.95±0.01) (all p<0.001).

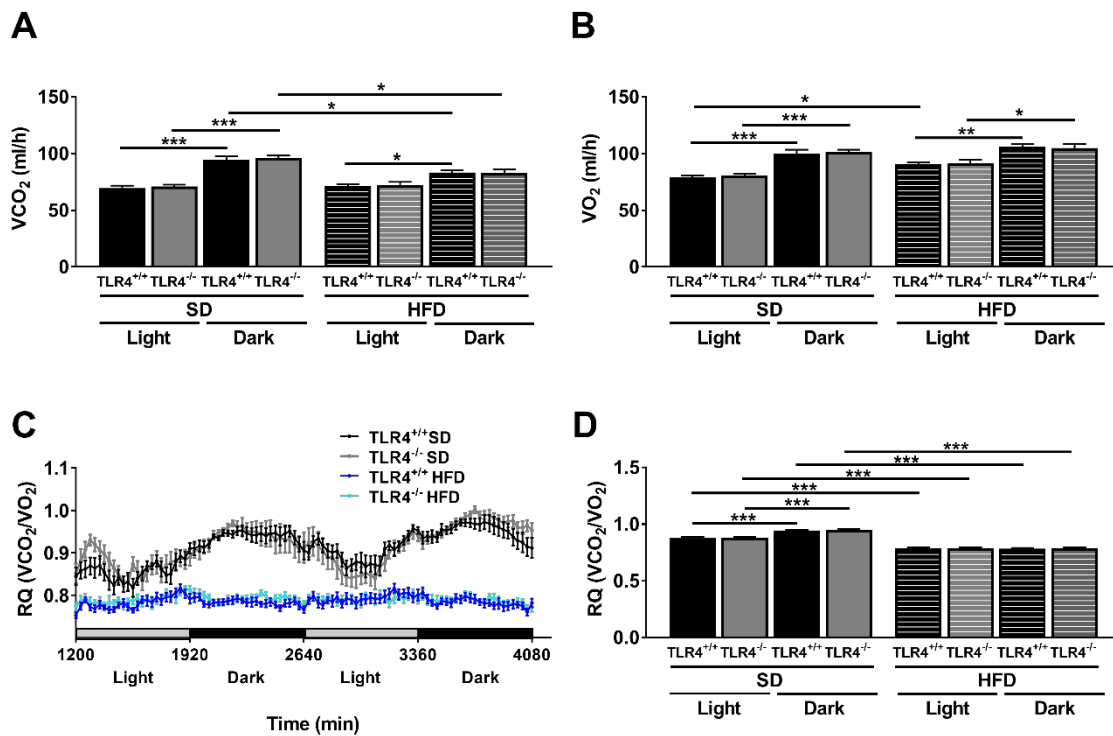


**Figure 58: Lower respiratory quotient in the light-phases and in the dark-phases in female prediabetic NOD TLR4<sup>+/+</sup> and NOD TLR4<sup>-/-</sup> mice fed with HFD compared to mice fed with SD.** The VCO<sub>2</sub>, VO<sub>2</sub> and RQ of female prediabetic NOD TLR4<sup>+/+</sup> and NOD TLR4<sup>-/-</sup> mice fed with SD or HFD were analyzed in a system that detects metabolic parameters over 2 light- and 2 dark-phases. The data show VCO<sub>2</sub> (A) and VO<sub>2</sub> (B) in ml/h and the RQ in VCO<sub>2</sub>/VO<sub>2</sub> (C+D) and the mean of both light-phases and both dark-phases. Data are given as means ± SEM. n= 7-11. \*p<0.05, \*\*p<0.01, \*\*\*p<0.001 by one-way ANOVA.

### 3.2.1.4 Energy expenditure

The energy expenditure was calculated from the VO<sub>2</sub> and VCO<sub>2</sub> parameters during 2 light- and 2 dark-phases. Similar to animals fed with SD, NOD TLR4<sup>+/+</sup> and NOD TLR4<sup>-/-</sup> mice fed with HFD showed the highest energy expenditure during the dark-phases and the lowest during the light-phases (Figure 59A).

The mean of energy expenditure was higher in the dark-phases (TLR4<sup>+/+</sup>: 19.3±0.7; TLR4<sup>-/-</sup>: 19.5±0.5 kcal·h<sup>-1</sup>·kg<sup>-1</sup>) compared to the light-phases (TLR4<sup>+/+</sup>: 16.6±0.6; TLR4<sup>-/-</sup>: 16.9±0.4 kcal·h<sup>-1</sup>·kg<sup>-1</sup>) in NOD TLR4<sup>+/+</sup> and NOD TLR4<sup>-/-</sup> mice fed with HFD (p<0.05-0.01) (Figure 59B). Furthermore, NOD TLR4<sup>+/+</sup> and NOD TLR4<sup>-/-</sup> mice fed with HFD (TLR4<sup>+/+</sup>: 19.3±0.7; TLR4<sup>-/-</sup>:

$19.5 \pm 0.5 \text{ kcal} \cdot \text{h}^{-1} \cdot \text{kg}^{-1}$ ) showed lower energy expenditure in the dark-phases compared to animals fed with SD (TLR4<sup>+/+</sup>:  $21.5 \pm 0.5$ ; TLR4<sup>-/-</sup>:  $22.0 \pm 0.4 \text{ kcal} \cdot \text{h}^{-1} \cdot \text{kg}^{-1}$ ) (both  $p < 0.05$ ).

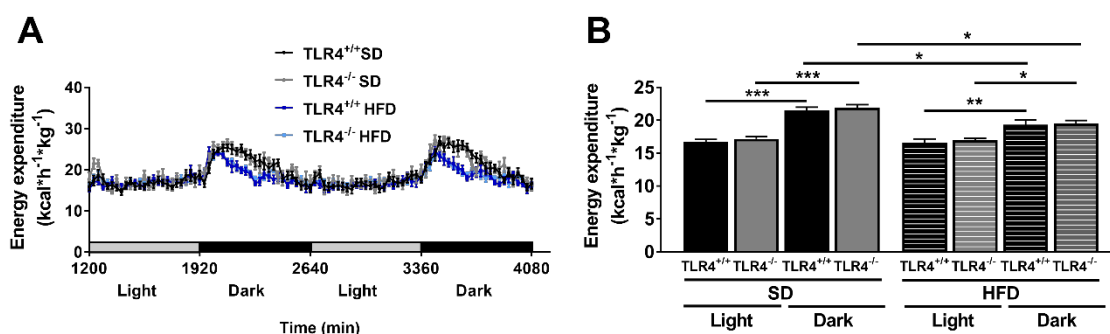


**Figure 59: Lower energy expenditure in the dark-phases in female prediabetic NOD TLR4<sup>+/+</sup> and NOD TLR4<sup>-/-</sup> mice fed with HFD compared to mice fed with SD.** The energy expenditure of female prediabetic NOD TLR4<sup>+/+</sup> and NOD TLR4<sup>-/-</sup> mice fed with SD or HFD was analyzed in a system that detects metabolic parameters over 2 light- and 2 dark-phases. The data show the energy expenditure (A+B) in  $\text{kcal} \cdot \text{h}^{-1} \cdot \text{kg}^{-1}$  and the mean of both light-phases and both dark-phases. Data are given as means  $\pm$  SEM.  $n = 7-11$ . \* $p < 0.05$ , \*\* $p < 0.01$ , \*\*\* $p < 0.001$  by one-way ANOVA.

### 3.2.1.5 Whole-body carbohydrate and fat oxidation rates

The whole-body CHO and FAO rates were calculated from the  $\text{VO}_2$  and  $\text{VCO}_2$  parameters during 2 light- and 2 dark-phases in NOD TLR4<sup>+/+</sup> and NOD TLR4<sup>-/-</sup> mice fed with SD and HFD. The whole-body CHO rates were comparable in the light-phases and the dark-phases in NOD TLR4<sup>+/+</sup> and NOD TLR4<sup>-/-</sup> mice fed with HFD (Figure 60A). Interestingly, NOD TLR4<sup>+/+</sup> and NOD TLR4<sup>-/-</sup> mice fed with HFD (light-phases: TLR4<sup>+/+</sup>:  $0.59 \pm 0.05$ ; TLR4<sup>-/-</sup>:  $0.61 \pm 0.06 \text{ mg/min}$ ; dark-phases: TLR4<sup>+/+</sup>:  $0.66 \pm 0.07$ ; TLR4<sup>-/-</sup>:  $0.70 \pm 0.06 \text{ mg/min}$ ) revealed lower CHO rates than animals fed with SD (light-phases: TLR4<sup>+/+</sup>:  $1.07 \pm 0.08$ ; TLR4<sup>-/-</sup>:  $1.10 \pm 0.05 \text{ mg/min}$ ; dark-phases: TLR4<sup>+/+</sup>:  $1.84 \pm 0.09$ ; TLR4<sup>-/-</sup>:  $1.92 \pm 0.04 \text{ mg/min}$ ) (all  $p < 0.001$ ).

The whole-body FAO rates of NOD TLR4<sup>+/+</sup> mice fed with HFD were higher in the dark-phases ( $0.64 \pm 0.02 \text{ mg/min}$ ) than in the light phases ( $0.54 \pm 0.02 \text{ mg/min}$ ) ( $p < 0.05$ ) (Figure 60B). NOD TLR4<sup>+/+</sup> mice fed with HFD (light-phases: TLR4<sup>+/+</sup>:  $0.54 \pm 0.02$ ; TLR4<sup>-/-</sup>:  $0.54 \pm 0.03 \text{ mg/min}$ ; dark-phases: TLR4<sup>+/+</sup>:  $0.64 \pm 0.02$ ; TLR4<sup>-/-</sup>:  $0.61 \pm 0.02 \text{ mg/min}$ ) showed higher whole-body FAO rates in the dark-phases and in the light-phases compared to animals fed with SD (light-phases: TLR4<sup>+/+</sup>:  $0.26 \pm 0.02$ ; TLR4<sup>-/-</sup>:  $0.26 \pm 0.02 \text{ mg/min}$ ; dark-phases: TLR4<sup>+/+</sup>:  $0.15 \pm 0.02$ ; TLR4<sup>-/-</sup>:  $0.13 \pm 0.02 \text{ mg/min}$ ) (all  $p < 0.001$ ).

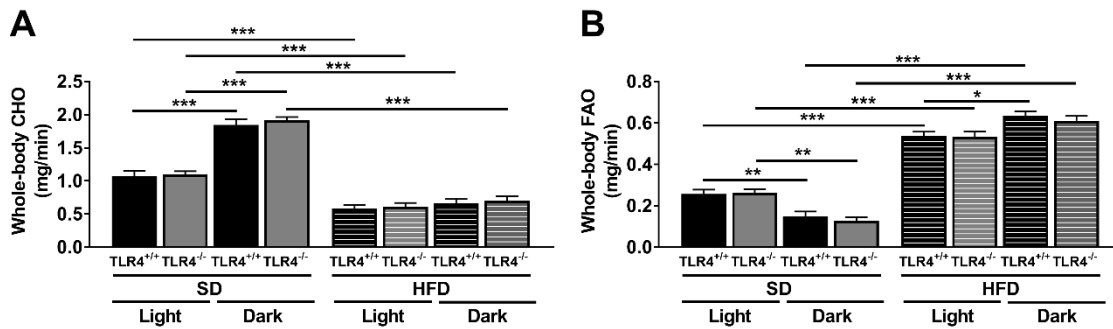


**Figure 60: Lower whole-body carbohydrate and higher fat oxidation rates in female prediabetic NOD TLR4<sup>+/+</sup> and NOD TLR4<sup>-/-</sup> mice fed with HFD compared to mice fed with SD.** The CHO and FAO rates of female prediabetic NOD TLR4<sup>+/+</sup> and NOD TLR4<sup>-/-</sup> mice fed with SD or HFD were analyzed in a system that detects metabolic parameters over 2 light- and 2 dark-phases. The data show the CHO rates (A) in mg/min and the FAO rates (B) in mg/min. The mean of both light-phases and both dark-phases is shown. Data are given as means  $\pm$  SEM. n= 7-11. \*p<0.05, \*\*p<0.01, \*\*\*p<0.001 by one-way ANOVA.

### 3.2.2 Body weight and weight of liver and visceral adipose tissue

To assess the potential effect of feeding a HFD on the body, liver and VAT weight, female prediabetic 70-90 days old NOD TLR4<sup>+/+</sup> and NOD TLR4<sup>-/-</sup> mice were analyzed before diabetes manifestation. NOD TLR4<sup>+/+</sup> and NOD TLR4<sup>-/-</sup> mice fed with HFD showed higher body weight compared to mice fed with SD (SD: TLR4<sup>+/+</sup>: 24.5 $\pm$ 0.3; TLR4<sup>-/-</sup>: 24.4 $\pm$ 0.6 g; HFD: TLR4<sup>+/+</sup>: 29.2 $\pm$ 0.6; TLR4<sup>-/-</sup>: 27.2 $\pm$ 0.7 g) (both p<0.001). Comparable body weight was found in NOD TLR4<sup>+/+</sup> and NOD TLR4<sup>-/-</sup> mice fed with HFD (Figure 61A). Additionally, the liver weight of NOD TLR4<sup>+/+</sup> and NOD TLR4<sup>-/-</sup> mice fed with HFD and SD was similar (SD: TLR4<sup>+/+</sup>: 1.15 $\pm$ 0.03; TLR4<sup>-/-</sup>: 1.14 $\pm$ 0.03 g; HFD: TLR4<sup>+/+</sup>: 1.12 $\pm$ 0.02; TLR4<sup>-/-</sup>: 1.10 $\pm$ 0.06 g) (Figure 61B). Furthermore, NOD TLR4<sup>+/+</sup> and NOD TLR4<sup>-/-</sup> mice fed with HFD showed higher amounts of VAT than mice fed with SD (SD: TLR4<sup>+/+</sup>: 0.23 $\pm$ 0.03; TLR4<sup>-/-</sup>: 0.35 $\pm$ 0.05 g; HFD: TLR4<sup>+/+</sup>: 1.27 $\pm$ 0.05; TLR4<sup>-/-</sup>: 0.96 $\pm$ 0.10 g) (both p<0.001). Interestingly, compared to NOD TLR4<sup>+/+</sup> mice fed with HFD, NOD TLR4<sup>-/-</sup> mice fed with HFD showed lower VAT weight (p<0.01) (Figure 61C).

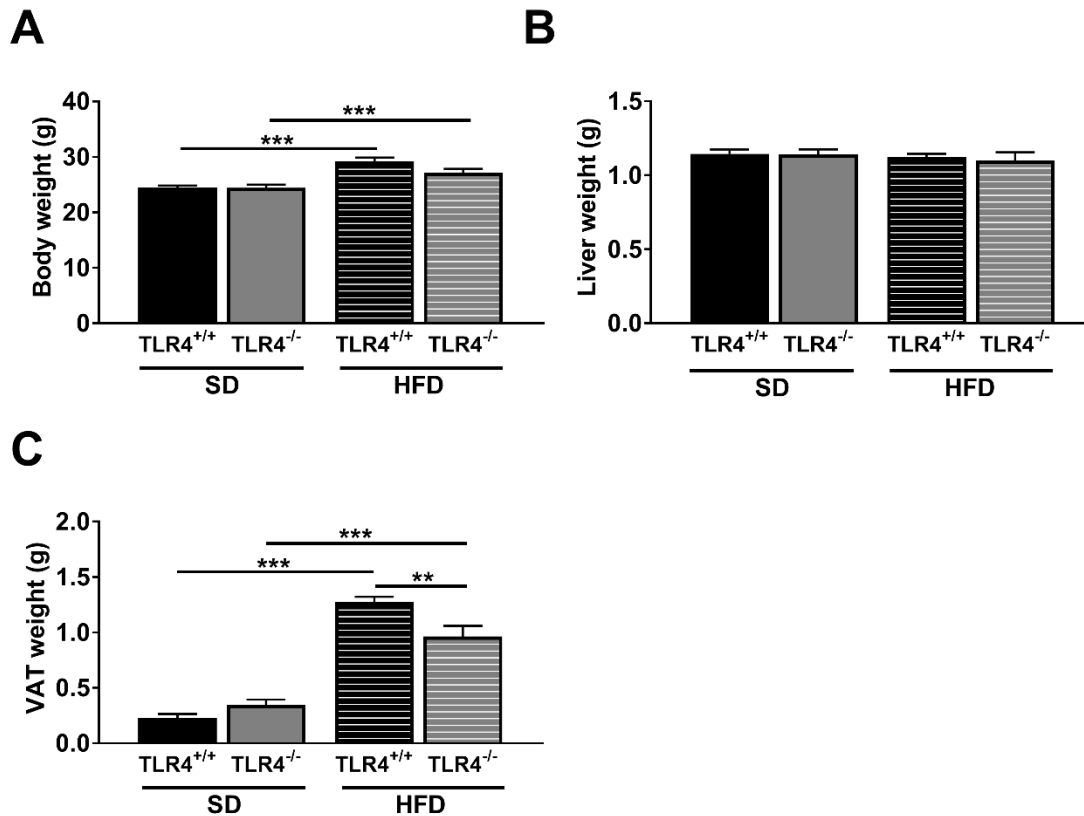


**Figure 61: Increased body and visceral adipose tissue weight, but similar liver weight in NOD TLR4<sup>+/+</sup> and NOD TLR4<sup>-/-</sup> mice fed with HFD compared to mice fed with SD.** The body weight (A) in g, liver weight (B) in g and VAT weight (C) in g were measured from female prediabetic NOD TLR4<sup>+/+</sup> and NOD TLR4<sup>-/-</sup> mice fed with SD or HFD at the age of 70-90 days. Data are given as means  $\pm$  SEM. n=6-8. \*\*p<0.01, \*\*\*p<0.001 by one-way ANOVA.

### 3.2.3 Development of body weight

To investigate the possible effect of a HFD on body weight development in female prediabetic NOD TLR4<sup>+/+</sup> and NOD TLR4<sup>-/-</sup> mice before the age of diabetes manifestation, the body weight was measured at seven time points between the age of 30 days and 72 days. The four groups started with a similar body weight in the range of 18.03-19.85 g at the age of 30 days. After two weeks (age 44 days) until age 72 days, NOD TLR4<sup>-/-</sup> mice fed with HFD showed higher body weight compared to NOD TLR4<sup>-/-</sup> mice fed with SD (p<0.05-0.001). Comparison of the body weight curves of the four groups revealed that NOD TLR4<sup>+/+</sup> and NOD TLR4<sup>-/-</sup> mice fed with HFD showed a higher body weight during the observation period compared to NOD TLR4<sup>+/+</sup> and NOD TLR4<sup>-/-</sup> mice fed with SD (p<0.001). Interestingly, NOD TLR4<sup>-/-</sup> mice fed with HFD showed an even higher body weight than NOD TLR4<sup>+/+</sup> mice fed with HFD (p<0.05) (Figure 62).

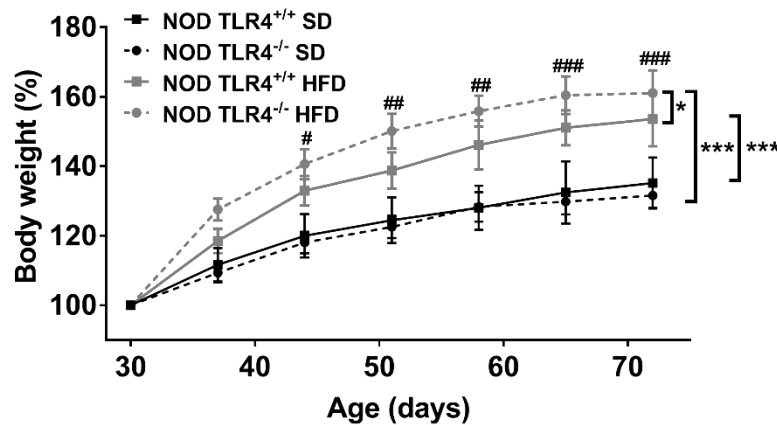


**Figure 62: Accelerated body weight development in female prediabetic NOD TLR4<sup>+/+</sup> mice and NOD TLR4<sup>-/-</sup> mice fed with HFD compared to mice fed with SD.** The body weight development was measured from female prediabetic NOD TLR4<sup>+/+</sup> and NOD TLR4<sup>-/-</sup> mice fed with SD or HFD at seven time points from an age of 30 to 72 days. The initial body weight of each animal was set to 100 %. Data are given as means  $\pm$  SEM.  $n=6-11$ . \* $p<0.05$ , \*\*\* $p<0.001$  by nonlinear regression. # $p<0.05$ , ## $p<0.01$ , ### $p<0.001$  comparison of NOD TLR4<sup>-/-</sup> mice fed with HFD and NOD TLR4<sup>-/-</sup> mice fed with SD by one-way ANOVA.

### 3.2.4 White and brown adipose tissue weight

The weights of the WAT and BAT of the neck were measured from female prediabetic NOD TLR4<sup>+/+</sup> and NOD TLR4<sup>-/-</sup> mice age 70-90 days fed with SD or HFD to examine the possible impact of HFD-feeding on the development of these two AT compartments. The weights of the WAT and BAT were determined separately and added to obtain the total weight of the NAT. NOD TLR4<sup>+/+</sup> and NOD TLR4<sup>-/-</sup> mice on HFD revealed comparable NAT, BAT and WAT weights (Figure 63). However, NOD TLR4<sup>+/+</sup> and NOD TLR4<sup>-/-</sup> mice on HFD showed higher NAT weights compared to mice on SD (SD: TLR4<sup>+/+</sup>: 51.9 $\pm$ 4.2; TLR4<sup>-/-</sup>: 53.0 $\pm$ 3.8 mg/10g body weight; HFD: TLR4<sup>+/+</sup>: 77.6 $\pm$ 2.2; TLR4<sup>-/-</sup>: 83.9 $\pm$ 4.7 mg/10g body weight) ( $p<0.01-0.001$ ) (Figure 63A). The BAT weight in NOD TLR4<sup>+/+</sup> mice fed with HFD was higher compared to NOD TLR4<sup>+/+</sup> mice fed with SD (SD: 20.8 $\pm$ 2.0; HFD: 29.5 $\pm$ 1.8 mg/10g body weight) ( $p<0.05$ ) (Figure 63B). There was no difference in the BAT weights of NOD TLR4<sup>-/-</sup> mice on HFD and SD. Furthermore, NOD TLR4<sup>+/+</sup> and NOD TLR4<sup>-/-</sup> mice on HFD showed higher WAT weights compared to mice on SD (SD: TLR4<sup>+/+</sup>: 31.1 $\pm$ 2.9; TLR4<sup>-/-</sup>: 30.2 $\pm$ 1.6 mg/10g body weight; HFD: TLR4<sup>+/+</sup>: 48.1 $\pm$ 2.4; TLR4<sup>-/-</sup>: 58.0 $\pm$ 4.5 mg/10g body weight) ( $p<0.05-0.001$ ) (Figure 63C).

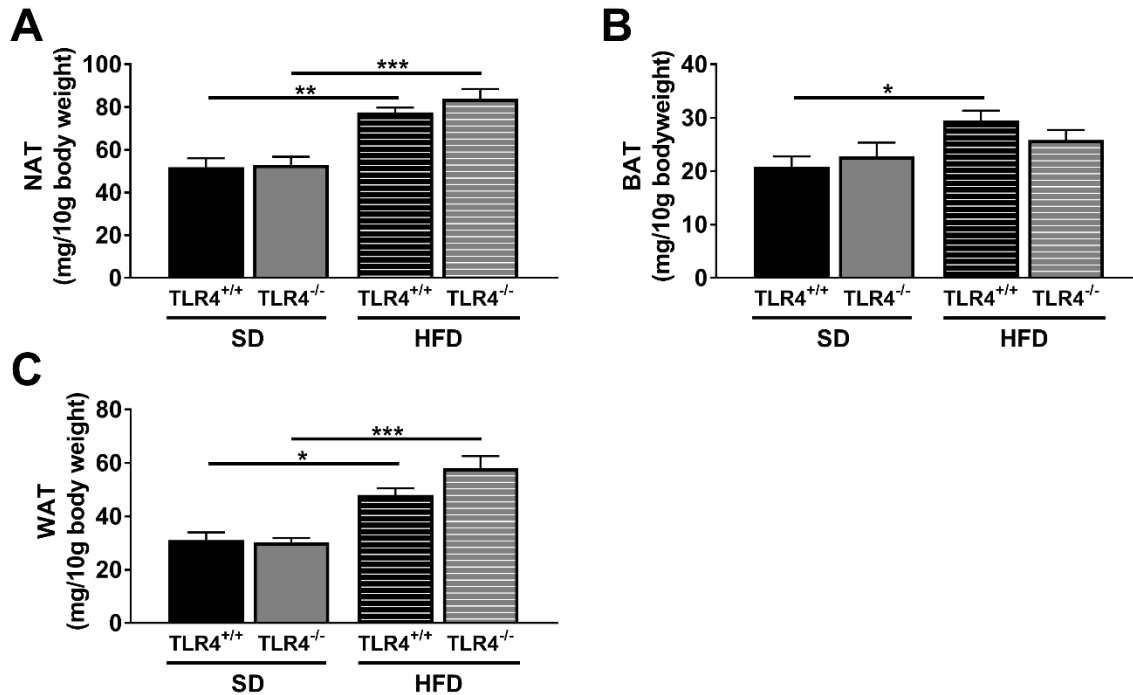


**Figure 63: Higher NAT, BAT and WAT weight in female prediabetic NOD TLR4<sup>+/+</sup> mice and NOD TLR4<sup>-/-</sup> mice fed with HFD compared to SD.** The total NAT weight (A), BAT weight (B) and WAT weight (C) were measured from female prediabetic NOD TLR4<sup>+/+</sup> and NOD TLR4<sup>-/-</sup> mice at the age of 70-90 days fed with SD or HFD. Data are given as means  $\pm$  SEM. n=6-11. \*p<0.05, \*\*p<0.01, \*\*\*p<0.001 by one-way ANOVA.

### 3.2.5 Liver, VAT, NAT and BAT volume

The possible effect of feeding a HFD to female prediabetic 70-90 days old NOD TLR4<sup>+/+</sup> and NOD TLR4<sup>-/-</sup> mice was analyzed with regard to the volumes of liver, VAT, NAT and BAT. The volume of each tissue was measured by encircling the shape of the tissue in each slice sequentially acquired by MRT in the axial direction and analyzing each slide to determine the entire tissue volume (Figure 64). NOD TLR4<sup>+/+</sup> and NOD TLR4<sup>-/-</sup> mice on HFD showed comparable liver, VAT, NAT and BAT volumes. The liver volume was similar in NOD TLR4<sup>+/+</sup> and NOD TLR4<sup>-/-</sup> mice on SD and on HFD (SD: TLR4<sup>+/+</sup>: 1.11 $\pm$ 0.04; TLR4<sup>-/-</sup>: 1.02 $\pm$ 0.05 ml; HFD: TLR4<sup>+/+</sup>: 1.17 $\pm$ 0.05; TLR4<sup>-/-</sup>: 1.10 $\pm$ 0.06 ml) (Figure 64A). Compared to NOD TLR4<sup>+/+</sup> and NOD TLR4<sup>-/-</sup> mice on SD, NOD TLR4<sup>+/+</sup> and NOD TLR4<sup>-/-</sup> mice on HFD showed higher VAT volumes (SD: TLR4<sup>+/+</sup>: 0.26 $\pm$ 0.02; TLR4<sup>-/-</sup>: 0.27 $\pm$ 0.05 ml; HFD: TLR4<sup>+/+</sup>: 1.64 $\pm$ 0.14; TLR4<sup>-/-</sup>: 1.66 $\pm$ 0.30 ml) (p<0.001) (Figure 64B). Additionally, NOD TLR4<sup>+/+</sup> and NOD TLR4<sup>-/-</sup> mice on HFD revealed higher NAT (SD: TLR4<sup>+/+</sup>: 89.0 $\pm$ 6.5; TLR4<sup>-/-</sup>: 92.3 $\pm$ 7.9  $\mu$ l; HFD: TLR4<sup>+/+</sup>: 192.7 $\pm$ 13.4; TLR4<sup>-/-</sup>: 176.6 $\pm$ 21.2  $\mu$ l) and higher BAT volumes than NOD TLR4<sup>+/+</sup> and NOD TLR4<sup>-/-</sup> mice on SD (SD: TLR4<sup>+/+</sup>: 43.3 $\pm$ 1.2; TLR4<sup>-/-</sup>: 43.0 $\pm$ 2.3  $\mu$ l; HFD: TLR4<sup>+/+</sup>: 68.4 $\pm$ 2.9; TLR4<sup>-/-</sup>: 60.1 $\pm$ 3.1  $\mu$ l) (p<0.01-0.001) (Figure 64C,D).

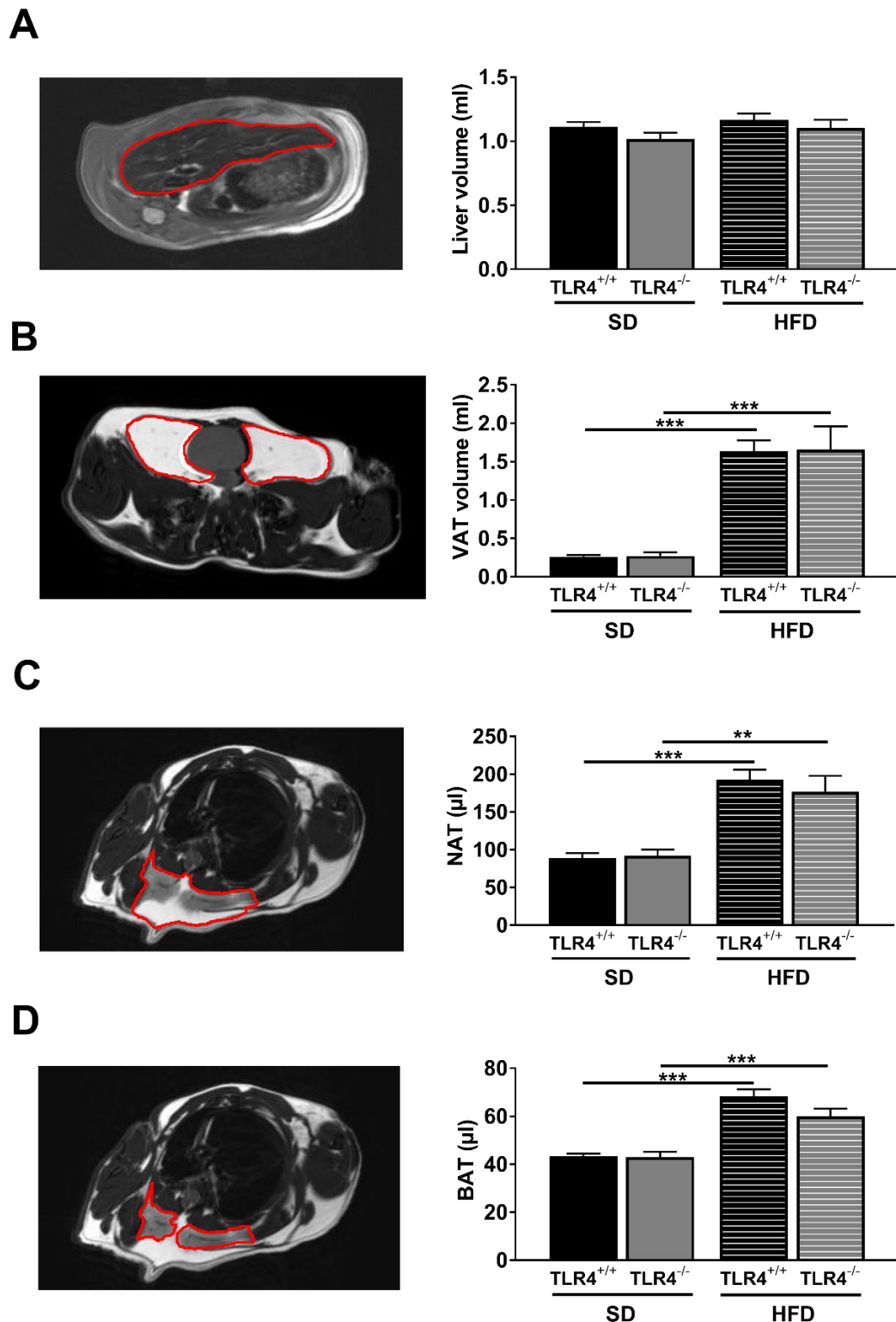


**Figure 64: Higher VAT, NAT and BAT volumes in female prediabetic NOD TLR4<sup>+/+</sup> and NOD TLR4<sup>-/-</sup> mice on HFD compared to mice on SD.** The volumes of the liver and fat depots were measured by encircling the MRT-derived tissue shapes in each slice in axial direction and analyzing each slice to determine the entire tissue volume from MRT-derived images from female prediabetic NOD TLR4<sup>+/+</sup> and NOD TLR4<sup>-/-</sup> mice on SD or HFD. The volume of liver (A), VAT (B), NAT (C) and BAT (D) was determined in NOD TLR4<sup>+/+</sup> and TLR4<sup>-/-</sup> mice. Data are given as means ± SEM. n=5-7. \*\*p<0.01, \*\*\*p<0.001 by one-way ANOVA.

### 3.2.6 Body fat mass

To analyze the potential effect of HFD-feeding on the fat mass development, the body composition was determined in female prediabetic NOD TLR4<sup>+/+</sup> and NOD TLR4<sup>-/-</sup> mice at the age of 30 and 70 days. NOD TLR4<sup>+/+</sup> and NOD TLR4<sup>-/-</sup> mice fed with HFD showed comparable body composition at the age of 30 and 70 days. However, NOD TLR4<sup>+/+</sup> and NOD TLR4<sup>-/-</sup> mice fed with HFD showed higher fat mass (SD: TLR4<sup>+/+</sup>: 13.1±1.1; TLR4<sup>-/-</sup>: 13.6±0.8 %; HFD: TLR4<sup>+/+</sup>: 28.1±1.5; TLR4<sup>-/-</sup>: 28.6±1.9 %) and lower fat free mass (SD: TLR4<sup>+/+</sup>: 82.1±0.8; TLR4<sup>-/-</sup>: 81.5±0.8 %; HFD: TLR4<sup>+/+</sup>: 69.1±1.4; TLR4<sup>-/-</sup>: 69.2±1.7 %) at the age of 70 days compared to NOD TLR4<sup>+/+</sup> and NOD TLR4<sup>-/-</sup> mice fed with SD (all p<0.001) (Figure 65). Interestingly, NOD TLR4<sup>+/+</sup> and NOD TLR4<sup>-/-</sup> mice fed with HFD revealed a higher fat mass and lower fat free mass at the age of 70 days (Fat mass: TLR4<sup>+/+</sup>: 28.1±1.5; TLR4<sup>-/-</sup>: 28.6±1.9 %; Fat free mass: TLR4<sup>+/+</sup>: 69.1±1.4; TLR4<sup>-/-</sup>: 69.2±1.7 %) compared to animals aged 30 days (Fat mass: TLR4<sup>+/+</sup>: 16.1±0.8; TLR4<sup>-/-</sup>: 16.0±0.7 %; Fat free mass: TLR4<sup>+/+</sup>: 80.3±0.8; TLR4<sup>-/-</sup>: 80.7±0.7 %) (p<0.001) (Figure 65).

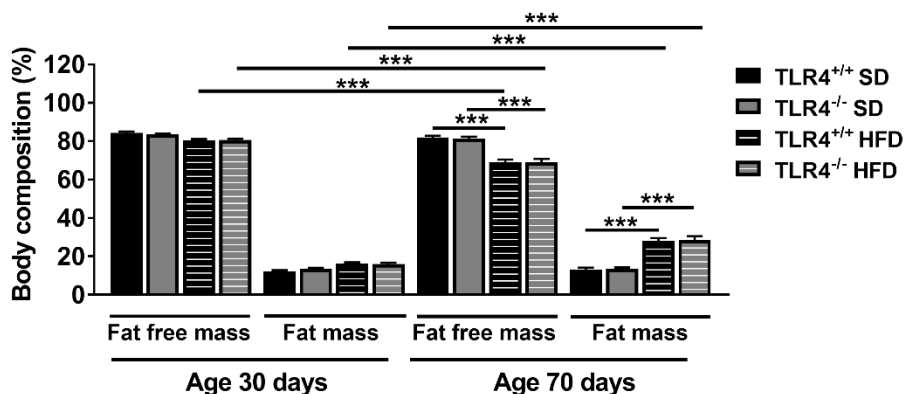


**Figure 65: Higher fat mass and lower fat free mass in female NOD TLR4<sup>+/+</sup> and NOD TLR4<sup>-/-</sup> mice on HFD compared to mice on SD at the age of 70 days.** The body composition of 30 and 70 days old female NOD TLR4<sup>+/+</sup> and NOD TLR4<sup>-/-</sup> mice fed with SD or HFD was analyzed by differentiating in fat free mass and fat mass by NMR. Data show the proportion of fat free mass and fat mass as percent of the whole body weight. Data are given as means ± SEM. n=6-11. \*\*\*p<0.001 by one-way ANOVA.

### 3.2.7 Effect of HFD on random blood glucose levels

To investigate the effect of HFD-feeding on blood glucose levels in both genotypes, the random blood glucose concentrations of unfasted female prediabetic NOD TLR4<sup>+/+</sup> and NOD TLR4<sup>-/-</sup> mice at the age of 70-90 days were determined. Blood glucose levels of 90-250 mg/dl were classified as normal range, whereas blood glucose levels above 250 mg/dl indicated hyperglycemia and diabetes development. Compared to NOD TLR4<sup>+/+</sup> mice fed with HFD, NOD TLR4<sup>-/-</sup> mice fed with HFD showed lower blood glucose concentrations (TLR4<sup>+/+</sup>: 139±2; TLR4<sup>-/-</sup>: 124±3 mg/dl) (p<0.05). Interestingly, NOD TLR4<sup>+/+</sup> mice on HFD showed higher blood

glucose levels than NOD TLR4<sup>+/+</sup> mice on SD (SD: 120±3; HFD: 139±2 mg/dl) ( $p<0.01$ ) (Figure 66).

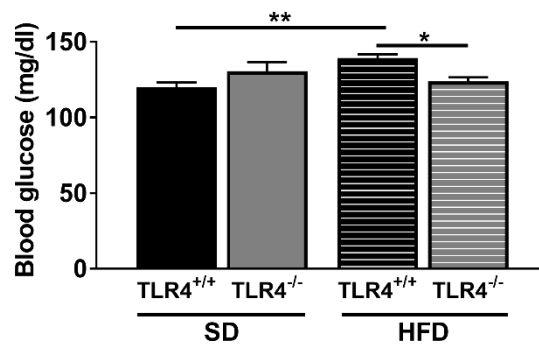


**Figure 66: Lower random blood glucose levels in NOD TLR4<sup>-/-</sup> mice on HFD compared to NOD TLR4<sup>+/+</sup> mice on HFD.** The random blood glucose levels were measured from non-fasted female prediabetic NOD TLR4<sup>+/+</sup> and NOD TLR4<sup>-/-</sup> mice on SD or HFD at the age of 70-90 days. Data are given as means ± SEM. n=6-8. \* $p<0.05$ , \*\* $p<0.01$  by one-way ANOVA.

### 3.2.8 Impact of HFD on the development of insulinitis and decline of beta cell mass in pancreatic islets

To elucidate a potential impact of a HFD on the size of pancreatic islets, islets from female prediabetic age 70-90 days old NOD TLR4<sup>+/+</sup> and NOD TLR4<sup>-/-</sup> mice were evaluated in pancreatic thin sections. Evaluation of the islets revealed that NOD TLR4<sup>+/+</sup> mice on HFD had a 42 % larger total area (65945±5950  $\mu\text{m}^2$ ) when compared to NOD TLR4<sup>+/+</sup> mice on SD (38291±3778  $\mu\text{m}^2$ ) ( $p<0.01$ ) (Figure 67A). NOD TLR4<sup>-/-</sup> mice on HFD (66266±5128  $\mu\text{m}^2$ ) showed comparable islet areas with NOD TLR4<sup>+/+</sup> mice on HFD, whereas NOD TLR4<sup>-/-</sup> mice had an islet area of 53792±4834  $\mu\text{m}^2$  (Figure 67A). Islets with an area less than 500  $\mu\text{m}^2$  were excluded from the evaluation in order to minimize errors.

To investigate the effect of HFD on the decline of the pancreatic beta-cell mass in NOD mice expressing or lacking TLR4, the insulin-positive areas of the pancreatic islets were determined. NOD TLR4<sup>+/+</sup> mice on SD (56.6±1.2 %) revealed a 6.6 % higher proportion of the insulin-positive area of the total islet area compared to the NOD TLR4<sup>+/+</sup> mice on HFD (50.0±1.1 %) ( $p<0.001$ ) (Figure 67B). In the SD and in the HFD fed groups, the TLR4 expression status had no effect on the insulin-positive area.

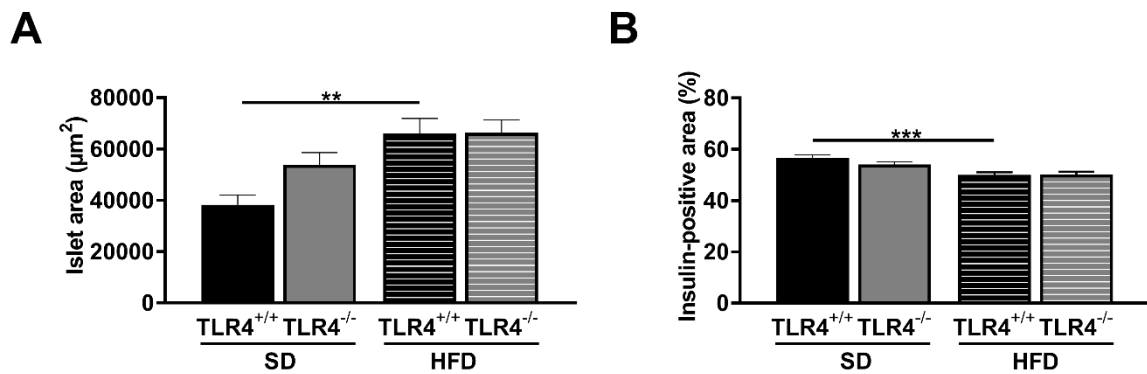


**Figure 67: Total area and insulin-positive area of pancreatic of NOD TLR4<sup>+/+</sup> and NOD TLR4<sup>-/-</sup> mice on SD or HFD.** The total area of pancreatic islets was measured (A). The relative insulin-positive area was measured in female prediabetic NOD TLR4<sup>+/+</sup> and NOD TLR4<sup>-/-</sup> mice on SD or HFD (B). 339-443 pancreatic islets were analyzed per genotype. Islet areas less than 500 µm<sup>2</sup> were excluded. Data are given as means ± SEM. n=9-10. \*\*p<0.01, \*\*\*p<0.001 by one-way ANOVA.

To further characterize the severity of islet inflammation, the immune cell infiltration of pancreatic islets of NOD TLR4<sup>+/+</sup> and NOD TLR4<sup>-/-</sup> mice on SD and HFD was determined and different stages of insulinitis were categorized into scores 0-3 (Figure 33A) based on the progression of inflammation (Figure 68). The numbers of islets with a certain immune cell infiltration rate were combined for each genotype and expressed as percent infiltrated islet area. There was no difference in immune cell infiltration between the genotypes and diets (Figure 68A).

Figure 68B shows the four scores and their proportion of the total islet number in the four experimental groups. NOD TLR4<sup>+/+</sup> and NOD TLR4<sup>-/-</sup> mice showed comparable proportions of score 0 under SD and HFD (SD: TLR4<sup>+/+</sup>: 55.5; TLR4<sup>-/-</sup>: 47.9 %; HFD: TLR4<sup>+/+</sup>: 45.4; TLR4<sup>-/-</sup>: 44.4 %) (Figure 68B). The highest amount of islets was assigned to score 0 and the lowest amount of islets to score 1 (SD: TLR4<sup>+/+</sup>: 4.4; TLR4<sup>-/-</sup>: 5.7 %; HFD: TLR4<sup>+/+</sup>: 2.5; TLR4<sup>-/-</sup>: 3.2 %). About 40-50 % of the islets account for score 2 and score 3 (SD: TLR4<sup>+/+</sup>: 40.1; TLR4<sup>-/-</sup>: 46.5 %; HFD: TLR4<sup>+/+</sup>: 52.1; TLR4<sup>-/-</sup>: 52.4 %). NOD TLR4<sup>+/+</sup> and NOD TLR4<sup>-/-</sup> mice on HFD showed 30 % in score 2, while mice on SD revealed 24-28 % (SD: TLR4<sup>+/+</sup>: 23.9; TLR4<sup>-/-</sup>: 27.8 %; HFD: TLR4<sup>+/+</sup>: 29.6; TLR4<sup>-/-</sup>: 29.4 %). Islet proportion in score 3 were also comparable between the genotypes and diets (SD: TLR4<sup>+/+</sup>: 16.2; TLR4<sup>-/-</sup>: 18.6 %; HFD: TLR4<sup>+/+</sup>: 22.6; TLR4<sup>-/-</sup>: 23.0 %).

Figure 68C shows the experimental groups only separated by their diets and their scores to identify a possible association between the islet area and the scores within the experimental groups. In particular, higher proportions of pancreatic islets with areas exceeding 200000 µm<sup>2</sup> showed score 2 and 3 than score 0-1 (all p<0.001) (Figure 68C). Animals fed with HFD showed

the highest proportion of islets  $>200000 \mu\text{m}^2$  with an infiltration  $<50\%$  and  $>50\%$  (SD: 33.1; HFD: 57.9 %) when compared to mice fed with SD ( $p<0.05$ ).

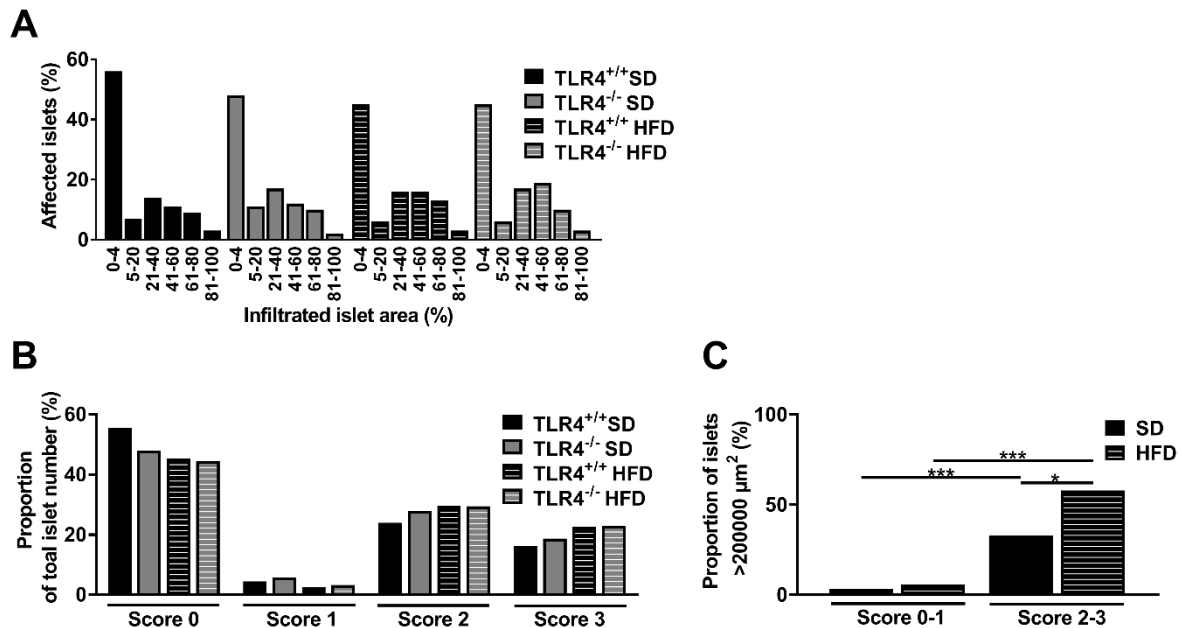


**Figure 68: Infiltrated islet area and the association of islet area and insulinitis-scores in NOD TLR4<sup>+/+</sup> and NOD TLR4<sup>-/-</sup> mice on SD or HFD.** The amount of islets with a certain infiltration rate were analyzed from female prediabetic NOD TLR4<sup>+/+</sup> and NOD TLR4<sup>-/-</sup> mice on SD or HFD and expressed as cumulative proportions of afflicted islets (A). The severity of insulinitis was assessed by categorizing into four insulinitis-scores: Score 0= no insulinitis, 1=  $<10\%$  and peri-insulinitis, 2=  $<50\%$  infiltration, 3=  $>50\%$  infiltration (B). The proportion of islets with an area  $>200000 \mu\text{m}^2$  and scores 0-1 and 2-3 were determined (C). Islet areas less than  $500 \mu\text{m}^2$  were excluded from the evaluation.  $n=9-10$ . \* $p<0.05$ , \*\*\* $p<0.001$  by Fisher's exact test.

### 3.2.9 Effect of HFD on lipid metabolism

To assess the effect of feeding a HFD to female prediabetic NOD TLR4<sup>+/+</sup> and NOD TLR4<sup>-/-</sup> mice at the age of 70-90 days on lipid metabolism, parameters such as plasma levels of FFA, TG and cholesterol were measured.

#### 3.2.9.1 Plasma free fatty acid and triglyceride levels

NOD TLR4<sup>+/+</sup> and NOD TLR4<sup>-/-</sup> mice fed with HFD showed similar FFA concentrations in the plasma compared to NOD TLR4<sup>+/+</sup> and NOD TLR4<sup>-/-</sup> mice fed with SD (SD: TLR4<sup>+/+</sup>:  $741.9 \pm 82.0$ ; TLR4<sup>-/-</sup>:  $920.7 \pm 102.4 \mu\text{mol/l}$ ; HFD: TLR4<sup>+/+</sup>:  $797.9 \pm 65.0$ ; TLR4<sup>-/-</sup>:  $604.9 \pm 93.4 \mu\text{mol/l}$ ) (Figure 69A). Furthermore, plasma triglyceride levels were comparable in NOD TLR4<sup>+/+</sup> and NOD TLR4<sup>-/-</sup> mice fed with HFD and SD (SD: TLR4<sup>+/+</sup>:  $143.1 \pm 12.2$ ; TLR4<sup>-/-</sup>:  $160.6 \pm 15.1 \text{ mg/dl}$ ; HFD: TLR4<sup>+/+</sup>:  $126.1 \pm 8.7$ ; TLR4<sup>-/-</sup>:  $160.8 \pm 12.3 \text{ mg/dl}$ ) (Figure 69B).

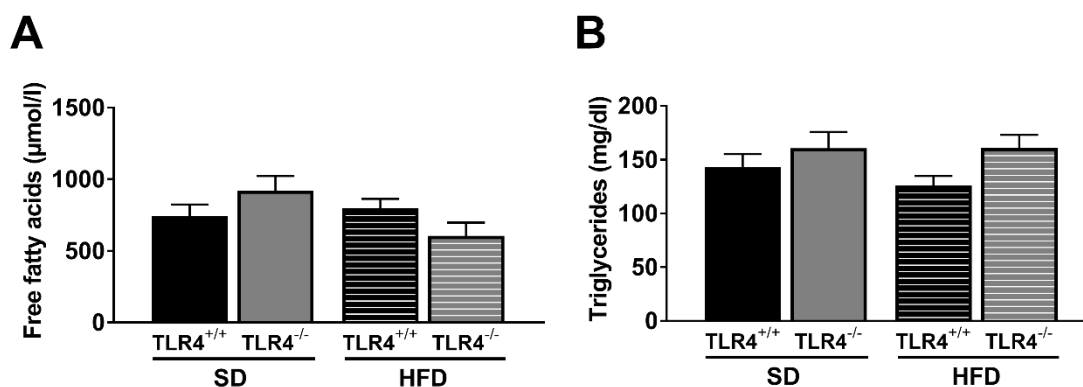


**Figure 69: Comparable plasma free fatty acid and triglyceride levels in female prediabetic NOD TLR4<sup>+/+</sup> and NOD TLR4<sup>-/-</sup> mice fed with SD or HFD.** Free fatty acid levels in µmol/l (A) and triglyceride concentrations in mg/dl (B) were measured in the plasma of female prediabetic NOD TLR4<sup>+/+</sup> and NOD TLR4<sup>-/-</sup> mice fed with SD or HFD. Data are given as means ± SEM. n=10.

### 3.2.9.2 Levels of plasma cholesterol, HDL, LDL and CRP

Plasma samples of female prediabetic NOD TLR4<sup>+/+</sup> and NOD TLR4<sup>-/-</sup> mice at the age of 70-90 days fed with SD or HFD were analyzed for their cholesterol, HDL, LDL and CRP content. NOD TLR4<sup>+/+</sup> and NOD TLR4<sup>-/-</sup> mice fed with HFD showed higher plasma cholesterol levels compared to mice fed with SD (SD: TLR4<sup>+/+</sup>: 78.3±2.4; TLR4<sup>-/-</sup>: 75.4±2.0 mg/dl; HFD: TLR4<sup>+/+</sup>: 119.2±1.6; TLR4<sup>-/-</sup>: 126.1±2.6 mg/dl) (Figure 70A). Additionally, NOD TLR4<sup>+/+</sup> and NOD TLR4<sup>-/-</sup> mice fed with HFD also revealed higher plasma HDL concentrations than mice fed with SD (SD: TLR4<sup>+/+</sup>: 48.9±1.6; TLR4<sup>-/-</sup>: 50.4±1.4 mg/dl; HFD: TLR4<sup>+/+</sup>: 88.0±4.1; TLR4<sup>-/-</sup>: 88.8±3.0 mg/dl) (Figure 70B). Furthermore, higher plasma levels of LDL were found in NOD TLR4<sup>+/+</sup> and NOD TLR4<sup>-/-</sup> mice fed with HFD compared to mice fed with SD (SD: TLR4<sup>+/+</sup>: 10.9±0.3; TLR4<sup>-/-</sup>: 10.4±0.4 mg/dl; HFD: TLR4<sup>+/+</sup>: 18.2±1.1; TLR4<sup>-/-</sup>: 17.6±0.6 mg/dl) (Figure 70C). Furthermore, NOD TLR4<sup>+/+</sup> and NOD TLR4<sup>-/-</sup> mice on HFD and SD showed comparable C-reactive protein levels in plasma SD (SD: TLR4<sup>+/+</sup>: 0.126±0.030; TLR4<sup>-/-</sup>: 0.128±0.029 mg/dl; HFD: TLR4<sup>+/+</sup>: 0.128±0.029; TLR4<sup>-/-</sup>: 0.164±0.024 mg/dl) (Figure 70D).

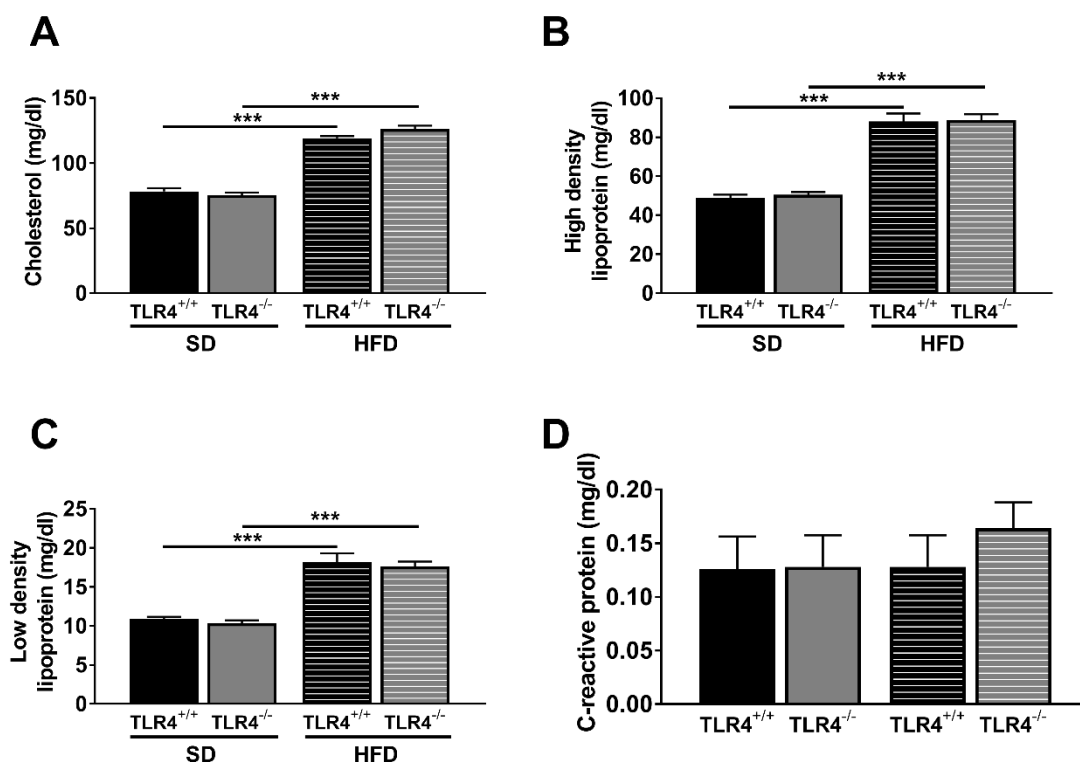


**Figure 70: Higher plasma cholesterol, high and low density lipoprotein but similar C-reactive protein levels in female prediabetic NOD TLR4<sup>+/+</sup> and NOD TLR4<sup>-/-</sup> mice fed with HFD compared to mice fed with SD.** Concentrations of cholesterol in mg/dl (A), high density lipoprotein in mg/dl (B), low density lipoprotein in mg/dl (C) and C-reactive protein in mg/dl (D) were measured in the plasma of female prediabetic NOD TLR4<sup>+/+</sup> and NOD TLR4<sup>-/-</sup> mice fed with SD or HFD. Data are given as means  $\pm$  SEM. n=10. \*\*\*p<0.001 by one-way ANOVA.

### 3.2.9.3 Composition of fat depots

To analyze a possible effect of feeding a HFD on the fat composition of different fat deposits in the mouse, <sup>1</sup>H MRS was applied in female prediabetic 70-90 days old NOD TLR4<sup>+/+</sup> and NOD TLR4<sup>-/-</sup> mice fed with SD or HFD. Fat depots such as VAT, NAT (BAT and WAT) and BAT were identified and their relative contents of SFA, MUFA and PUFA were quantified. The voxel positioning in axial direction in the VAT of the mice to measure the FA composition (Figure 71A) is shown as well as a representative <sup>1</sup>H MRS spectrum of VAT with the H<sub>2</sub>O reference peak (Figure 71B). The peak assignments of SFA, MUFA and PUFA with location and type were determined (Table 12). NOD TLR4<sup>+/+</sup> and NOD TLR4<sup>-/-</sup> mice fed with HFD showed no differences in the proportion of SFA in the VAT between each other and NOD TLR4<sup>+/+</sup> and NOD TLR4<sup>-/-</sup> mice fed with SD also showed similar proportions of SFA (SD TLR4<sup>+/+</sup>: 19.6 $\pm$ 3.8; TLR4<sup>-/-</sup>: 24.9 $\pm$ 3.9 %; HFD: TLR4<sup>+/+</sup>: 10.3 $\pm$ 1.9; TLR4<sup>-/-</sup>: 16.1 $\pm$ 1.4 %) (Figure 71C). Interestingly, NOD TLR4<sup>+/+</sup> and NOD TLR4<sup>-/-</sup> mice fed with HFD had higher proportions of MUFA in the VAT than NOD TLR4<sup>+/+</sup> and NOD TLR4<sup>-/-</sup> mice fed with SD (SD TLR4<sup>+/+</sup>: 52.1 $\pm$ 2.6; TLR4<sup>-/-</sup>: 53.9 $\pm$ 3.0 %; HFD: TLR4<sup>+/+</sup>: 68.4 $\pm$ 2.3; TLR4<sup>-/-</sup>: 64.2 $\pm$ 1.6 %) (p<0.05-0.01) (Figure 71D). The proportion of PUFA was higher in NOD TLR4<sup>+/+</sup> mice on SD compared to

NOD TLR4<sup>-/-</sup> mice on SD and NOD TLR4<sup>+/+</sup> mice on HFD (SD: TLR4<sup>+/+</sup>: 28.7±2.0; TLR4<sup>-/-</sup>: 21.2±1.5 %; HFD: TLR4<sup>+/+</sup>: 21.3±1.1 %) (all p<0.01) (Figure 71E).

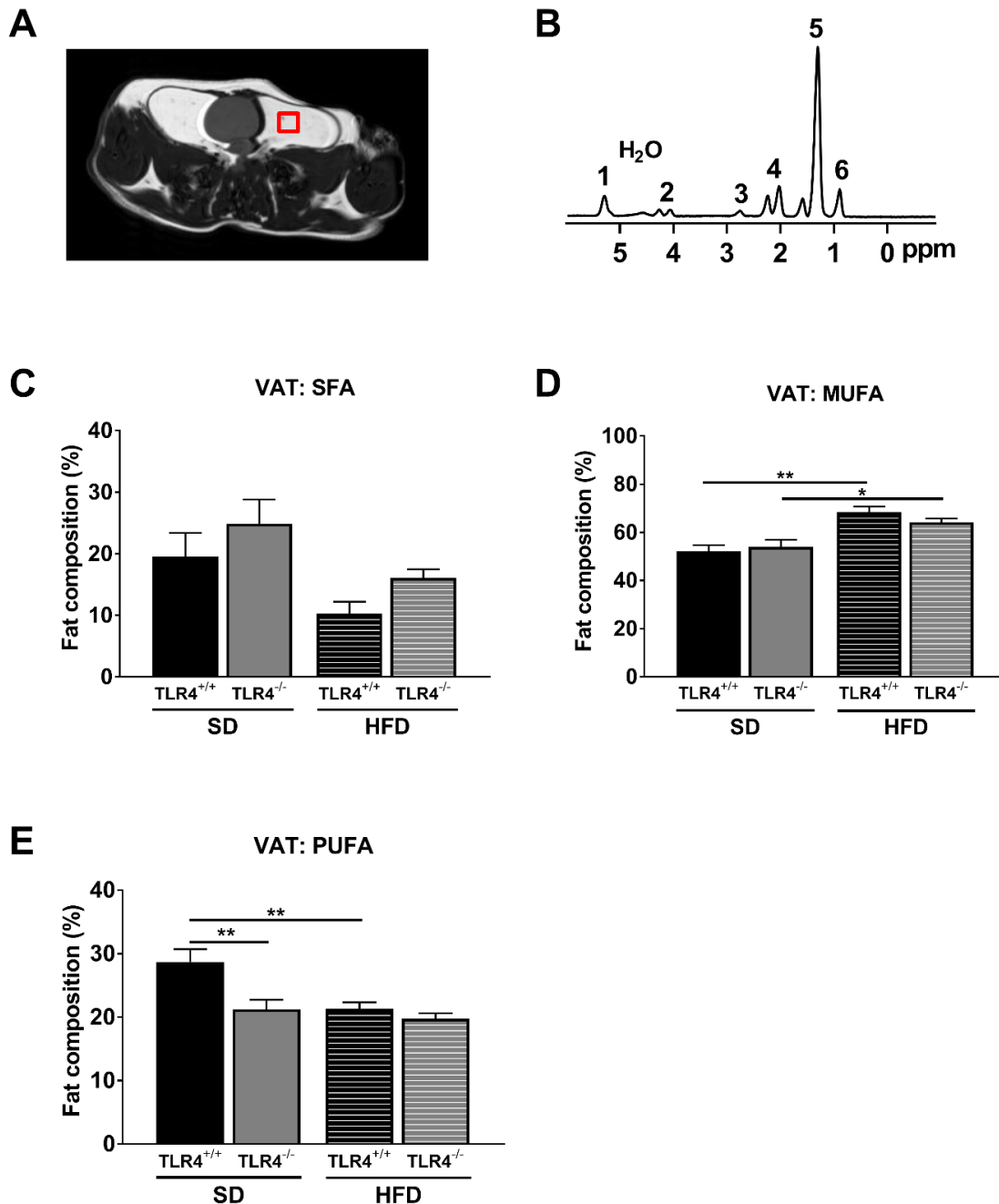


**Figure 71: Effect of the TLR4-expression status on the fat composition of VAT in female prediabetic NOD TLR4<sup>+/+</sup> and NOD TLR4<sup>-/-</sup> mice fed with SD or HFD.** Voxel positioning in axial direction in VAT to measure the FA composition in female prediabetic NOD TLR4<sup>+/+</sup> and NOD TLR4<sup>-/-</sup> mice (A) and a representative <sup>1</sup>H MRS VAT spectrum with fat peak assignments (B). Fat peak assignment: 1: -CH=CH- and -CH-O-CO-, 2: -CH<sub>2</sub>-O-CO-, 3: -CH=CH-CH<sub>2</sub>-CH=CH-, 4: -CO-CH<sub>2</sub>-CH<sub>2</sub>- and -CH<sub>2</sub>-CH=CH-CH<sub>2</sub>-, 5: -CO-CH<sub>2</sub>-CH<sub>2</sub>- and -(CH<sub>2</sub>)<sub>n</sub>-, 6: -(CH<sub>2</sub>)<sub>n</sub>-CH<sub>3</sub>. The percentage of SFA (C), MUFA (D) and PUFA (E) in VAT in NOD TLR4<sup>+/+</sup> and NOD TLR4<sup>-/-</sup> mice was determined by MRS. Data are given as means ± SEM. n=11-19. \*p<0.05, \*\*p<0.01 by one-way ANOVA.

## Results

The NAT composition was analyzed in female prediabetic 70-90 days old NOD TLR4<sup>+/+</sup> and NOD TLR4<sup>-/-</sup> mice fed with SD or HFD. For the measurement of the FA composition, the voxel was positioned in axial direction in the NAT of the mice (Figure 72A). A representative <sup>1</sup>H MRS spectrum of NAT with the H<sub>2</sub>O reference peak is shown in Figure 72B. The peak assignments of SFA, MUFA and PUFA with location and type were determined (Table 12).

NOD TLR4<sup>+/+</sup> and NOD TLR4<sup>-/-</sup> mice on SD and HFD showed no differences in the proportion of SFA in the NAT (SD: TLR4<sup>+/+</sup>: 38.2±4.6; TLR4<sup>-/-</sup>: 31.7±5.0 %; HFD: TLR4<sup>+/+</sup>: 19.5±4.4; TLR4<sup>-/-</sup>: 32.0±3.6 %) (Figure 72C). Interestingly, NOD TLR4<sup>+/+</sup> mice on HFD revealed higher proportions of MUFA in the NAT compared to NOD TLR4<sup>+/+</sup> mice on SD (SD: 58.1±3.5; HFD: 68.8±4.2 %) (p<0.05) (Figure 72D). There was no difference in MUFA proportions between the genotypes and NOD TLR4<sup>-/-</sup> mice on SD and HFD. Moreover, NOD TLR4<sup>+/+</sup> and NOD TLR4<sup>-/-</sup> mice on SD and HFD had comparable proportions of PUFA in the NAT (SD: TLR4<sup>+/+</sup>: 13.8±1.6; TLR4<sup>-/-</sup>: 13.4±1.7 %; HFD: TLR4<sup>+/+</sup>: 11.7±1.3; TLR4<sup>-/-</sup>: 10.0±1.1 %) (Figure 72E).

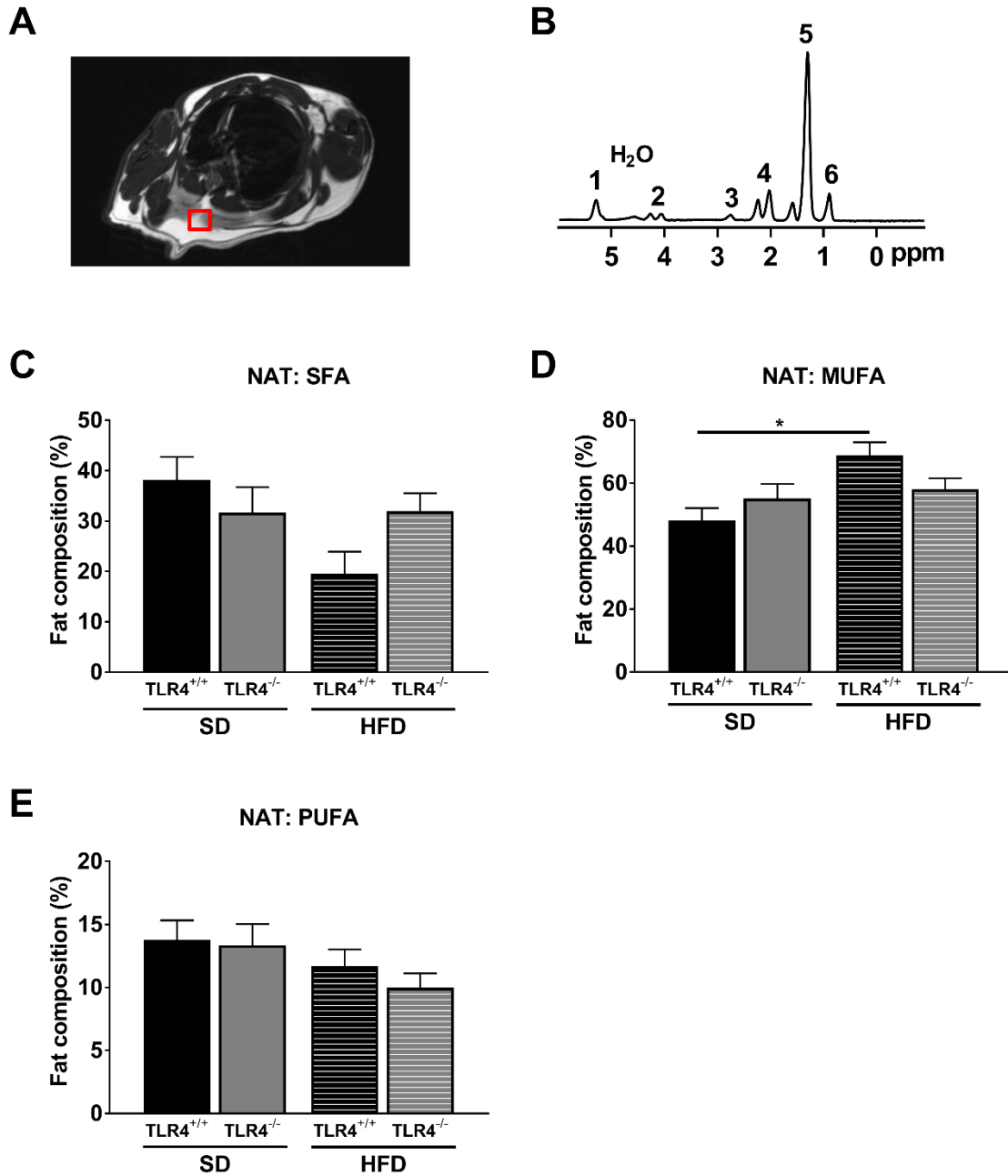


**Figure 72: Effect of the TLR4-expression status on the fat composition of the NAT in female prediabetic NOD TLR4<sup>+/+</sup> and NOD TLR4<sup>-/-</sup> mice fed with either SD or HFD.** Voxel positioning in axial direction in the NAT to measure the FA composition in female prediabetic NOD TLR4<sup>+/+</sup> and NOD TLR4<sup>-/-</sup> mice on SD or HFD (A) and a representative <sup>1</sup>H MRS neck fat spectrum with fat peak assignments (B). Fat peak assignment: 1: -CH=CH- and -CH-O-CO-, 2: -CH<sub>2</sub>-O-CO-, 3: -CH=CH-CH<sub>2</sub>-CH=CH-, 4: -CO-CH<sub>2</sub>-CH<sub>2</sub>- and -CH<sub>2</sub>-CH=CH-CH<sub>2</sub>-, 5: -CO-CH<sub>2</sub>-CH<sub>2</sub>- and -(CH<sub>2</sub>)<sub>n</sub>-, 6: -(CH<sub>2</sub>)<sub>n</sub>-CH<sub>3</sub>. The percentage of SFA (C), MUFA (D) and PUFA (E) in NAT in NOD TLR4<sup>+/+</sup> and NOD TLR4<sup>-/-</sup> mice was determined by MRS. Data are given as means ± SEM. n=11-22. \*p<0.05 by one-way ANOVA.

## Results

The composition of fatty acids in VAT was compared to the fatty acid composition in NAT in female prediabetic 70-90 days old NOD TLR4<sup>+/+</sup> and NOD TLR4<sup>-/-</sup> mice on SD or HFD. NOD TLR4<sup>+/+</sup> and NOD TLR4<sup>-/-</sup> mice fed with SD and HFD showed similar proportions of SFA in VAT (SD: TLR4<sup>+/+</sup>: 19.6±3.8; TLR4<sup>-/-</sup>: 24.9±3.9 %; HFD: TLR4<sup>+/+</sup>: 10.3±1.9; TLR4<sup>-/-</sup>: 16.1±1.4 %) and NAT (SD: TLR4<sup>+/+</sup>: 38.2±4.6; TLR4<sup>-/-</sup>: 31.7±5.0 %; HFD: TLR4<sup>+/+</sup>: 19.5±4.4; TLR4<sup>-/-</sup>: 31.9±3.6 %).

Furthermore, NOD TLR4<sup>+/+</sup> and NOD TLR4<sup>-/-</sup> mice on SD and HFD showed comparable proportions of MUFA in VAT (SD: TLR4<sup>+/+</sup>: 52.1±2.6; TLR4<sup>-/-</sup>: 53.9±3.0 %; HFD: TLR4<sup>+/+</sup>: 68.4±2.3; TLR4<sup>-/-</sup>: 64.2±1.6 %) and NAT (SD: TLR4<sup>+/+</sup>: 48.1±4.0; TLR4<sup>-/-</sup>: 55.1±4.6 %; HFD: TLR4<sup>+/+</sup>: 68.8±4.2; TLR4<sup>-/-</sup>: 58.1±3.5 %), except that NOD TLR4<sup>+/+</sup> mice on HFD revealed a higher MUFA proportion in NAT than NOD TLR4<sup>+/+</sup> mice on SD ( $p < 0.01$ ).

Interestingly, a higher proportion of PUFA was found in VAT (SD: TLR4<sup>+/+</sup>: 28.7±2.0; TLR4<sup>-/-</sup>: 21.2±1.5 %; HFD: TLR4<sup>+/+</sup>: 21.3±1.1; TLR4<sup>-/-</sup>: 19.7±0.9 %) compared to NAT (SD: TLR4<sup>+/+</sup>: 13.8±1.6; TLR4<sup>-/-</sup>: 13.4±1.7 %; HFD: TLR4<sup>+/+</sup>: 11.7±1.3; TLR4<sup>-/-</sup>: 10.0±1.1 %) in both NOD TLR4<sup>+/+</sup> and NOD TLR4<sup>-/-</sup> mice on SD and HFD ( $p < 0.05-0.001$ ).

To determine a potential effect of feeding a HFD on the fat composition of BAT in mice, <sup>1</sup>H MRS was applied in female prediabetic 70-90 days old NOD TLR4<sup>+/+</sup> and NOD TLR4<sup>-/-</sup> mice on SD or HFD. The voxel positioning in axial direction in the BAT of the mice to measure the FA composition is shown in Figure 73A and a representative <sup>1</sup>H MRS spectrum of BAT with the H<sub>2</sub>O reference peak is shown in Figure 73B. The peak assignments of SFA, MUFA and PUFA with location and type were determined (Table 12). No differences in SFA proportion in BAT of NOD TLR4<sup>+/+</sup> and NOD TLR4<sup>-/-</sup> mice fed with SD or HFD were detectable (SD TLR4<sup>+/+</sup>: 19.0±8.0; TLR4<sup>-/-</sup>: 33.4±9.0 %; HFD: TLR4<sup>+/+</sup>: 26.6±9.1; TLR4<sup>-/-</sup>: 21.0±6.8 %) (Figure 73C). Furthermore, NOD TLR4<sup>+/+</sup> and NOD TLR4<sup>-/-</sup> mice fed with SD or HFD showed similar MUFA proportions in the BAT (SD TLR4<sup>+/+</sup>: 51.7±4.0; TLR4<sup>-/-</sup>: 40.2±9.9 %; HFD: TLR4<sup>+/+</sup>: 62.3±9.3; TLR4<sup>-/-</sup>: 59.7±5.6 %) (Figure 73D). The proportion of PUFA in BAT of NOD TLR4<sup>+/+</sup> and NOD TLR4<sup>-/-</sup> mice on HFD and SD was comparable (SD TLR4<sup>+/+</sup>: 29.3±6.5; TLR4<sup>-/-</sup>: 26.4±5.3 %; HFD: TLR4<sup>+/+</sup>: 11.1±1.0; TLR4<sup>-/-</sup>: 19.3±5.6 %) (Figure 73E).

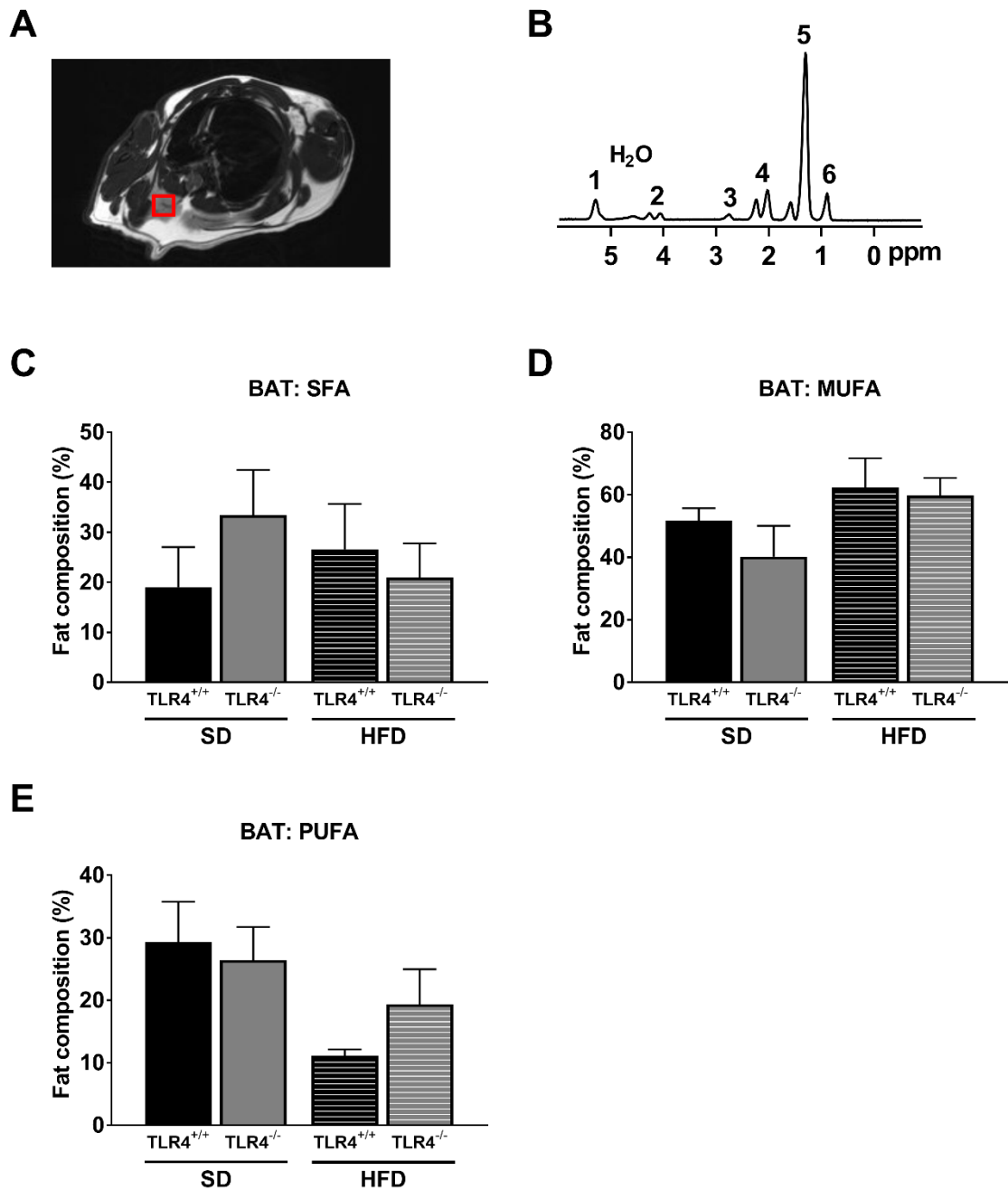


**Figure 73: Effect of the TLR4-expression status on the fat composition of the BAT in female prediabetic NOD TLR4<sup>+/+</sup> and NOD TLR4<sup>-/-</sup> mice fed with SD or HFD.** Voxel positioning in axial direction in the BAT to measure the FA composition in female prediabetic NOD TLR4<sup>+/+</sup> and NOD TLR4<sup>-/-</sup> mice fed with SD or HFD (A) and a representative <sup>1</sup>H MRS BAT spectrum with fat peak assignments (B). Fat peak assignment: 1:  $-\text{CH}=\text{CH}-$  and  $-\text{CH}-\text{O}-\text{CO}-$ , 2:  $-\text{CH}_2-\text{O}-\text{CO}-$ , 3:  $-\text{CH}=\text{CH}-\text{CH}_2-\text{CH}=\text{CH}-$ , 4:  $-\text{CO}-\text{CH}_2-\text{CH}_2-$  and  $-\text{CH}_2-\text{CH}=\text{CH}-\text{CH}_2-$ , 5:  $-\text{CO}-\text{CH}_2-\text{CH}_2-$  and  $-(\text{CH}_2)_n-$ , 6:  $-(\text{CH}_2)_n-\text{CH}_3$ . The percentage of SFA (C), MUFA (D) and PUFA (E) in BAT in NOD TLR4<sup>+/+</sup> and NOD TLR4<sup>-/-</sup> mice was determined by MRS. Data are given as means  $\pm$  SEM. n=5-6.

### 3.2.9.4 Hepatocellular lipid content

To investigate the possible effect of a HFD-feeding on the accumulation of liver fat, the HCL content of female prediabetic 70-90 days old NOD TLR4<sup>+/+</sup> and NOD TLR4<sup>-/-</sup> mice on SD or HFD was quantified via MRS. The voxel was positioned in coronal (left) and axial (right) direction in the liver as shown in Figure 74A. A representative <sup>1</sup>H MRS liver spectrum with the H<sub>2</sub>O reference peak and CH<sub>2</sub> and CH<sub>3</sub> peaks is shown in Figure 74B.

NOD TLR4<sup>+/+</sup> and NOD TLR4<sup>-/-</sup> mice fed with HFD showed higher HCL levels compared to mice fed with SD (SD: TLR4<sup>+/+</sup>: 4.2±0.7; TLR4<sup>-/-</sup>: 2.4±0.3 %; HFD: TLR4<sup>+/+</sup>: 9.2±1.5; TLR4<sup>-/-</sup>: 15.4±2.0 %) (p<0.05-0.001) (Figure 74C). Interestingly, compared to NOD TLR4<sup>+/+</sup> mice fed with HFD, NOD TLR4<sup>-/-</sup> mice fed with HFD revealed higher HCL levels (TLR4<sup>+/+</sup>: 9.2±1.5; TLR4<sup>-/-</sup>: 15.4±2.0 %) (p<0.01) (Figure 74C).

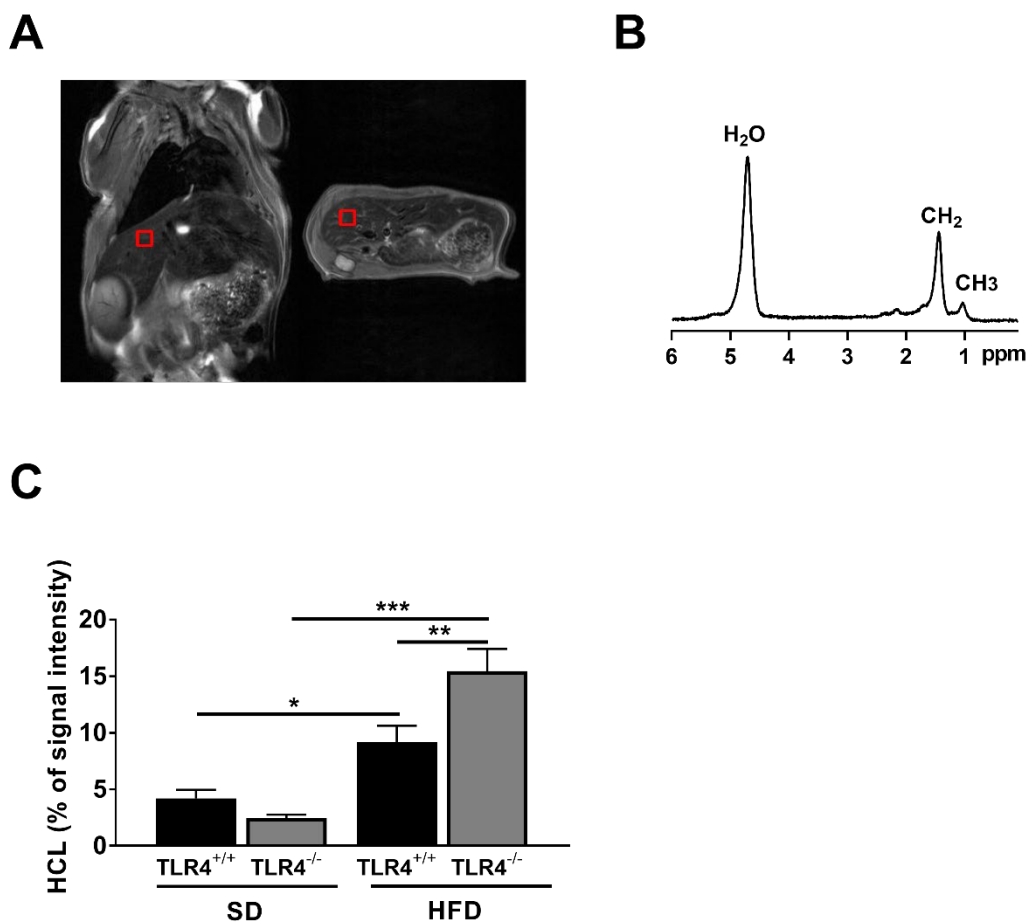


**Figure 74: Higher HCL levels in female prediabetic NOD TLR4<sup>+/+</sup> and NOD TLR4<sup>-/-</sup> mice on HFD compared to mice on SD.** Voxel positioning in coronal (left) and axial (right) direction in the liver to measure lipids in female prediabetic NOD TLR4<sup>+/+</sup> and NOD TLR4<sup>-/-</sup> mice on HFD and SD (A) and a representative <sup>1</sup>H MRS liver spectrum (B). HCL content was analyzed in NOD TLR4<sup>+/+</sup> and NOD TLR4<sup>-/-</sup> mice fed with SD or HFD (C). Data are given as means ± SEM. SD n=17-18, HFD: n=11-12. \*p<0.05, \*\*p<0.01, \*\*\*p<0.001 by one-way ANOVA.

### 3.2.10 Hepatic energy metabolism in NOD TLR4<sup>-/-</sup> mice

To analyze the potential effect of HFD-feeding on the hepatic energy metabolism,  $\gamma$ -ATP, Pi, PME and PDE contents were measured in NOD TLR4<sup>+/+</sup> and NOD TLR4<sup>-/-</sup> mice on SD and HFD by MRS.

#### 3.2.10.1 Hepatic ATP and Pi concentrations

To assess the potential effect of feeding a HFD on liver energy metabolism, hepatic  $\gamma$ -ATP and Pi content was determined in female prediabetic 70-90 days old NOD TLR4<sup>+/+</sup> and NOD TLR4<sup>-/-</sup> mice by MRS. For the measurements, the voxel was positioned in coronal (left) and axial (right) direction in the liver (Figure 75A) and hepatic  $\gamma$ -ATP and Pi content were measured by <sup>31</sup>P MRS in NOD TLR4<sup>+/+</sup> and NOD TLR4<sup>-/-</sup> mice fed with SD and HFD (Figure 75B). Interestingly, NOD TLR4<sup>+/+</sup> and NOD TLR4<sup>-/-</sup> mice on HFD showed higher hepatic  $\gamma$ -ATP concentrations compared to NOD TLR4<sup>+/+</sup> and NOD TLR4<sup>-/-</sup> mice on SD (SD: TLR4<sup>+/+</sup>: 1.62±0.09; TLR4<sup>-/-</sup>: 1.42±0.07 mmol/l; HFD: TLR4<sup>+/+</sup>: 2.05±0.15; TLR4<sup>-/-</sup>: 2.03±0.10 mmol/l) ( $p < 0.05-0.01$ ) (Figure 75C). Furthermore, NOD TLR4<sup>+/+</sup> and NOD TLR4<sup>-/-</sup> mice on SD and HFD showed similar Pi concentrations in the liver (SD: TLR4<sup>+/+</sup>: 1.12±0.08; TLR4<sup>-/-</sup>: 1.11±0.05 mmol/l; HFD: TLR4<sup>+/+</sup>: 1.37±0.07; TLR4<sup>-/-</sup>: 1.28±0.11 mmol/l) (Figure 75D).

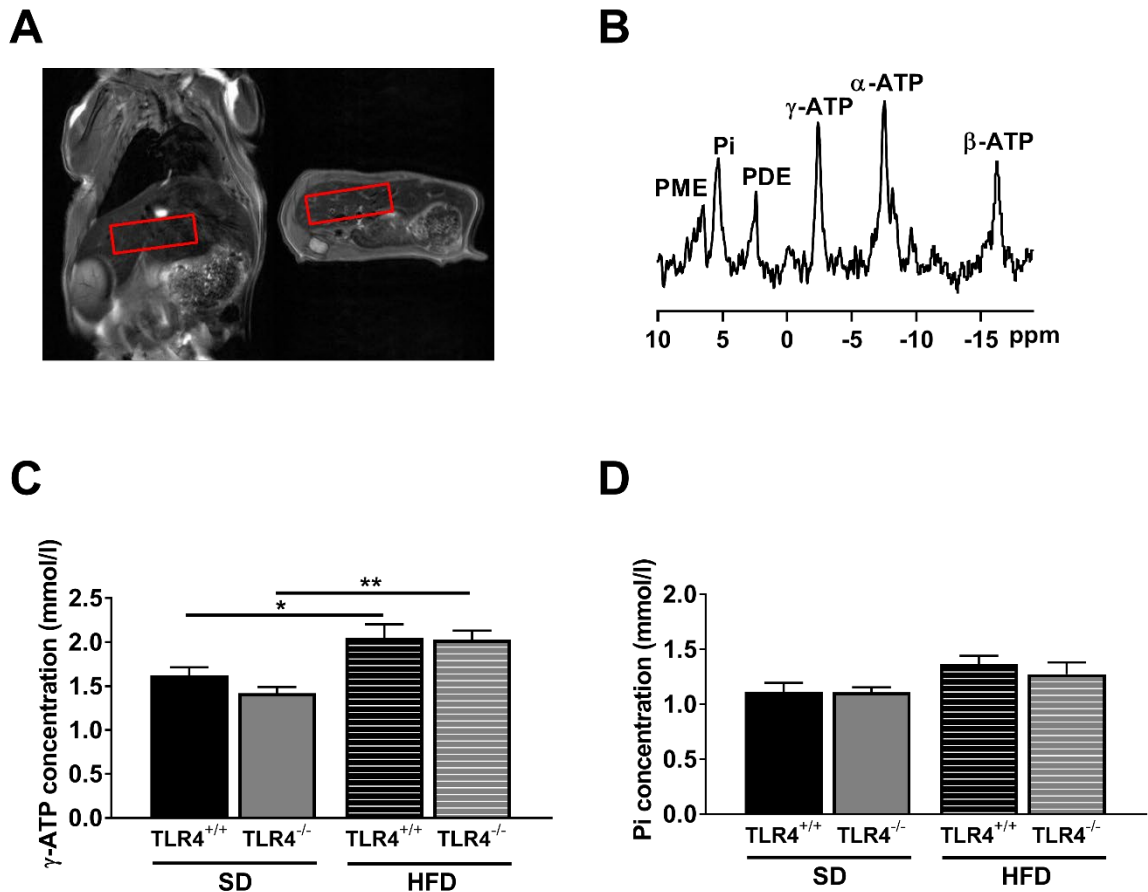


**Figure 75: Higher  $\gamma$ -ATP levels in the liver of female prediabetic NOD TLR4<sup>+/+</sup> and NOD TLR4<sup>-/-</sup> mice fed with HFD compared to mice fed with SD.** Voxel positioning in coronal (left) and axial (right) direction in the liver to measure  $\gamma$ -ATP and Pi concentrations in female prediabetic NOD TLR4<sup>+/+</sup> and NOD TLR4<sup>-/-</sup> mice fed with SD or HFD (A) and a representative  $^{31}\text{P}$  MRS liver spectrum (B). Hepatic  $\gamma$ -ATP (C) and Pi (D) content was analyzed in NOD TLR4<sup>+/+</sup> and NOD TLR4<sup>-/-</sup> mice. Data are given as means  $\pm$  SEM. n=13-16.

$^{31}\text{P}$  measurements were performed before and after intraperitoneal injection of 2g/kg glucose and the  $\gamma$ -ATP and Pi content was determined in the identical liver area before and 15 minutes after the glucose injection in female prediabetic 70-90 days old NOD TLR4<sup>+/+</sup> and NOD TLR4<sup>-/-</sup> mice fed with SD or HFD. Interestingly, 15 minutes after glucose injection, NOD TLR4<sup>+/+</sup> mice on HFD revealed higher hepatic  $\gamma$ -ATP concentrations than NOD TLR4<sup>+/+</sup> mice on SD (SD: 1.50 $\pm$ 0.09; HFD: 2.04 $\pm$ 0.13 mmol/l) ( $p$ <0.01) and before glucose injection, NOD TLR4<sup>-/-</sup> mice fed with HFD showed higher hepatic  $\gamma$ -ATP concentrations than NOD TLR4<sup>-/-</sup> mice on SD (SD: 1.42 $\pm$ 0.07; HFD: 2.03 $\pm$ 0.10 mmol/l) ( $p$ <0.01) (Figure 76A).  $\gamma$ -ATP concentrations measured before and after glucose injection were comparable within the groups fed with SD and in the HFD fed groups. Interestingly, calculation of the difference in  $\gamma$ -ATP concentrations measured before and after glucose injection indicated that NOD TLR4<sup>-/-</sup> mice on HFD have a stronger decrease of  $\gamma$ -ATP levels compared to NOD TLR4<sup>-/-</sup> mice on SD after glucose injection (SD: 0.23 $\pm$ 0.06; HFD: -0.14 $\pm$ 0.07 mmol/l) ( $p$ <0.01) (Figure 76B). Additionally, NOD TLR4<sup>+/+</sup> and

NOD TLR4<sup>-/-</sup> mice on SD and HFD showed similar concentrations of Pi in the liver before (SD: TLR4<sup>+/+</sup>: 1.12±0.08; TLR4<sup>-/-</sup>: 1.11±0.05 mmol/l; HFD: TLR4<sup>+/+</sup>: 1.37±0.07; TLR4<sup>-/-</sup>: 1.28±0.11 mmol/l) and after (SD: TLR4<sup>+/+</sup>: 1.07±0.08; TLR4<sup>-/-</sup>: 1.06±0.06 mmol/l; HFD: TLR4<sup>+/+</sup>: 1.40±0.06; TLR4<sup>-/-</sup>: 1.37±0.08 mmol/l) glucose injection (Figure 76C). Furthermore, Pi concentrations measured before and after glucose injection showed no differences between the genotypes and diets (SD: TLR4<sup>+/+</sup>: -0.046±0.070; TLR4<sup>-/-</sup>: -0.049±0.067 mmol/l; HFD: TLR4<sup>+/+</sup>: 0.03±0.06; TLR4<sup>-/-</sup>: 0.10±0.13 mmol/l) (Figure 76D).

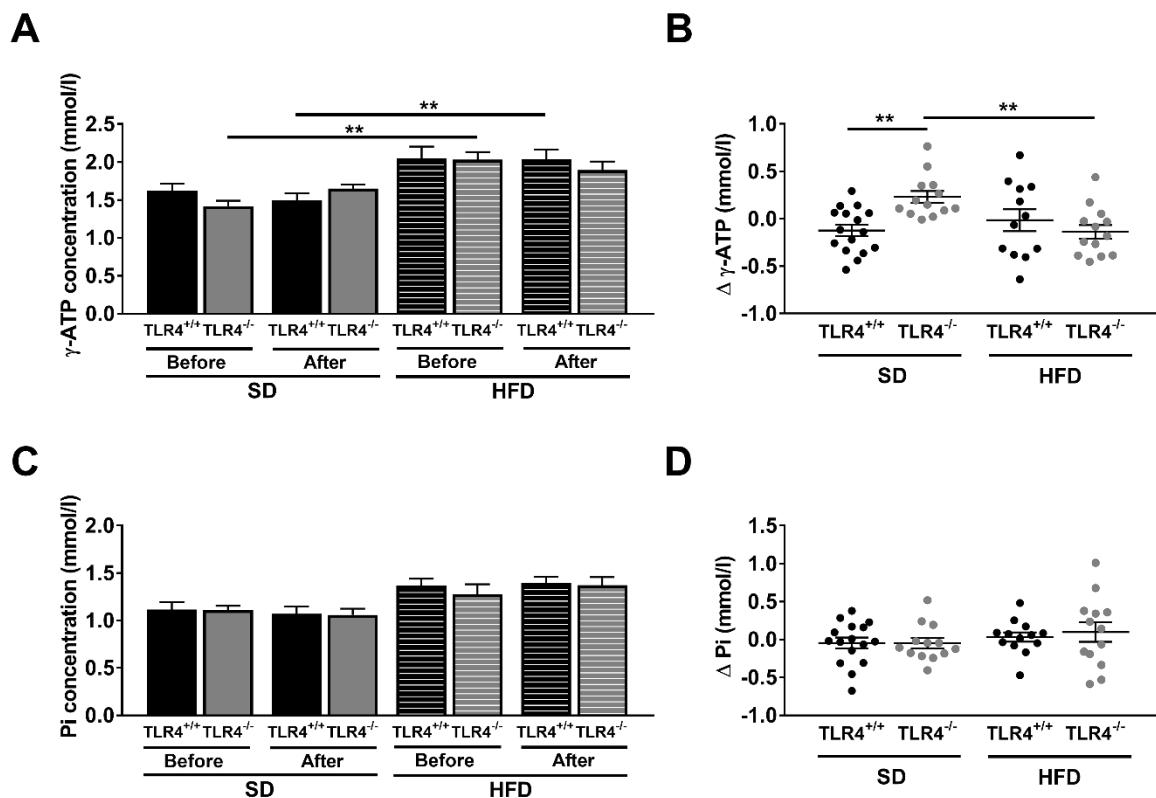


**Figure 76: Hepatic  $\gamma$ -ATP and Pi concentrations before and after glucose injection in female prediabetic NOD TLR4<sup>+/+</sup> and NOD TLR4<sup>-/-</sup> mice fed with SD or HFD.** The hepatic  $\gamma$ -ATP (A) concentrations of female prediabetic NOD TLR4<sup>+/+</sup> and TLR4<sup>-/-</sup> mice fed with SD or HFD before and after glucose injection were analyzed and their differences were calculated (B). The hepatic Pi concentrations (C) and Pi differences (D) of NOD TLR4<sup>+/+</sup> and TLR4<sup>-/-</sup> mice on SD or HFD were calculated.  $\Delta$ =  $\gamma$ -ATP and Pi levels after – before glucose injection in mmol/l. Data are given as means  $\pm$  SEM. n=13-16. \*\*p<0.01 one-way ANOVA.

### 3.2.10.2 Hepatic PME and PDE concentrations

The effect of HFD feeding on PME and PDE concentrations in the liver was assessed in female prediabetic 70-90 days old NOD TLR4<sup>+/+</sup> and NOD TLR4<sup>-/-</sup> mice. For these measurements, the voxel was positioned in coronal (left) and axial (right) direction in the liver (Figure 77A) and hepatic PME and PDE content were measured by <sup>31</sup>P MRS (Figure 77B). NOD TLR4<sup>+/+</sup> and NOD TLR4<sup>-/-</sup> mice on SD and HFD showed comparable PME (SD: TLR4<sup>+/+</sup>: 1.13±0.08; TLR4<sup>-/-</sup>:

$^-$ :  $1.08 \pm 0.07$  mmol/l; HFD: TLR4<sup>+/+</sup>:  $1.11 \pm 0.06$ ; TLR4<sup>-/-</sup>:  $1.04 \pm 0.07$  mmol/l) content in the liver (Figure 77C). Interestingly, NOD TLR4<sup>+/+</sup> mice on HFD showed higher PDE content than NOD TLR4<sup>+/+</sup> mice on SD (SD:  $0.20 \pm 0.04$ ; HFD:  $0.42 \pm 0.07$  mmol/l) ( $p < 0.05$ ) (Figure 77D).

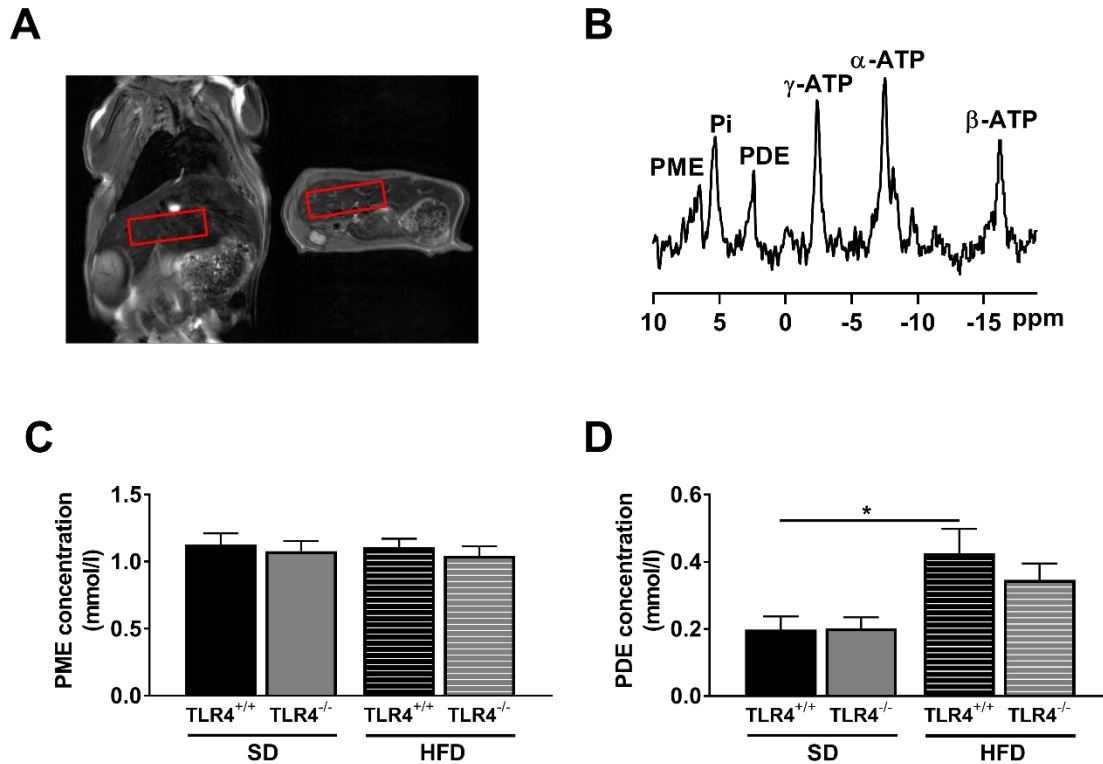


**Figure 77: Similar PME and PDE levels in the liver of female prediabetic NOD TLR4<sup>+/+</sup> and NOD TLR4<sup>-/-</sup> mice on SD or HFD.** Voxel positioning in coronal (left) and axial (right) direction in the liver to measure PME and PDE concentrations in female prediabetic NOD TLR4<sup>+/+</sup> and NOD TLR4<sup>-/-</sup> mice on SD or HFD (A) and a representative <sup>31</sup>P MRS liver spectrum (B). Hepatic PME (C) and PDE (D) contents were analyzed in NOD TLR4<sup>+/+</sup> and NOD TLR4<sup>-/-</sup> mice. Data are given as means  $\pm$  SEM.  $n=11-13$ . \* $p < 0.05$  by one-way ANOVA.

<sup>31</sup>P measurements were performed before and after intraperitoneal injection of 2g/kg glucose and the PME and PDE contents in the liver were determined in the identical liver area before and 15 minutes after the glucose injection in female prediabetic 70-90 days old NOD TLR4<sup>+/+</sup> and NOD TLR4<sup>-/-</sup> mice on SD or HFD. Similar amounts of hepatic PME were measured in NOD TLR4<sup>+/+</sup> and NOD TLR4<sup>-/-</sup> mice on SD and HFD before and after glucose injection (Figure 78A). Calculation of the differences of PMA concentrations showed no alterations in NOD TLR4<sup>+/+</sup> and NOD TLR4<sup>-/-</sup> mice on SD and HFD (SD: TLR4<sup>+/+</sup>:  $0.31 \pm 0.18$ ; TLR4<sup>-/-</sup>:  $0.19 \pm 0.09$  mmol/l; HFD: TLR4<sup>+/+</sup>:  $0.08 \pm 0.08$ ; TLR4<sup>-/-</sup>:  $0.27 \pm 0.39$  mmol/l) (Figure 78B). NOD TLR4<sup>+/+</sup> and NOD TLR4<sup>-/-</sup> mice on SD and HFD showed comparable concentrations of PDE in the liver before and after glucose injection (Figure 78C). Additionally, the difference of PDE concentrations measured before and after glucose injection showed no alterations of PDE levels between the

genotypes (SD: TLR4<sup>+/+</sup>: 0.01±0.05; TLR4<sup>-/-</sup>: -0.04±0.03 mmol/l; HFD: TLR4<sup>+/+</sup>: -0.04±0.07; TLR4<sup>-/-</sup>: -0.06±0.05 mmol/l) (Figure 78D).

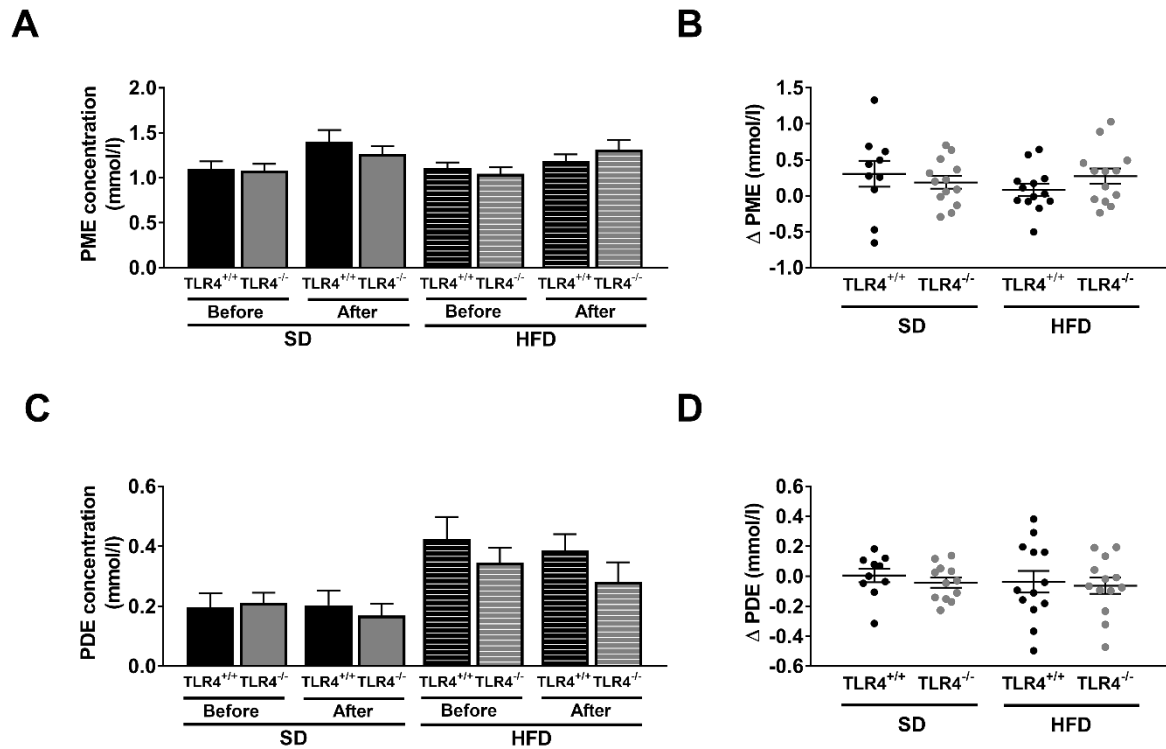


**Figure 78: Hepatic PME and PDE concentrations before and after glucose injection in female prediabetic NOD TLR4<sup>+/+</sup> and NOD TLR4<sup>-/-</sup> mice fed with SD or HFD.** The hepatic PME (A) concentration in female prediabetic NOD TLR4<sup>+/+</sup> and TLR4<sup>-/-</sup> mice fed with SD or HFD before and after glucose injection were analyzed and their differences calculated (B). The hepatic PDE concentration (C) and their differences (D) in NOD TLR4<sup>+/+</sup> and TLR4<sup>-/-</sup> mice was determined.  $\Delta$  = PME and PDE levels after – before glucose injection in mmol/l. Data are given as means  $\pm$  SEM. n=10-13.

## 4 Discussion

### 4.1 Metabolic phenotyping of the NOD TLR4<sup>-/-</sup> mouse, as a model of accelerated development of insulin-deficient diabetes

In recent years, the incidence of T1D in young children is increasing. However, the mechanisms underlying this development are still unknown. The manifestation of T1D is frequently preceded by metabolic disorders, which might contribute to accelerated disease development. However, the metabolic factors controlling diabetes progression in the prediabetic phase are not fully understood. To identify the potential mechanisms underlying this accelerated disease development, an animal model was developed based on the NOD mouse, the currently best characterized and most widely used model of T1D. The NOD mouse lacking TLR4 is known for an accelerated development of insulin-deficient diabetes. Because of the comparability with the increasing incidence of T1D in younger children, the NOD TLR4<sup>-/-</sup> mouse represents an adequate model for detailed analyses of the glucose, lipid and energy metabolism before diabetes manifestation and for identifying possible mechanisms underlying the accelerated development of insulin-deficient diabetes/T1D.

Earlier findings in the NOD TLR4<sup>-/-</sup> mouse model and indications from the literature led to the hypothesis that accelerated diabetes development in NOD TLR4<sup>-/-</sup> mice is associated with impaired glucose, lipid and energy metabolism as well as decreased intestinal and peripheral SCFA levels before the age of diabetes onset.

#### 4.1.1 Effect of TLR4-deficiency in NOD mice on manifestation of insulin-deficient diabetes

The diabetes incidence in the NOD mouse is variable and depends on the NOD colony. Until the age of 200 days, around 60-90 % of female and 10-30 % of male NOD mice develop insulin-deficient diabetes [162, 215, 216]. In the current study, diabetes manifestation of NOD mice was monitored as well as the blood glucose levels at diabetes onset were determined. NOD mice developed diabetes at an age of about 170 days with mean blood glucose concentrations of 437 mg/dl at diabetes onset.

To test if TLR4 is involved in metabolic and inflammatory processes in the pathogenesis of insulin-deficient diabetes/T1D an NOD mouse line with TLR4-deficiency was generated. The NOD TLR4<sup>-/-</sup> mouse line was established by backcrossing NOD mice with C57BL/10ScCr mice, a line that carries a spontaneous deletion of 74723 base pairs of the TLR4 encoding region on chromosome 4 [217-219]. To proof the successful transfer of the TLR4-deficiency onto the NOD mouse background, macrophage-enriched spleen cells from NOD TLR4<sup>+/+</sup> and NOD TLR4<sup>-/-</sup> mice were exposed to the TLR4 ligand LPS. NOD TLR4<sup>+/+</sup> mice cells released large amounts of TNF $\alpha$  and IL-6, in contrast, NOD TLR4<sup>-/-</sup> mice cells were entirely unresponsive to LPS [30].

In the present study, the diabetes incidence of NOD TLR4<sup>+/+</sup> and NOD TLR4<sup>-/-</sup> mice was monitored for more than 10 generations and revealed that female NOD TLR4<sup>+/+</sup> and NOD TLR4<sup>-/-</sup> mice developed diabetes more frequently in their life span (70 % and 76 %, respectively) compared to male NOD TLR4<sup>+/+</sup> and NOD TLR4<sup>-/-</sup> mice (21 % and 31 %). The finding of sex-dependent diabetes development was also seen previously in the NOD TLR4<sup>+/+</sup> and NOD TLR4<sup>-/-</sup> mouse model and also corresponds to findings in the wildtype NOD mouse strain [30, 220]. Other studies showed different outcomes of diabetes development in association with TLR4. A recent study showed, that TLR4 inhibition protects NOD mice from developing autoimmune diabetes [221]. In this approach TLR4-deficiency was achieved by intraperitoneal treatment of 8-week old NOD mice with CLI-095, a selective inhibitor of TLR4 [221]. Another group showed that TLR4-deficiency reduces the proinflammatory state of diabetes in C57BL/6 mice after induction of diabetes by administration of STZ [222]. However, these studies used models with TLR4-deficiencies induced by inhibitors or chemicals, which might have side effects on the metabolism of the animals and cannot be compared to the deletion of TLR4 in the model used in the present study. Furthermore, one of the studies used a mouse model without a diabetes background and therefore can also not be compared to the NOD TLR4<sup>-/-</sup> mouse. Additionally, female NOD TLR4<sup>+/+</sup> and NOD TLR4<sup>-/-</sup> mice developed diabetes much earlier (166 and 151 days, respectively) than male NOD TLR4<sup>+/+</sup> and NOD TLR4<sup>-/-</sup> mice (191 and 187 days, respectively), which was also observed previously in the same model and in the wildtype NOD mice [30, 220].

Because of these findings, all further experiments of this thesis were performed exclusively with female NOD TLR4<sup>+/+</sup> and NOD TLR4<sup>-/-</sup> mice. Interestingly, as shown in the present thesis, NOD TLR4<sup>-/-</sup> mice developed diabetes even earlier than NOD TLR4<sup>+/+</sup> mice. NOD TLR4<sup>-/-</sup> mice manifested the disease at about 151 days of age, two weeks earlier than NOD TLR4<sup>+/+</sup> mice which developed diabetes at a mean age of 166 days. The accelerated diabetes development of NOD mice lacking TLR4 confirms the findings of an earlier study, in which NOD TLR4<sup>-/-</sup> mice developed diabetes at a mean age of 118 days and NOD TLR4<sup>+/+</sup> mice 59 days later at a mean age of 177 days [30].

Previous studies in animal models of the BB rat and the NOD mouse showed that the incidence of insulin-deficient diabetes is associated with the hygienic conditions of the housing [223]. As a result, the diabetes incidence in female NOD mice housed under specific pathogen-free conditions adds up to 80 %. In contrast, NOD mice that were infected with various bacteria, parasites and viruses were mostly protected against the development of insulin-deficient diabetes [30, 224]. The animals in the present study were kept under specific-pathogen free conditions and had a diabetes incidence of 70-76 %. These findings suggest that early stimulation of the immune system via the TLR4 by microbial pathogens is necessary for the development of an intact immune system along with the establishment of a stable

immunological tolerance to reliably differentiate between autologous and exogenous antigenic structures. Mice lacking TLR4 obviously suffer from impaired tolerance induction.

Further studies showed that T<sub>reg</sub> cells are important for the limitation of immune responses and the inhibition of the development of autoreactivity. Adequate T<sub>reg</sub> cell activation requires the presence of TLR4, which is expressed on their surface [155, 225]. Lack of TLR4 on T<sub>reg</sub> could lead to decreased inhibitory activity resulting in a reduced suppression of autoimmune responses and potentially in an accelerated development of insulin-deficient diabetes in NOD TLR4<sup>-/-</sup> mice.

Taken together, the female NOD TLR4<sup>-/-</sup> mouse model represents an adequate model for analyzing metabolic and inflammatory processes involved in the pathogenesis of insulin-deficient diabetes/T1D.

Besides the accelerated development of insulin-deficient diabetes, the blood glucose levels at diabetes onset were analyzed and showed similar concentrations between the two genotypes. These findings are in contrast to earlier studies which revealed increased blood glucose levels at diabetes onset in NOD TLR4<sup>-/-</sup> mice compared to NOD TLR4<sup>+/+</sup> mice [1]. These contrasting results may be explained by shifts in the observed mouse colony over generations, which might result from subtle alterations in housing conditions.

To analyze possible metabolic changes occurring before disease onset, all further experiments of this study were performed as comparative analyses of female NOD TLR4<sup>+/+</sup> and NOD TLR4<sup>-/-</sup> mice during the prediabetic phase at the age of 70-90 days, before diabetes manifestation at the age of 151-166 days.

### 4.1.2 Effect of TLR4-deficiency on body- and tissue weight of NOD mice

Lately, obesity is diagnosed at an increasingly early age and the numbers are reaching alarming levels. Worldwide, more than 340 million children and adolescents were overweight or obese in 2016 [187]. It is assumed that the body weight development has an impact on the progression of T1D. Because earlier findings in mouse models showed an impact of the TLR4-expression status on the body weight development [226], female prediabetic 70-90 days old NOD TLR4<sup>+/+</sup> and NOD TLR4<sup>-/-</sup> mice were analyzed with regard to their body weight and whole-body fat mass. NOD TLR4<sup>-/-</sup> mice showed higher body weights than NOD TLR4<sup>+/+</sup> mice, but similar whole-body fat mass. In a previous study, NOD TLR4<sup>-/-</sup> mice also showed higher body weight but also a higher whole-body fat mass [1]. These discrepancies can result from shifts in the animal colonies due to alterations in housing conditions. In humans, one of the main causes of overweight and obesity is an unbalanced nutrition from hypercaloric diets [187].

The observations in the present study and in humans correspond to the findings in the C57BL/6J mouse model, where a TLR4-deficiency combined with an application of a HFD led to an increase of body weight [226]. Another study showed contrasting results, demonstrating

that HFD-feeding protects TLR4-deficient C57BL/10 mice against the development of adiposity [227]. These contradictory findings in the literature can be explained by the use of different mouse models, which are metabolically and immunologically normal and showed no genetic predisposition for the development of insulin-deficient diabetes like the NOD mouse model used in this thesis. Despite the contrasting results as compared to the NOD TLR4<sup>-/-</sup> mouse, the findings in this thesis support the view that the TLR4-expression status controls the body weight development in the NOD mouse model. The higher body weight was observed after feeding a SD to both NOD TLR4<sup>+/+</sup> and NOD TLR4<sup>-/-</sup> mice. Findings from the literature suggest that under HFD conditions, NOD TLR4<sup>-/-</sup> mice could show an even larger increase of the body weight.

Investigations of weights and volumes of various tissues such as liver and different fat depots which are particularly important for glucose and lipid metabolism were performed to determine the impact of the TLR4-expression status on fat depot and liver development of female prediabetic NOD TLR4<sup>+/+</sup> and NOD TLR4<sup>-/-</sup> mice. The tissue weight and volume of the liver, VAT, BAT, NAT and WAT was similar between NOD TLR4<sup>+/+</sup> and NOD TLR4<sup>-/-</sup> mice suggesting that the TLR4-expression status has no impact on the weight and volume of these organs. This observation corresponds to a previous study, which showed, that a TLR4-deficiency in hepatocytes of C57BL/6 mice did not affect their liver weight [228].

Taken together, the finding of an increased body weight in NOD TLR4<sup>-/-</sup> mice suggest that the TLR4 controls basic metabolic processes involved in the pathogenesis of insulin-deficient diabetes/T1D.

### 4.1.3 Effect of TLR4-deficiency on metabolic parameters of NOD mice

Because of the observation that higher body weight is often accompanied by the development of adiposity, a broad spectrum of metabolic parameters with a focus on variables of the glucose and lipid metabolism was analyzed in female prediabetic NOD TLR4<sup>+/+</sup> and NOD TLR4<sup>-/-</sup> mice. In an initial approach, the water and food intake, as well as the physical activity and the RQ were measured over two light- and two dark-phases. The water and food intake of NOD TLR4<sup>+/+</sup> and NOD TLR4<sup>-/-</sup> mice was comparable in the light- and in the dark-phases. The increased water and food intake during the dark-phases can be explained by the circadian rhythm of the nocturnal animals. These findings further match recent findings in the NOD TLR4<sup>-/-</sup> mouse model [1].

As expected, the physical activity of both genotypes was higher in the dark-phases than in the light-phases which can be explained by the typical circadian rhythm of these nocturnal animals. However, the physical activity of NOD TLR4<sup>+/+</sup> and NOD TLR4<sup>-/-</sup> mice showed no differences between the two strains in the light- and dark-phases.

Because the CO<sub>2</sub> production and the O<sub>2</sub> consumption provide important, basic information for the substrate preference in energy production and therefore for the glucose- and lipid-metabolism, these parameters were determined in female prediabetic NOD TLR4<sup>+/+</sup> and NOD TLR4<sup>-/-</sup> mice. The CO<sub>2</sub> production and the O<sub>2</sub> consumption were similar in NOD TLR4<sup>+/+</sup> and NOD TLR4<sup>-/-</sup> mice during the light-phases and the dark-phases. The RQ and the energy expenditure were determined via the CO<sub>2</sub> production and the O<sub>2</sub> consumption (VCO<sub>2</sub>/VO<sub>2</sub>). In the dark-phases, the RQ was higher compared to the light-phases in both genotypes. The energy expenditure also was higher in the dark-phases than in the light-phases in both NOD TLR4<sup>+/+</sup> and NOD TLR4<sup>-/-</sup> mice. The enhanced RQ and energy expenditure can also be explained by the circadian rhythm of the nocturnal animals and their higher physical activity in the dark-phases.

Additionally, the whole-body CHO and FAO rates were calculated from the VO<sub>2</sub> and VCO<sub>2</sub> parameters during two light- and two dark-phases in NOD TLR4<sup>+/+</sup> and NOD TLR4<sup>-/-</sup> mice. In the dark phases, whole-body CHO levels were higher and whole-body FAO rates were lower in the dark-phases than in the light-phases in NOD TLR4<sup>+/+</sup> and NOD TLR4<sup>-/-</sup> mice. Higher CHO rates and lower FAO rates in the dark-phases can also be explained by the circadian rhythm of the nocturnal animals and furthermore by the higher physical activity, higher RQ and higher energy expenditure in the dark-phases in NOD TLR4<sup>+/+</sup> and NOD TLR4<sup>-/-</sup> mice. The different results in energy expenditure, physical activity and RQ of the present study compared to the earlier findings can result from changes in the animal populations due to changes in housing conditions [1]. The comparable results from NOD TLR4<sup>+/+</sup> and NOD TLR4<sup>-/-</sup> mice regarding the energy expenditure, the RQ, CHO and FAO rates indicate a balanced substrate utilization for energy production in NOD TLR4<sup>-/-</sup> mice.

Taken together, NOD TLR4<sup>+/+</sup> and NOD TLR4<sup>-/-</sup> mice showed similar levels of the measured metabolic parameters indicating no impact of the TLR4-expression status on glucose utilization. In addition, water- and food intake as well as physical activity may not have an impact on the accelerated development of insulin-deficient diabetes and increased body weight observed in NOD TLR4<sup>-/-</sup> mice.

#### **4.1.4 Effect of TLR4-deficiency in NOD mice on islet inflammation**

In an approach complementary to the study on the impact of the TLR4-expression status on metabolic parameters, the islet inflammation in NOD TLR4<sup>-/-</sup> mice was analyzed by determining the development of insulinitis in pancreatic islets. By using histological analyses, the total islet area, insulin-positive area and infiltrated islet area were determined in female prediabetic 70-90 days old NOD TLR4<sup>+/+</sup> and NOD TLR4<sup>-/-</sup> mice. Interestingly, NOD TLR4<sup>-/-</sup> mice showed an enhanced islet area compared to NOD TLR4<sup>+/+</sup> mice. It can be assumed that NOD TLR4<sup>-/-</sup> mice reveal higher islet areas to compensate the increased insulin requirement caused by an

increased IR resulting from elevated FA levels in the periphery. Matching results were described in a study, in which non-diabetic patients suffering from IR revealed increased islet sizes compared to insulin-sensitive individuals [229]. There was no difference between the two genotypes in insulin-positive area and infiltrated islet area. In addition, pancreatic islets were categorized into one of four insulinitis-scores and their proportion of the total islet number. There was also no difference in each score between the two genotypes. Most of the islets showed no insulinitis and about 40-50 % of the islets accounted for score 2 and 3. These findings indicate that the TLR4-expression status has no impact on the development of insulinitis in pancreatic islets of NOD mice. Previous findings revealed that 120 days old NOD TLR4<sup>-/-</sup> mice showed an enhanced islet infiltration of immune cells and a reduction of insulin-producing beta cells in the islets [30]. These results, which are in contrast to the findings in the present thesis, might result from the age difference in the investigated animals. It could be assumed that the accelerated progression of infiltration in the islets of NOD TLR4<sup>-/-</sup> mice starts later than at the age of 70-90 days but earlier than 120 days.

Another factor of systemic inflammation is the plasma levels of CRP. The CRP concentrations were measured in the plasma of NOD TLR4<sup>+/+</sup> and NOD TLR4<sup>-/-</sup> mice and were found comparable in both genotypes around 0.13 mg/dl. A study in C57BL/6 mice showed that the baseline level of CRP in these mice is around 0.2 mg/dl and in humans between 0.1-0.3 mg/dl [230]. These findings demonstrate that the blood samples of the animals used in the current study are in the normal range and do not indicate elevated systemic inflammatory conditions. Taken together, the finding of comparable degrees of insulinitis in NOD TLR4<sup>-/-</sup> mice and NOD TLR4<sup>+/+</sup> mice indicates that the accelerated progression of the immune cell infiltration starts later as assumed in the prediabetic phase of NOD TLR4<sup>-/-</sup> mice. In the context of the previous findings in 120 days old NOD TLR4<sup>-/-</sup> mice, the observations of the current study suggest that the TLR4 controls not only metabolic but also immunologic processes involved in the pathogenesis of insulin-deficient diabetes/T1D.

### 4.1.5 Effect of TLR4-deficiency in NOD mice on glucose metabolism

Earlier studies in the NOD mouse model showed, that diabetes development is not only associated with the deletion of insulin-producing beta cells but might also be associated with the development of IR [231]. To support the assumption that NOD TLR4<sup>-/-</sup> mice develop an impaired insulin sensitivity, an ipGTT was performed and the insulin levels were measured at two different time points. The random blood glucose concentrations were elevated in NOD TLR4<sup>-/-</sup> mice compared to NOD TLR4<sup>+/+</sup> mice [1]. Additionally, NOD TLR4<sup>-/-</sup> mice showed higher blood glucose levels during the ipGTT than NOD TLR4<sup>+/+</sup> mice [1]. The peak blood glucose levels at 15 minutes after glucose injection were 157 mg/dl in NOD TLR4<sup>+/+</sup> mice but were 33 % higher in NOD TLR4<sup>-/-</sup> mice with 202 mg/dl. The reduced glucose tolerance in NOD TLR4<sup>-/-</sup>

mice might be a sign for an impaired insulin sensitivity and/or an impaired glucose-induced insulin secretory capacity in these mice.

To clarify if the beta cells are still able to produce and release insulin, pancreatic islets of NOD mice were isolated and exposed to different glucose concentrations. The insulin release of islets treated with high glucose concentrations was higher than islets treated with low glucose concentrations. Previous findings showed, that NOD TLR4<sup>+/+</sup> and NOD TLR4<sup>-/-</sup> mice revealed comparable glucose-stimulated insulin release from isolated cultivated pancreatic islets [1]. Furthermore, prediabetic NOD mice showed an impaired glucose-stimulated insulin secretion during an ipITT, where their blood glucose concentrations did not return to their initial levels but stayed lower from 60 minutes until 120 minutes. This finding is in line with the results of an ipITT in NOD TLR4<sup>+/+</sup> and NOD TLR4<sup>-/-</sup> mice [1]. NOD TLR4<sup>-/-</sup> mice revealed a higher HOMA-IR than NOD TLR4<sup>+/+</sup> mice published earlier, which could not be reproduced in the present study [1]. These results prove that NOD mice, independent of the TLR4-expression status, suffer from an impaired glucose-stimulated insulin secretion but their pancreatic islets are still able to produce insulin. These findings further support the suggestion that NOD TLR4<sup>-/-</sup> mice show an even more severe impairment of glucose-induced insulin secretory capacity than NOD TLR4<sup>+/+</sup> mice.

As an additional finding supporting the impairment of glucose tolerance and/or glucose-induced insulin secretion in NOD TLR4<sup>-/-</sup> mice, NOD TLR4<sup>+/+</sup> and NOD TLR4<sup>-/-</sup> mice revealed comparable levels of insulin in the plasma under fasting conditions, but after glucose injection NOD TLR4<sup>-/-</sup> mice showed lower plasma levels of insulin than NOD TLR4<sup>+/+</sup> mice.

Taken together, the findings support the notion that impaired insulin-sensitivity and/or impaired glucose-induced insulin secretion might contribute to the accelerated diabetes development in NOD TLR4<sup>-/-</sup> mice.

### 4.1.6 Effect of TLR4-deficiency in NOD mice on lipid metabolism

Besides an impaired glucose metabolism, patients with T1D frequently also suffer from abnormalities in lipid metabolism such as higher plasma TG and LDL cholesterol levels, especially under poor glycemic control [232]. In addition, insulin stimulates the FA uptake into the adipose tissue and inhibits lipolysis, which depends on the levels of insulin in the periphery [16, 17, 94]. Based on this close association between lipid metabolism and whole-body glucose homeostasis, it could be speculated that the TLR4-expression status controls diabetes development in NOD mice also via affecting the lipid metabolism.

To follow up on this assumption and considering the impaired lipid metabolism but the similar fat depot weights and volumes, the fat depot composition of female prediabetic NOD TLR4<sup>+/+</sup> and NOD TLR4<sup>-/-</sup> mice was analyzed to identify possible changes due to the TLR4-expression status. In the VAT, NAT and BAT, the SFA, MUFA and PUFA content was analyzed in both

genotypes. NOD TLR4<sup>-/-</sup> mice showed lower PUFA levels in the VAT, but the levels of SFA and MUFA in VAT, NAT and BAT were comparable to NOD TLR4<sup>+/+</sup> mice. Both genotypes were on the same SD and showed similar food intake and physical activity. Therefore, less PUFA in the VAT of NOD TLR4<sup>-/-</sup> mice could neither result from different food intake or composition nor altered physical activity. It might be speculated that NOD TLR4<sup>-/-</sup> mice exhibit an altered absorption of nutrients, especially PUFA, and/or as implicated by a previous study by an impaired gut barrier, which might lead to an altered absorption of FA from the gut to the periphery [1].

Another explanation for the lower PUFA concentrations in the VAT of NOD TLR4<sup>-/-</sup> mice could also result from increased ectopic storage of PUFA in tissues such as the liver.

To further investigate the lipid metabolism in NOD TLR4<sup>+/+</sup> and NOD TLR4<sup>-/-</sup> mice, peripheral levels of FFA, TG, cholesterol, LDL and HDL were analyzed in plasma samples. However, there was no difference in FFA, TG, cholesterol, LDL and HDL concentrations between the two genotypes. These findings were in contrast to the findings published previously, showing higher FFA and TG levels in the plasma of NOD TLR4<sup>-/-</sup> mice [1]. These changes could result from shifts in the animal colony over time due to alterations in housing conditions.

The previous findings of higher FFA and TG levels in NOD TLR4<sup>-/-</sup> mice match with results from studies in humans and in animal models, describing higher FFA and TG levels in the plasma as a consequence of reduced insulin-sensitivity resulting in enhanced lipolysis. Less insulin binds to the insulin receptor; consequently, less suppression of the lipolysis by insulin can occur resulting in an increased release of FFA and TG from the tissues into the periphery [233-235].

Taken together, NOD TLR4<sup>-/-</sup> mice showed an altered lipid metabolism, which might be the result of reduced insulin-sensitivity and/or an impaired gut barrier.

### 4.1.7 Effect of TLR4-deficiency in NOD mice on SCFA levels

Because of the suggested gut barrier impairment, altered lipid metabolism and known impaired gut morphology and microbiome composition [1] in NOD TLR4<sup>-/-</sup> mice, products of the gut microbiome were further analyzed to identify a possible link between gut microbiome and metabolism. Intestinal bacteria are known to release SCFA, which exit the gut and enter the circulation thereby providing a possible link between gut microbiome and host metabolism [236, 237]. Because of the above-mentioned evidence of an altered lipid metabolism before diabetes onset in NOD TLR4<sup>-/-</sup> mice, SCFA levels were determined in three different gut segments (small intestine, cecum and colon) and in plasma samples of female prediabetic NOD TLR4<sup>+/+</sup> and NOD TLR4<sup>-/-</sup> mice. The SCFA concentrations in small intestine, cecum and colon were comparable in NOD TLR4<sup>+/+</sup> and NOD TLR4<sup>-/-</sup> mice supporting the view that the TLR4-expression status does not affect intestinal SCFA concentrations. Interestingly, when

compared to NOD TLR4<sup>+/+</sup> mice, NOD TLR4<sup>-/-</sup> mice showed changes in gut bacteria composition, especially a decrease in the abundance of Firmicutes and an increase of Bacteroidetes [1]. Nevertheless, this change did not result in alterations of the SCFA content in the gut of these animals.

Interestingly, NOD TLR4<sup>-/-</sup> mice showed lower SCFA levels in the plasma than NOD TLR4<sup>+/+</sup> mice, with a most pronounced reduction in butyrate. Butyrate is known for its ability to stabilize tight junctions in gastrointestinal epithelia [238]. Less butyrate might further destabilize the gut barrier in NOD TLR4<sup>-/-</sup> mice, which would lead to an impaired transition of small molecules from the gut lumen to the periphery.

Decreased SCFA in plasma but not in the gut segments of NOD TLR4<sup>-/-</sup> mice might result from altered peripheral consumption of SCFA. These findings in the NOD TLR4<sup>-/-</sup> mouse model suggest that SCFA in the plasma and not in the gut lumen are relevant for the more rapid progression of insulin-deficient diabetes/T1D. Recently, a study confirmed the relevance of SCFA in the plasma but not in the gut for the regulation of insulin sensitivity and lipolysis in humans. Circulating concentrations of the three most abundant SCFA acetate, propionate and butyrate were associated with the body mass index, FFA levels, triacylglycerol levels, GLP-1 concentrations, fasting plasma glucose and insulin sensitivity. These findings suggest that SCFA in plasma are more closely linked to a healthy metabolism than intestinal SCFA and should be determined in probiotic intervention studies and as biomarkers of the effects on metabolism [194]. Additionally, the observations in this thesis are in line with findings of a gut metagenome analysis in children on the protective effect of SCFA in early-onset T1D. In this study, SCFA such as acetate, propionate and butyrate were increased in healthy controls compared to children developing T1D/ with T1D [239].

Taken together, by using the NOD TLR4<sup>-/-</sup> mouse model, the association between alterations of gut morphology [1] and microbiome composition could be identified in the context of metabolic disorders potentially involved in the progression of insulin-deficient diabetes/T1D. SCFA might serve as important mediators in the metabolic processes involved in accelerated diabetes progression in NOD TLR4<sup>-/-</sup> mice.

### **4.1.8 Effect of TLR4-deficiency in NOD mice on hepatic lipid, glucose and energy metabolism**

Because of an assumed ectopic fat accumulation in NOD TLR4<sup>-/-</sup> mice, HCL were determined in female prediabetic 70-90 days old NOD TLR4<sup>+/+</sup> and NOD TLR4<sup>-/-</sup> mice via MRS. In (young) prediabetic patients, no information on hepatic lipid contents are available. However, multiple studies point to impaired lipid metabolism before the appearance of beta cell-directed autoimmune processes. Impaired levels of TG in children were observed months before seroconversion to autoantibody positivity as an indicator of emerging beta cell-directed

immunity [240]. Another study using lipidomics revealed lipid signatures that characterize children who develop islet autoimmunity or even T1D later in life [241].

Interestingly, NOD TLR4<sup>-/-</sup> mice showed lower levels of HCL compared to NOD TLR4<sup>+/+</sup> mice before the age of diabetes onset. While NOD TLR4<sup>+/+</sup> mice showed HCL levels in the normal range of metabolically healthy mice [242], NOD TLR4<sup>-/-</sup> mice showed almost 50 % lower HCL levels.

Human studies showed, that patients with long-standing T1D revealed lower HCL compared to healthy individuals [243-245]. A study in mice with a hepatocyte-selective TLR4-deletion showed that animals with an alcohol intake over 4 weeks are protected from triglyceride accumulation in the liver, partly due to increased expression of genes involved in FA oxidation and decreased expression of endogenous lipogenic genes [228]. There are no data available on HCL content in the prediabetic phase of T1D.

The HCL could not be separated into SFA, MUFA and PUFA due to the low amounts of fat in the liver. Not only the lipid metabolism but also the hepatic energy metabolism was analyzed in NOD TLR4<sup>+/+</sup> and NOD TLR4<sup>-/-</sup> mice. The livers showed similar concentrations of phosphorous metabolites such as  $\gamma$ -ATP, Pi, PME and PDE, indicating that the hepatic ATP content and consequential energy metabolism are not affected by the TLR4-deficiency. These findings are in line with a study in long-standing T1D patients, who revealed the same amounts of hepatic  $\gamma$ -ATP and Pi as healthy individuals [243].

The observation on the reduced HCL content in NOD TLR4<sup>-/-</sup> mice expands the finding of a marked dyslipidemia in female prediabetic NOD TLR4<sup>-/-</sup> mice, which was described previously [1]. The amount of HCL might differ in the two genotypes because of mechanisms involved in hepatic lipid acquisition and disposal [100]. As the cellular FA uptake depends on FA receptors such as CD36 and FFAR2, the hepatic protein expression of these receptors was analyzed. However, as revealed by Western Blot analyses, female prediabetic 70-90 days old NOD TLR4<sup>+/+</sup> and NOD TLR4<sup>-/-</sup> mice showed similar levels of CD36 and FFAR2 expression in the liver. Based on these findings, it appears unlikely that the lower HCL content is caused by an impaired FA uptake in NOD TLR4<sup>-/-</sup> mice.

Another explanation for the decreased HCL levels in NOD TLR4<sup>-/-</sup> mice might be an increased FA consumption in the liver due to increased rates of FA oxidation. Recently, it was demonstrated that hepatic lipid content is controlled by lipid consumption and disposal, specifically by FA oxidation and export of lipids in VLDL [242]. Previous findings showed higher mitochondrial respiration in the liver of NOD TLR4<sup>-/-</sup> mice than NOD TLR4<sup>+/+</sup> mice [1]. An increased hepatic mitochondrial respiration rate leads to more ATP production in the mitochondria, thereby possibly increasing the FA oxidation, which in turn results in decreased HCL levels in NOD TLR4<sup>-/-</sup> mice. This assumption might be supported by an earlier study in diabetic NOD mice describing an increase in mRNA levels for enzymes involved in FA

oxidation specifically in the liver leading to liver-specific upregulation of these enzymes [246]. Taken together, based on these earlier findings and the findings of the present study, it might be speculated that because of the impaired lipid metabolism observed in prediabetic NOD TLR4<sup>-/-</sup> mice, increased FA oxidative enzymatic activity results in higher degradation of lipids in the liver leading to decreased HCL.

Additionally, the impaired glucose metabolism could also play a role in the decrease of HCL in prediabetic NOD TLR4<sup>-/-</sup> mice. Insulin is known to stimulate lipogenesis and to suppress lipolysis in the liver [94]. Decreased insulin levels in NOD TLR4<sup>-/-</sup> mice as described in the current study might lead to reduced insulin-induced suppression of hepatic lipolysis resulting in higher conversion of TG to FA and to a higher release of FA subsequently leading to decreased HCL content.

Furthermore, insulin stimulates the hepatic TG synthesis resulting in the conversion of FA to TG and subsequently in the release of hepatic TG into the periphery [92]. Consequently, less insulin in NOD TLR4<sup>-/-</sup> mice might result in lower rates of insulin-stimulated TG synthesis in the liver leading to reduced generation of TG and fewer release of TG into the periphery. Reduced TG synthesis rates might be associated with higher rates of hepatic lipolysis leading to an enhanced release of FA from the liver into the blood stream resulting in lower HCL content in these animals. To follow up on this issue, the TG content in the liver was measured and revealed comparable levels in NOD TLR4<sup>+/+</sup> and NOD TLR4<sup>-/-</sup> mice. This finding further implies that NOD TLR4<sup>-/-</sup> mice have a lower hepatic TG synthesis rate but increased hepatic lipolytic activity (Figure 79).

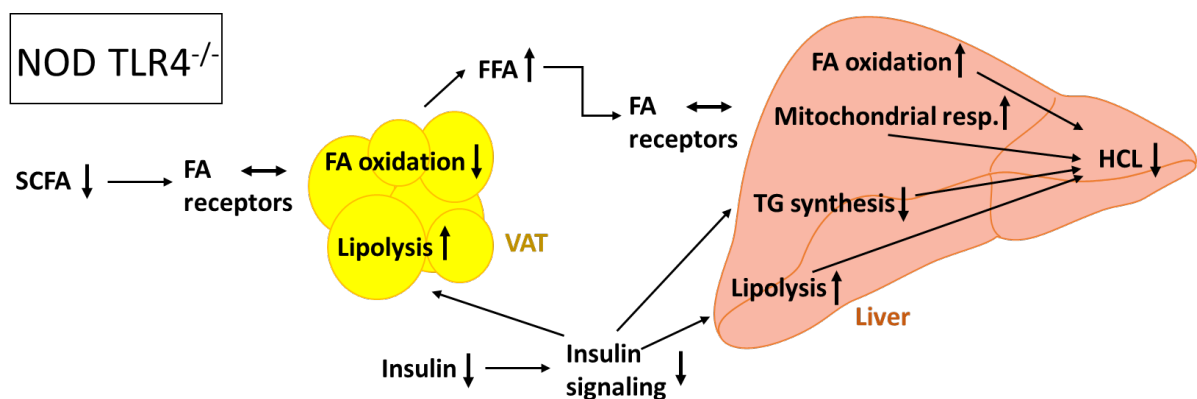


**Figure 79: Hypothetical processes associated with lower HCL in NOD TLR4<sup>-/-</sup> mice.** NOD TLR4<sup>-/-</sup> mice showed lower levels of short-chain fatty acids (SCFA) in plasma but no change in free fatty acid (FFA) receptor expression in visceral adipose tissue (VAT). Additionally, NOD TLR4<sup>-/-</sup> mice revealed lower insulin levels suggesting less insulin signaling. NOD TLR4<sup>-/-</sup> mice showed higher levels of FFA in the plasma, leading to the assumption of lower rates of FA oxidation and/or a decreased insulin-suppression of lipolysis in the VAT. In the liver of NOD TLR4<sup>-/-</sup> mice, the FFA receptor expression was also not changed, but an elevated mitochondrial respiration was observed. It is assumed that an increase in hepatic lipolysis and/or decrease of insulin-stimulated triglyceride (TG)-synthesis but also the increase in mitochondrial respiration and/or FA oxidation contribute to the lower levels of HCL observed in NOD TLR4<sup>-/-</sup> mice.

Earlier findings of increased FFA and TG levels in plasma of NOD TLR4<sup>-/-</sup> mice indicate an impaired hepatic lipid storage capacity possibly due to higher release of FA and TG contributing to higher plasma FFA and TG levels.

Hepatic lipid metabolism plays an essential role in the maintenance of whole-body glucose homeostasis [247]. Impairments of the HCL content in NOD TLR4<sup>-/-</sup> mice in the prediabetic phase, preceding the manifestation of insulin-deficient diabetes/T1D, might have effects on the pathogenesis and progression of the disease. A recent study in NOD mice showed that an impaired regulation of hepatic lipid metabolism observed in the neonatal phase is an early feature of insulin-deficient diabetes/T1D [248].

Hyperlipidemia might lead to alterations of whole-body insulin sensitivity resulting from increased blood glucose levels in prediabetic NOD TLR4<sup>-/-</sup> mice. In prediabetic animals, hyperglycemia associated with hyperlipidemia may lead to glucolipotoxic conditions which result in impairments of beta cell functions [249]. Taken together, the damaging impact of glucolipotoxicity on beta cell function, the stress of increased insulin secretion on demand under conditions of impaired insulin sensitivity and the inflammatory stress resulting from the progressing autoimmune process might accelerate the decline of insulin secretory capacity and the manifestation of insulin-deficient diabetes/T1D in NOD TLR4<sup>-/-</sup> mice. In the context of the literature, the findings of the present thesis support the assumption that impaired lipid metabolism in the liver in the prediabetic phase contributes to the development of insulin-deficient diabetes/T1D in NOD TLR4<sup>-/-</sup> mice.

### **4.2 Effect of HFD on metabolic parameters in the prediabetic phase of NOD TLR4<sup>-/-</sup> mice, a model of accelerated development of insulin-deficient diabetes**

Lately, obesity is diagnosed at an increasingly early age and the numbers are still rising. In 2019, around 38 million children under the age of five were diagnosed as overweight or obese. Suffering from obesity, these patients have an increased risk of developing chronic diseases such as diabetes [187]. Overweight and obesity are mostly caused by lifestyle changes, such as an unbalanced nutrition and/or a lack of physical activity [187].

These findings in early life led to the hypothesis that feeding NOD TLR4<sup>-/-</sup> mice a high caloric diet before diabetes manifestation further promotes diabetes-accelerating metabolic changes in these animals. NOD TLR4<sup>-/-</sup> mice were fed a HFD during the prediabetic phase from 30 to 70-90 days of age to test this hypothesis and to investigate metabolic changes evoked by a high caloric diet.

#### 4.2.1 Effect of HFD on body- and tissue weight

Under SD conditions, NOD TLR4<sup>-/-</sup> mice showed higher body weight compared to NOD TLR4<sup>+/+</sup> mice. The findings from the literature suggested that under HFD condition, NOD TLR4<sup>-/-</sup> mice might even have a more rapid increase in body weight [226]. Female NOD TLR4<sup>+/+</sup> and NOD TLR4<sup>-/-</sup> mice were fed a HFD during the prediabetic phase from the age of 30 days to the age of 70-90 days. NOD TLR4<sup>+/+</sup> and NOD TLR4<sup>-/-</sup> mice had higher body weights under HFD condition than under SD condition, but no difference between the genotypes was observed. Other studies confirmed these findings of higher body weight by feeding NOD mice a HFD for 6-8 weeks [250, 251]. Another study using TLR4 knockout mice on a C57BL/6J background showed, that TLR4-deficiency protected these mice from body weight gain induced by feeding a HFD for 18 weeks [252]. These contrasting results can be explained by using different mouse models with TLR4-deficiency on a genetic background that does not predispose to diabetes development.

Interestingly, when comparing the kinetics of body weight development of the two genotypes, NOD TLR4<sup>-/-</sup> mice fed with HFD showed an even higher body weight gain than HFD fed NOD TLR4<sup>+/+</sup> mice. These observations suggest that the TLR4-expression status has an impact on the body weight development under hypercaloric conditions in NOD mice.

The whole-body fat mass was analyzed using NMR in NOD TLR4<sup>+/+</sup> and NOD TLR4<sup>-/-</sup> mice fed with HFD which revealed higher fat mass at the age of 70 days in animals fed with HFD compared to animals fed with SD. There were again no differences between the genotypes in whole-body fat mass content. The increased body weight in NOD TLR4<sup>+/+</sup> and NOD TLR4<sup>-/-</sup> mice fed with HFD was found to be associated with enhanced whole-body fat mass. Based on the findings of higher whole-body fat mass, weights and volumes of the liver, VAT, NAT, BAT and WAT were determined. The liver weight and volume was the same for both genotypes under both conditions, suggesting that neither the TLR4-expression status nor the hypercaloric diet have an impact on the liver size. These findings could be confirmed by a study with NOD mice, showing comparable liver weight in animals fed with SD and HFD [250]. The VAT weight and volume were higher in animals fed with HFD compared to animals fed with SD. Interestingly, NOD TLR4<sup>-/-</sup> mice showed lower VAT weight than NOD TLR4<sup>+/+</sup> mice after HFD feeding. This finding may lead to the assumption that NOD TLR4<sup>-/-</sup> mice have increased rates of lipolysis and/or FA oxidation in the VAT resulting in higher rates of fat-degradation/fat-release from the VAT into the periphery. In contrast, a previous study in TLR4-deficient mice on the C57BL/6J background showed no effect of HFD-feeding on VAT weight [252]. These different findings could also be explained by a different mouse model, which has no genetic predisposition for the development of insulin-deficient diabetes like the NOD mouse model. The NAT, BAT and WAT weights and volumes were increased in NOD TLR4<sup>+/+</sup> and NOD TLR4<sup>-/-</sup> mice fed with HFD compared to animals fed with SD.

Taken together, the higher body weight of NOD TLR4<sup>+/+</sup> and NOD TLR4<sup>-/-</sup> mice is associated with increased whole-body fat mass during HFD-feeding in the prediabetic phase. The increased whole-body fat mass results from higher fat intake and enhanced fat storage in the different fat depots. Interestingly, while on HFD, the TLR4-expression status seems to have an effect on the body weight development and the fat storage.

### 4.2.2 Effect of HFD on metabolic parameters

Because of the HFD-effect on body weight and inflammation in NOD TLR4<sup>+/+</sup> and NOD TLR4<sup>-/-</sup> mice, central parameters of energy metabolism were investigated. The water and food intake of NOD TLR4<sup>+/+</sup> and NOD TLR4<sup>-/-</sup> mice were determined under HFD conditions. Interestingly, both genotypes showed a lower water and food intake under HFD conditions compared to SD. NOD TLR4<sup>+/+</sup> and NOD TLR4<sup>-/-</sup> mice revealed no difference in water intake during the light- and the dark-phases. These findings suggest that mice under HFD condition drink and eat less than mice under SD conditions, which could be explained by a faster feeling of satiety because of more fat and perhaps less thirst due to the texture of the HFD. Findings in the literature confirm the results of the present thesis regarding less water and food intake during HFD feeding. In a previous study, C57BL6/J mice fed a HFD also showed lower water intake compared to animals fed a SD [253]. In addition, another study showed that C57BL/6 mice on HFD revealed lower food intake compared to mice on SD [254].

The physical activity in animals fed with HFD was similar to animals fed with SD. In the dark-phases, animals showed higher physical activity compared to the light-phases, which can be explained by the circadian rhythm of the nocturnal animals. These findings suggest that neither HFD-feeding nor the TLR4-expression status have an impact on the diurnal rhythm of physical activity of NOD mice. The energy expenditure was measured in NOD TLR4<sup>+/+</sup> and NOD TLR4<sup>-/-</sup> mice on HFD. Mice on HFD showed lower energy expenditure during the dark-phases than mice fed with SD. Additionally, mice on HFD showed higher energy expenditure in the dark-phases compared to the light-phases, which also can be explained by the circadian rhythm of the nocturnal animals.

The CO<sub>2</sub> production and the O<sub>2</sub> consumption as well as the RQ were determined in mice fed with HFD. Interestingly, NOD TLR4<sup>+/+</sup> and NOD TLR4<sup>-/-</sup> mice on HFD showed lower CO<sub>2</sub> production in the dark phases than animals on SD. Additionally, when compared to NOD TLR4<sup>-/-</sup> mice, NOD TLR4<sup>+/+</sup> mice revealed higher CO<sub>2</sub> production in the dark-phases than during the light-phases. The O<sub>2</sub> consumption was higher in the dark-phases than in the light-phases in animals fed with HFD, but comparable to animals fed with SD except for NOD TLR4<sup>+/+</sup> mice in the light-phases. The RQ was similar between the genotypes and the phases in animals fed with HFD but lower than in animals fed with SD. In HFD fed animals, low RQ during dark-phases indicates continuous preference of the utilization of fat and proteins. Similar findings in

human studies revealed, that patients with T1D show an impaired substrate utilization which might result from an increased metabolic inflexibility resulting in a decreased RQ because of a reduced ability to oxidize carbohydrates [235, 255].

Taken together, the decreased RQ and energy consumption in animals fed with HFD could result from lower glucose utilization resulting from IR. Furthermore, the TLR4-expression status during HFD feeding does not seem to have an impact on energy expenditure and RQ. The issue of impaired carbohydrate oxidation and higher protein and fat oxidation was further investigated by determining the whole-body CHO and whole-body FAO rates in NOD TLR4<sup>+/+</sup> and NOD TLR4<sup>-/-</sup> mice on HFD. Mice on HFD showed lower CHO rates compared to animals on SD. Furthermore, mice on HFD revealed higher FAO rates than animals on SD. These findings confirm the assumption that under HFD conditions, NOD TLR4<sup>+/+</sup> and NOD TLR4<sup>-/-</sup> mice decrease glucose utilization. For compensation, they increase the utilization of proteins and fat as energy substrates leading to lower energy consumption and RQ.

Taken together, under HFD condition, the TLR4-expression status does not seem to affect basic parameters of substrate utilization in NOD mice, as HFD feeding of both genotypes revealed comparable effects on water and food intake, RQ, energy expenditure and CHO and FAO rates.

Because of impaired carbohydrate oxidation in NOD TLR4<sup>+/+</sup> and NOD TLR4<sup>-/-</sup> mice fed with HFD, random blood glucose concentrations were determined. NOD TLR4<sup>+/+</sup> mice showed higher blood glucose levels under HFD condition compared to SD condition. The increase of blood glucose levels of NOD TLR4<sup>+/+</sup> mice fed with HFD was confirmed by other studies in NOD mice [250, 251]. Interestingly, NOD TLR4<sup>-/-</sup> mice revealed lower blood glucose concentrations than NOD TLR4<sup>+/+</sup> mice under HFD condition. The blood glucose levels of NOD TLR4<sup>-/-</sup> mice remained largely unaltered under HFD and SD conditions. The findings of lower blood glucose levels in NOD TLR4<sup>-/-</sup> mice fed with HFD may allow the speculation that HFD might have a protective effect on the glucose metabolism. However, these assumptions need to be tested in further experiments.

### 4.2.3 Effect of HFD on islet inflammation

Because of the impact of the HFD on metabolic parameters and the plasma glucose concentrations, the islet inflammation in NOD TLR4<sup>-/-</sup> mice was examined by determining the development of insulinitis in pancreatic islets. By using histological analyses, the total islet area, insulin-positive area and infiltrated islet area were determined in pancreatic sections of female prediabetic 70-90 days old NOD TLR4<sup>+/+</sup> and NOD TLR4<sup>-/-</sup> mice fed with SD or HFD. Pancreatic islets of NOD TLR4<sup>+/+</sup> mice revealed larger islet areas under HFD than SD. There was neither a difference in islet area between NOD TLR4<sup>-/-</sup> mice fed with SD or HFD nor between the two genotypes. The larger islet areas in NOD TLR4<sup>+/+</sup> mice on HFD might result from the attempt

to compensate for the increased insulin requirement caused by an elevated IR due to larger fat mass after the prolonged uptake of a HFD. The findings in the present thesis match the results from other studies showing that an increased fat cell mass leads to an increase of islet size and contributes to IR [226, 256-258]. Moreover, various other studies in different animal models found that HFD leads to enhanced beta cell mass [259-262].

The insulin-positive area of pancreatic islets of animals fed with HFD was determined and NOD TLR4<sup>+/+</sup> mice were found to show lower proportions of insulin-positive areas compared to NOD TLR4<sup>+/+</sup> mice on SD. There was no difference between the genotypes or NOD TLR4<sup>-/-</sup> mice fed with SD or HFD regarding the proportions of the insulin-positive area of pancreatic islets. These findings were unexpected, since other studies commonly report that as a result of HFD feeding, IR develops and the beta cell mass consequentially increases [45, 259, 260, 262, 263]. Further detailed studies and analysis of the islet structure of NOD TLR4<sup>+/+</sup> and NOD TLR4<sup>-/-</sup> mice fed with SD and HFD are required to explain the unexpected finding of the lower insulin-positive islet area in NOD TLR4<sup>+/+</sup> mice fed with HFD. In complementary analyses, the infiltrated islet area was determined in pancreatic islets of NOD TLR4<sup>+/+</sup> and NOD TLR4<sup>-/-</sup> mice fed with SD or HFD. The proportion of the infiltrated islet area from all affected islets was comparable between the genotypes and the diets. In addition, the classification in insulinitis-scores to assess the degree of insulinitis showed no differences within the experimental groups. Furthermore, regardless of the TLR4 expression status, the HFD showed the highest proportion of large islets being infiltrated compared to SD. This might be explained by the presence of higher amounts of beta cell specific antigens, which attract increasing numbers of immune cells thereby accelerating insulinitis in larger islets. Previous studies showed that as a consequence of the HFD-induced IR, the stress on beta-cells to synthesize higher amounts of insulin increases and therefore their metabolic activity enhances, which consequently makes them a more preferred target for the immune system [45, 264]. Another study found that beta-cells with high activity showed increased antigen expression, which makes them more vulnerable to inflammatory attacks [265].

As an indicator of systemic inflammation, the plasma levels of CRP were measured in NOD TLR4<sup>+/+</sup> and NOD TLR4<sup>-/-</sup> mice on SD and HFD. The plasma concentrations of CRP were similar in both genotypes and diets around 0.13-0.16 mg/dl. The findings in the present thesis regarding the levels of CRP were similar to results in a study in C57BL/6 mice and healthy individuals [230]. These findings confirmed that the plasma CRP levels of NOD TLR4<sup>+/+</sup> and NOD TLR4<sup>-/-</sup> mice on HFD are in normal range and do not indicate systemic inflammatory conditions.

Taken together, under HFD NOD TLR4<sup>+/+</sup> mice showed higher islet areas and insulin-positive areas, whereas islets of NOD TLR4<sup>-/-</sup> mice remained largely unchanged suggesting that HFD has a rather protective effect on islets of NOD TLR4<sup>-/-</sup> mice. Under HFD condition, the highest

proportion of large islets was infiltrated compared to SD conditions, indicating that the TLR4-expression status has no impact on the immune cell infiltration of islets. The plasma CRP levels were comparable between the two genotypes and diets suggesting that neither the TLR4-expression status nor the diet has an effect on systemic inflammation.

### 4.2.4 Effect of HFD on lipid metabolism

Because of the impaired insulin secretion in NOD TLR4<sup>-/-</sup> mice on SD and the altered fat depot weights and volumes, the lipid metabolism was analyzed in female prediabetic NOD TLR4<sup>+/+</sup> and NOD TLR4<sup>-/-</sup> mice in order to investigate the potential impact of HFD-feeding on the fat depot composition and parameters in the plasma. Regarding the fat depot composition, the VAT, NAT and BAT were analyzed. Under HFD conditions, animals showed higher MUFA content in the VAT than mice fed with SD. In addition, NOD TLR4<sup>+/+</sup> mice fed with HFD revealed lower PUFA content compared to NOD TLR4<sup>+/+</sup> mice fed with SD. In the NAT, NOD TLR4<sup>+/+</sup> mice showed higher MUFA content when fed with HFD than SD. The SFA, MUFA and PUFA content in the BAT was comparable between the two genotypes and the diets. No difference was observed between the genotypes on HFD. The differences in lipid composition between SD and HFD fed mice could be a result of the different compositions of the diets. The SD consists of 0.7 % SFA, 1.1 % MUFA and 2.7 % PUFA per 100 g meal whereas the HFD contains much higher FA proportions and consist of 11.2 % SFA, 12.5 % MUFA and 11.2 % PUFA. The ratio between HFD/SD amounted to 15.5 for SFA, 11.4 for MUFA and 4.1 for PUFA. Animals on SD take up much more PUFA in comparison to SFA and MUFA than animals on HFD which could contribute to the lower PUFA contents in the VAT of NOD TLR4<sup>+/+</sup> mice fed with HFD. NOD TLR4<sup>+/+</sup> mice showed higher MUFA content in the VAT and NAT, which could also result from the HFD composition. Interestingly, only NOD TLR4<sup>+/+</sup> mice revealed differences in the FA content of fat depots under HFD condition. These observations lead to the speculation that under HFD condition NOD TLR4<sup>-/-</sup> mice might be better protected from changes in the lipid metabolism than NOD TLR4<sup>+/+</sup> mice. Additionally, FFA, TG, cholesterol, HDL, and LDL levels were determined in the plasma. Surprisingly, the FFA and TG concentrations showed no change under HFD conditions compared to SD condition and no differences between the genotypes suggesting that HFD-feeding has no impact on peripheral FA and TG levels. Based on these findings, the levels of other lipids in the periphery were investigated such as cholesterol, HDL and LDL levels, which were found to be higher in animals fed with HFD than in animals fed with SD.

Taken together, feeding a HFD to NOD TLR4<sup>+/+</sup> and NOD TLR4<sup>-/-</sup> mice led to higher lipid concentrations in the plasma and to a partly different FA composition in fat depots, suggesting that the HFD and the TLR4-expression status both have an effect on the lipid metabolism in

these animals. Further studies are required to clarify the association between FA composition in fat depots, high caloric diet and the TLR4-expression status in NOD mice.

### 4.2.5 Effect of HFD on hepatic lipid-, glucose- and energy metabolism

Because of the differences in the HCL content under SD condition and the alterations in lipid metabolism in animals fed with HFD, HCL content was determined in female prediabetic NOD TLR4<sup>+/+</sup> and NOD TLR4<sup>-/-</sup> mice using MRS. As expected, the HCL content in animals fed with HFD was higher than in mice fed with SD. This increased ectopic fat storage could be explained by reaching the limits of the fat storage capacity of the adipose tissue. These findings match with results from the literature showing that C57BL/6J mice on HFD have higher liver TG levels than mice on SD [266]. Interestingly, NOD TLR4<sup>-/-</sup> mice had even higher levels of HCL than NOD TLR4<sup>+/+</sup> mice on HFD.

Not only the lipid metabolism but also the hepatic energy metabolism was analyzed in NOD TLR4<sup>+/+</sup> and NOD TLR4<sup>-/-</sup> mice on HFD. Interestingly, the liver of animals fed with HFD showed higher  $\gamma$ -ATP concentrations, but similar Pi levels compared to animals fed with SD. There was no difference between the genotypes in  $\gamma$ -ATP and Pi concentrations. The PME levels in the liver of NOD TLR4<sup>+/+</sup> and NOD TLR4<sup>-/-</sup> mice revealed no differences between the genotypes and diets. In contrast, the PDE levels of NOD TLR4<sup>+/+</sup> mice were higher in animals fed with HFD than SD. In summary, the hepatic energy metabolism is affected by the HFD, but not by the TLR4-expression status of the animals. A previous study showed that after feeding a HFD to C57BL/6J mice, the liver mitochondria have a higher respiratory capacity and increased ATP levels compared to mitochondria of animals fed with SD [267].

The higher HCL levels in NOD TLR4<sup>-/-</sup> mice on HFD could be explained by an assumed normal glucose metabolism in these animals as indicated by their random blood glucose levels which were in the normal range and lower than NOD TLR4<sup>+/+</sup> mice on HFD. This could lead to the assumption that the HFD might protect NOD TLR4<sup>-/-</sup> mice from hyperglycemia and alterations of the glucose metabolism. The normal range of blood glucose levels in NOD TLR4<sup>-/-</sup> mice could presumably result from normal insulin release of beta cells and/or unimpaired insulin sensitivity of the liver and other tissues. The presumably normal insulin release into the periphery and the assumed normal insulin sensitivity of the liver but the increased levels of LDL, HDL and cholesterol measured in the periphery might lead to higher FA uptake into the liver. Higher FA uptake but an assumed normal hepatic insulin-stimulated TG synthesis and hepatic insulin-suppressed lipolysis might result in normal release of hepatic FA and TG into the periphery which could explain the normal levels of FA and TG in the periphery of NOD TLR4<sup>-/-</sup> mice. The excess of FA in the liver but the assumed regular hepatic FA degradation might lead to the increased HCL content observed in NOD TLR4<sup>-/-</sup> mice fed with HFD.

Taken together, NOD TLR4<sup>-/-</sup> mice on HFD showed higher HCL content than NOD TLR4<sup>+/+</sup> mice on HFD, which could result from higher FA uptake into the liver while FA degradation is in the normal range. However, these assumptions need to be further investigated.

### 4.3 Limitations of this study

Basic problems arising from animal studies, the heterogeneity of the mouse model and the effects of isoflurane are seen as limitations of this study and are further outlined in this section.

#### 4.3.1 Basic problem arising from animal studies

Evaluation of multiple parameters requires the use of animals over many generations. The explanation for unexpected observations in the current study compared to previously published findings in the model may be caused by marginal shifts in the metabolic phenotype of the animals over generations. To minimize these shifts, the housing conditions were kept as stable as possible. To further reduce variations by shifts of phenotype between generations, the NOD TLR4 colony was maintained by following a breeding strategy that relied on a larger number of breeding pairs over all generations. In addition, in all experiments, littermates were compared with homozygous TLR4-expression or TLR4-deficiency. However, basic parameters, particularly the accelerated diabetes development, were stable as shown by monitoring diabetes manifestation over many generations. Because of the possible shift of parameters over generations, the parameters of the SD group were always measured again together with the groups receiving HFD.

#### 4.3.2 Heterogeneity of NOD TLR4<sup>+/+</sup> and NOD TLR4<sup>-/-</sup> mice

The number of animals that actually have developed insulin-deficient diabetes can explain the partially contrasting results to findings published earlier and the standard deviation of measured data in the present thesis. Around 70-76 % of female NOD TLR4<sup>+/+</sup> and NOD TLR4<sup>-/-</sup> mice develop diabetes during their life span. At the time of the experiments, the mice are in the prediabetic phase at the age of 70-90 days, but diabetes manifestation typically starts at the age of 151-166 days. As a consequence, at the time point of the analyses it is not clear which mouse will develop diabetes later in life. This leads to a heterogeneity of the examined animals with regard to their “prediabetes” status. This heterogeneity may contribute to the deviation of measured data. To address this problem, larger numbers of animals per group were included and the blood glucose levels were measured before every experiment to ensure the inclusion of normoglycemic animals. Despite the deviation of measured data, the NOD TLR4<sup>-/-</sup> mouse model is still regarded as the best model to analyze the processes involved in

the pathogenesis of T1D. Based on the model of the NOD mouse, the NOD TLR4<sup>-/-</sup> mouse model used in this thesis represents an adequate model to analyze the energy and glucose metabolism as well as the insulinitis linked to the development of insulin-deficient diabetes/T1D. Because of its comparability with the increased incidence of T1D in younger children, the model of the NOD TLR4<sup>-/-</sup> mouse allows to study possible mechanisms underlying the accelerated diabetes development and to identify possible strategies to counteract the development of T1D.

### 4.3.3 Anesthesia effects

Isoflurane is a commonly used inhalation anesthetic, which has impacts on multiple cellular processes including the glucose metabolism. To estimate possible isoflurane effects on parameters determined in the present study, the plasma glucose and insulin levels in isoflurane anesthetized female prediabetic NOD TLR4<sup>+/+</sup> and NOD TLR4<sup>-/-</sup> mice were extensively analyzed in pilot studies. The plasma glucose levels were increased in both genotypes during isoflurane anesthesia, but the plasma insulin levels were higher during anesthesia only in NOD TLR4<sup>-/-</sup> mice. These findings confirm the elevation of blood glucose levels by isoflurane in different animal models [268-271]. Regarding the effect of isoflurane on insulin secretion, various studies showed that isoflurane has no impact on the insulin levels or insulin secretion in different animal models, whereas other studies revealed decreased plasma insulin levels by isoflurane [268-272]. Potential alternative anesthetics such as ketamine and xylazine (Ket/Xyl), pentobarbital (PENTO), sevoflurane (SEVO), ketamine-medetomidine-atropine (KMA), sufentanil-propofol-morphine (SPM), fentanyl-ketamine-midazolam (FKM), fentanyl-midazolam-haldol (FMH), fentanyl-fluanisone-midazolam (FFM), fentanyl-midazolam-acepromazine (FMA), propofol-fentanyl-midazolam (PFM) and hypnorm and midazolam (Hyp/Mid) were found to have similar adverse effects as isoflurane on plasma glucose and insulin levels, but also partly on plasma FFA levels [268-271]. SPM, FFM, FMH and PFM showed minor or no effects on the glucose metabolism of the investigated animals. Moreover, these anesthetics have to be applied intraperitoneally, which takes longer to show an effect than inhalation anesthetics and might increase the stress of the animals [269, 271]. In addition, injecting anesthetics intraperitoneally several times during MRI/MRS would challenge the protocols and their duration.

In summary, there is no optimal anesthesia for MRS experiments regarding the whole-body metabolism in animals. Different anesthetics may be preferred in different animal models selected on their physiological conditions and experimental protocols. There is no good alternative for isoflurane for the experiments of the present thesis. However, most parameters in the present study are largely unaffected by isoflurane effects except the <sup>31</sup>P-metabolite measurements.

### 5 Conclusion and outlook

The present thesis combines published data and unpublished experiments that provide new insights into metabolic and immunologic alterations during the prediabetic phase in an animal model of accelerated development of insulin-deficient diabetes/T1D. The newly described metabolic and immunologic changes might contribute to the accelerated development of insulin-deficient diabetes observed in the present mouse model and could explain the accelerated T1D development in younger children.

The findings in the present thesis indicate that the accelerated development of diabetes in prediabetic NOD TLR4<sup>-/-</sup> mice is associated with reduced plasma SCFA levels as well as an impaired glucose tolerance and lipid metabolism. It was shown that lower HCL content precedes the manifestation of accelerated diabetes development in NOD TLR4<sup>-/-</sup> mice, which might result from reduced activity of insulin-mediated TG synthesis or increased lipolysis. On HFD, NOD TLR4<sup>-/-</sup> mice revealed less metabolic and immunologic changes than NOD TLR4<sup>+/+</sup> mice, suggesting that HFD-feeding rather protects from unfavorable alterations of metabolic and immunologic processes in NOD TLR4<sup>-/-</sup> mice. As expected, HFD-feeding led to higher body weight and increased fat mass in both genotypes. In contrast, NOD TLR4<sup>-/-</sup> mice on HFD revealed higher HCL than NOD TLR4<sup>+/+</sup> mice suggesting an increased FA uptake into the liver while the rate of hepatic FA degradation remains unaffected.

Future experiments should include tissue or cell-type specific TLR4-knockout mouse models, especially hepatocyte-specific, to further investigate the impact of the TLR4-deficiency on distinct tissues. Furthermore, not only FA receptors on the surface but also proteins involved in intracellular lipid metabolism such as ATGL and HSL should be examined in liver tissue of NOD TLR4<sup>+/+</sup> and NOD TLR4<sup>-/-</sup> mice. Additionally, performing a hyperinsulinemic-euglycemic clamp in NOD TLR4<sup>-/-</sup> mice would clarify the degree of insulin sensitivity and proof insulin resistance in these animals. To investigate the impact of HFD on diabetes development and incidence in NOD TLR4<sup>+/+</sup> and NOD TLR4<sup>-/-</sup> mice, these animals should be fed a HFD until the age of 250 days. In addition, their glucose tolerance and insulin sensitivity should be determined to further characterize a potential protective effect of the HFD in NOD TLR4<sup>-/-</sup> mice. Taken together, the NOD TLR4<sup>-/-</sup> mouse is an adequate model to investigate the metabolic processes underlying the accelerated development of T1D, as recently seen in younger children. The present study reveals possible processes and mechanisms that might contribute to and partly clarify the acceleration of T1D development. The findings further emphasize the importance of studies in the prediabetic phase of animal models, in order to develop strategies to prevent or delay the progression of T1D.

## 6 Personal contribution to the manuscripts

Personal contribution of Corinna Wessel (C.W.) to the manuscript “**Distinct alterations of gut morphology and microbiota characterize accelerated diabetes onset in nonobese diabetic mice**“, which was published in the Journal of Biological Chemistry in 2020.

**Name of the journal:** Journal of Biological Chemistry  
**Impact factor:** 4.238 (2019)  
**Author position:** Third author, equal contribution to first authorship  
**Tasks:** Curation and visualization of data. Correction of manuscript and figures.

### Author’s contribution (as written in the manuscript):

M.-C. S., A. L. R., **C.W.**, J. H., K. K., J. A.-C., A. S., M. B., F. B., and V. B. data curation; M.-C. S., A. L. R., **C. W.**, J. H., K. K., M. B., F. B., and V. B. formal analysis; M.-C. S., F. B., and V. B. funding acquisition; M.-C. S., A. L. R., **C. W.**, J. H., T. J., K. K., J. A.-C., A. S., M. B., F. B., and V. B. investigation; M.-C. S., A. L. R., **C. W.**, J. H., T. J., K. K., A. S., M. B., F. B., and V. B. methodology; M.-C. S., F. B., and V. B. writing-original draft; A. L. R., **C. W.**, J. H., T. J., K. K., J. A.-C., A. S., F. B., and V. B. visualization; T. J., F. B., V. B., and M. R. conceptualization; F. B. and V. B. resources; F. B. software; F. B., V. B., and M. R. supervision; V. B. and M. R. project administration; V. B. and M. R. writing-review and editing.

### Contribution by C.W. in detail:

Planning, performance and evaluation of experiments to characterize metabolic parameters and determine lipid levels; collecting, processing and visualization of data; writing and revising the original draft.

**In sum, Corinna Wessel contributed to the work of this manuscript with approximately 25 %.**

## Personal contribution

Personal contribution of Corinna Wessel (C.W.) to the manuscript “**In vivo absolute quantification of hepatic  $\gamma$ -ATP concentration in mice using  $^{31}\text{P}$  MRS at 11.7 T**”, which was published in the journal of NMR in Biomedicine in 2020.

**Name of the journal:** NMR in Biomedicine  
**Impact factor:** 3.221 (2019)  
**Author position:** Second author  
**Tasks:** Providing the NOD mouse model. Performance of MRI/MRS measurements. Revision of the manuscript.

### **Author’s contribution (as written in the manuscript):**

Not required by the journal’s publication guidelines and therefore not stated in the manuscript.

### **Contribution by C.W. in detail:**

Collecting and evaluation of basic parameters of the experimental animals. Performance of MRI/MRS measurements based on validated protocols. Revision of the original draft of the manuscript.

**In sum, Corinna Wessel contributed to the work of this manuscript with approximately 15 %.**

## 7 List of abbreviations

### Symbols and numbers

$^1\text{H}$ MRS	Proton magnetic resonance spectroscopy
$^{31}\text{P}$ MRS	Phosphorus magnetic resonance spectroscopy
3D	Three-dimensional
$\Delta$	Delta
<b>A</b>	
Acetyl-CoA	Acetyl coenzyme A
ADP	Adenosine diphosphate
Akt	Protein kinase B
AMARES	Advanced method for accurate, robust, and efficient spectral fitting
ANOVA	Analysis of variance
APS	Ammonium persulfate
ATGL	Adipose triglyceride lipase
ATP	Adenosine triphosphate
AUC	Area under the curve
<b>B</b>	
BAT	Brown adipose tissue
BB rat	Bio Breeding rat
BCA	Bicinchoninic acid
BSA	Bovine Serum Albumin
<b>C</b>	
CaCl <sub>2</sub>	Calcium chloride
CD36	Cluster of differentiation 36
CHO	Carbohydrate oxidation
CO <sub>2</sub>	Carbon dioxide
CRP	C-reactive protein
CTLA4	Cytotoxic T-lymphocyte-associated Protein 4
Cu <sup>+</sup> / Cu <sup>2+</sup>	Cuprous ion
<b>D</b>	
DNA	Deoxyribonucleic acid
DDG	Deutsche Diabetes Gesellschaft
DEPC	Diethyl pyrocarbonate
DMEM	Dulbecco's modified eagle's medium
dNTP	Deoxynucleoside triphosphate
<b>E</b>	
EASD	European association for the study of diabetes
EDTA	Ethylenediaminetetraacetic acid
ELISA	Enzyme-linked Immunosorbent Assay
EMCL	Extramycellular lipids
ER	Endoplasmic reticulum
<b>F</b>	
FA	Fatty acid
FADH <sub>2</sub>	Flavin adenine dinucleotide
FAO	Fat oxidation
FCS	Fetal calf serum
FFA	Free fatty acid
FFAR2	Free fatty acid receptor 2
FFM	Fentanyl-fluanisone- midazolam
FKM	Fentanyl-ketamine-midazolam
FMA	Fentanyl-midazolam-acepromazine
FMH	Fentanyl-midazolam-haldol

## List of abbreviations

FWHM	Full width at half maximum
<b><u>G</u></b>	
G6P	Glucose 6-phosphate
GAD65	Glutamate decarboxylase
GC-MS	Gas chromatography-mass spectrometry
GLP-1	Glucagon-like peptide-1
GLUT2	Glucose transporter 2
GLUT4	Glucose transporter 4
GPR43	G-protein-coupled receptor 4
GSV	GLUT4 storage vesicle
<b><u>H</u></b>	
H <sub>2</sub> O	Water
H <sub>2</sub> O <sub>2</sub>	Hydrogen peroxide
HBSS	Harks' Balanced Salts
HCl	Hydrogen chloride
HCL	Hepatocellular lipid
HDL	High density lipoprotein
HEPES	4-(2-hydroxyethyl)-1-piperazineethanesulfonic acid
HFD	High fat diet
HLA	Human leukocyte antigen
HOMA-IR	Homeostatic model assessment-insulin resistance
HRP	Horseradish peroxidase
HSL	Hormone sensitive lipase
HSP60	Heat shock protein 60
Hyp/Mid	Hypnorm/Midazolam
<b><u>I</u></b>	
IAA	Insulin autoantibody
iAUC	Incremental area under the curve
ICA	Islet cell antigens
IFN $\gamma$	Interferon gamma
IgG	Immunoglobulin G
IL2RA	Interleukin-2 receptor alpha chain
IL-6	Interleukin 6
IMCL	Intramyocellular lipid
ipGTT	Intraperitoneal glucose tolerance test
ipITT	Intraperitoneal insulin tolerance test
IR	Insulin resistance
IRS	Insulin receptor substrate
ISIS	Image-selected in vivo spectroscopy
<b><u>K</u></b>	
K <sub>ATP</sub>	ATP sensitive potassium channels
KCl	Potassium chloride
kDa	Kilodalton
Ket/Xyl	Ketamine/Xylazine
KH <sub>2</sub> PO <sub>4</sub>	Monopotassium phosphate
KMA	Ketamine-medetomidine-atropine
KRH-buffer	Krebs-Ringer-HEPES buffer
<b><u>L</u></b>	
LCFA	Long-chain fatty acids
LDL	Low density lipoprotein
LPS	Lipopolysaccharide
<b><u>M</u></b>	
MDPA	Methylenediphosphonic acid
MgSO <sub>4</sub>	Magnesium sulfate

## List of abbreviations

MHC	Major histocompatibility complex
MRI	Magnetic resonance imaging
mRNA	Messenger ribonucleic acid
MRS	Magnetic resonance spectroscopy
MUFA	Monounsaturated fatty acid
MyD88	Myeloid differentiation primary response 88
<b><u>N</u></b>	
NaCl	Sodium chloride
NADH	Nicotinamide adenine dinucleotide
NAFLD	Nonalcoholic fatty liver disease
NASH	Nonalcoholic steatohepatitis
NAT	Neck adipose tissue
NF-κB	Nuclear factor κ-light-chain-enhancer of activated B cells
NK cells	Natural killer cells
NLR	Nucleotide oligomerization domain -like receptors
NMR	Nuclear magnetic resonance
NOD	Non-obese diabetic
<b><u>O</u></b>	
O <sub>2</sub>	Oxygen
ob/ob	Leptin-deficient mouse
<b><u>P</u></b>	
PAMPs	Pathogen-associated molecular patterns
PBS	Phosphate-buffered saline
PCR	Polymerase chain reaction
PDE	Phosphodiester
PENTO	Pentobarbital
PFA	Paraformaldehyde
PFM	Propofol-fentanyl-midazolam
pH	Potential of hydrogen
Pi	Inorganic phosphate
PME	Phosphomonoester
Ppm	Parts per million
PRESS	Point resolved spectroscopy
PTMs	Post-translational modifications
PUFA	Polyunsaturated fatty acid
<b><u>R</u></b>	
RARE	Turbo Rapid Acquisition with Relaxation Enhancement
RQ	Respiratory quotient
rRNA	Ribosomal ribonucleic acid
<b><u>S</u></b>	
SAT	Subcutaneous adipose tissue
SCFA	Short-chain fatty acid
SD	Standard diet
SEM	Standard error of the mean
SEVO	Sevoflurane
SFA	Saturated fatty acid
SPM	Sufentanil-propofol-morphine
STEAM	Stimulated echo acquisition mode
STZ	Streptozotocin
<b><u>T</u></b>	
T1D	Type 1 diabetes
T2D	Type 2 diabetes
TCA	Tricarboxylic acid
TEMED	Tetramethylethylenediamine

## List of abbreviations

TG	Triglyceride
TLR	Toll-like receptor
TLR2	Toll-like receptor 2
TLR4	Toll-like receptor 4
TNF $\alpha$	Tumor necrosis factor
T <sub>reg</sub>	Regulatory T cell
TRIF	Toll-like receptor domain-containing adapter-inducing interferon- $\beta$
<b><u>U</u></b>	
UV	Ultraviolet
<b><u>V</u></b>	
VAPOR	Variable power radiofrequency pulses with optimized relaxation delays
VAT	Visceral adipose tissue
VDCC	Voltage-dependent calcium ion channels
VLDL	Very low density lipoprotein
<b><u>W</u></b>	
WAT	White adipose tissue
<b><u>Z</u></b>	
ZnT8	Zinc transporter 8

## 8 Figure index

Figure 1:	Glucose stimulated insulin secretion from pancreatic beta cells.	13
Figure 2:	Insulin signaling pathway in mammalian cells.	14
Figure 3:	Pathway of energy generation by glucose degradation from glycolysis to the tricarboxylic acid cycle and finally to the respiratory chain in mammals.	22
Figure 4:	Schematic representation of the fatty acid (FA) metabolism in the liver.	23
Figure 5:	Schematic representation of the interplay between the gut microbiome and energy homeostasis in T1D.	33
Figure 6:	Schematic representation of insulin detection using specific antibodies and the Avidin-Biotin complex formation.	51
Figure 7:	Procedure of BCA for protein quantification in a 96-well plate format.	53
Figure 8:	The order of the blotting stack for Western Blot analysis from the anode to the cathode.	54
Figure 9:	Schematic presentation of the time course of the intraperitoneal glucose-tolerance-test (ipGTT) under isoflurane-anesthesia.	56
Figure 10:	Schematic representation of the <sup>1</sup> H MRS protocol.	58
Figure 11:	Schematic representation of the <sup>31</sup> P MRS protocol.	59
Figure 12:	Age and blood glucose concentrations at diabetes onset in female NOD mice.	60
Figure 13:	Blood glucose levels during an intraperitoneal insulin tolerance test in NOD mice.	61
Figure 14:	Higher insulin release from cultivated pancreatic islets of NOD mice exposed to 28 mM glucose compared to islets treated with lower glucose concentrations.	61
Figure 15:	Diabetes incidence in female and male NOD TLR4 <sup>+/+</sup> and NOD TLR4 <sup>-/-</sup> mice.	62
Figure 16:	Accelerated diabetes development in female NOD TLR4 <sup>-/-</sup> mice compared to NOD TLR4 <sup>+/+</sup> .	63
Figure 17:	Comparable blood glucose concentrations in female NOD TLR4 <sup>+/+</sup> mice and NOD TLR4 <sup>-/-</sup> mice at the time of diabetes manifestation.	63
Figure 18:	Comparable water and food intake of female prediabetic NOD TLR4 <sup>+/+</sup> and NOD TLR4 <sup>-/-</sup> mice.	65
Figure 19:	Comparable physical activity in female prediabetic NOD TLR4 <sup>+/+</sup> and NOD TLR4 <sup>-/-</sup> mice.	66
Figure 20:	Comparable respiratory quotient in female prediabetic NOD TLR4 <sup>+/+</sup> and NOD TLR4 <sup>-/-</sup> mice.	67
Figure 21:	Comparable energy expenditure in female prediabetic NOD TLR4 <sup>+/+</sup> and NOD TLR4 <sup>-/-</sup> mice.	68
Figure 22:	Comparable whole-body carbohydrate and fat oxidation rates in female prediabetic NOD TLR4 <sup>+/+</sup> and NOD TLR4 <sup>-/-</sup> mice.	69
Figure 23:	Increased body weight, but comparable liver and visceral adipose tissue weight in NOD TLR4 <sup>-/-</sup> mice compared to NOD TLR4 <sup>+/+</sup> mice.	69
Figure 24:	Comparable body weight development in female prediabetic NOD TLR4 <sup>+/+</sup> mice and NOD TLR4 <sup>-/-</sup> mice.	70

Figure 25:	Comparable weights of NAT, BAT and WAT in female prediabetic NOD TLR4 <sup>+/+</sup> mice and NOD TLR4 <sup>-/-</sup> mice.	71
Figure 26:	Volumes of liver, VAT, NAT and BAT of female prediabetic NOD TLR4 <sup>+/+</sup> and NOD TLR4 <sup>-/-</sup> mice.	72
Figure 27:	Comparable body composition of female NOD TLR4 <sup>+/+</sup> and NOD TLR4 <sup>-/-</sup> mice at 30 and 70 days of age.	73
Figure 28:	Increased random blood glucose levels in NOD TLR4 <sup>-/-</sup> compared to NOD TLR4 <sup>+/+</sup> mice.	74
Figure 29:	Increased blood glucose levels during an intraperitoneal glucose tolerance test in NOD TLR4 <sup>-/-</sup> mice compared to NOD TLR4 <sup>+/+</sup> mice.	75
Figure 30:	Lower insulin levels 15 minutes after glucose injection in NOD TLR4 <sup>-/-</sup> mice compared to NOD TLR4 <sup>+/+</sup> mice.	76
Figure 31:	Comparable HOMA-IR of female prediabetic NOD TLR4 <sup>+/+</sup> and NOD TLR4 <sup>-/-</sup> mice.	76
Figure 32:	Total area and insulin-positive area of pancreatic islets of NOD TLR4 <sup>+/+</sup> and NOD TLR4 <sup>-/-</sup> mice.	77
Figure 33:	Representative histological images of pancreatic islets and their classification into insulinitis-scores, the infiltrated islet area and the association of islet area and insulinitis-scores in NOD TLR4 <sup>+/+</sup> and NOD TLR4 <sup>-/-</sup> mice.	78
Figure 34:	The effect of the anesthetic isoflurane on the blood glucose levels during an ipGTT in female prediabetic NOD TLR4 <sup>+/+</sup> and NOD TLR4 <sup>-/-</sup> mice.	80
Figure 35:	Effect of isoflurane anesthesia on blood glucose levels of NOD TLR4 <sup>+/+</sup> and NOD TLR4 <sup>-/-</sup> mice at the beginning and the end of an ipGTT.	81
Figure 36:	Area under the glucose concentration time curve and incremental area under the curve of an ipGTT in female prediabetic NOD TLR4 <sup>+/+</sup> and NOD TLR4 <sup>-/-</sup> mice.	82
Figure 37:	Effect of isoflurane anesthesia on plasma insulin levels in female prediabetic NOD TLR4 <sup>+/+</sup> and NOD TLR4 <sup>-/-</sup> mice.	83
Figure 38:	Comparable plasma free fatty acid and triglyceride levels in female prediabetic NOD TLR4 <sup>+/+</sup> and NOD TLR4 <sup>-/-</sup> mice.	84
Figure 39:	Comparable plasma cholesterol, high and low density lipoprotein and C-reactive protein levels in female prediabetic NOD TLR4 <sup>+/+</sup> and NOD TLR4 <sup>-/-</sup> mice.	85
Figure 40:	Effect of the TLR4-expression status on fat composition of VAT in female prediabetic NOD TLR4 <sup>+/+</sup> and NOD TLR4 <sup>-/-</sup> mice.	86
Figure 41:	Effect of the TLR4-expression status on fat composition of the NAT in female prediabetic NOD TLR4 <sup>+/+</sup> and NOD TLR4 <sup>-/-</sup> mice.	87
Figure 42:	Effect of TLR4-expression status on fat composition of the BAT in female prediabetic NOD TLR4 <sup>+/+</sup> and NOD TLR4 <sup>-/-</sup> mice.	88
Figure 43:	Lower HCL levels in NOD TLR4 <sup>-/-</sup> mice compared to NOD TLR4 <sup>+/+</sup> mice.	89
Figure 44:	Effect of the TLR4-expression status on the triglyceride content in liver tissue in female prediabetic NOD TLR4 <sup>+/+</sup> and NOD TLR4 <sup>-/-</sup> mice.	90
Figure 45:	Effect of the TLR4-expression status on protein expression of the FA receptors CD36 and FFAR2 in liver tissue of female prediabetic NOD TLR4 <sup>+/+</sup> and NOD TLR4 <sup>-/-</sup> mice.	91
Figure 46:	Effect of the TLR4-expression status on protein expression of the FA receptors CD36 and FFAR2 in skeletal muscle tissue of female	

	prediabetic NOD TLR4 <sup>+/+</sup> and NOD TLR4 <sup>-/-</sup> mice.	92
Figure 47:	Effect of the TLR4-expression status on protein expression of the FA receptors CD36 and FFAR2 in VAT of female prediabetic NOD TLR4 <sup>+/+</sup> and NOD TLR4 <sup>-/-</sup> mice.	92
Figure 48:	Lower SCFA plasma concentrations in NOD TLR4 <sup>-/-</sup> mice compared to NOD TLR4 <sup>+/+</sup> mice.	94
Figure 49:	Comparable total SCFA concentrations in small intestine, cecum and colon of female prediabetic NOD TLR4 <sup>+/+</sup> and NOD TLR4 <sup>-/-</sup> mice.	95
Figure 50:	Effect of the TLR4-expression status on intraluminal concentrations of SCFA in gut segments of female prediabetic NOD TLR4 <sup>+/+</sup> and NOD TLR4 <sup>-/-</sup> mice.	96
Figure 51:	Ratios of SCFA concentrations between plasma and gut segments in female prediabetic NOD TLR4 <sup>+/+</sup> and NOD TLR4 <sup>-/-</sup> mice.	98
Figure 52:	Similar $\gamma$ -ATP and Pi levels in the liver of female prediabetic NOD TLR4 <sup>+/+</sup> and NOD TLR4 <sup>-/-</sup> mice.	99
Figure 53:	Hepatic $\gamma$ -ATP and Pi concentrations before and after glucose injection in female prediabetic NOD TLR4 <sup>+/+</sup> and NOD TLR4 <sup>-/-</sup> mice.	100
Figure 54:	Similar PME and PDE levels in the liver of female prediabetic NOD TLR4 <sup>+/+</sup> and NOD TLR4 <sup>-/-</sup> mice.	101
Figure 55:	Hepatic PME and PDE concentrations before and after glucose injection in female prediabetic NOD TLR4 <sup>+/+</sup> and NOD TLR4 <sup>-/-</sup> mice.	102
Figure 56:	Comparable water and food intake in female prediabetic NOD TLR4 <sup>+/+</sup> and NOD TLR4 <sup>-/-</sup> mice fed with either SD or HFD.	104
Figure 57:	Comparable physical activity in female prediabetic NOD TLR4 <sup>+/+</sup> and NOD TLR4 <sup>-/-</sup> mice fed with SD or HFD.	105
Figure 58:	Lower respiratory quotient in the light-phases and in the dark-phases in female prediabetic NOD TLR4 <sup>+/+</sup> and NOD TLR4 <sup>-/-</sup> mice fed with HFD compared to mice fed with SD.	106
Figure 59:	Lower energy expenditure in the dark-phases in female prediabetic NOD TLR4 <sup>+/+</sup> and NOD TLR4 <sup>-/-</sup> mice fed with HFD compared to mice fed with SD.	107
Figure 60:	Lower whole-body carbohydrate and higher fat oxidation rates in female prediabetic NOD TLR4 <sup>+/+</sup> and NOD TLR4 <sup>-/-</sup> mice fed with HFD compared to mice fed with SD.	108
Figure 61:	Increased body and visceral adipose tissue weight, but similar liver weight in NOD TLR4 <sup>+/+</sup> and NOD TLR4 <sup>-/-</sup> mice fed with HFD compared to mice fed with SD.	109
Figure 62:	Accelerated body weight development in female prediabetic NOD TLR4 <sup>+/+</sup> mice and NOD TLR4 <sup>-/-</sup> mice fed with HFD compared to mice fed with SD.	110
Figure 63:	Higher NAT, BAT and WAT weight in female prediabetic NOD TLR4 <sup>+/+</sup> mice and NOD TLR4 <sup>-/-</sup> mice fed with HFD compared to SD.	111
Figure 64:	Higher VAT, NAT and BAT volumes in female prediabetic NOD TLR4 <sup>+/+</sup> and NOD TLR4 <sup>-/-</sup> mice on HFD compared to mice on SD.	112
Figure 65:	Higher fat mass and lower fat free mass in female NOD TLR4 <sup>+/+</sup> and NOD TLR4 <sup>-/-</sup> mice on HFD compared to mice on SD at the age of 70 days.	113
Figure 66:	Lower random blood glucose levels in NOD TLR4 <sup>-/-</sup> mice on HFD compared to NOD TLR4 <sup>+/+</sup> mice on HFD.	114

## Figure index

Figure 67:	Total area and insulin-positive area of pancreatic of NOD TLR4 <sup>+/+</sup> and NOD TLR4 <sup>-/-</sup> mice on SD or HFD.	115
Figure 68:	Infiltrated islet area and the association of islet area and insulinitis-scores in NOD TLR4 <sup>+/+</sup> and NOD TLR4 <sup>-/-</sup> mice on SD or HFD.	116
Figure 69:	Comparable plasma free fatty acid and triglyceride levels in female prediabetic NOD TLR4 <sup>+/+</sup> and NOD TLR4 <sup>-/-</sup> mice fed with SD or HFD.	117
Figure 70:	Higher plasma cholesterol, high and low density lipoprotein but similar C-reactive protein levels in female prediabetic NOD TLR4 <sup>+/+</sup> and NOD TLR4 <sup>-/-</sup> mice fed with HFD compared to mice fed with SD.	118
Figure 71:	Effect of the TLR4-expression status on the fat composition of VAT in female prediabetic NOD TLR4 <sup>+/+</sup> and NOD TLR4 <sup>-/-</sup> mice fed with SD or HFD.	119
Figure 72:	Effect of the TLR4-expression status on the fat composition of the NAT in female prediabetic NOD TLR4 <sup>+/+</sup> and NOD TLR4 <sup>-/-</sup> mice fed with either SD or HFD.	121
Figure 73:	Effect of the TLR4-expression status on the fat composition of the BAT in female prediabetic NOD TLR4 <sup>+/+</sup> and NOD TLR4 <sup>-/-</sup> mice fed with SD or HFD.	123
Figure 74:	Higher HCL levels in female prediabetic NOD TLR4 <sup>+/+</sup> and NOD TLR4 <sup>-/-</sup> mice on HFD compared to mice on SD.	124
Figure 75:	Higher $\gamma$ -ATP levels in the liver of female prediabetic NOD TLR4 <sup>+/+</sup> and NOD TLR4 <sup>-/-</sup> mice fed with HFD compared to mice fed with SD.	126
Figure 76:	Hepatic $\gamma$ -ATP and Pi concentrations before and after glucose injection in female prediabetic NOD TLR4 <sup>+/+</sup> and NOD TLR4 <sup>-/-</sup> mice fed with SD or HFD.	127
Figure 77:	Similar PME and PDE levels in the liver of female prediabetic NOD TLR4 <sup>+/+</sup> and NOD TLR4 <sup>-/-</sup> mice on SD or HFD.	128
Figure 78:	Hepatic PME and PDE concentrations before and after glucose injection in female prediabetic NOD TLR4 <sup>+/+</sup> and NOD TLR4 <sup>-/-</sup> mice fed with SD or HFD.	129
Figure 79:	Hypothetical processes associated with lower HCL in NOD TLR4 <sup>-/-</sup> mice.	140

## 9 Table index

Table 1:	Fat composition of the SD and HFD per 100 g fat and per 100 g meal. Additionally, the ratio of HFD to SD per 100 g fat and per 100 g meal was calculated.	35
Table 2:	Nucleotide sequences of the primers for detection of the TLR4-expression status.	42
Table 3:	List of primary antibodies with information of species, dilution, molecular weight and company.	42
Table 4:	List of secondary antibodies with information of species, dilution, molecular weight and company.	42
Table 5:	The components for each sample for the genotyping of mouse ears.	43
Table 6:	The PCR program for the detection of the TLR4-gene.	44
Table 7:	The PCR program for the detection of the TLR4-defect.	44
Table 8:	The preparation of standards for the BCA assay.	52
Table 9:	The amount of the components used for Western Blotting.	54
Table 10:	The components of the 15 % separating gel of the Western Blot.	55
Table 11:	The components of the 4 % stacking gel of the Western Blot.	55
Table 12:	Peak assignments with location (ppm) and type [214].	86

## 10 References

1. Simon, M.C., et al., *Distinct alterations of gut morphology and microbiota characterize accelerated diabetes onset in nonobese diabetic mice*. J Biol Chem, 2020. **295**(4): p. 969-980.
2. Rothe, M., et al., *In vivo absolute quantification of hepatic gamma-ATP concentration in mice using (31) P MRS at 11.7 T*. NMR Biomed, 2020: p. e4422.
3. Kulkarni, R.N., *The islet beta-cell*. Int J Biochem Cell Biol, 2004. **36**(3): p. 365-71.
4. Brissova, M., et al., *Assessment of human pancreatic islet architecture and composition by laser scanning confocal microscopy*. J Histochem Cytochem, 2005. **53**(9): p. 1087-97.
5. Komatsu, M., et al., *Glucose-stimulated insulin secretion: A newer perspective*. J Diabetes Investig, 2013. **4**(6): p. 511-6.
6. Jensen, M.V., et al., *Metabolic cycling in control of glucose-stimulated insulin secretion*. Am J Physiol Endocrinol Metab, 2008. **295**(6): p. E1287-97.
7. Ashcroft, F.M. and P. Rorsman, *Diabetes mellitus and the beta cell: the last ten years*. Cell, 2012. **148**(6): p. 1160-71.
8. Chang, L., S.H. Chiang, and A.R. Saltiel, *Insulin signaling and the regulation of glucose transport*. Mol Med, 2004. **10**(7-12): p. 65-71.
9. Santoleri, D. and P.M. Titchenell, *Resolving the Paradox of Hepatic Insulin Resistance*. Cell Mol Gastroenterol Hepatol, 2019. **7**(2): p. 447-456.
10. Leto, D. and A.R. Saltiel, *Regulation of glucose transport by insulin: traffic control of GLUT4*. Nat Rev Mol Cell Biol, 2012. **13**(6): p. 383-96.
11. Boucher, J., A. Kleinridders, and C.R. Kahn, *Insulin receptor signaling in normal and insulin-resistant states*. Cold Spring Harb Perspect Biol, 2014. **6**(1).
12. Bevan, P., *Insulin signalling*. J Cell Sci, 2001. **114**(Pt 8): p. 1429-30.
13. Dashty, M., *A quick look at biochemistry: carbohydrate metabolism*. Clin Biochem, 2013. **46**(15): p. 1339-52.
14. Hatting, M., et al., *Insulin regulation of gluconeogenesis*. Ann N Y Acad Sci, 2018. **1411**(1): p. 21-35.
15. Rui, L., *Energy metabolism in the liver*. Compr Physiol, 2014. **4**(1): p. 177-97.
16. Taniguchi, C.M., B. Emanuelli, and C.R. Kahn, *Critical nodes in signalling pathways: insights into insulin action*. Nat Rev Mol Cell Biol, 2006. **7**(2): p. 85-96.
17. Fisher, S.J. and C.R. Kahn, *Insulin signaling is required for insulin's direct and indirect action on hepatic glucose production*. J Clin Invest, 2003. **111**(4): p. 463-8.
18. Reddy, S.S., V. Lauris, and C.R. Kahn, *Insulin receptor function in fibroblasts from patients with leprechaunism. Differential alterations in binding, autophosphorylation, kinase activity, and receptor-mediated internalization*. J Clin Invest, 1988. **82**(4): p. 1359-65.
19. Baumeister, F.A., I. Engelsberger, and A. Schulze, *Pancreatic agenesis as cause for neonatal diabetes mellitus*. Klin Padiatr, 2005. **217**(2): p. 76-81.
20. World Health Organization, *Diabetes*, <https://www.who.int/health-topics/diabetes>. (accessed on 28.07.2020).
21. International Diabetes Federation. *IDF Diabetes Atlas, 9th edn. 2019 Brussels*, <https://www.diabetesatlas.org/en/>. (accessed 28.07.2020).
22. American Diabetes, A., *2. Classification and Diagnosis of Diabetes: Standards of Medical Care in Diabetes-2020*. Diabetes Care, 2020. **43**(Suppl 1): p. S14-S31.
23. Henning, R.J., *Type-2 diabetes mellitus and cardiovascular disease*. Future Cardiol, 2018. **14**(6): p. 491-509.
24. Wu, Y., et al., *Risk factors contributing to type 2 diabetes and recent advances in the treatment and prevention*. Int J Med Sci, 2014. **11**(11): p. 1185-200.
25. Shanik, M.H., et al., *Insulin resistance and hyperinsulinemia: is hyperinsulinemia the cart or the horse?* Diabetes Care, 2008. **31** Suppl 2: p. S262-8.
26. Hundal, R.S. and S.E. Inzucchi, *Metformin: new understandings, new uses*. Drugs, 2003. **63**(18): p. 1879-94.

27. Atkinson, M.A., G.S. Eisenbarth, and A.W. Michels, *Type 1 diabetes*. Lancet, 2014. **383**(9911): p. 69-82.
28. Pearson, J.A., F.S. Wong, and L. Wen, *The importance of the Non Obese Diabetic (NOD) mouse model in autoimmune diabetes*. J Autoimmun, 2016. **66**: p. 76-88.
29. American Diabetes, A., *2. Classification and Diagnosis of Diabetes: Standards of Medical Care in Diabetes-2018*. Diabetes Care, 2018. **41**(Suppl 1): p. S13-S27.
30. Gulden, E., et al., *Toll-like receptor 4 deficiency accelerates the development of insulin-deficient diabetes in non-obese diabetic mice*. PLoS One, 2013. **8**(9): p. e75385.
31. Burrack, A.L., T. Martinov, and B.T. Fife, *T Cell-Mediated Beta Cell Destruction: Autoimmunity and Alloimmunity in the Context of Type 1 Diabetes*. Front Endocrinol (Lausanne), 2017. **8**: p. 343.
32. Atkinson, M.A., *The pathogenesis and natural history of type 1 diabetes*. Cold Spring Harb Perspect Med, 2012. **2**(11).
33. Melendez-Ramirez, L.Y., R.J. Richards, and W.T. Cefalu, *Complications of type 1 diabetes*. Endocrinol Metab Clin North Am, 2010. **39**(3): p. 625-40.
34. Patterson, C.C., et al., *Incidence trends for childhood type 1 diabetes in Europe during 1989-2003 and predicted new cases 2005-20: a multicentre prospective registration study*. Lancet, 2009. **373**(9680): p. 2027-33.
35. Quinn, M., et al., *Characteristics at diagnosis of type 1 diabetes in children younger than 6 years*. J Pediatr, 2006. **148**(3): p. 366-71.
36. Goonetilleke, R., M. Pollitzer, and N. Mann, *Insulin for toddlers with difficult diabetes*. Diabetes Care, 2004. **27**(6): p. 1505.
37. Jayasimhan, A., K.P. Mansour, and R.M. Slattery, *Advances in our understanding of the pathophysiology of Type 1 diabetes: lessons from the NOD mouse*. Clin Sci (Lond), 2014. **126**(1): p. 1-18.
38. Barrett, J.C., et al., *Genome-wide association study and meta-analysis find that over 40 loci affect risk of type 1 diabetes*. Nat Genet, 2009. **41**(6): p. 703-7.
39. Polychronakos, C. and Q. Li, *Understanding type 1 diabetes through genetics: advances and prospects*. Nat Rev Genet, 2011. **12**(11): p. 781-92.
40. van Belle, T.L., K.T. Coppieters, and M.G. von Herrath, *Type 1 diabetes: etiology, immunology, and therapeutic strategies*. Physiol Rev, 2011. **91**(1): p. 79-118.
41. Dang, M.N., R. Buzzetti, and P. Pozzilli, *Epigenetics in autoimmune diseases with focus on type 1 diabetes*. Diabetes Metab Res Rev, 2013. **29**(1): p. 8-18.
42. Knip, M. and H. Siljander, *Autoimmune mechanisms in type 1 diabetes*. Autoimmun Rev, 2008. **7**(7): p. 550-7.
43. Furlanos, S., L.C. Harrison, and P.G. Colman, *The accelerator hypothesis and increasing incidence of type 1 diabetes*. Curr Opin Endocrinol Diabetes Obes, 2008. **15**(4): p. 321-5.
44. Wilkin, T.J., *The accelerator hypothesis: a review of the evidence for insulin resistance as the basis for type I as well as type II diabetes*. Int J Obes (Lond), 2009. **33**(7): p. 716-26.
45. Wilkin, T.J., *The accelerator hypothesis: weight gain as the missing link between Type I and Type II diabetes*. Diabetologia, 2001. **44**(7): p. 914-22.
46. Furlanos, S., et al., *Insulin resistance is a risk factor for progression to type 1 diabetes*. Diabetologia, 2004. **47**(10): p. 1661-7.
47. Nokoff, N.J., M. Rewers, and M. Cree Green, *The interplay of autoimmunity and insulin resistance in type 1 diabetes*. Discov Med, 2012. **13**(69): p. 115-22.
48. Wellen, K.E. and G.S. Hotamisligil, *Obesity-induced inflammatory changes in adipose tissue*. J Clin Invest, 2003. **112**(12): p. 1785-8.
49. Weisberg, S.P., et al., *Obesity is associated with macrophage accumulation in adipose tissue*. J Clin Invest, 2003. **112**(12): p. 1796-808.
50. Svensson, M.K. and J.W. Eriksson, *Change in the amount of body fat and IL-6 levels is related to altered insulin sensitivity in type 1 diabetes patients with or without diabetic nephropathy*. Horm Metab Res, 2011. **43**(3): p. 209-15.

51. Konner, A.C. and J.C. Bruning, *Toll-like receptors: linking inflammation to metabolism*. Trends Endocrinol Metab, 2011. **22**(1): p. 16-23.
52. Norris, J.M., et al., *Omega-3 polyunsaturated fatty acid intake and islet autoimmunity in children at increased risk for type 1 diabetes*. JAMA, 2007. **298**(12): p. 1420-8.
53. Oh, D.Y., et al., *GPR120 is an omega-3 fatty acid receptor mediating potent anti-inflammatory and insulin-sensitizing effects*. Cell, 2010. **142**(5): p. 687-98.
54. Ilonen, J., et al., *Environmental factors and primary prevention in type 1 diabetes*. Pediatr Endocrinol Diabetes Metab, 2009. **15**(4): p. 227-32.
55. Akerblom, H.K., et al., *Environmental factors in the etiology of type 1 diabetes*. Am J Med Genet, 2002. **115**(1): p. 18-29.
56. Group, T.S., *The Environmental Determinants of Diabetes in the Young (TEDDY) Study*. Ann N Y Acad Sci, 2008. **1150**: p. 1-13.
57. Karjalainen, J., et al., *A bovine albumin peptide as a possible trigger of insulin-dependent diabetes mellitus*. N Engl J Med, 1992. **327**(5): p. 302-7.
58. Moltchanova, E.V., et al., *Seasonal variation of diagnosis of Type 1 diabetes mellitus in children worldwide*. Diabet Med, 2009. **26**(7): p. 673-8.
59. Mathieu, C., et al., *Prevention of autoimmune diabetes in NOD mice by 1,25 dihydroxyvitamin D3*. Diabetologia, 1994. **37**(6): p. 552-8.
60. Mathieu, C., et al., *1,25-Dihydroxyvitamin D3 prevents insulinitis in NOD mice*. Diabetes, 1992. **41**(11): p. 1491-5.
61. D'Ambrosio, D., et al., *Inhibition of IL-12 production by 1,25-dihydroxyvitamin D3. Involvement of NF-kappaB downregulation in transcriptional repression of the p40 gene*. J Clin Invest, 1998. **101**(1): p. 252-62.
62. Hyponen, E., et al., *Intake of vitamin D and risk of type 1 diabetes: a birth-cohort study*. Lancet, 2001. **358**(9292): p. 1500-3.
63. Walter, M., et al., *No effect of the 1alpha,25-dihydroxyvitamin D3 on beta-cell residual function and insulin requirement in adults with new-onset type 1 diabetes*. Diabetes Care, 2010. **33**(7): p. 1443-8.
64. Vaarala, O., M.A. Atkinson, and J. Neu, *The "perfect storm" for type 1 diabetes: the complex interplay between intestinal microbiota, gut permeability, and mucosal immunity*. Diabetes, 2008. **57**(10): p. 2555-62.
65. Samuel, V.T. and G.I. Shulman, *The pathogenesis of insulin resistance: integrating signaling pathways and substrate flux*. J Clin Invest, 2016. **126**(1): p. 12-22.
66. Yaribeygi, H., et al., *Insulin resistance: Review of the underlying molecular mechanisms*. J Cell Physiol, 2019. **234**(6): p. 8152-8161.
67. Kubes, P. and C. Jenne, *Immune Responses in the Liver*. Annu Rev Immunol, 2018. **36**: p. 247-277.
68. Franko, A., et al., *Identification of the Secreted Proteins Originated from Primary Human Hepatocytes and HepG2 Cells*. Nutrients, 2019. **11**(8).
69. Smith, U. and B.B. Kahn, *Adipose tissue regulates insulin sensitivity: role of adipogenesis, de novo lipogenesis and novel lipids*. J Intern Med, 2016. **280**(5): p. 465-475.
70. Turner, N., et al., *Distinct patterns of tissue-specific lipid accumulation during the induction of insulin resistance in mice by high-fat feeding*. Diabetologia, 2013. **56**(7): p. 1638-48.
71. Samuel, V.T., et al., *Mechanism of hepatic insulin resistance in non-alcoholic fatty liver disease*. J Biol Chem, 2004. **279**(31): p. 32345-53.
72. Hernandez, E.A., et al., *Acute dietary fat intake initiates alterations in energy metabolism and insulin resistance*. J Clin Invest, 2017. **127**(2): p. 695-708.
73. Ibrahim, M.M., *Subcutaneous and visceral adipose tissue: structural and functional differences*. Obes Rev, 2010. **11**(1): p. 11-8.
74. Marlatt, K.L. and E. Ravussin, *Brown Adipose Tissue: an Update on Recent Findings*. Curr Obes Rep, 2017. **6**(4): p. 389-396.
75. Fenzl, A. and F.W. Kiefer, *Brown adipose tissue and thermogenesis*. Horm Mol Biol Clin Investig, 2014. **19**(1): p. 25-37.

76. van Marken Lichtenbelt, W.D., et al., *Cold-activated brown adipose tissue in healthy men*. N Engl J Med, 2009. **360**(15): p. 1500-8.
77. Frontera, W.R. and J. Ochala, *Skeletal muscle: a brief review of structure and function*. Calcif Tissue Int, 2015. **96**(3): p. 183-95.
78. Popadic Gacesa, J., et al., *Intramyocellular lipids and their dynamics assessed by (1) H magnetic resonance spectroscopy*. Clin Physiol Funct Imaging, 2017. **37**(6): p. 558-566.
79. Hua, N., et al., *Influence of muscle fiber type composition on early fat accumulation under high-fat diet challenge*. PLoS One, 2017. **12**(8): p. e0182430.
80. Shulman, G.I., *Unraveling the cellular mechanism of insulin resistance in humans: new insights from magnetic resonance spectroscopy*. Physiology (Bethesda), 2004. **19**: p. 183-90.
81. Cree, M.G. and R.R. Wolfe, *Postburn trauma insulin resistance and fat metabolism*. Am J Physiol Endocrinol Metab, 2008. **294**(1): p. E1-9.
82. Perseghin, G., et al., *Insulin resistance, intramyocellular lipid content, and plasma adiponectin in patients with type 1 diabetes*. Am J Physiol Endocrinol Metab, 2003. **285**(6): p. E1174-81.
83. Schauer, I.E., et al., *Insulin resistance, defective insulin-mediated fatty acid suppression, and coronary artery calcification in subjects with and without type 1 diabetes: The CACTI study*. Diabetes, 2011. **60**(1): p. 306-14.
84. Bonora, M., et al., *ATP synthesis and storage*. Purinergic Signal, 2012. **8**(3): p. 343-57.
85. Friedman, J.R. and J. Nunnari, *Mitochondrial form and function*. Nature, 2014. **505**(7483): p. 335-43.
86. Martinez-Reyes, I. and N.S. Chandel, *Mitochondrial TCA cycle metabolites control physiology and disease*. Nat Commun, 2020. **11**(1): p. 102.
87. Larosa, V. and C. Rémacle, *Insights into the respiratory chain and oxidative stress*. Biosci Rep, 2018. **38**(5).
88. van der Blik, A.M., M.M. Sedensky, and P.G. Morgan, *Cell Biology of the Mitochondrion*. Genetics, 2017. **207**(3): p. 843-871.
89. Nicholls, D.G., *Mitochondrial function and dysfunction in the cell: its relevance to aging and aging-related disease*. Int J Biochem Cell Biol, 2002. **34**(11): p. 1372-81.
90. Mishra, P. and D.C. Chan, *Mitochondrial dynamics and inheritance during cell division, development and disease*. Nat Rev Mol Cell Biol, 2014. **15**(10): p. 634-46.
91. Petersen, M.C., D.F. Vatner, and G.I. Shulman, *Regulation of hepatic glucose metabolism in health and disease*. Nat Rev Endocrinol, 2017. **13**(10): p. 572-587.
92. Alves-Bezerra, M. and D.E. Cohen, *Triglyceride Metabolism in the Liver*. Compr Physiol, 2017. **8**(1): p. 1-8.
93. Wueest, S., et al., *Mesenteric Fat Lipolysis Mediates Obesity-Associated Hepatic Steatosis and Insulin Resistance*. Diabetes, 2016. **65**(1): p. 140-8.
94. Petersen, M.C. and G.I. Shulman, *Mechanisms of Insulin Action and Insulin Resistance*. Physiol Rev, 2018. **98**(4): p. 2133-2223.
95. Lampidonis, A.D., et al., *The resurgence of Hormone-Sensitive Lipase (HSL) in mammalian lipolysis*. Gene, 2011. **477**(1-2): p. 1-11.
96. Bartlett, K. and S. Eaton, *Mitochondrial beta-oxidation*. Eur J Biochem, 2004. **271**(3): p. 462-9.
97. Sevastianova, K., et al., *Effect of short-term carbohydrate overfeeding and long-term weight loss on liver fat in overweight humans*. Am J Clin Nutr, 2012. **96**(4): p. 727-34.
98. Roden, M., *Mechanisms of Disease: hepatic steatosis in type 2 diabetes--pathogenesis and clinical relevance*. Nat Clin Pract Endocrinol Metab, 2006. **2**(6): p. 335-48.
99. Birkenfeld, A.L. and G.I. Shulman, *Nonalcoholic fatty liver disease, hepatic insulin resistance, and type 2 diabetes*. Hepatology, 2014. **59**(2): p. 713-23.
100. Ipsen, D.H., J. Lykkesfeldt, and P. Tveden-Nyborg, *Molecular mechanisms of hepatic lipid accumulation in non-alcoholic fatty liver disease*. Cell Mol Life Sci, 2018. **75**(18): p. 3313-3327.

101. Luukkonen, P.K., et al., *Saturated Fat Is More Metabolically Harmful for the Human Liver Than Unsaturated Fat or Simple Sugars*. *Diabetes Care*, 2018. **41**(8): p. 1732-1739.
102. Cotter, T.G. and M. Rinella, *Nonalcoholic Fatty Liver Disease 2020: The State of the Disease*. *Gastroenterology*, 2020. **158**(7): p. 1851-1864.
103. Dewidar, B., et al., *Metabolic liver disease in diabetes - From mechanisms to clinical trials*. *Metabolism*, 2020: p. 154299.
104. Byrne, C.D. and G. Targher, *NAFLD: a multisystem disease*. *J Hepatol*, 2015. **62**(1 Suppl): p. S47-64.
105. Wang, X.J. and H. Malhi, *Nonalcoholic Fatty Liver Disease*. *Ann Intern Med*, 2018. **169**(9): p. ITC65-ITC80.
106. D'Aversa, F., et al., *Gut microbiota and metabolic syndrome*. *Intern Emerg Med*, 2013. **8** **Suppl 1**: p. S11-5.
107. Rashid, M. and E.A. Roberts, *Nonalcoholic steatohepatitis in children*. *J Pediatr Gastroenterol Nutr*, 2000. **30**(1): p. 48-53.
108. Pepino, M.Y., et al., *Structure-function of CD36 and importance of fatty acid signal transduction in fat metabolism*. *Annu Rev Nutr*, 2014. **34**: p. 281-303.
109. Glatz, J.F., J.J. Luiken, and A. Bonen, *Membrane fatty acid transporters as regulators of lipid metabolism: implications for metabolic disease*. *Physiol Rev*, 2010. **90**(1): p. 367-417.
110. Abumrad, N.A. and N.O. Davidson, *Role of the gut in lipid homeostasis*. *Physiol Rev*, 2012. **92**(3): p. 1061-85.
111. Silverstein, R.L., et al., *Mechanisms of cell signaling by the scavenger receptor CD36: implications in atherosclerosis and thrombosis*. *Trans Am Clin Climatol Assoc*, 2010. **121**: p. 206-20.
112. Lopez-Carmona, M.D., et al., *CD36 overexpression: a possible etiopathogenic mechanism of atherosclerosis in patients with prediabetes and diabetes*. *Diabetol Metab Syndr*, 2017. **9**: p. 55.
113. Zhu, W., W. Li, and R.L. Silverstein, *Advanced glycation end products induce a prothrombotic phenotype in mice via interaction with platelet CD36*. *Blood*, 2012. **119**(25): p. 6136-44.
114. Gautam, S. and M. Banerjee, *The macrophage Ox-LDL receptor, CD36 and its association with type II diabetes mellitus*. *Mol Genet Metab*, 2011. **102**(4): p. 389-98.
115. Melis, M., et al., *Polymorphism rs1761667 in the CD36 Gene Is Associated to Changes in Fatty Acid Metabolism and Circulating Endocannabinoid Levels Distinctively in Normal Weight and Obese Subjects*. *Front Physiol*, 2017. **8**: p. 1006.
116. Rac, M.E., et al., *CD36 gene polymorphism and plasma sCD36 as the risk factor in higher cholesterolemia*. *Arch Pediatr*, 2018. **25**(3): p. 177-181.
117. Villa, S.R., et al., *Loss of Free Fatty Acid Receptor 2 leads to impaired islet mass and beta cell survival*. *Sci Rep*, 2016. **6**: p. 28159.
118. Alvarez-Curto, E. and G. Milligan, *Metabolism meets immunity: The role of free fatty acid receptors in the immune system*. *Biochem Pharmacol*, 2016. **114**: p. 3-13.
119. Tolhurst, G., et al., *Short-chain fatty acids stimulate glucagon-like peptide-1 secretion via the G-protein-coupled receptor FFAR2*. *Diabetes*, 2012. **61**(2): p. 364-71.
120. Smith, P.M., et al., *The microbial metabolites, short-chain fatty acids, regulate colonic Treg cell homeostasis*. *Science*, 2013. **341**(6145): p. 569-73.
121. Maslowski, K.M., et al., *Regulation of inflammatory responses by gut microbiota and chemoattractant receptor GPR43*. *Nature*, 2009. **461**(7268): p. 1282-6.
122. Bibbo, S., et al., *The role of diet on gut microbiota composition*. *Eur Rev Med Pharmacol Sci*, 2016. **20**(22): p. 4742-4749.
123. Jandhyala, S.M., et al., *Role of the normal gut microbiota*. *World J Gastroenterol*, 2015. **21**(29): p. 8787-803.
124. Topping, D.L. and P.M. Clifton, *Short-chain fatty acids and human colonic function: roles of resistant starch and nonstarch polysaccharides*. *Physiol Rev*, 2001. **81**(3): p. 1031-64.

## References

125. Morrison, D.J. and T. Preston, *Formation of short chain fatty acids by the gut microbiota and their impact on human metabolism*. Gut Microbes, 2016. **7**(3): p. 189-200.
126. den Besten, G., et al., *The role of short-chain fatty acids in the interplay between diet, gut microbiota, and host energy metabolism*. J Lipid Res, 2013. **54**(9): p. 2325-40.
127. Wong, J.M., et al., *Colonic health: fermentation and short chain fatty acids*. J Clin Gastroenterol, 2006. **40**(3): p. 235-43.
128. Aron-Wisnewsky, J., et al., *Gut microbiota and non-alcoholic fatty liver disease: new insights*. Clin Microbiol Infect, 2013. **19**(4): p. 338-48.
129. Dhiman, R.K., *Gut microbiota and hepatic encephalopathy*. Metab Brain Dis, 2013. **28**(2): p. 321-6.
130. Bibbo, S., et al., *Is there a role for gut microbiota in type 1 diabetes pathogenesis?* Ann Med, 2017. **49**(1): p. 11-22.
131. Stewart, C.J., et al., *Temporal development of the gut microbiome in early childhood from the TEDDY study*. Nature, 2018. **562**(7728): p. 583-588.
132. Kostic, A.D., et al., *The dynamics of the human infant gut microbiome in development and in progression toward type 1 diabetes*. Cell Host Microbe, 2015. **17**(2): p. 260-73.
133. Secondulfo, M., et al., *Ultrastructural mucosal alterations and increased intestinal permeability in non-celiac, type I diabetic patients*. Dig Liver Dis, 2004. **36**(1): p. 35-45.
134. Maffei, C., et al., *Association between intestinal permeability and faecal microbiota composition in Italian children with beta cell autoimmunity at risk for type 1 diabetes*. Diabetes Metab Res Rev, 2016. **32**(7): p. 700-709.
135. Li, X. and M.A. Atkinson, *The role for gut permeability in the pathogenesis of type 1 diabetes--a solid or leaky concept?* Pediatr Diabetes, 2015. **16**(7): p. 485-92.
136. Yiu, J.H., B. Dorweiler, and C.W. Woo, *Interaction between gut microbiota and toll-like receptor: from immunity to metabolism*. J Mol Med (Berl), 2017. **95**(1): p. 13-20.
137. Hansson, G.K. and K. Edfeldt, *Toll to be paid at the gateway to the vessel wall*. Arterioscler Thromb Vasc Biol, 2005. **25**(6): p. 1085-7.
138. Beutler, B., *Tlr4: central component of the sole mammalian LPS sensor*. Curr Opin Immunol, 2000. **12**(1): p. 20-6.
139. Beutler, B., *TLR4 as the mammalian endotoxin sensor*. Curr Top Microbiol Immunol, 2002. **270**: p. 109-20.
140. Kawai, T. and S. Akira, *The role of pattern-recognition receptors in innate immunity: update on Toll-like receptors*. Nat Immunol, 2010. **11**(5): p. 373-84.
141. Kumar, H., T. Kawai, and S. Akira, *Toll-like receptors and innate immunity*. Biochem Biophys Res Commun, 2009. **388**(4): p. 621-5.
142. Akira, S., S. Uematsu, and O. Takeuchi, *Pathogen recognition and innate immunity*. Cell, 2006. **124**(4): p. 783-801.
143. Kawai, T. and S. Akira, *Pathogen recognition with Toll-like receptors*. Curr Opin Immunol, 2005. **17**(4): p. 338-44.
144. Pasare, C. and R. Medzhitov, *Toll-like receptors: linking innate and adaptive immunity*. Microbes Infect, 2004. **6**(15): p. 1382-7.
145. Wagner, H., *Endogenous TLR ligands and autoimmunity*. Adv Immunol, 2006. **91**: p. 159-73.
146. Habich, C., et al., *The receptor for heat shock protein 60 on macrophages is saturable, specific, and distinct from receptors for other heat shock proteins*. J Immunol, 2002. **168**(2): p. 569-76.
147. Vabulas, R.M., et al., *The endoplasmic reticulum-resident heat shock protein Gp96 activates dendritic cells via the Toll-like receptor 2/4 pathway*. J Biol Chem, 2002. **277**(23): p. 20847-53.
148. Termeer, C., et al., *Oligosaccharides of Hyaluronan activate dendritic cells via toll-like receptor 4*. J Exp Med, 2002. **195**(1): p. 99-111.
149. Beutler, B. and A. Poltorak, *The sole gateway to endotoxin response: how LPS was identified as Tlr4, and its role in innate immunity*. Drug Metab Dispos, 2001. **29**(4 Pt 2): p. 474-8.

150. Jiang, D., J. Liang, and P.W. Noble, *Regulation of non-infectious lung injury, inflammation, and repair by the extracellular matrix glycosaminoglycan hyaluronan*. *Anat Rec (Hoboken)*, 2010. **293**(6): p. 982-5.
151. Rakoff-Nahoum, S., et al., *Recognition of commensal microflora by toll-like receptors is required for intestinal homeostasis*. *Cell*, 2004. **118**(2): p. 229-41.
152. Tai, N., F.S. Wong, and L. Wen, *The role of the innate immune system in destruction of pancreatic beta cells in NOD mice and humans with type 1 diabetes*. *J Autoimmun*, 2016. **71**: p. 26-34.
153. Huurman, V.A., et al., *Immunological efficacy of heat shock protein 60 peptide DiaPep277 therapy in clinical type 1 diabetes*. *Clin Exp Immunol*, 2008. **152**(3): p. 488-97.
154. Ohashi, K., et al., *Cutting edge: heat shock protein 60 is a putative endogenous ligand of the toll-like receptor-4 complex*. *J Immunol*, 2000. **164**(2): p. 558-61.
155. Caramalho, I., et al., *Regulatory T cells selectively express toll-like receptors and are activated by lipopolysaccharide*. *J Exp Med*, 2003. **197**(4): p. 403-11.
156. Brusko, T. and M. Atkinson, *Treg in type 1 diabetes*. *Cell Biochem Biophys*, 2007. **48**(2-3): p. 165-75.
157. Pasare, C. and R. Medzhitov, *Toll-like receptors: balancing host resistance with immune tolerance*. *Curr Opin Immunol*, 2003. **15**(6): p. 677-82.
158. Jin, C., J. Henao-Mejia, and R.A. Flavell, *Innate immune receptors: key regulators of metabolic disease progression*. *Cell Metab*, 2013. **17**(6): p. 873-82.
159. Dasu, M.R., et al., *Increased toll-like receptor (TLR) activation and TLR ligands in recently diagnosed type 2 diabetic subjects*. *Diabetes Care*, 2010. **33**(4): p. 861-8.
160. van der Werf, N., et al., *Viral infections as potential triggers of type 1 diabetes*. *Diabetes Metab Res Rev*, 2007. **23**(3): p. 169-83.
161. von Herrath, M. and G.T. Nepom, *Animal models of human type 1 diabetes*. *Nat Immunol*, 2009. **10**(2): p. 129-32.
162. King, A.J., *The use of animal models in diabetes research*. *Br J Pharmacol*, 2012. **166**(3): p. 877-94.
163. Szkudelski, T., *The mechanism of alloxan and streptozotocin action in B cells of the rat pancreas*. *Physiol Res*, 2001. **50**(6): p. 537-46.
164. Sandler, S. and I. Swenne, *Streptozotocin, but not alloxan, induces DNA repair synthesis in mouse pancreatic islets in vitro*. *Diabetologia*, 1983. **25**(5): p. 444-7.
165. Nakhooa, A.F., et al., *The spontaneously diabetic Wistar rat (the "BB" rat): the significance of transient glycosuria*. *Diabetes Metab*, 1978. **4**(4): p. 255-9.
166. Hanenberg, H., et al., *Macrophage infiltration precedes and is a prerequisite for lymphocytic insulinitis in pancreatic islets of pre-diabetic BB rats*. *Diabetologia*, 1989. **32**(2): p. 126-34.
167. Ikehara, S., et al., *Prevention of type 1 diabetes in nonobese diabetic mice by allogeneic bone marrow transplantation*. *Proc Natl Acad Sci U S A*, 1985. **82**(22): p. 7743-7.
168. Kolb, H., *Mouse models of insulin dependent diabetes: low-dose streptozocin-induced diabetes and nonobese diabetic (NOD) mice*. *Diabetes Metab Rev*, 1987. **3**(3): p. 751-78.
169. Wucherpfennig, K.W., *MHC-linked susceptibility to type 1 diabetes: a structural perspective*. *Ann N Y Acad Sci*, 2003. **1005**: p. 119-27.
170. Schmid, S., et al., *Delayed exposure to wheat and barley proteins reduces diabetes incidence in non-obese diabetic mice*. *Clin Immunol*, 2004. **111**(1): p. 108-18.
171. Marietta, E.V., et al., *Low incidence of spontaneous type 1 diabetes in non-obese diabetic mice raised on gluten-free diets is associated with changes in the intestinal microbiome*. *PLoS One*, 2013. **8**(11): p. e78687.
172. Wen, L., et al., *Innate immunity and intestinal microbiota in the development of Type 1 diabetes*. *Nature*, 2008. **455**(7216): p. 1109-13.
173. Hansen, C.H., et al., *Early life treatment with vancomycin propagates *Akkermansia muciniphila* and reduces diabetes incidence in the NOD mouse*. *Diabetologia*, 2012. **55**(8): p. 2285-94.

174. Tormo-Badia, N., et al., *Antibiotic treatment of pregnant non-obese diabetic mice leads to altered gut microbiota and intestinal immunological changes in the offspring*. Scand J Immunol, 2014. **80**(4): p. 250-60.
175. Cooke, A., et al., *Infection with Schistosoma mansoni prevents insulin dependent diabetes mellitus in non-obese diabetic mice*. Parasite Immunol, 1999. **21**(4): p. 169-76.
176. Zaccone, P., et al., *Salmonella typhimurium infection halts development of type 1 diabetes in NOD mice*. Eur J Immunol, 2004. **34**(11): p. 3246-56.
177. Drescher, K.M., et al., *Coxsackievirus B3 infection and type 1 diabetes development in NOD mice: insulinitis determines susceptibility of pancreatic islets to virus infection*. Virology, 2004. **329**(2): p. 381-94.
178. Coleman, D.L., J.E. Kuzava, and E.H. Leiter, *Effect of diet on incidence of diabetes in nonobese diabetic mice*. Diabetes, 1990. **39**(4): p. 432-6.
179. Lefebvre, D.E., et al., *Dietary proteins as environmental modifiers of type 1 diabetes mellitus*. Annu Rev Nutr, 2006. **26**: p. 175-202.
180. Flohe, S.B., et al., *A wheat-based, diabetes-promoting diet induces a Th1-type cytokine bias in the gut of NOD mice*. Cytokine, 2003. **21**(3): p. 149-54.
181. Kagohashi, Y., et al., *Maternal dietary n-6/n-3 fatty acid ratio affects type 1 diabetes development in the offspring of non-obese diabetic mice*. Congenit Anom (Kyoto), 2010. **50**(4): p. 212-20.
182. Calcinaro, F., et al., *Oral probiotic administration induces interleukin-10 production and prevents spontaneous autoimmune diabetes in the non-obese diabetic mouse*. Diabetologia, 2005. **48**(8): p. 1565-75.
183. Maslowski, K.M. and C.R. Mackay, *Diet, gut microbiota and immune responses*. Nat Immunol, 2011. **12**(1): p. 5-9.
184. Hansen, A.K., et al., *Diabetes preventive gluten-free diet decreases the number of caecal bacteria in non-obese diabetic mice*. Diabetes Metab Res Rev, 2006. **22**(3): p. 220-5.
185. Heinrichsdorff, J. and J.M. Olefsky, *Fetuin-A: the missing link in lipid-induced inflammation*. Nat Med, 2012. **18**(8): p. 1182-3.
186. Woods, S.C., et al., *Signals that regulate food intake and energy homeostasis*. Science, 1998. **280**(5368): p. 1378-83.
187. World Health Organization, *Obesity*, <https://www.who.int/topics/obesity>. (accessed on 15.07.2020).
188. Hu, J., et al., *Short-chain fatty acids in control of energy metabolism*. Crit Rev Food Sci Nutr, 2018. **58**(8): p. 1243-1249.
189. Tarini, J. and T.M. Wolever, *The fermentable fibre inulin increases postprandial serum short-chain fatty acids and reduces free-fatty acids and ghrelin in healthy subjects*. Appl Physiol Nutr Metab, 2010. **35**(1): p. 9-16.
190. Ley, R.E., et al., *Obesity alters gut microbial ecology*. Proc Natl Acad Sci U S A, 2005. **102**(31): p. 11070-5.
191. Schwartz, A., et al., *Microbiota and SCFA in lean and overweight healthy subjects*. Obesity (Silver Spring), 2010. **18**(1): p. 190-5.
192. Teixeira, T.F., et al., *Higher level of faecal SCFA in women correlates with metabolic syndrome risk factors*. Br J Nutr, 2013. **109**(5): p. 914-9.
193. Rahat-Rozenbloom, S., et al., *Evidence for greater production of colonic short-chain fatty acids in overweight than lean humans*. Int J Obes (Lond), 2014. **38**(12): p. 1525-31.
194. Muller, M., et al., *Circulating but not faecal short-chain fatty acids are related to insulin sensitivity, lipolysis and GLP-1 concentrations in humans*. Sci Rep, 2019. **9**(1): p. 12515.
195. Shah, J.H., N. Wongsurawat, and P.P. Aran, *Effect of ethanol on stimulus-induced insulin secretion and glucose tolerance. A study of mechanisms*. Diabetes, 1977. **26**(4): p. 271-7.
196. Patel, D.G. and S.P. Singh, *Effect of ethanol and its metabolites on glucose mediated insulin release from isolated islets of rats*. Metabolism, 1979. **28**(1): p. 85-9.

## References

197. Tiengo, A., et al., *Effect of ethanol, acetaldehyde, and acetate on insulin and glucagon secretion in the perfused rat pancreas*. *Diabetes*, 1981. **30**(9): p. 705-9.
198. Bloemen, J.G., et al., *Short chain fatty acids exchange: Is the cirrhotic, dysfunctional liver still able to clear them?* *Clin Nutr*, 2010. **29**(3): p. 365-9.
199. den Besten, G., et al., *Short-Chain Fatty Acids Protect Against High-Fat Diet-Induced Obesity via a PPARgamma-Dependent Switch From Lipogenesis to Fat Oxidation*. *Diabetes*, 2015. **64**(7): p. 2398-408.
200. Fushimi, T., et al., *Acetic acid feeding enhances glycogen repletion in liver and skeletal muscle of rats*. *J Nutr*, 2001. **131**(7): p. 1973-7.
201. Boillot, J., et al., *Effects of dietary propionate on hepatic glucose production, whole-body glucose utilization, carbohydrate and lipid metabolism in normal rats*. *Br J Nutr*, 1995. **73**(2): p. 241-51.
202. Sakakibara, S., et al., *Acetic acid activates hepatic AMPK and reduces hyperglycemia in diabetic KK-A(y) mice*. *Biochem Biophys Res Commun*, 2006. **344**(2): p. 597-604.
203. Endesfelder, D., et al., *Compromised gut microbiota networks in children with anti-islet cell autoimmunity*. *Diabetes*, 2014. **63**(6): p. 2006-14.
204. Brown, C.T., et al., *Gut microbiome metagenomics analysis suggests a functional model for the development of autoimmunity for type 1 diabetes*. *PLoS One*, 2011. **6**(10): p. e25792.
205. Harbison, J.E., et al., *Gut microbiome dysbiosis and increased intestinal permeability in children with islet autoimmunity and type 1 diabetes: A prospective cohort study*. *Pediatr Diabetes*, 2019.
206. Marino, E., et al., *Gut microbial metabolites limit the frequency of autoimmune T cells and protect against type 1 diabetes*. *Nat Immunol*, 2017. **18**(5): p. 552-562.
207. Burrows, M.P., et al., *Microbiota regulates type 1 diabetes through Toll-like receptors*. *Proc Natl Acad Sci U S A*, 2015. **112**(32): p. 9973-7.
208. Chadt, A., et al., *Tbc1d1 mutation in lean mouse strain confers leanness and protects from diet-induced obesity*. *Nat Genet*, 2008. **40**(11): p. 1354-9.
209. Davis, R.C., et al., *Systems genetics of susceptibility to obesity-induced diabetes in mice*. *Physiol Genomics*, 2012. **44**(1): p. 1-13.
210. Matthews, D.R., et al., *Homeostasis model assessment: insulin resistance and beta-cell function from fasting plasma glucose and insulin concentrations in man*. *Diabetologia*, 1985. **28**(7): p. 412-9.
211. Garcia-Villalba, R., et al., *Alternative method for gas chromatography-mass spectrometry analysis of short-chain fatty acids in faecal samples*. *J Sep Sci*, 2012. **35**(15): p. 1906-13.
212. Moreau, N.M., et al., *Simultaneous measurement of plasma concentrations and <sup>13</sup>C-enrichment of short-chain fatty acids, lactic acid and ketone bodies by gas chromatography coupled to mass spectrometry*. *J Chromatogr B Analyt Technol Biomed Life Sci*, 2003. **784**(2): p. 395-403.
213. Weickert, M.O., et al., *Changes in dominant groups of the gut microbiota do not explain cereal-fiber induced improvement of whole-body insulin sensitivity*. *Nutr Metab (Lond)*, 2011. **8**: p. 90.
214. Hamilton, G., et al., *In vivo characterization of the liver fat (1)H MR spectrum*. *NMR Biomed*, 2011. **24**(7): p. 784-90.
215. Pozzilli, P., et al., *NOD mouse colonies around the world--recent facts and figures*. *Immunol Today*, 1993. **14**(5): p. 193-6.
216. Hanafusa, T., et al., *The NOD mouse*. *Diabetes Res Clin Pract*, 1994. **24** Suppl: p. S307-11.
217. Poltorak, A., et al., *Limits of a deletion spanning Tlr4 in C57BL/10ScCr mice*. *J Endotoxin Res*, 2000. **6**(1): p. 51-6.
218. Poltorak, A., et al., *A point mutation in the IL-12R beta 2 gene underlies the IL-12 unresponsiveness of Lps-defective C57BL/10ScCr mice*. *J Immunol*, 2001. **167**(4): p. 2106-11.
219. Poltorak, A., et al., *Defective LPS signaling in C3H/HeJ and C57BL/10ScCr mice: mutations in Tlr4 gene*. *Science*, 1998. **282**(5396): p. 2085-8.

## References

220. Makino, S., et al., *Breeding of a non-obese, diabetic strain of mice*. Jikken Dobutsu, 1980. **29**(1): p. 1-13.
221. Alibashe-Ahmed, M., et al., *Toll-like receptor 4 inhibition prevents autoimmune diabetes in NOD mice*. Sci Rep, 2019. **9**(1): p. 19350.
222. Devaraj, S., P. Tobias, and I. Jialal, *Knockout of toll-like receptor-4 attenuates the pro-inflammatory state of diabetes*. Cytokine, 2011. **55**(3): p. 441-5.
223. Okada, H., et al., *The 'hygiene hypothesis' for autoimmune and allergic diseases: an update*. Clin Exp Immunol, 2010. **160**(1): p. 1-9.
224. Bach, J.F., *The effect of infections on susceptibility to autoimmune and allergic diseases*. N Engl J Med, 2002. **347**(12): p. 911-20.
225. Bauer, S., T. Muller, and S. Hamm, *Pattern recognition by Toll-like receptors*. Adv Exp Med Biol, 2009. **653**: p. 15-34.
226. Shi, H., et al., *TLR4 links innate immunity and fatty acid-induced insulin resistance*. J Clin Invest, 2006. **116**(11): p. 3015-25.
227. Davis, J.E., et al., *Tlr-4 deficiency selectively protects against obesity induced by diets high in saturated fat*. Obesity (Silver Spring), 2008. **16**(6): p. 1248-55.
228. Jia, L., et al., *Hepatocyte toll-like receptor 4 deficiency protects against alcohol-induced fatty liver disease*. Mol Metab, 2018. **14**: p. 121-129.
229. Mezza, T., et al., *Insulin resistance alters islet morphology in nondiabetic humans*. Diabetes, 2014. **63**(3): p. 994-1007.
230. Pogue, A.I., et al., *Systemic Inflammation in C57BL/6J Mice Receiving Dietary Aluminum Sulfate; Up-Regulation of the Pro-Inflammatory Cytokines IL-6 and TNFalpha, C-Reactive Protein (CRP) and miRNA-146a in Blood Serum*. J Alzheimers Dis Parkinsonism, 2017. **7**(6).
231. Chaparro, R.J., et al., *Nonobese diabetic mice express aspects of both type 1 and type 2 diabetes*. Proc Natl Acad Sci U S A, 2006. **103**(33): p. 12475-80.
232. Verges, B., *Lipid disorders in type 1 diabetes*. Diabetes Metab, 2009. **35**(5): p. 353-60.
233. Bergman, B.C., et al., *The importance of palmitoleic acid to adipocyte insulin resistance and whole-body insulin sensitivity in type 1 diabetes*. J Clin Endocrinol Metab, 2013. **98**(1): p. E40-50.
234. Heptulla, R.A., et al., *In situ evidence that peripheral insulin resistance in adolescents with poorly controlled type 1 diabetes is associated with impaired suppression of lipolysis: a microdialysis study*. Pediatr Res, 2003. **53**(5): p. 830-5.
235. Wohl, P., et al., *Inflexibility of energy substrate oxidation in type 1 diabetic patients*. Metabolism, 2004. **53**(5): p. 655-9.
236. Canfora, E.E., J.W. Jocken, and E.E. Blaak, *Short-chain fatty acids in control of body weight and insulin sensitivity*. Nat Rev Endocrinol, 2015. **11**(10): p. 577-91.
237. Gancheva, S., et al., *Interorgan Metabolic Crosstalk in Human Insulin Resistance*. Physiol Rev, 2018. **98**(3): p. 1371-1415.
238. Ploger, S., et al., *Microbial butyrate and its role for barrier function in the gastrointestinal tract*. Ann N Y Acad Sci, 2012. **1258**: p. 52-9.
239. Vatanen, T., et al., *The human gut microbiome in early-onset type 1 diabetes from the TEDDY study*. Nature, 2018. **562**(7728): p. 589-594.
240. Oresic, M., et al., *Dysregulation of lipid and amino acid metabolism precedes islet autoimmunity in children who later progress to type 1 diabetes*. J Exp Med, 2008. **205**(13): p. 2975-84.
241. Lamichhane, S., et al., *Dynamics of Plasma Lipidome in Progression to Islet Autoimmunity and Type 1 Diabetes - Type 1 Diabetes Prediction and Prevention Study (DIPP)*. Sci Rep, 2018. **8**(1): p. 10635.
242. Lede, V., et al., *Altered hepatic lipid metabolism in mice lacking both the melanocortin type 4 receptor and low density lipoprotein receptor*. PLoS One, 2017. **12**(2): p. e0172000.
243. Wolf, P., et al., *Reduced hepatocellular lipid accumulation and energy metabolism in patients with long standing type 1 diabetes mellitus*. Sci Rep, 2019. **9**(1): p. 2576.

244. Perseghin, G., et al., *Reduced intrahepatic fat content is associated with increased whole-body lipid oxidation in patients with type 1 diabetes*. *Diabetologia*, 2005. **48**(12): p. 2615-21.
245. Llaurodo, G., et al., *Liver fat content and hepatic insulin sensitivity in overweight patients with type 1 diabetes*. *J Clin Endocrinol Metab*, 2015. **100**(2): p. 607-16.
246. Kurtz, D.M., et al., *Transgenic studies of fatty acid oxidation gene expression in nonobese diabetic mice*. *J Lipid Res*, 2000. **41**(12): p. 2063-70.
247. Bechmann, L.P., et al., *The interaction of hepatic lipid and glucose metabolism in liver diseases*. *J Hepatol*, 2012. **56**(4): p. 952-64.
248. Serrano, D., et al., *Dysregulated liver lipid metabolism and innate immunity associated with hepatic steatosis in neonatal BBdp rats and NOD mice*. *Sci Rep*, 2019. **9**(1): p. 14594.
249. Kim, J.W. and K.H. Yoon, *Glucolipotoxicity in Pancreatic beta-Cells*. *Diabetes Metab J*, 2011. **35**(5): p. 444-50.
250. Wang, H., et al., *Maternal obesity exacerbates insulinitis and type 1 diabetes in non-obese diabetic mice*. *Reproduction*, 2014. **148**(1): p. 73-9.
251. Clark, A.L.Y., Z.; Chen, S.X.; Fuess, M.; McGinn, G.; Remedi, M.S., *High-fat diet prevents autoimmune diabetes in NOD mice*. *Diabetes*, 2020. **vol. 69**: p. 86 no. Supplement 1.
252. Pierre, N., et al., *Toll-like receptor 4 knockout mice are protected against endoplasmic reticulum stress induced by a high-fat diet*. *PLoS One*, 2013. **8**(5): p. e65061.
253. Gelineau, R.R., et al., *The behavioral and physiological effects of high-fat diet and alcohol consumption: Sex differences in C57BL6/J mice*. *Brain Behav*, 2017. **7**(6): p. e00708.
254. Lang, P., et al., *Effects of different diets used in diet-induced obesity models on insulin resistance and vascular dysfunction in C57BL/6 mice*. *Sci Rep*, 2019. **9**(1): p. 19556.
255. Corpeleijn, E., W.H. Saris, and E.E. Blaak, *Metabolic flexibility in the development of insulin resistance and type 2 diabetes: effects of lifestyle*. *Obes Rev*, 2009. **10**(2): p. 178-93.
256. Verbeeten, K.C., et al., *Association between childhood obesity and subsequent Type 1 diabetes: a systematic review and meta-analysis*. *Diabet Med*, 2011. **28**(1): p. 10-8.
257. Dahlquist, G., *Can we slow the rising incidence of childhood-onset autoimmune diabetes? The overload hypothesis*. *Diabetologia*, 2006. **49**(1): p. 20-4.
258. Maffei, C. and A. Morandi, *Body composition and insulin resistance in children*. *Eur J Clin Nutr*, 2018. **72**(9): p. 1239-1245.
259. Mosser, R.E., et al., *High-fat diet-induced beta-cell proliferation occurs prior to insulin resistance in C57Bl/6J male mice*. *Am J Physiol Endocrinol Metab*, 2015. **308**(7): p. E573-82.
260. Seferovic, M.D., et al., *Increases in bioactive lipids accompany early metabolic changes associated with beta-cell expansion in response to short-term high-fat diet*. *Am J Physiol Endocrinol Metab*, 2018. **315**(6): p. E1251-E1263.
261. Oliveira, R.B., et al., *Influence of gender and time diet exposure on endocrine pancreas remodeling in response to high fat diet-induced metabolic disturbances in mice*. *Ann Anat*, 2015. **200**: p. 88-97.
262. d Oliveira, R.B., et al., *Impaired compensatory beta-cell function and growth in response to high-fat diet in LDL receptor knockout mice*. *Int J Exp Pathol*, 2014. **95**(4): p. 296-308.
263. Butler, A.E., et al., *Beta-cell deficit and increased beta-cell apoptosis in humans with type 2 diabetes*. *Diabetes*, 2003. **52**(1): p. 102-10.
264. Gale, E.A., *Spring harvest? Reflections on the rise of type 1 diabetes*. *Diabetologia*, 2005. **48**(12): p. 2445-50.
265. Buschard, K., *What causes type 1 diabetes? Lessons from animal models*. *APMIS Suppl*, 2011(132): p. 1-19.

## References

266. Siersbaek, M., et al., *High fat diet-induced changes of mouse hepatic transcription and enhancer activity can be reversed by subsequent weight loss*. *Sci Rep*, 2017. **7**: p. 40220.
267. Guo, Y., et al., *Quantitative proteomic and functional analysis of liver mitochondria from high fat diet (HFD) diabetic mice*. *Mol Cell Proteomics*, 2013. **12**(12): p. 3744-58.
268. Pomplun, D., et al., *Elevation of blood glucose following anaesthetic treatment in C57BL/6 mice*. *Horm Metab Res*, 2004. **36**(1): p. 67-9.
269. Zuurbier, C.J., et al., *Anesthesia's effects on plasma glucose and insulin and cardiac hexokinase at similar hemodynamics and without major surgical stress in fed rats*. *Anesth Analg*, 2008. **106**(1): p. 135-42, table of contents.
270. Windelov, J.A., J. Pedersen, and J.J. Holst, *Use of anesthesia dramatically alters the oral glucose tolerance and insulin secretion in C57Bl/6 mice*. *Physiol Rep*, 2016. **4**(11).
271. Zuurbier, C.J., et al., *Optimizing anesthetic regimen for surgery in mice through minimization of hemodynamic, metabolic, and inflammatory perturbations*. *Exp Biol Med (Maywood)*, 2014. **239**(6): p. 737-46.
272. Kim, S.P., J.L. Broussard, and C.M. Kolka, *Isoflurane and Sevoflurane Induce Severe Hepatic Insulin Resistance in a Canine Model*. *PLoS One*, 2016. **11**(11): p. e0163275.

## **Statutory declaration**

I hereby declare that I wrote the dissertation “Die Rolle des Toll-like Rezeptor 4 als Modulator metabolischer Prozesse im Tiermodell des Typ 1 Diabetes“ independently and without other resources as indicated in according to “Grundsätze zur Sicherung guter wissenschaftlicher Praxis an der Heinrich-Heine-Universität Düsseldorf”.

Furthermore, I declare that I did not submit this dissertation, either in full or modified, to any other academic institute and did not absolve any promotion trials before.

---

Corinna Wessel

Düsseldorf,

## **Eidesstattliche Erklärung**

Ich versichere an Eides Statt, dass die Dissertation „Die Rolle des Toll-like Rezeptor 4 als Modulator metabolischer Prozesse im Tiermodell des Typ 1 Diabetes“ von mir selbstständig und ohne unzulässige fremde Hilfe unter Beachtung der „Grundsätze zur Sicherung guter wissenschaftlicher Praxis an der Heinrich-Heine-Universität Düsseldorf“ erstellt worden ist.

Darüber hinaus versichere ich, dass ich die Dissertation weder in der hier vorgelegten noch in einer ähnlichen Form bei einem anderen Institut eingereicht habe und bisher keine Promotionsversuche unternommen habe.

---

Corinna Wessel

Düsseldorf,

### Acknowledgements

First, I would like to thank my supervisor PD Dr. Volker Burkart for giving me the opportunity to write my PhD thesis in his lab and introducing me into the field of Type 1 Diabetes and the NOD mouse. I am very grateful for your excellent scientific advice, your guidance and support. Thank you for a very comfortable work environment and for always taking time for discussion.

I want to thank Prof. Dr. Eckhard Lammert for being my second supervisor. For helpful comments and supervision.

Furthermore, I would like to thank Prof. Dr. Michael Roden for the opportunity to write my PhD thesis in the Institute for Clinical Diabetology at the German Diabetes Center in Düsseldorf.

I want to thank all lab members of the AG Burkart and AG Herder for the enjoyable work environment, helpful discussions and assistance. A special thanks to Waltraud Fingberg and Robert Wischeidt for all their help and lots of fun. I would also like to thank Prof. Dr. Christian Herder, Dr. Corinna Niersmann and Ulrike Partke for all their support and great moments over the last years.

Special thanks goes to Dr. Jong-Hee Hwang and Maik Rothe of the Research Group Metabolic Imaging of the Institute for Clinical Diabetology for introducing me to the world of magnetic resonance imaging and spectroscopy. Thank you Maik Rothe, for all experimental help and the patience to teach me, but also for all the fun and laughter.

I would further like to thank Sandra Cames, Dr. Bengt-Frederik Belgardt, Dr. Jürgen Weiß, Kay Jeruschke, Dr. Olaf Spörkel, Birgit Knobloch, Angelika Horrigs, Lena Espelage, Prof. Dr. Michael Blaut, Maximilian Jüdt, Katharina Hemme and Andrea Scheffel-Clausewitz for all their help.

I especially thank my family. My parents, grandma and my sister who always believed in me. Very special thanks to Silvia Kerner, for your encouragement, great support and love.